THE UNIVERSITY
of EDINBURGH

The Geochemistry of Eclogites from Western Norway: Implications from High-Precision Whole-Rock and Rutile Analyses

THE UNIVERSITY *of* EDINBURGH

Darren James Wilkinson

A Thesis Submitted for the Degree of Doctor of Philosophy

2014

Declaration

I declare that this thesis has been composed soley by myself and that it has not been submitted, either in whole or part, in any previous application for a degree. Except where otherwise acknowledged, the work presented is entirely my own.

Darren James Wilkinson
25/08/2014 (initial submission)
29/05/2015 (final submission)

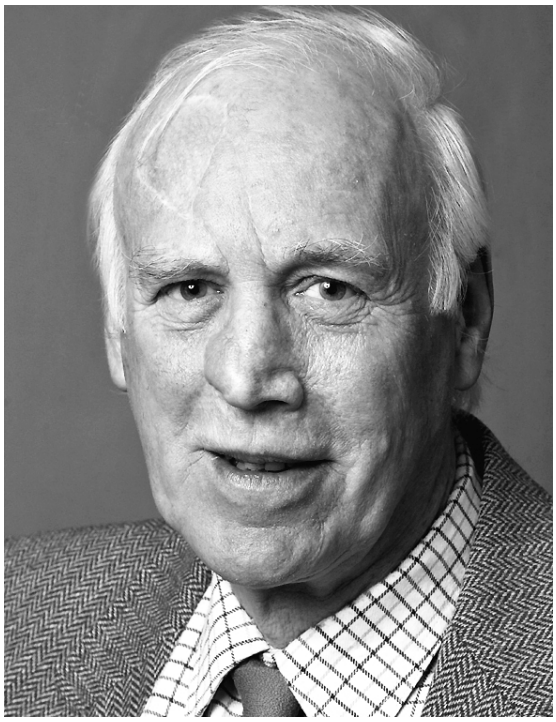

Dedicated to Barry Dawson

A inspirational scientist, dearest friend, true gentleman, a chap and a legend. Cheers, Barry!

Abstract

The Western Gneiss Region (WGR) in Norway is home to some of the world's most spectacular exposures of high pressure (HP) and ultrahigh pressure (UHP) eclogites. Despite extensive petrological studies into their pressure, temperature and time (PTt) histories, relatively few have reported on their trace element compositions. Such data can be used to supplement our understanding of the provenance and history of Norwegian eclogites, as well as to further our understanding of trace element fluxes during HP to UHP metamorphism in subduction zone settings.

In order to address this shortfall in data availability, the first step was to investigate and apply the best dissolution techniques for preparing eclogite samples for chemical analysis. Eclogites commonly contain up to a few weight percent rutile (TiO_2), which is known to be an important host for a variety of major and trace elements (e.g. Ti, Nb and Ta). However, typical rock digestion procedures are incapable of dissolving rutile, and thus may lead to inaccurate measurements. It was found that that total dissolution of rutile can be achieved by dissolving samples in sealed pressure vessels at increased pressures and temperatures, ultimately leading to greatly increased data accuracy for analyses of any rutile-bearing lithology. The solutions were analysed by standard ICP-MS techniques and the results compared to analyses of powders by XRF spectrometry.

Our high-accuracy and high-precision data were subjected to immobile trace element discriminant analyses that suggested eclogites belonged to three broad geochemical groups: eclogites with mid ocean ridge Basalt (MORB)-like composition; eclogites with arc-like composition; and eclogites with geochemical signatures significantly perturbed by metamorphism. The geochemistry of eclogites in the first two groups are shown to likely reflect protolith composition, and as such we used model protolith compositions to calculate estimated element mobilities (EMMs) for those elements considered relatively mobile during metamorphism. It was not possible to determine protoliths for eclogites in the third category using trace elements alone.

Finally, the trace element geochemistry of a large number of separated eclogite-hosted rutiles was studied. The data collected were used to demonstrate that rutile contains

significant amounts of the whole-rock's high field strength element (HFSE) budget, and may exert significant control on the HFSE composition of passing hydrothermal fluids. Furthermore, Zr-in-rutile thermometry (ZRT) was applied to separated rutiles. This temperature information was used to better our understanding of the thermal history of the WGR, as well as to create a map of eclogite temperatures in the Nordfjord-Statlandet area. This high-resolution thermal map of arguably the most important area of the WGR, supports current interpretations that during the Caledonian Orogeny the leading edge of the Baltica plate was consumed in a northwest to north-northwest-dipping subduction zone under Laurentia. Furthermore, isotherms on this map mimic several major fold hinges in the region rather well, thus providing support to the hypothesis that such structures were most likely formed during the collapse of the Scandinavian Caledonian Orogen after the peak metamorphism of most eclogites.

Acknowledgements

Now that I approach the conclusion to the past three and half years of research, I am humbled when I look back at the good will and generosity of others that has carried me through such an important and often turbulent chapter of my professional and personal life. I know that I can give only an abstract of the debt I owe, and the gratefulness I bear.

First, an elaboration on why I dedicated this thesis to Barry Dawson. Barry was undoubtedly a self-appointed additional project supervisor, one whom would regularly visit my office to talk about both my work and his own. In doing so he became the most unique of friends and colleagues, and I know that he would have been excited to see this thesis in its final form. Barry certainly had wings of a sort, and I felt welcomed beneath them.

Funding for this project was provided by Natural Environment Research Council (NERC), the Scottish Universities Environmental Research Centre (SUERC), The School of GeoSciences at The University of Edinburgh, and in part by Craig Storey at The University of Portsmouth. Their financial support has been the most obvious and fundamental contribution to this project and its outcomes.

Long before they were my supervisors, Godfrey Fitton and Simon Harley were both equally strong yet utterly unique points of inspiration and intrigue for me. Since day one of this project, both have let me take real ownership and control, treated me as a colleague rather than subordinate, and equipped me with the skills necessary to make a strong and independent career wherever I go next. I hold them both with the highest possible regard, and have been lucky to have worked alongside such eminent scientists and patient mentors.

My parents, Rosalyn and Keith, are undoubtedly responsible for helping me find situations of which I have been able to take full advantage as a young scientist. Without their unflinching and hefty support, both financial and moral, I would never have come so close to my dreams. I must also mention my Grandfather Richard, a man who defines for me the word *inquisition*. His love for logic, reason and philosophy is where I often turn to for motivation and advice.

How can I even begin to acknowledge my wife in her support of myself and this project? She has invested significant time and energy herself into supporting me in every possible way as the project evolved, and is in large part responsible for the existence of this thesis. It is perhaps to her I owe the greatest debt.

There are countless staff and technicians at various institutions whose good-will and hard work always left me flummoxed as to why on Earth they have been so kind. Nic Odling must be recognised not only for his flexible and generous attitude to my rock analyses, but for his willingness to dedicate significant parts of his day to teach me laboratory techniques and discuss analytical ideas and problems. Mike Hall is truly one of the best thin-section makers one may encounter, and must be praised for his meticulous work that allows others to do theirs. Chris Hayward with his warm and witty personality has given me access to very good EMP data and training, all the while treating me with a respect and professional friendship I find now so familiar in the world of research. Similarly, John Craven and Richard Hinton provided me with much laboratory support and advice at several key stages in my project.

A large component of my data comes from analyses performed at the Scottish Universities Environmental Research Centre (SUERC) in East Kilbride, Scotland. First and foremost, director of the facility Rob Ellam has no doubt been instrumental in laying a path of unfettered access to technical staff, time on analytical equipment, and funds for expensive laboratory equipment. Valerie Olive is perhaps the person with whom I have worked most closely with in this project. She has dedicated months of her time, and applied her impressive insights into analytical geochemistry to help develop a rigorous analytical procedure for rutile-bearing eclogites. Her colleagues Anne Kelly and Vince Gallagher have too given significant time and effort to this project. All welcomed me as a colleague at the SUERC facility.

Craig Storey is yet another who has devoted time, energy and funds to this project. Craig truly went out of his way to help me gather the data I needed by giving me access to his laser ablation inductively-coupled plasma mass spectrometry (LA-ICP-MS) laboratory in Southampton. I have an ongoing debt of gratitude to him for the work we did together.

I have a lot to thank my fellow PhD students who have made my time in the Grant Institute full of many fond memories. These people have been my bothers and sisters in arms, and we've shared frustrations and successes together. Romesh in particular has been my sidekick now for over 6 years and I was lucky to have been able to work with him so much. His inspiring positive attitude and strong ambitions have no doubt helped keep me motivated and positive in his presence. Andrew Miles went from being my demonstrator to my colleague, friend to field assistant, and all the while he has been a constant source of inspiration. I often find myself trying to fill his shoes and follow his lead. As for the rest of my PhD colleagues - too many to list or describe, I'm sure they know how much they are appreciated.

How can I possibly write my acknowledgements without including Milo and Sophie, the loyal and character-rich dogs that have in succession acted as my shadow for the past three and half years. Never one without the other, I never knew who was more welcome at work: me or the dog. They have fulfilled their roles as therapy dogs for countless PhD students, and I'm sure Milo will be by my side to the very end.

Contents

Symbols, Acronyms & Abbreviations

BSE	backscattered electron
CAB	calc-alkali basalt
CPS	counts per second
CRB	continental rift basalt
GLOSS	globally subducted sediment
E-MORB	enriched mid-ocean ridge basalt
EMM	estimated minimum mobility
HFSE	high field strength element
HREE	heavy rare earth element
HP	high pressure
HPTS	high pressure and temperature solution
HT	high temperature
IAT	island arc tholeiite
IAB	island arc basalt
ICE	iceland array
ICP-MS	inductively coupled plasma mass spectrometry
HP	high pressure
KDE	kernel density estimate
LA-ICP-MS	laser ablation inductively-coupled plasma mass spectrometry
LFSE	low field strength element
LILE	large ion lithophile element
LOI	loss on ignition
LPTS	low pressure and temperature solution
LREE	light rare earth element
LT	low temperature
MP	medium pressure
MT	medium temperature

MORB	mid-ocean ridge basalt
N-MORB	normal mid-ocean ridge basalt
NERC	Natural Environment Research Council
NIST	National Institute of Standards and Technology
NSDZ	Nordfjord-Sogn detachment zone
OIB	ocean island basalt
PTt	pressure-temperature-time
PTX	pressure-temperature-composition
REE	rare earth element
SEES	School of Earth and Environmental Sciences
SEM	scanning electron microscope
SILLS	signal integration for laboratory laser systems
SIMS	secondary ionisation mass spectrometry
SRM	standard reference material
SSO	Southwest Scandinavian Orogen
SUERC	the Scottish Universities Environmental Research Centre
T-MORB	transitional mid-ocean ridge basalt
TAS	total alkali silica
TIB	trans-Scandinavian igneous belt
UCC	upper continental crust
UHP	ultra-high pressure
UHT	ultra-high temperature
VAB	volcanic arc basalt
WGR	Western Gneiss Region
WPAB	within-plate alkali basalt
WPB	within-plate basalt
WPT	within-plate tholeiite
XRF	X-ray fluorescence
ZRT	Zr-in-rutile thermometer

c) Mineral name abbreviations

Ap	Apatite
Amp	Amphibole
Aug	Augite
Bar	Barriosite
Bt	Biotite
Cpx	Clinopyroxene
Coe	Coesite
Czo	Clinozoisite
Di	Diopside
Ep	Epidote
Grs	Grossular
Grt	Garnet
Gt	Garnet
Hbl	Hornblende
Jd	Jadeite
Ky	Kyanite
Mag	Magnetite
Ol	Olivine
Omp	Omphacite
Opx	Orthopyroxene
Pl	Plagioclase
Phe	Phengite
Prp	Pyrope
Py	Pyrite
Qtz	Quartz
Qz	Quartz
Rt	Rutile
Spl	Spinel
Su	Sulphide Mineral
Trem	Tremolite
Zo	Zoisite

Chapter 1

Introduction

1.1 Eclogites and Eclogites

1.1.1 Early Discoveries and Descriptions

Eclogites were first described by Horace-Bénédict de Saussure (Figure 1.1) in his Voyages dans les Alps in the mid 1700s. He found pebbles of eclogite in the Rhône Valley not far from Geneva, and described it as 'a beautiful rock...not yet described'. Other early observations were made by Déodat Gratet de Dolomieu (Dolomieu, 1794) and Abraham Gottlob Werner (Werner, 1917).

The term eclogite (after the Greek 'ekloga', meaning 'choice') was not actually coined until much later by the mineralogist René J. Haüy (Figure 1.2) in his 1822 "Traité de Minéralogie" in which he wrote about eclogite: "...diallage (i.e. clinopyroxene) is considered the main mineral and constitutes with garnet a binary association to which can be unevenly added kyanite, quartz, epidote and lamellar amphibole. I gave to this rock the name eclogite, which means 'choice' or 'selection' because its components, which do not usually coexist together in primitive rocks, as do the feldspar, mica and amphibole, seem to have chosen themselves to constitute a peculiar association."

1.1.2 The Eclogite Enigma

For over a century there would exist an often undignified and dogmatic controversy over the origin of eclogites, as the idea that eclogite was a metamorphic rock was radical one. Until the late 19th Century it was thought that metamorphic rocks were only ever sedimentary in origin, formed by the effects of temperature and fluids (Hunt, 1884; Williams, 1890; Zittel, 1899, e.g.). This was soon followed by the first reported geochemical analyses of eclogites (e.g. Mauthner, 1872; Gerichten, 1874), which showed their bulk composition was basaltic. Unfortunately this observation

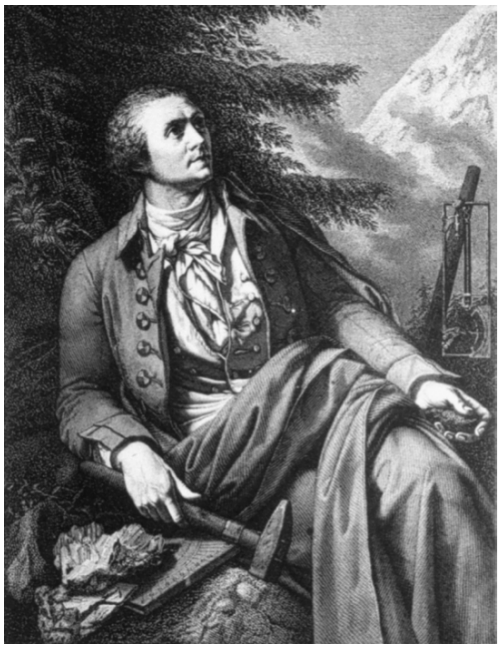

Figure 1.1: Horace-Bénédict de Saussure, (1740-1799) by Jean-Pierre Saint-Ours, 1976.

Figure 1.2: René J. Haüy (1743-1822) was the first to coin the term 'eclogite'.

was unable to resolve the debate.

Although Pentti Eskola (i.e. Eskola, 1920, 1921) is considered one of the pioneers of the eclogite facies, until ca. 1939 he was actually a supporter of a magmatic origin for eclogites. Based on the eclogites he saw in Norway, he concluded that they had crystallised from a 'high pressure eclogite magma'.

Convincing evidence in favour of a metamorphic origin began with the observation of transitions between 'fresh' gabbros and basalts, glaucoaphanites and eclogites (e.g. Bonney, 1879; Koto, 1887; Lepsius, 1893). Brière (1920) noticed that eclogites in France were gabbroic in composition and followed geochemical variations typical of fresh gabbros, but this was received rather negatively by her peers (Godard, 2001, see).

The controversy came to an end in the late 1930s, compelled in following years by three main lines of argument: firstly, detailed geochemical studies showed that the major element, trace element, and isotopic composition of eclogites and basaltic rocks were very similar; secondly, original textural and structural features of basaltic protoliths in some eclogites can be identified (e.g. Chenevoy, 1958; Miller, 1970); and finally, experimental studies (e.g. Ringwood and Green, 1966; Green and Ringwood, 1967, 1972) have proven the gabbro-to-eclogite transition to exist.

The accepted modern definition of the rock-type eclogite comes from Carswell (1990) who defined it as "a plagioclase-free rock, of broadly basaltic composition, composed of >70 % red pyropic garnet and green omphacitic pyroxene solid solution".

1.1.3 The Eclogite Facies

Once a metamorphic origin for eclogites was widely accepted, it became necessary for the mineralogical differences between basaltic rocks and eclogites to be explained. The solution lay in the Clausius Clapeyron equation (or "volume law") which predicts higher pressures result in the formation of more dense minerals. In fact it was petrologist Friedrich Becke who first tested the volume law on eclogites (Becke, 1903), suggesting they had indeed crystallised at relatively high pressure.

The eclogite *facies* (Figures 1.3 and 1.4), established by (Eskola, 1915, 1921), is the highest pressure metamorphic facies. Pressures start from around 8 kbar, and temperatures can vary from a few hundred to over a thousand degrees Celsius. Not all rocks metamorphosed in the eclogite facies become *true* eclogites, but may be described as *eclogite facies* rocks.

Since the work of Becke (1903), for much of the 20^{th} century eclogites and blueschists were known to have formed under high pressures. However, our understanding of the range of pressures of metamorphism preserved in rocks in orogenic belts was redefined after the discovery of the mineral coesite (a ultra-high pressure SiO_2 polymorph) in high grade blueschists by Chopin (1984) in the Dora Maira province of the Italian Alps, and in eclogites from Western Norway by Smith (1984). Smith and

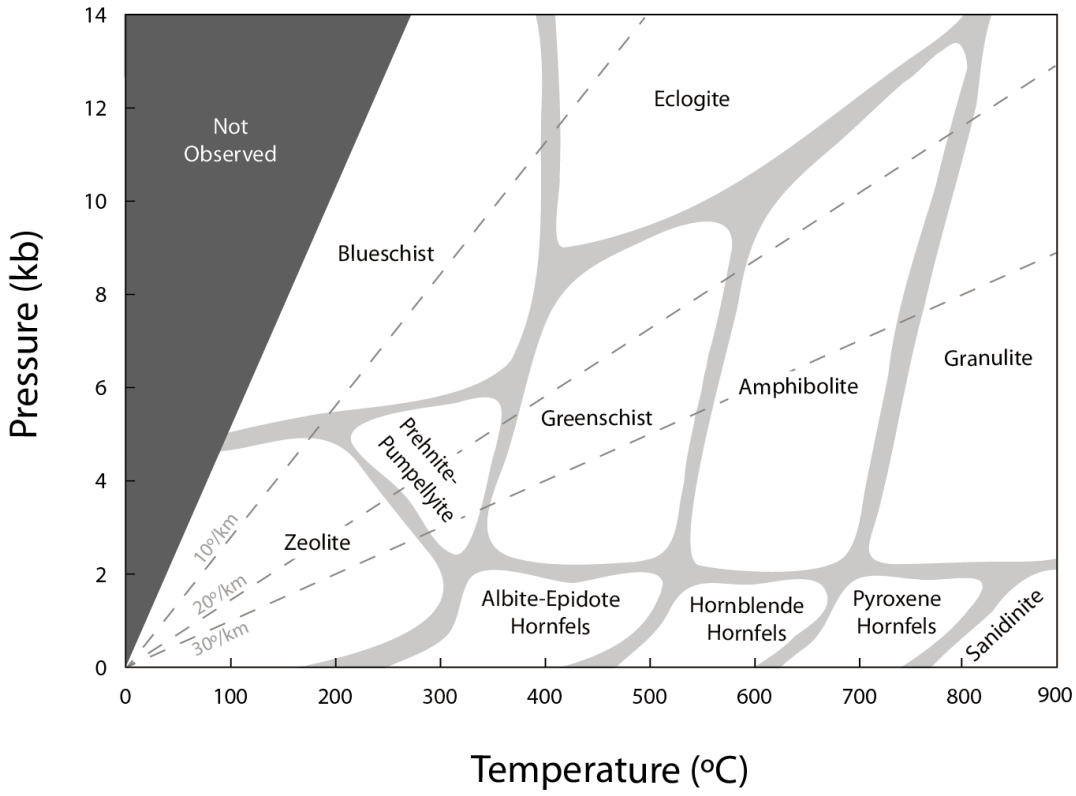

Figure 1.3: Overview of Metamorphic Facies observed in the terrestrial geological record. The dark shaded area represents conditions not though to exist in the Earth. The light shaded area indicates transitional conditions between adjacent facies. Dashed lines show geothermal gradients typically followed by rocks undergoing metamorphism in a range of tectonic settings.

Chopin's discoveries were closely followed by many others, as not only coesite but diamond-bearing rocks continue to be found in many of the worlds orogens. It was at this time the term ultra-high pressure (UHP) metamorphism was coined, and became a milestone in modern metamorphic geology.

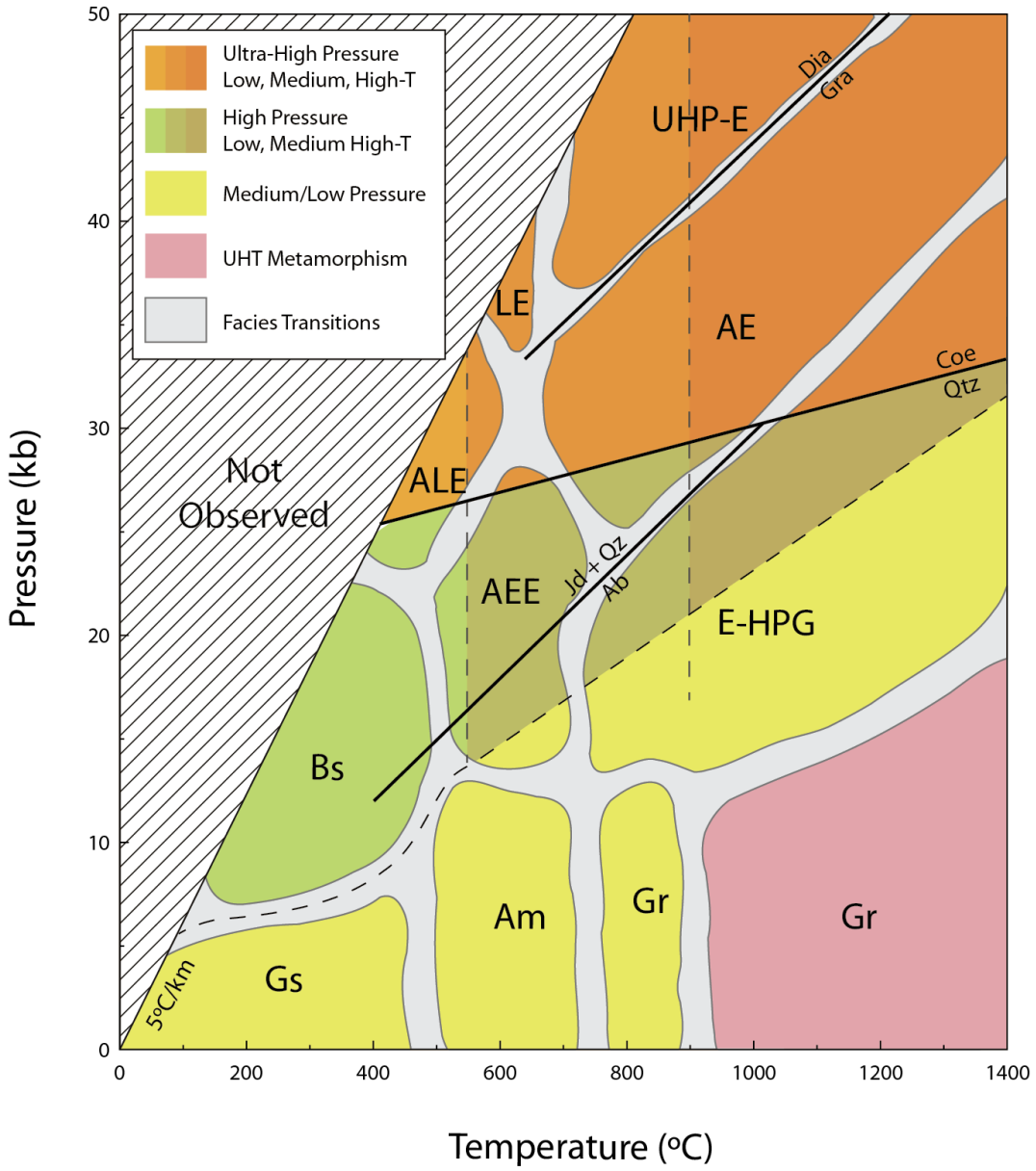

Figure 1.4: Petrogenetic grid showing MP to UHT and LT to UHT facies, as well as the various subdivisions divisions of the eclogite facies: AE, Amphibole Eclogite; AEE, Amphibole-Epidote Eclogite; ALE, Amphibole-Lawsonite Eclogite; E-HPG, Eclogite-High Pressure Granulite; LE, Lawsonite Eclogite; UHP-E, Ultra-High Pressure Eclogite. Other facies are: Am, Amphibolite; Bs, Blueschist; Gr, Granulite; Gs, Greenschist. Mineral abbreviations for reaction lines: Coe, Coesite; Dia, Diamond; Gra, Graphite; Qtz, Quartz. Modified after Johnson and Harley (2012).

1.1.4 Eclogite Petrogenesis

The transformation of basaltic igneous rocks into eclogites can be summarised by the following reaction:

$$Pl + Cpx \pm Ol \pm Opx \rightarrow Grt \pm Omp \pm Qtz \pm Rt^{*} \tag{1.1}$$

In addition to the typical eclogite facies parageneses, there are as many as 30 or more other minerals that are stable as accessory phases in typical basaltic eclogites. The exact assemblage is dependent upon the specific composition of the basaltic protolith as well as the pressure-temperature-composition (PTX) conditions experienced along the prograde path (Coleman et al., 1965, e.g.).

Totally recrystallised eclogites do not preserve information on the petrological evolution of their protoliths, yet coarse grained rocks (i.e. metagabbros) that are not deformed can often preserve textural relics of prograde recrystallisation. Figure 1.5 shows a common 'dry' basalt-to-eclogite prograde reaction sequence preserved in a olivine gabbro from Flemsøy, Western Norway (after Mørk, 1985). This reaction sequence explains some several petrological features of even heavily recrystallised eclogites, such as the abundance of omphacite inclusions in garnet.

More specifically, the breakdown of plagioclase is ultimately controlled by reactions either in the presence of absence of water (reaction equations 1.2 and 1.3 respectively):

$$Pl + H_2O \rightarrow Jd + Zo + Ky + Qtz \tag{1.2}$$

$$Pl \rightarrow Jd + Grs + Ky + Qtz \tag{1.3}$$

Surplus Na and Al ions generated by the recrystallisation of plagioclase can then exchange with Ca, Mg and Fe in augite, leading to sodic pseudomorphs most commonly of omphacite composition. In response, the exchanged Ca, Mg and Fe can diffuse back into reacting plagioclase to provide the diopside component for omphacite formation. As shown in Figure 1.5, the replacement of olivine under

*See page 17 for mineral abbreviations.

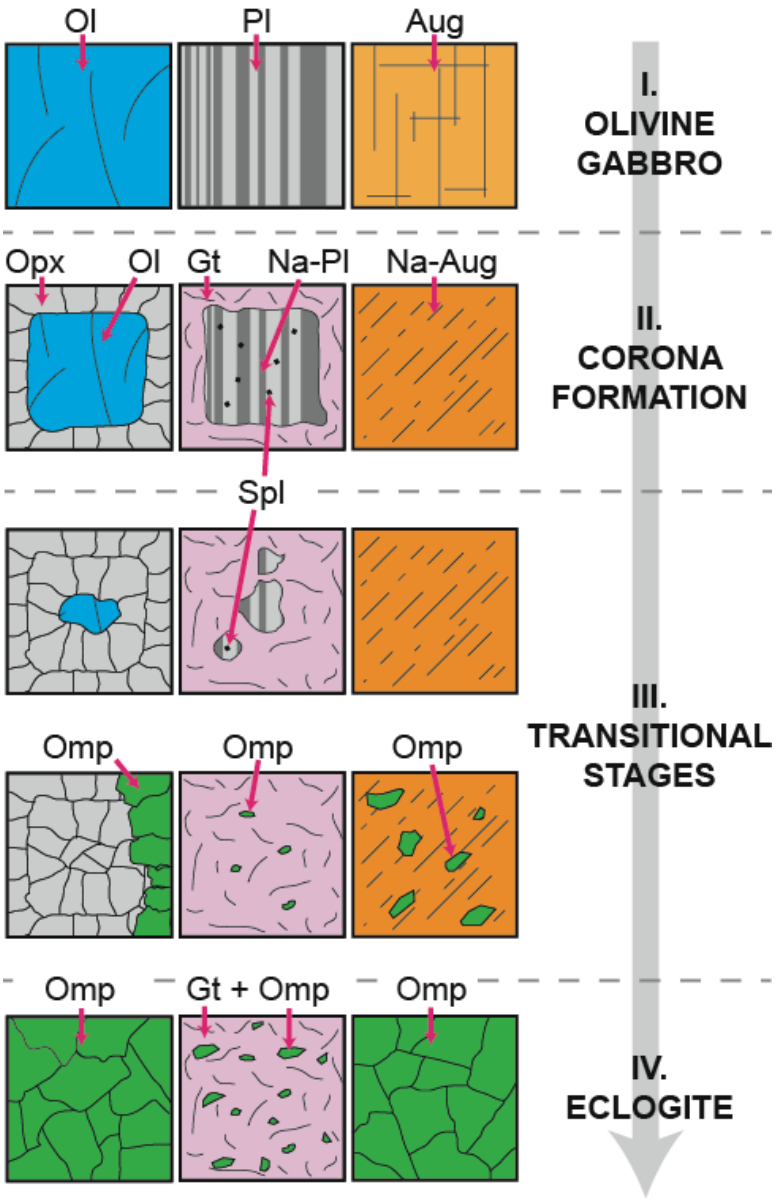

Figure 1.5: The local domain phase changes associated with the 'dry' reaction of primary minerals in an olivine gabbro during eclogite facies metamorphism. The first metamorphic stage involves the formation of corona around olivine (Ol) and plagioclase (Pl), whilst augite (Aug) undergoes pseudomorphism to a Na-rich augite (Na-Aug). Ultimately, olivine is recrystallised to omphacite (Omp), plagioclase to garnet (Grt) with omphacite inclusions, and augite to omphacite. Spinel (Spl) forms within plagioclase during transitional stages of recrystallisation. The sequence is modelled on the Flemsøy eclogite body, Norway and the diagram redrawn from Mørk (1985).

'dry' conditions typically occurs by rim-to-core replacement with orthopyroxene followed by omphacite, which is probably facilitated by the incorporation of free silica generated in plagioclase breakdown, and the increased availability of Na, Al, and Ca ions generated from plagioclase and augite reactions. Under hydrous conditions, talc and chlorite probably the products of the breakdown of olivine.

As will be demonstrated in this thesis, the length-scale of diffusion during eclogitisation is often relatively short in relation to the protolith's grain size, and thus prograde reaction and recrystallisation tends to occur in local mineralogical domains within the rock (Koons et al., 1986, e.g.). It is therefore not uncommon to observe mineralogical disequilibrium within eclogites on the centimetre scale and above (e.g. Årsheimsneset eclogite).

1.1.5 Eclogite Parageneses

True basaltic eclogites commonly have the basic mineral assemblage:

$$Grt + Omp \pm Rt \pm Qtz \pm Py$$

As mentioned above, there are around 30 different accessory phases stable within basaltic eclogites, but the most common ones outside rutile (Rt) and pyrite (Py) include kyanite, (clino) zoisite, epidote (Ep), othopyroxene, amphibole, phengite, and carbonate, depending on the unique PTX evolution of the eclogite.

Garnets in eclogites are solid solutions with dominant components of Almandine (Alm, 20-60%), pyrope (Prp, 10-55%) and grossular (Grs, ca. 30%), and minor amounts of spessartine (Sps, $<8\%$) especially in cores (Mottana et al., 1990). Garnets typically show prograde zoning characterised by decreasing almandine and increasing pyrope ($Alm_{60}Prp_{10}$ to $Alm_{20}Prp_{55}$).

Omphacite pyroxene, a solid solution between diopside (Di) and jadeite (Jd), also experiences prograde zoning in composition from around $Di_{75}Jd_{25}$ to around $Di_{40}Jd_{60}$ (Mottana et al., 1990). In 'dry' eclogites, omphacite typically crystallises *after* garnet (see Figure 1.5), whereas in 'wet' eclogites omphacite crystallises *before* garnet.

Amphiboles grown on the prograde path often belong to solid solution series that are often adept at keeping pace with changes in P-T conditions as well as local changes in composition caused by reactions of other minerals. As summarised by Carswell (1990), the vast majority of prograde amphiboles crystallise as galucophane (Gln, low whole rock Fe/Al) or crossite (Crs, high whole rock Fe/Al). Increasing P at low T yields more pure Gln followed by nyböite ($NaNa_2(Al_2Mg_3)(Si_7Al)O_{22}(OH)_{22}$), whilst medium temperature (MT) gradients lead to more Na-Ca-rich amphiboles (e.g. barriosite, $NaCa(Mg_3Al_2)(Si_8)O_{22}(OH)_{22}$).

Prograde micas (phengite and paragonite) typically react to form kyanite, contribute Na to omphacite, and/or provide K which instigates reactions between garnet and calcic amphiboles that form biotite. Prograde epidote group minerals typically present as zoisite (Zo) which later reacts to clino-zoisite.

1.1.6 Eclogite Retrogression

Although the preservation of eclogite facies parageneses requires high rates of exhumation, eclogites commonly show variable degrees of retrograde recrystallisation, most commonly in the amphibolite facies. Amphibolitisation of eclogites mostly composed of garnet and omphacite can be expodited by the addition of H_2O, and thus the degree and distribution of retrograde amphibolitisation is highly dependent on the availability of fluids and the permeability of the eclogite.

Retrogression of basaltic eclogites involves a relatively simple hydration reaction:

$$Grt + Omp + Ky + H_2O \rightarrow Hbl + Pl \tag{1.4}$$

The resulting growth of retrograde hornblende and plagioclase is typically symplectic (Figure 1.6) and dominated by hornblende, especially around garnet rims. However, solid-solid reactions involving jadeite and quartz, or omphacite and quartz can also yield albite, or albite and diopside respectively.

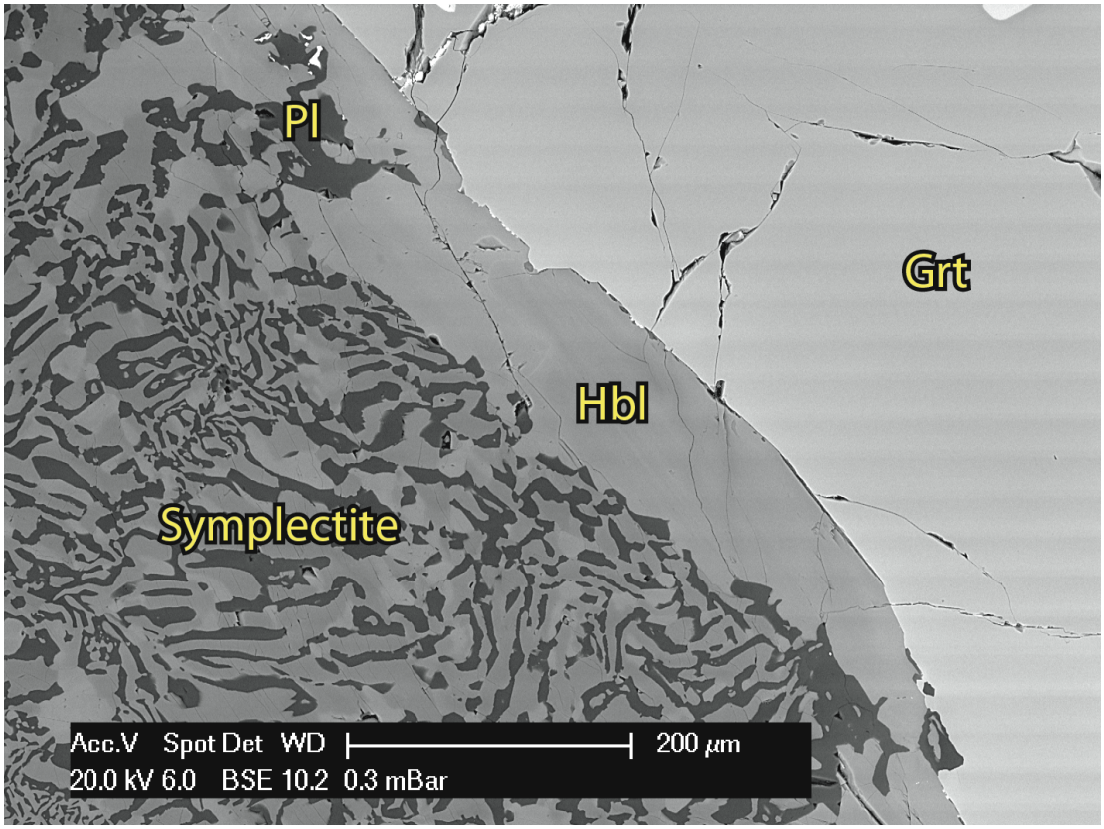

Figure 1.6: Backscatter electron (BSE) image of an hornblende-plagioclase symplectite surrounding garnet (WGR-73-DW). Plagioclase (Pl) and hornblende (Hbl) are formed by the hydration of the eclogite assemblage. The image shows that around the garnet (Grt) rim, hornblende dominates the symplectite.

1.1.7 Eclogites and the Global Nb/Ta Problem

Both Nb and Ta are HFSEs with a charge of 5^+ and almost indistinguishable ionic radius (0.64 Å in VI coordination, Shannon (1976)). Elemental partitioning in most magmatic processes are known to be **ch**arge- **a**nd **ra**dius-**c**ontrolled (CHARAC, Bau (1996)), therefore Nb/Ta would be expected to be present in most rock in the chondritic ratio of around 17 (McDonough and Sun, 1995; Sun and McDonough, 1989, e.g.). Despite this, in the 1970s workers began to notice an apparent lack of Nb within the crust-mantle system as a whole. For example, continental crust has Nb/Ta of only around 11-12 (Rudnick and Fountain, 1995; Taylor and McLennan, 1985, e.g.) and MORB-melt has Nb/Ta generally 9-18 (Nui and Hekinian, 1997; Nui and Batiza, 1997, e.g.). Therefore, there is an enigma in that the depleted mantle and continental crust are not considered to be complementary reservoirs of Nb/Ta.

McDonough (1991) was the first to suggest that, given our observations of crust and mantle Nb/Ta ratios, a complementary reservoir for Nb/Ta must exist somewhere inside the Earth, isolated from the upper mantle and continental crust. Rudnick et al. (2000) suggest that this reservoir is, at least in part, refractory eclogite produced by slab melting, which sinks into the lower mantle and is isloated from mantle involved in the formation of new crust. Indeed, Green and Pearson (1987) and then Brenan et al. (1994) showed that Nb and Ta can actually be fractionated from one another by Ti-rich accessory minerals such as rutile. More recently, there is a growing body of evidence suggesting that rutile does indeed dominate the budget of, and even fractionate Nb and Ta in subducted basic rocks, and may therefore help explain the observed subchrondritic nature of the crust-mantle system.

The Nb/Ta enigma is very much a current and relatively immature problem in the geochemistry community. It is hoped that we may use comprehensive high-precision analyses of Nb and Ta in rutiles and their host rutiles that may prove useful in the discussion of the behaviour of Nb/Ta in the crust-mantle system.

1.2 Geological Setting

The Western Gneiss Region (WGR) of Norway is an area of mostly para-autochthonous Precambrian basement that covers an area of over 25 $\times$ 10^3 km^2 from Sogn in the south, to Nord Trøndelag in the north (Figure 1.7). Its basement, which is dominated by Proterozoic orthogneisses, belongs to the Baltic Shield, which formed during the mid-Archaean (3.5 to 3.1 Ga). The oldest rocks *within* the WGR belong to the Geitfjell Granite that formed 1.83-1.84 Ga ago (Johansson et al., 1993). The geology of the WGR is largely the product of three main orogenic events (see Figure 1.9): the Southwest Scandinavian Orogen (SSO), composed of the Gothian (1750 to 1500 Ma) and Sveconorwegian (12500 to 970 Ma) events; and the Caledonian Orogeny (450-380 Ma). These main large-scale orogenic events are discussed in the sections below.

1.2.1 Precambrian Norway

Before the breakup of Pangaea, the Proterozoic rocks of the Western Gneiss Region (WGR) belonged to the Fennoscandian Shield. This shield is dated to 3.5-3.73 Ga (Siurua Gneiss in Northern Finland, Mutanen and Huhma, 2003), but the WGR only began to form 1.83-1.84 Ga (Gjeitfjell Granite Johansson et al., 1993)). The oldest parts of the WGR probably formed in a continuation of the trans-Scandinavian igneous belt (TIB) in Sweden, which represents a significant crustal accretion event (1.85 to 1.65 Ga) in northern Fennoscandia (Ramberg et al., 2008).

The majority of the basement in the WGR was formed in the Late Palaeoproterozoic to Early Neoproterozoic Southwest Scandinavian Orogen (SSO), which affected south-western parts of the Fennoscandian Shield. Approximately 80 % of the rocks exposed in the southern WGR were formed in the former Gothian (Figure 1.9, Skår, 2000), an important period of crustal accretion for the region. Gothian lithologies are typically dioritic to granitic orthogneisses (Kildal, 1969; Lutro and Tveten, 1996; Skår, 2000), the protoliths of which formed in a setting of sustained eastward-dipping oceanic-continental convergence on the south-western margin of the Fennoscandian shield (Figure 1.10 Brewer et al., 1998), much like the eastern Pacific Ocean margin

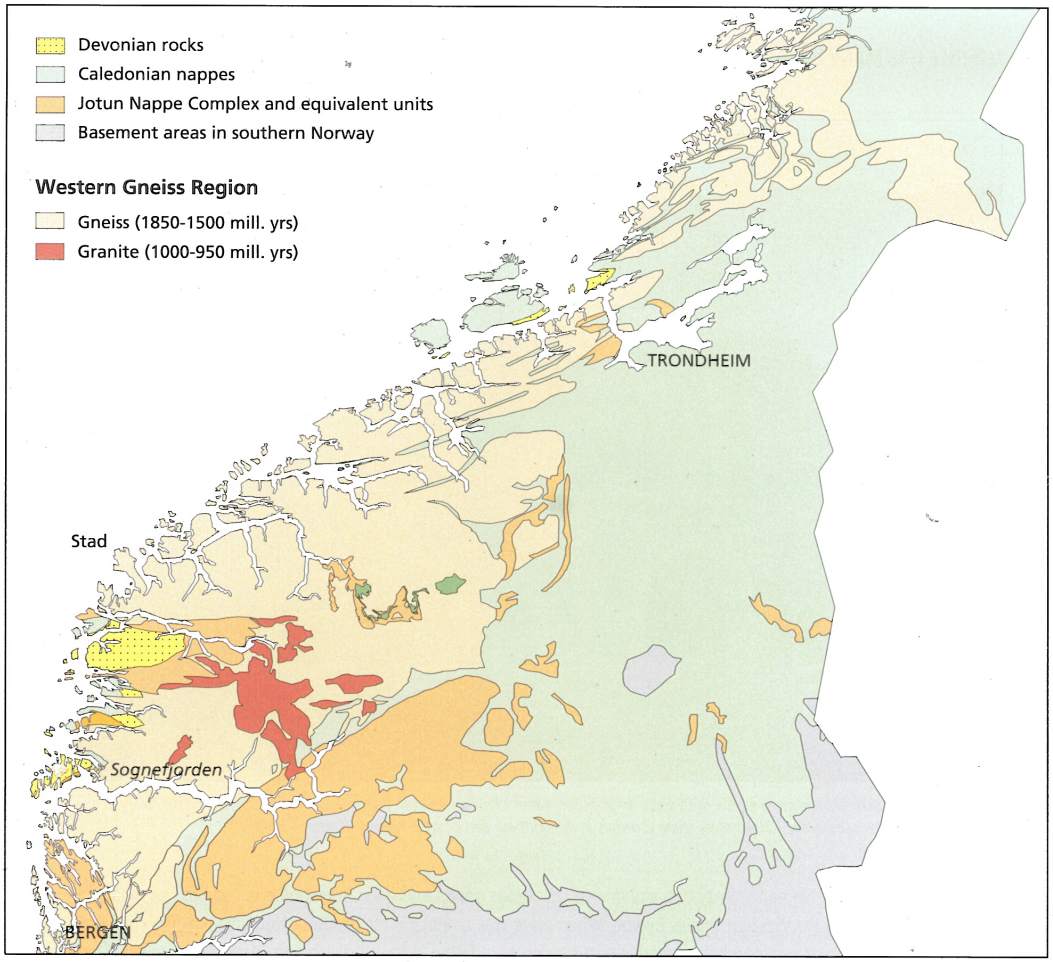

Figure 1.7: Simplified geological map of the WGR of Norway. The WGR extends from Sognefjorden in the south to beyond Trondheim to Trøndelag in the north. The WGR is broken by significant pre-Caledonian granites (red) and younger Devonian rocks (yellow, i.e. the Hornelen Basin). Taken from Ramberg et al. (2008).

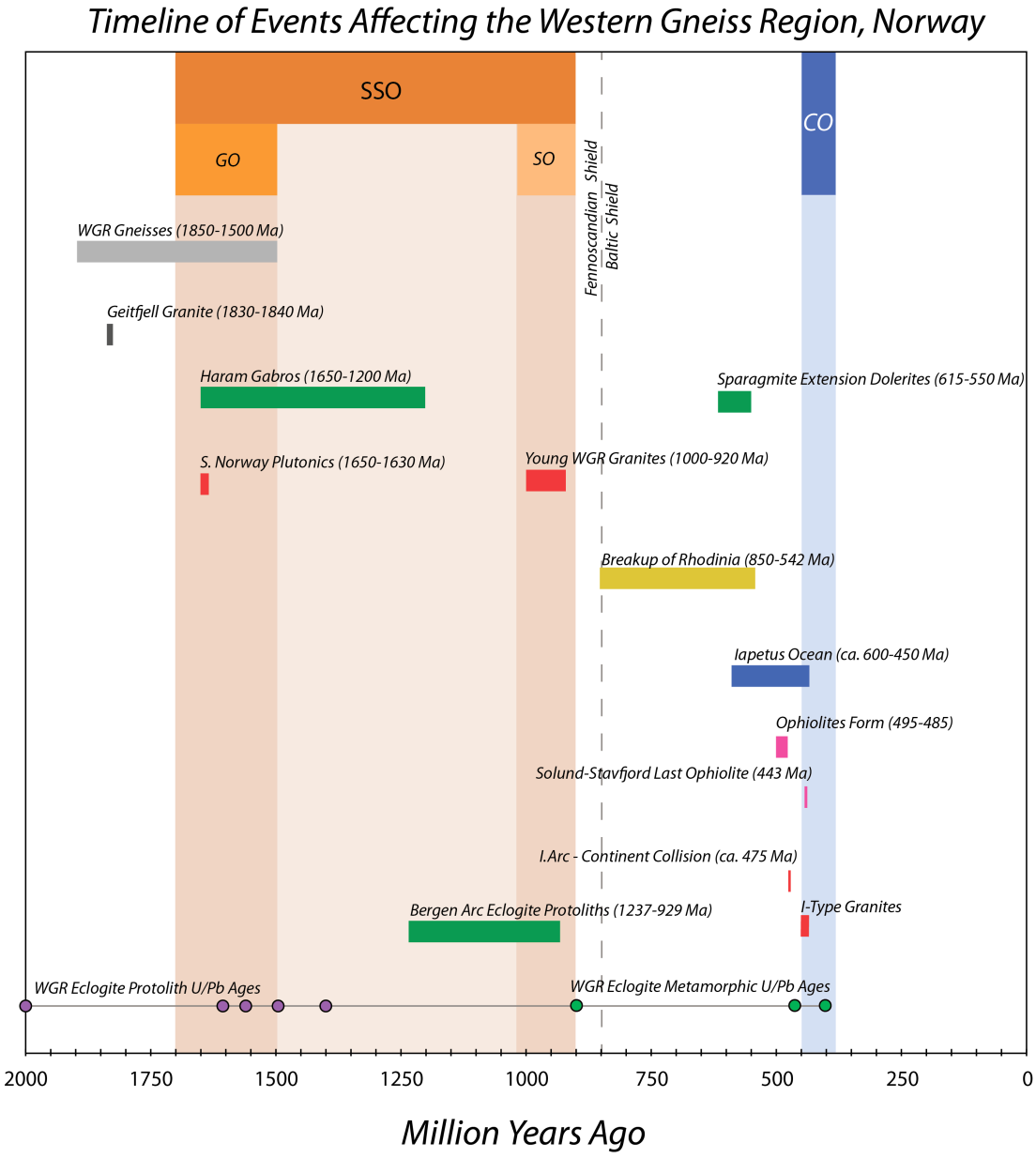

Figure 1.8: Timeline of events affecting the WGR from 2.0 Ga to present. The timeline covers the two main orogenic events that affected the region: the Southwest Scandinavian Orogen (SSO) including the Gothian (GO) and Sveconorwegian (SO), and the Caledonian Orogen (CO).

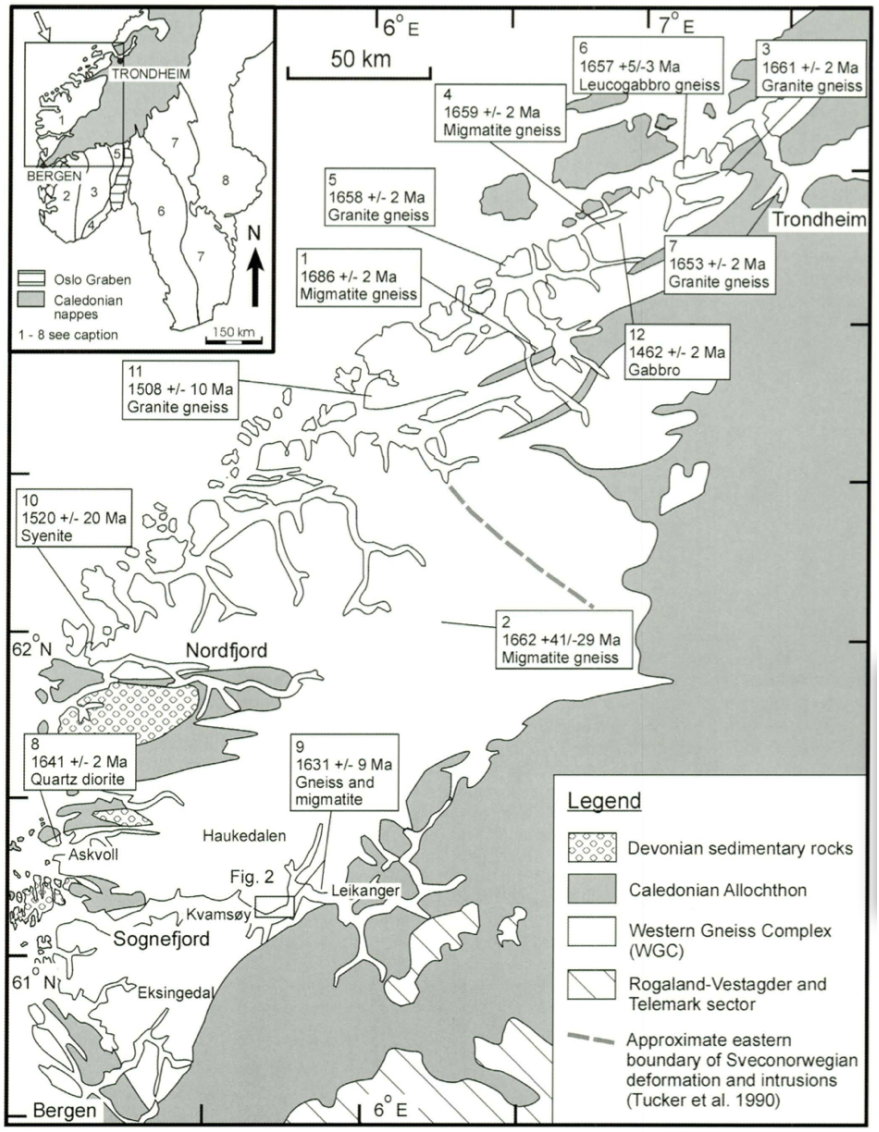

Figure 1.9: Locations for rocks dated using U-Pb. Inset map: 1-6, Southwest Scandinavian Domain (SSD) (1750-900Ma); 1, WGR; 2, Rodaland-Vestagder sector; 3, Telemark sector; 4, Bamble Sector; 5, Kongsberg sector; 6, Østfold sector and coeval sectors in Sweden; 7, Trans-Scandinavian Granite-Porphyry Belt (or Trans-Scandinavian Igneous Belt, TIB) (1780-1600 Ma)); 8, Sveconorwegian Orogen (2000-1750 Ma). From Skår (2000), after Gaál and Gorbatschev (1987); Gower et al. (1990); Tucker et al. (1990).

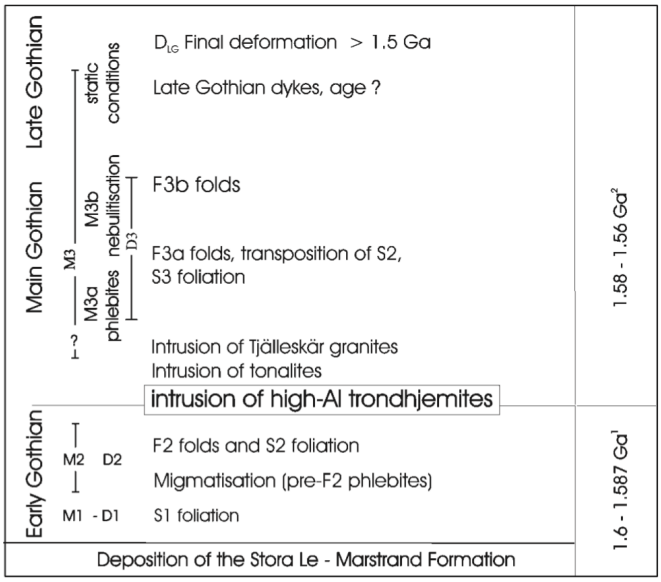

Figure 1.10: Timeline of events in the Gothian Orogeny highlighting at least three distinct events of crustal accretion and deformation. Taken from (Hageskov and Mørch, 2000)

of today. Relatively little is known about the Gothian, but so far at least three crust-generating events, and four deformation events have been identified (Hageskov and Mørch, 2000).

The Sveconorwegian Orogen was a major final stage in the formation of the super-continent of Rhodinia, and resulted from the collision of Fennoscandia and another continent during the Mesoproterozoic. The orogen itself is best preserved in southern parts of Norway and Sweden and is typified by Sveconorwegian-aged granites (see Figure 1.7) and high temperature (HT) and medium pressure (MP) metamorphic rocks (e.g. Røhr et al., 2004). These rocks are correlated with similar lithologies of around the same age found in the basement gneisses of Southern Norway suggesting that the basement gneisses of the southern WGR and southern Norway are continuations of one another (Ramberg et al., 2008).

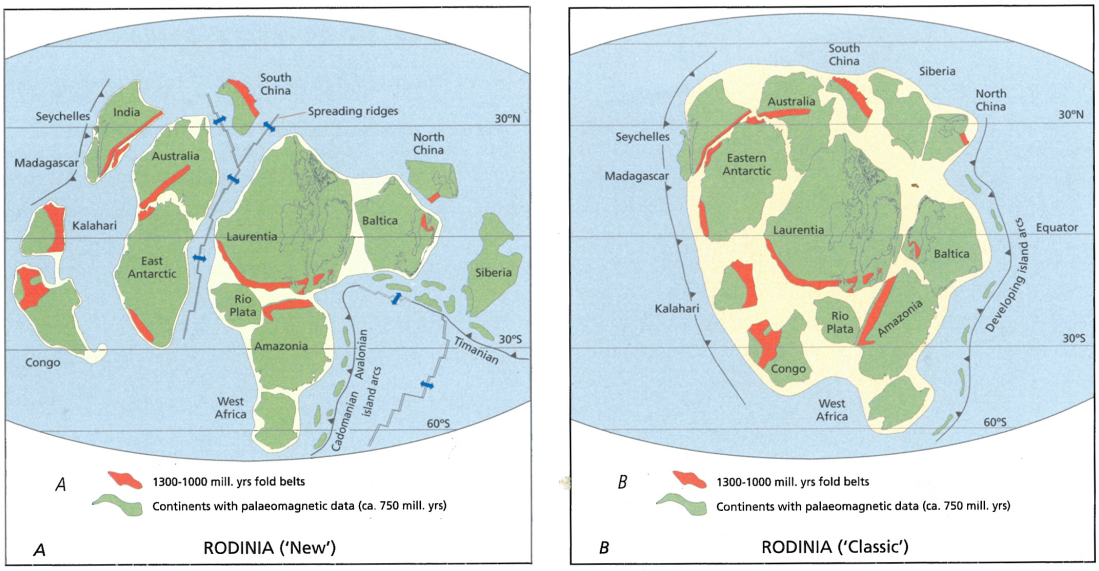

Figure 1.11: New vs. classic models for the breakup of Rhodinia. More recent interpretations involve the Baltican continent rotated 180° from previous models and its current orientation. From Ramberg et al. (2008)

1.2.2 Break-Up of Rhodinia and the Iapetus Ocean

Rifting of the super-continent of Rhodinia took place over a long period of time at end of the Neoproterozoic era (1000-542 Ma). Rifting eventually led to the formation of the Iapetus Ocean around 650 Ma (Figure 1.11), reaching its widest towards the beginning of the Ordovician (ca. 510 Ma), at approximately 5000 km wide. The Iapetus was bordered by the palaeocontinents of Avalonia (Southern Britain), Baltica (Scandinavia and Russia), Gondwana (southern Britain, South America, Africa, Australia, Eastern Antarctica, Western Europe), and Laurentia (Northern Britain, Greenland and North America).

Evidence of the earliest rifting of Baltica is found in the form of mafic dyke swarms of Late Riphean to Vendian age (Solyom et al., 1979, 1992; Roberts, 1990; Andréasson, 1994; Stølen, 1994; Svenningsen, 1994, 2001). The Atlantic-type passive margin sequence which formed on the edge of Baltica in the earliest stages of the Iapetus is preserved today in the middle allochthon of the Scandinavian Caledonides.

The closure of the Iapetus (Figure 1.12) is marked by the appearance of subduction-related magmatism around the margins of the ocean from the early Cambrian (ca. 542 Ma) to late Ordovician (443 Ma), preserved as obducted slices of crust such as the late Cambrian to early Ordovician Ballantrae ophiolite complex in southern Scotland (Stone, 2012). Similar ophiolites are found all along the coast of western Norway (Figure 1.13), and are dated mostly to 495-485 Ma, but as young as 443 Ma (the Stavfjord ophiolite). These ophiolites have geochemical characteristics typical of immature islands arcs: otherwise MORB-like lavas inter-bedded with light rare earth element (LREE) and low field strength element (LFSE) enriched island arc tholeiites (IATs) and boninites (Pedersen and Heterogen, 1990).

1.2.3 The Caledonian Orogeny in Norway

Closure of the Iapetus culminated in the Caledonian Orogeny, a major event which contributed to the accretion of the last supercontinent, Pangaea. The orogeny itself is named after Scotland (*Caledonia*), where the first inferences of a so-called Caledonian Orogen in Scotland, Ireland and Wales were made (e.g. Haug (1900); Suess (1906); Stille (1924)). However, we now understand that the orogen affected a much greater area: North America (Appalachian Mountains), Scotland and Ireland, Greenland and Svalbard (Laurentian Caledonides), Norway (Scandinavian Caledonides), as well as parts of Germany and Poland (North German-Polish Caledonides).

At the apex of their existence, the Caledonian mountains would have rivalled the dimensions of the modern day Himalayan and Alpine mountains. Whereas the Himalayas stretch over a longitudinal distance of around 3000 km, the Caledonian Mountain chain was likely over 7500 km in length, and would have likely hosted some of the worlds tallest mountains of the time.

Norway is arguably the home of the best developed and preserved remnants of any of the Caledonides. Its geology is dominated by the effects of the Caledonian Orogen, and has been a fount of information for those researching the development of major orogens.

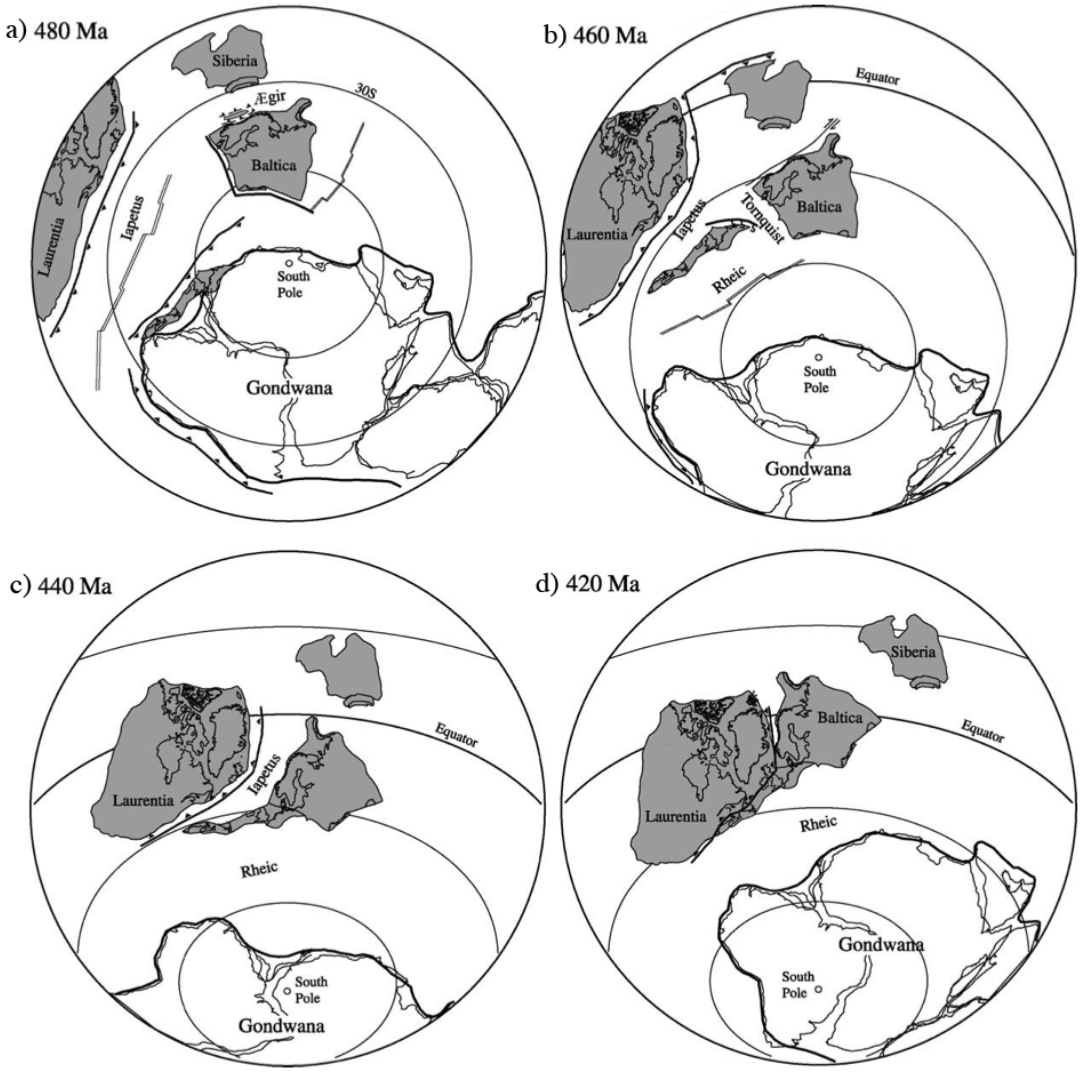

Figure 1.12: Simplified illustration showing the progressive closure of the Iapetus Ocean from the Early Ordovician to Late Silurian. A) Baltica is rotating anticlockwise, and the Baltoscandian margin is facing Siberia; B) Baltica is still rotating anticlockwise and has moved southward. Avalonia approaches Baltica from the north; C) Avalonia has docked with Baltica, as Baltica moves towards Laurentia across the narrowing Iapetus Ocean; D) Continental collision between Baltica and Laurentia during the Scandian event. The oblique collision results in development of major sinistral shear zones which are observed today across the entire orogen. Taken from Ramberg et al. (2008) based on reconstructions by Torsvik (2001), Torsvik et al. (1996), and Cocks and Torsvik (2002).

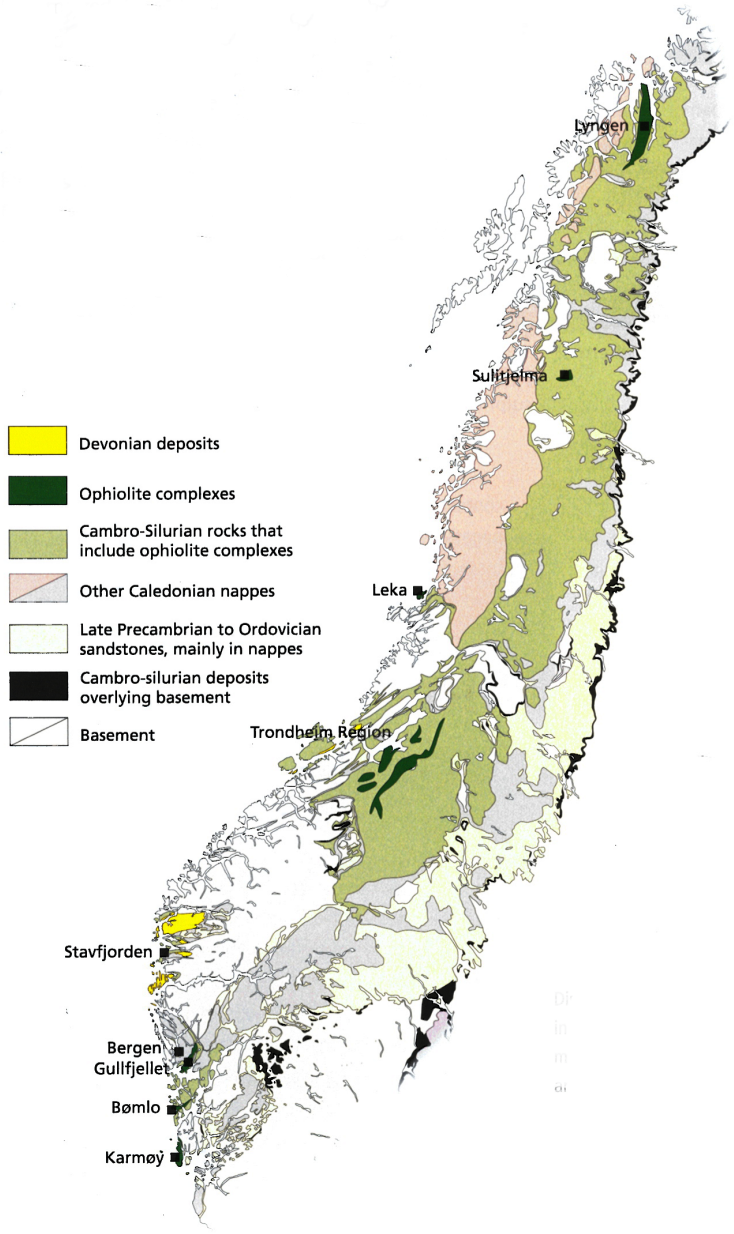

Figure 1.13: Distribution of ophiolite complexes (dark green) in the Norwegian Caledonides. The most significant ophiolite complexes are named. Taken from Ramberg et al. (2008)

The WGR or Norway is a window of Proterozoic autochthonous to parautochthonous basement gneisses belonging to the former continent of Baltica, to which the protoliths of the HP- to UHP eclogites in this study belong. These rocks, and others, preserve information related to the subduction of this part of the crust to HP-UHP conditions as a consequence of the Caledonian continent-continent collusion during the Silurian to Devonian. The origins and history of their protoliths are discussed in the section above on Precambrian Norway, which briefly describes the former Fennoscandian history of the basement in which the majority of the WGR basement was formed in the Southwest Scandinavian Orogen.

Closure of the Iapetus Ocean at around 435 Ma resulted in the emplacement of a stack of allochthonous units eastwards over and on top of the underlying basement rocks of the former Baltican margin (i.e. the WGR). These allochthons may be generally divided into four large structural domains with broad scale differences in structural paragenesis and lithological provenance; they are the Lower-, Middle-, Upper-, and Uppermost Allochthons. The Lower Allochthon represents Baltican platform and shelf successions on the edge of the Iapetus Ocean. The Middle and Basal-Upper Allochthons are composed of thick passive margin sequences which are heavily dissected by dyke swarms. The Upper Allochthon represents mostly Oceanic lithologies, and the Uppermost Allochthon is made of highly allochthonous thrust sheets of Laurentian origin. Samples in this study do not belong to these domains, and thus they are not considered further here.

Within the main Caledonian orogen, as many as five tectono-thermal events have been recognised: the Finnmarkian, Trondheim, Taconian, Scandian, and Late- to Post-Scandian events. A timeline for most of the the Caledonian is shown in Figure 1.14. Figure 1.15 shows that the first three events record discrete arc-continent accretion events over a period of 50 Ma from the Late Cambrian to the Mid-Late Ordovician (Roberts, 2003). Following this, the most significant event in the development of the Scandinavian Caledonides, the Scandian event, took place. The Scandian records the oblique collision of Baltica with Laurentia, the ensuing crustal thickening, and the extensional collapse and formation of major shears.

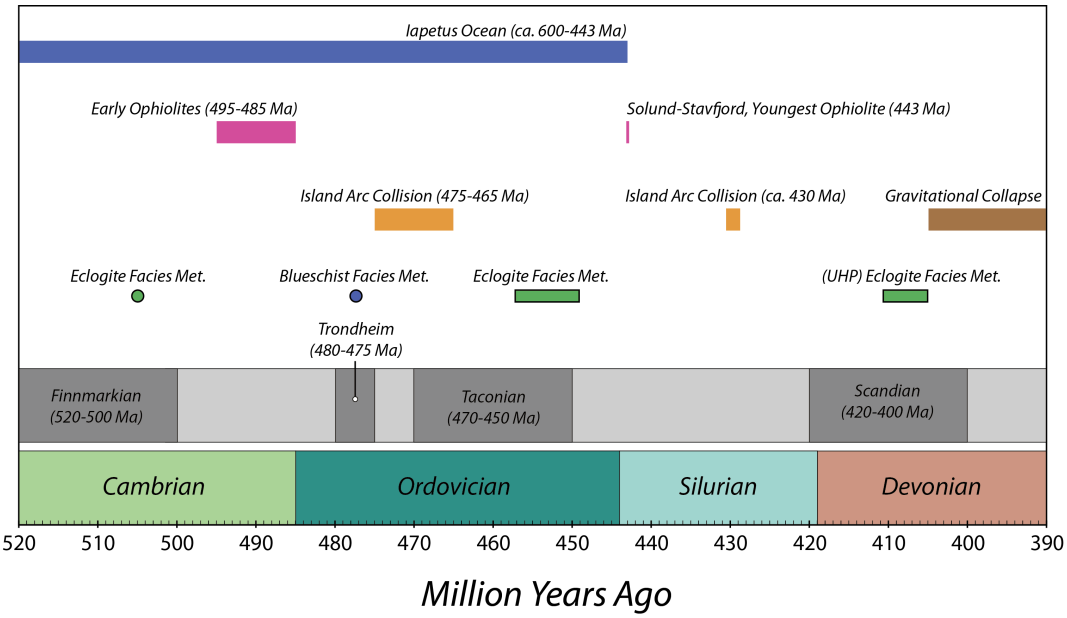

Figure 1.14: Timeline of the most tectonically significant events of the Caledonian Orogeny as seen in the Scandinavian Caledonides.

The Finnmarkian event

The Late Cambrian (ca. 520-500 Ma) Finnmarkian event is preserved within the Basal-Upper and (parts of the) Middle Allochthons. It records the first signs of Iapetus contraction, whereby the Baltoscandian margin collided with an oceanic island arc above a seaward facing subduction zone (Figure 1.15, Dallmeyer and Gee, 1986b; Sturt and Roberts, 1991; Torsvik and Rehnström, 2001b; Hartz and Torsvik, 2002). The associated subduction resulted in significant metamorphism, which peaked in the eclogite facies at ca. 505 Ma (Mørk et al., 1988; Dallmeyer et al., 1991; Essex et al., 1997).

Trondheim event

First noted by Holtedahl (1920), the Trondheim Event (493-482 Ma) was the first phase of significant high grade (blueschist) metamorphism and obduction of early ophiolites associated with a still oceanward-dipping subduction zone (e.g. Dunning, 1987; Eide and Lardeaux, 2002). Ophiolitic sediments are dominated by

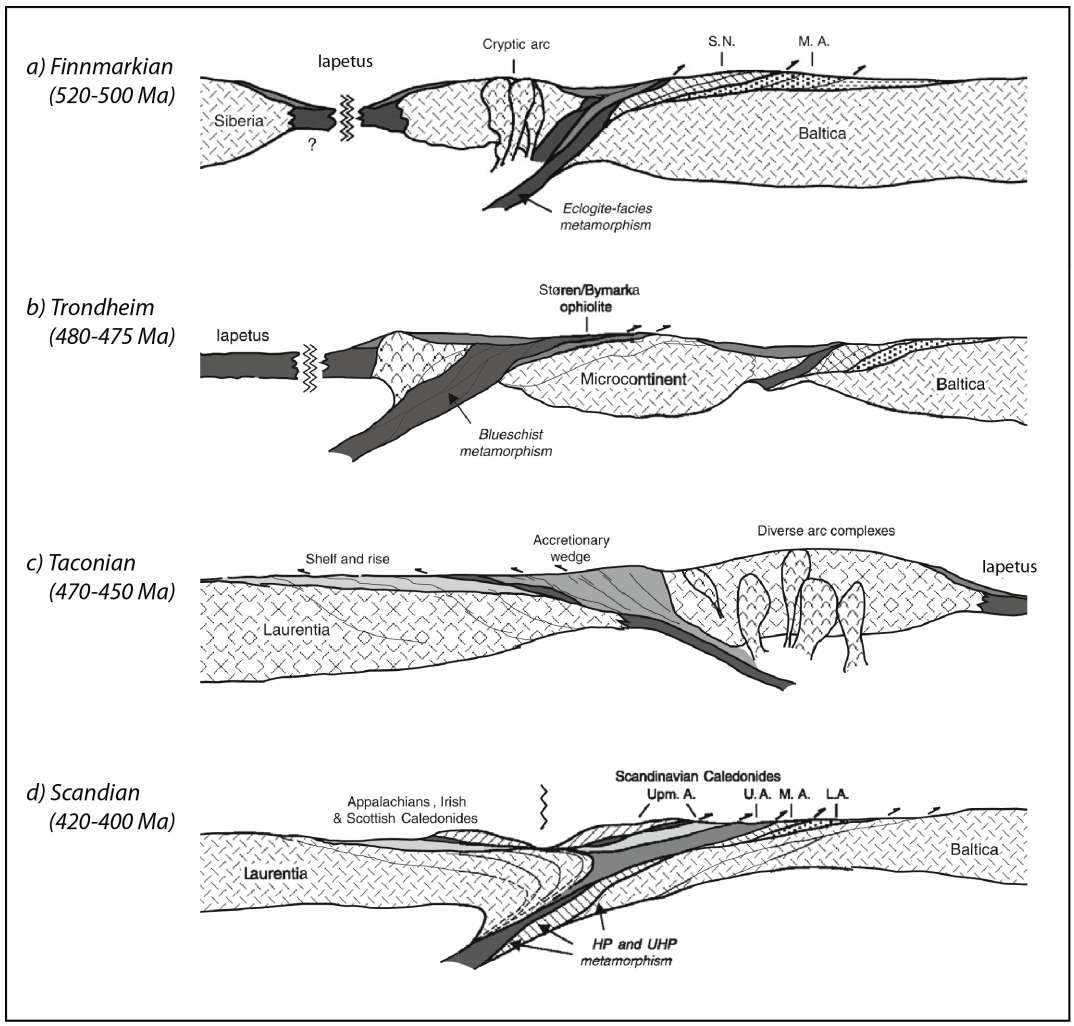

Figure 1.15: Model for the evolution of the Scandinavian Caledonides covering the the collisional Finnmarkian, Trondheim, Taconian, Scandian events. S.N. - Seve Nappes; L.A. Lower Allochthon; M.A. Middle Allochthon; U.A. Upper Allochthon. From (Roberts, 2003).

predominantly Laurentian fauna, suggesting genesis in a so-called 'peri-Laurentian' setting. At this time, Baltica had started to rotate anticlockwise away from Siberia (Torsvik et al., 1996; Torsvik and Rehnström, 2001a) and was approaching Laurentia in a narrowing seaway (Roberts, 2003) which could explain the ever dominating input of Laurentian fauna.

Taconian event

The Taconian is thought to be largely coeval with the *Grampian* orogenic event of Britain and Ireland (Soper et al., 1999). In parts of the Uppermost Allochthon in the Scandinavian Caledonides, the event records the Mid- to Late Ordovician accretion of microcontinents onto the Laurentian margin at 470-465 Ma (Roberts, 2003), following oceanward subduction. This included the accretion of the ophiolite at Karmøy and the Bergen Arcs complex. At this time, a sedimentary sequence which includes shelf limestones analogous to the Durness Limestone of Scotland (Bruton and Brockelie, 1979), were metamorphosed and deformed under low grade conditions. In the Mid- to early Late Ordovician time, locally high-grade eclogite facies metamorphism and ophiolite obduction occurred followed by a stage of rapid exhumation (Roberts, 2003). Finally, in the Late Ordovician to Early Silurian the Upper Allochthon records intrusion of evolved plutons of arc affinity (Gautneb and Roberts, 1989; Nordgulen et al., 1995).

Scandian event

The Scandian Event was very important in defining the large scale structure we observe in the Scandinavian Caledonides today, affecting all the allochthonous units to some extent. From the Late Silurian to Early Devonian, it records the oblique north-westward collision of Baltica and Laurentia, culminating with the transient subduction of the continental margin of Baltica to conditions of at least 3.6 GPa and 800^{o}C (Cuthbert et al., 2000; Dobrzhinetskaya et al., 1995; Krogh-Ravna and Terry, 2004; Terry et al., 2000; Wain, 1997) between $\sim$420 Ma and $\sim$400 Ma (Kylander-Clark et al., 2009). Timing of the event varies significantly at different parts of the orogen (Roberts, 2003), but it is estimated that the event itself (including

subduction and exhumation) may have lasted as little as 10 Ma (Terry et al., 2000; Roberts, 2003).

The Scandian is responsible for the formation of the majority of HP to UHP metamorphic assemblages, most notably so in the WGR where UHP rocks are exposed in three main domains from Nordfjord to Nordøyene (Figure 1.16, Walsh et al., 2013). Timing of HP-UHP metamorphism during the Scandian is constrained by several isotopic systems: two separate three-point Sm-Nd isochrons with ages of 408 $\pm$ 8 Ma (Mearns, 1986) and 400 $\pm$ 16 Ma (Mørk and Mearns, 1986); U-Pb zircon ages of 401.6 $\pm$ 1.6 Ma (Carswell et al., 2003) and 405-400 Ma (Root et al., 2004); and finally a Th-Pb monozite age of 415 $\pm$ 6.8 Ma (Terry et al., 2000).

Late- to post Scandian events

Numerous models have attempted to explain the Late- to post-Scandian cessation of subduction and subsequent exhumation of the roots of the Caledonian orogen, with particular reference to the HP/UHP domains within the WGR. The true mechanisms remain largely unsettled, but the strongest candidates have the same overall theme: initial rapid uplift from the mantle to the base of the continental crust, followed by relatively slower exhumation through the crust itself.

It is perhaps this initial, relatively rapid stage in uplift that has divided opinion most, and there exist some very interesting and diverse models that attempt to explain it. A relatively long-standing model involves the drop-opp of a dense lithospheric root from the terminus of the down-going Baltican slab (Andersen and Jamtveit, 1990; Austrheim, 1991, e.g.). Around a decade later, Fossen (2000) and Dewey and Strachan (2003) suggested an alternative model involving a change in plate motion, whilst Terry and Robinson (2004) proposed a model involving forced return flow. All the while, and continuing until recently, convincing models invoking slab break-off and eduction (Andersen et al., 1991; Brueckner and van Roermund, 2004; Duretz et al., 2012, e.g.) or delamination due to as-yet unidentified gravitational instabilities (Hacker, 2007; Labrousse, 2004; Peterman et al., 2009; Walsh and Hacker, 2004, e.g.) have provided yet more plausible explanations as to initial rapid exhumation during the final stages of the Caledonian.

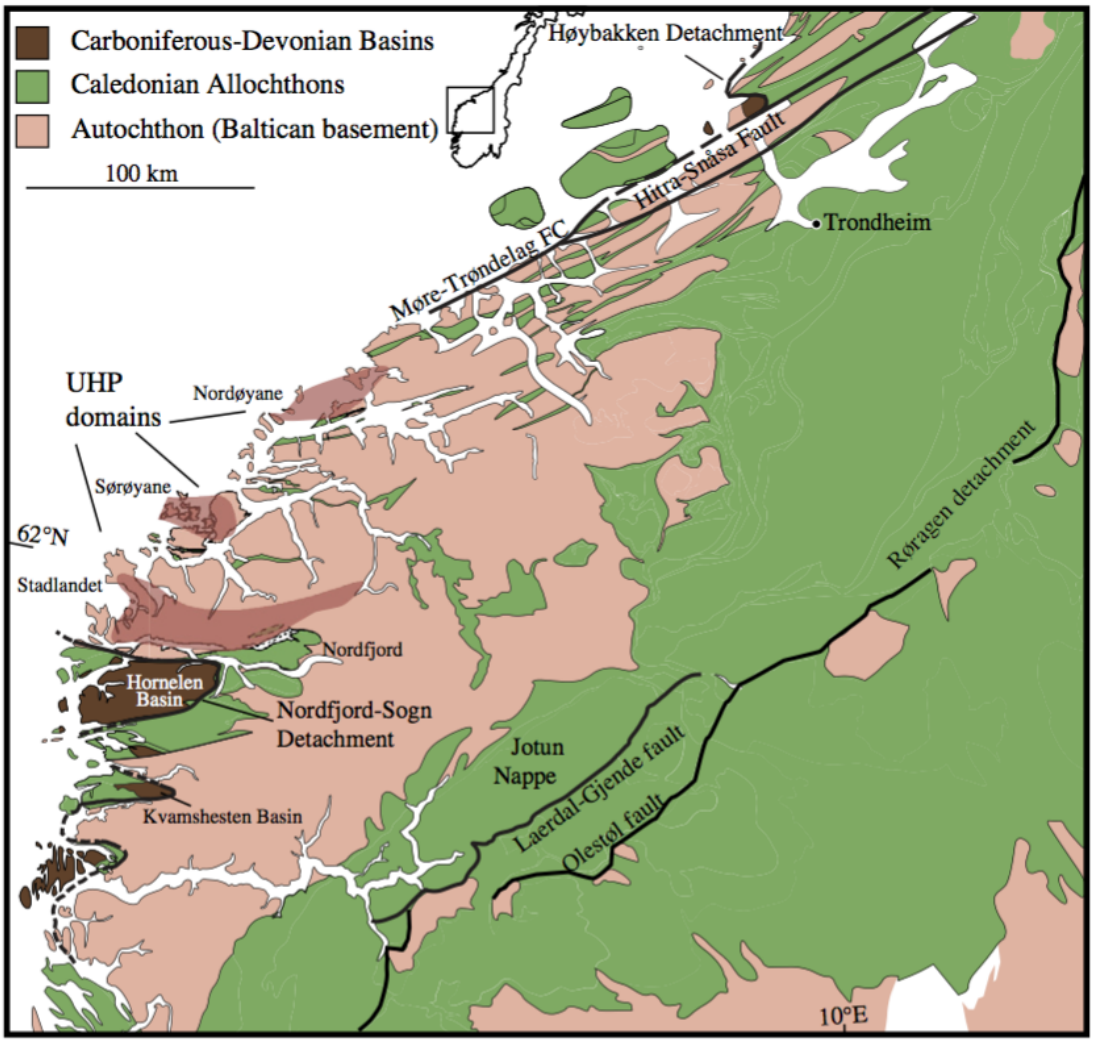

Figure 1.16: Simplified geological map of the WGR highlighting the three Caledonian UHP domains known to exist (from Walsh et al., 2013). Eclogites collected in relation to this thesis mainly belong to the Nordfjord-Statlandet HP and UHP regions, the latter being the largest and most southerly of the WGR UHP domains.

Exhumation from the amphibolite faces at the base of the continental crust is still relatively poorly understood, but most agree that extensional tectonism is the most likely mechanism. At around 400 Ma collisional orogenisis had largely ceased and gravitational collapse of the orogen and exhumation of HP-UHP lithologies began (Andersen, 1998; Roberts, 1983). At this time, the lateral support for the great thickness of amassed Caledonian Nappes had been drastically diminished. As a consequence, large parts of the Caledonian nappe pile began to slide back to the west and north west (Figure 1.17), driven by their great unsupported mass, and lubricated by the swathes of phyllitic lithologies on which they lay (Ramberg et al., 2008).

Soon enough, extension was concentrated into major shear zones. The first to form was the Nordfjord-Sogn detachment zone (NSDZ) (Figure 1.17): one of the largest detachments in the world. It has a mylonite zone several kilometres thick that can be traced from Nordfjord all the way to the Bergen Arcs in the southern WGR, and an inferred displacement of 50-100 km.

Brittle extension within backsliding nappes occurred as early as 415-422 Ma, whereas major shear zones became brittle at from around 395 Ma in the Nordland and Bergen areas (Ramberg et al., 2008). This alone shows that exhumation was fast paced, and that several extensional regimes were likely operating concurrently along the rapidly collapsing orogen.

The most convincing models that explain the uplift of HP-UHP rocks specifically, invoke two main stages: the first involves rapid buoyancy-driven uplift from mantle depths to the base of the continental crust; secondly, relatively slow exhumation through the continental crust itself.

Possible triggers for the initial rapid buoyancy-driven uplift ($\sim$10 mm a^{-1} or more: e.g. Carswell et al., 2003; Krabbendam and Dewey, 1998; Kylander-Clark et al., 2008; Terry et al., 2000; Walsh et al., 2013) include slab-break-off (Andersen et al., 1991; Brueckner and van Roermund, 2004; Duretz et al., 2012), lithospheric root drop-off (Andersen and Jamtveit, 1990; Austrheim, 1991) and slab delamination (Hacker, 2007; Hurich, 1996; Johnston et al., 2007; Peterman et al., 2009; Walsh and Hacker, 2004). Whatever the trigger, it is clear that wide-scale amphibolite- to granulite-facies

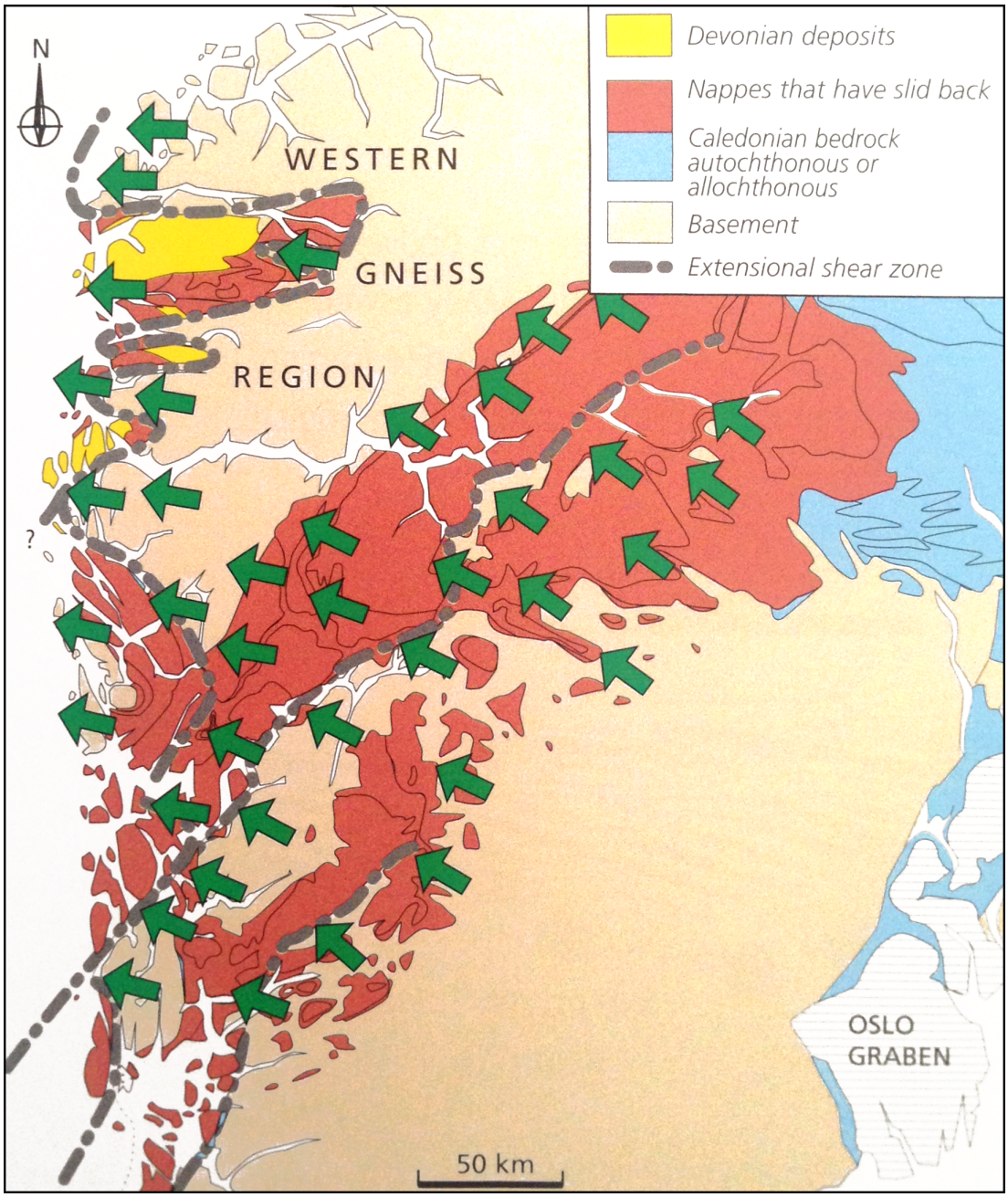

Figure 1.17: Simplified geological map showing the inferred direction of collapse (green arrows) of the Caledonian Nappes during the Early Devonian. Broken lines are extensional shear zones that developed *after* back-sliding of the nappes occurred. From Ramberg et al. (2008)

overprinting of HP-UHP rocks occurred as the slab reached the base of the continental crust as the initial rapid exhumation was heavily retarded (e.g. Labrousse, 2004; Root, 2005; Spencer, 2013; Terry and Robinson, 2003; Walsh and Hacker, 2004).

Models for slower, shallower exhumation of rocks in the Western Gneiss Region are to-date less uncertain. Extensional tectonics is the favoured explanation given obvious westward extension along the NSDZ (Johnston et al., 2007; Marques et al., 2007; Norton, 1986) and normal shear in the Møre-Trøndelag Fault Complex (Braathen, 2000; Krabbendam and Dewey, 1998). The most recent thermo-chronology study by Walsh et al. (2013) suggests that basal- to mid-crustal exhumation occurred mostly between around 400 and 380 Ma, whilst UHP domains were still experiencing crustal uplift until around 374 Ma.

1.2.4 The Nature of Eclogite in the WGR

Eclogite is widespread in across the whole of the Scandinavian Caledonides at various tectonostratigraphic levels. It has been discovered in all of-, and only in the continental tectonostratigraphic units of the orogen, most famously so in the para-autochthonous Baltic basement in the WGR (Cuthbert & Carswell, 1990). Within the WGR, eclogite occurs all the way from the Sognefjord area in the south up to the Trondheimsfjord area in the north (Krogh and Carswell, 1995).

Eclogites across the whole Scandinavian Caledonides typically occur as lenses or bands within felsic host gneisses, but also migmatites, supracrustal rocks (e.g. marbles), anorthosites in layered igneous complexes, and in garnet peridotites. Host rocks are typically of amphibolite-, granulite-, or even eclogite facies (Bryhni, 1966; Mysen and Heier, 1972; Griffin and Mørk, 1981; Krogh, 1980; Harvey, 1983; Griffin et al., 1985; Cuthbert, 1985). In addition, eclogites are locally developed in doleritic sills and dykes which cross-cut the surrounding country rocks. Most eclogites in the Caledonides have tectonic contact relationships with these country rocks, with the margins of eclogites being strongly sheared and often heavily retrogressed (Krogh and Carswell, 1995). More specifically, in the WGR eclogite mostly occurs as pods or

lenses, apparently representing boudinaged layers (Lappin, 1966) within amphibolite to granulite facies gneisses (Krogh and Carswell, 1995).

1.2.5 The Norwegian Eclogite Controversy

The controversy as to the origins of Norwegian eclogites began in 1966 with the publications of Bryhni (1966) and Lappin (1966): both publications provided contrasting interpretations of equally lengthy petrological and structural research conducted on a wide range of lithologies from closely associated regions within the WGR. Bryhni (1966) argued that eclogites were formed *in-situ* in their host gneisses, and thus both gneiss and eclogite endured the same pressure-temperature-time (PTt) paths. Lappin (1966) argued that eclogites in the region had been introduced tectonically into the host gneisses during exhumation. Indeed, one of the main problems was that eclogites often occur in host rocks of apparently significantly lower metamorphic grade. The 'foreign' versus 'in-situ' debate was to ensue for nearly two decades after the initial publications of Bryhni (1966) and Lappin (1966).

The presence of relict eclogite-facies assemblages in host rocks provides good evidence that at least some eclogites in the Caledonides formed by metamorphism of in-situ protoliths (Cuthbert and Carswell, 1990). In addition, omphacite relicts do occur in quartzofeldspathic gneisses at several localities in the WGR, typically as CPX + Pl or Amp + Pl symplectites, or as inclusions in garnets (Mysen and Heier, 1972; Green and Mysen, 1972; Brueckner, 1977; Krogh, 1980; Carswell and Harvey, 1985; Cuthbert, 1985).

There are many models that have attempted to explain the tectonic evolution of the Caledonides over the past 45 years (Krogh, 1977; Lappin and Smith, 1978; Smith, 1980; Cuthbert et al., 1983; Jamtveit, 1987; Cuthbert and Carswell, 1990; Hacker, 2010; Walsh et al., 2013). Although the matter remains far from resolved, it is clear to the author that Norwegian eclogites can be considered *in-situ* in their host gneisses.

1.3 Thesis Motivation, Objectives and Layout

Eclogite is probably a common lithology in the mantle, yet its exposure at the surface is rare since rapid exhumation from HP and UHP conditions must occur. Such exhumation appears to be a relatively common feature in major collisional orogens, of which the Caledonian Western Gneiss Region is a world-class example. These eclogites therefore have the potential to record and preserve valuable information about the most extreme and inaccessible parts of collisional tectonic settings such as subduction zones and continental orogens.

The geological value of eclogite has historically driven investigations into unravelling their metamorphic histories In Western Norway, studies have concentrated on eclogite PTt trajectories, metamorphic mineral transformations, and the occurrence of UHP mineral discoveries (i.e. coesite). However, recent advances in trace element geochemistry mean that eclogites can be further exploited to better our understanding of the geochemical evolution of the crust-mantle system. This is because they may be used as natural analogues for studying the processes and changes affecting basaltic crust that experiences subduction into the mantle, most of which is not exhumed as preserved eclogites. Furthermore, micro-analytical techniques are now able to accurately sample very small volumes of material, and thus many recent geochemical studies have targeted important trace element hosts and fluid inclusions to better understand geochemical fluxes the subduction zone (Becker et al., 2000; Nadeau et al., 1993; Marschall et al., 2013; Brenan et al., 1994; Gao and Klemd, 2001; Gao et al., 2010; Manning, 1998; Svensen et al., 2001; Zack et al., 2002a, e.g.). Rutile, a common accessory mineral in eclogite, has only recently shown that it is an important and robust host for many trace elements in eclogites, and may play an important role in controlling the flux of these elements during subduction or subduction-like burial in collisional settings.

Despite the fact that Norwegian eclogites are amongst the best exposed, most diverse and best studied eclogites in the world, there exist very little modern and comprehensive trace-element data sets for whole-rock eclogites and associated accessory minerals. Eclogites and eclogite-hosted rutile therefore represent a potentially significant untapped resource to the geologist studying geochemical

processes collisional parts of the crust-mantle system.

As a consequence of these motivations, the objectives of this project were to:

- Sample a representative suite of eclogites from the Western Gneiss Region, Norway
- Develop a rigorous and proven technique for gathering high-precision trace-element data for each of the those samples.
- Use the whole-rock geochemical data to determine the likely tectonic setting of emplacement of the eclogite protoliths.
- Assess the apparent mobilities of so-called mobile and immobile elements by comparing the compositions of eclogites and their anticipated protoliths.
- Gather comprehensive and reliable trace element data on eclogite-hosted rutiles such that the following questions can be addressed:
  - How does rutile control the trace element inventories of its host eclogites?
  - What can the eclogite-hosted rutiles tell us about the thermal histories of the whole-rocks?
  - To what extent may out-of-context rutiles be used to characterise their former host rocks?

Since the scope of this study relied on gathering high-precision trace element compositional data, size of the sample set was duly limited to ensure both time and cost budgets could be conserved. Gathering additional data on other rocks such as the enclosing gneisses, veins, and less highly metamorphosed analogous mafic rocks in other parts of the Baltic basement was not considered viable, despite the assumption such data would be useful. In the case of comparing with other analogous mafic lithologies elsewhere in the Baltican basement, it will be illustrated in order for such data to be compared with our sampled eclogites in a rigorous manner, we would need to ensure the data was obtained by the high-pressure dissolution techniques used on our own samples. Data from the literature is not called upon for comparison because of this reason.

The objectives will be addressed in the following 4 chapters, which take the form of reports that are currently being redrafted into papers pending submission for publication. Chapters in this thesis mostly follow the chronological order in which investigations were undertaken and the data processed.

- **Chapter 2** deals with the preparation of rutile-bearing lithologies for ICP-MS analysis. In this chapter we show that 'normal' acid digestion techniques are clearly incapable of dissolving refractory minerals that can contribute significantly to the whole rock abundance of trace elements such as Nb and Ta. To achieve total sample dissolution one must combine standard dissolution procedures with one in which the sample is placed in a sealed acid digestion vessels and exposed to a mix of strong acids at 220 ^{o}C for several hours. We show that whilst this method increases the reliability of whole rock concentrations of elements such as Nb, Ta, Zr and Hf, volatile elements such as Pb and Sn are often lost even when vessels apparently maintain good seals.

- **Chapter 3** uses the highly accurate and comprehensive suite of trace-element measurements obtained in chapter 2 to: 1) identify the geochemical characteristics of the protoliths to Norwegian eclogites and thereby comment on their potential origins; and 2) assess the mobility of both so-called mobile and immobile elements with specific reference to subduction zone fluids, metasomatism and retrogression. We show that a significant number of eclogites have apparently maintained protolith geochemical signatures that indicate protoliths derived from both MORB-like and enriched mantle sources. We show that both rare earth elements (REEs) and high field strength elements (HFSEs) have the capacity to remain largely immobile during subduction to UHP conditions and exhumation during orogenic collapse.

- **Chapter 4** delves into one of the most detailed and comprehensive studies on eclogitic rutiles published to date. We show that rutile can control significant amounts of the whole-rock HFSE budget, illustrating the important role rutile can play in controlling HFSE mobility whenever it is present. We provide the first evidence from natural samples that corroborate experimental findings that Ta is more compatible in rutile than Nb. Finally, we show that rutile geochemistry in any one sample can be highly heterogeneous, something of

which those using detrital rutiles in sediment provenance studies should be acutely aware.

- **Chapter 5** expands on rutile trace element data by presenting the results of Zr-in-rutile thermometer (ZRT) for over 400 analyses. The temperature data allows us to present a thermal map of perhaps the most important part of the WGR with reference to eclogites: the Nordfjord-Statlandet region. Our thermal map suggests isotherms for the region that reflect not only the thermal profile of Caledonian-aged transient subduction of the leading edge of the Baltican continent, but also the subsequent deformation the basement experienced during orogenic collapse.

Chapter 2

Dissolution of Rutile-Bearing Eclogites for Chemical Analysis*

Abstract

Rutile (TiO_2) is a common accessory mineral in amphibolite- to eclogite-facies metabasites, in which as little as 0.5-2.0 wt.% rutile may contain 20 to 100 % of the whole-rock Nb and Ta; up to 40 % Sn and Mo; and up to 5% V, Cr, Hf and Zr. Furthermore, rutile commonly contains inclusions of zircon which is an important host for Zr and Hf. These elements are key in protolith determination and fractionation studies, and it is thus imperative that total dissolution of rutile occurs when preparing samples for solution inductively coupled plasma mass spectrometry (ICP-MS) analysis. In a preliminary investigation, we found that the majority of rutile and a small amount of zircon often remain undissolved during typical acid digestion procedures conducted at 1 atmosphere and 100^{o}C (i.e. Low Pressure-Temperature Solution, LPTS). Although acid digestion vessels are known to greatly increase the extent of analyte dissolution, few authors report their use in the preparation of rutile-bearing lithologies. We investigated the efficacy of using pressure digestion vessels on rutile-bearing eclogite samples at around 70 atmospheres (7×10^6)Pa) and 220^{o}C (i.e. High Pressure-Temperature Solution, HPTS) using a variety of solvents. High pressures ensured solvents remained liquid, whilst high temperatures greatly increased ion mobility, lowered viscosity and as a consequence rutile dissolution was effectively increased to 100 %. Our results showed marked increases in measured concentrations from LPTS to HPTS techniques for elements with high partition coefficients for rutile (e.g. Nb, Ta, and Mo). We show that HPTS achieves total rutile dissolution by comparing both LPTS- and HPTS-ICP-MS data with high-precision X-Ray Fluorescence data and modelled whole-rock compositions

*Contributors: Godfrey Fitton - *the University of Edinburgh*; Simon Harley *the University of Edinburgh*; Valerie Olive - *Scottish Universities Environmental Research Center*

calculated using independently determined rutile compositions. Despite increases in nearly all rutile-hosted elements, significant volatilisation of Pb and Sn occurred during HPTS, and therefore their concentrations cannot be considered reliable. We conclude that the dissolution of rutile-bearing lithologies via HPTS acid digestion is essential for those wishing to gain accurate concentrations of many important trace elements in rutile-bearing rocks of metamorphic, igneous and sedimentary origin.

2.1 Introduction

Many mass spectrometry and other instrumental techniques require analytes to be dissolved into solution before analysis. In a procedure we call LPTS, most Earth materials (e.g. soils and rocks) may be dissolved with relative ease in a mixture of acids (typically HNO_3, HCl, and HF) at room pressure and maximum temperatures of around 100 to 120^oC. Rutile (TiO_2) is an accessory mineral common in a wide range of igneous, metamorphic and sedimentary rocks, and although often a volumetrically minor phase, this study and others (e.g. Zack et al., 2002b; Aulbach et al., 2008; Marschall et al., 2013) show that rutile can contain significant amounts of the whole-rock Nb, Ta, Sn, Mo, V, Cr, Hf and Zr. As such, it is important to ensure rutile is completely dissolved along with the rest of the analyte.

Several authors have provided good evidence that rutile resists dissolution under common geological conditions (Schuiling and Vink, 1967; Barsukova et al., 1979; Agapova et al., 1989; Audetat and Keppler, 2005; Tropper and Manning, 2005; Manning et al., 2008; Marsh, 1979; Czemanske et al., 1981). However, it has also been known for some time that acids rich in Cl and F ions are very effective at breaking down the rutile lattice (Weyer et al., 2002; Yu et al., 2000). Indeed, the notion that rutile may be highly soluble under certain geochemical conditions has been supported most recently by the experimental work of Rapp et al. (2010).

Rapp et al. (2010) found that, compared with H_2O solutions under the same conditions, rutile solubility was 2-4 and 20-100 times greater in Cl-rich and F-rich brines respectively. Fluoride (F^-) and chloride (Cl^-) ions are thought to form particularly strong electrostatic bonds with Ti^{4+} ions in rutile, thereby increasing

the efficacy of rutile dissolution. It is therefore of no surprise that hydrochloric and hydrofluoric acids are commonly used to dissolve earth materials containing acid resistant minerals. However, even when HF and HCl are used in LPTS techniques, complete digestion is often not attained (as we show below). Reaction kinetics in the LPTS technique are limited by the boiling and melting temperatures of acids and containers respectively. Sealed vessles (so-called Tölg bombs) allow for a higher temperatures (200-260^oC) and pressures (up to 200 bar) to be used, thereby dramatically increasing reaction kinetics.

Despite the not uncommon use of this high pressure and temperature solution (HPTS) technique in some geochemical investigations, there appear to be no publications that explicitly investigate its efficacy. We therefore set out to compare ICP-MS digestion procedures for rutile-bearing eclogites using a large number of trace elements. We qualify our observations by comparing collected data with complementary XRF and separated rutile LA-ICP-MS analyses.

2.2 Samples

A total of 37 samples of eclogite were used in this study. Petrographic descriptions for each sample can be found in Appendix B (pg. 285) and availability of geochemical data for each sample is shown in Table 2.1. The sample set is composed of 36 eclogites from the Western Gneiss Region (WGR) of Norway, and one eclogite from the Scottish Highlands (GEg, Glen Elg).

2.3 Sample Preparation

2.3.1 Rock Powders

Over 3000 cm^3 of unweathered eclogite for each sample was crushed and milled into a fine powder using agate barrel components in order to avoid contamination with Ta from the standard tungsten carbide crushing units. Barrel components were blasted with a high pressure air hose followed by a thorough wipe-down using acetone in between samples.

Table 2.1: Chart showing data availability for each sample of eclogite in this study

	ICP-MS			
Sample	**LPTS**	**HPTS**	**LA**	**XRF**
1	●	●	○	●
8	●	●	●	●
14	●	●	●	●
22	●	●	○	●
30	●	●	●	●
32	●	●	●	●
37	●	●	●	●
41	●	●	○	●
46	●	●	●	●
47	●	●	○	●
51	●	●	●	●
53	○	●	●	●
60	○	●	○	●
64	○	●	●	●
65	○	●	●	●
67	○	●	●	●
69	○	●	●	●
70	○	●	●	●
71	○	●	●	●
72	○	●	●	●
73	○	●	●	●
74	○	●	●	●
75	○	●	●	●
76	○	●	●	●
77	○	●	●	●
78	○	●	●	●
79	○	●	●	●
80	○	●	●	●
81	○	●	●	●
82	○	●	●	●
83	○	●	●	●
84	○	●	○	●
85	○	●	●	●
Geg	●	●	○	●
kval	●	●	○	●
Lef1	●	●	●	●
Lef2	●	●	●	●

● - Analysed, ○ - Not analysed

2.3.2 Low Pressure and Temperature Solution (LPTS) ICP-MS

1. 0.095 - 0.125 g of sample was weighed into a sealable PTFE (Teflon^{TM}) beaker.
2. Approximately 10 ml of 50 % hydrofluoric acid (HF) was added. The beaker was sealed and left on a hotplate at 100^{o}C for a period of 24 hours.
3. The beaker cap was removed and the HF acid allowed to completely evaporate, leaving behind a residue.
4. Steps 2 and 3 were repeated using 50 % nitric acid (HNO_3) instead of HF.
5. The dissolved sample was then placed into 100 ml of 5 % HNO_3.
6. A standard sequential dilution procedure was followed to achieve a target dissolution of 1/10^3.

2.3.3 High-Pressure and Temperature Solution (HPTS) ICP-MS

For this procedure, we purchased four general purpose acid digestion vessels (Parr Instrument Company, Vessel 4749) along with complementary PTFE beakers (Figure 2.1). The acid digestion vessels consist of a stainless steel outer casing with a removable lid and base. Inside the top of the housing is a spring-piston system which ensures a tight seal of the beaker, but also allows degassing should the beaker pressure exceed the maximum threshold of about 120 atmospheres (1.2×10^7 Pa). The beaker fits snugly in the metal housing, protected on its top and bottom by a replaceable foil made of stainless steel. The beakers were completely new, and used only for this study.

1. Approximately 0.095-0.0125 g of powdered sample was placed into the bomb's PTFE beaker along with approximately 5 ml of 50 % hydrofluoric acid and 5 ml of 50 % nitric acid.
2. The beakers were then placed inside the digestion capsule casing and placed in an oven at 230^{o}C for approximately 12 hours, and allowed to cool to room temperature for a further 4 - 5 hours.
3. The sample was recovered from the bomb and then subjected to the standard LPTS dissolution procedure detailed above.

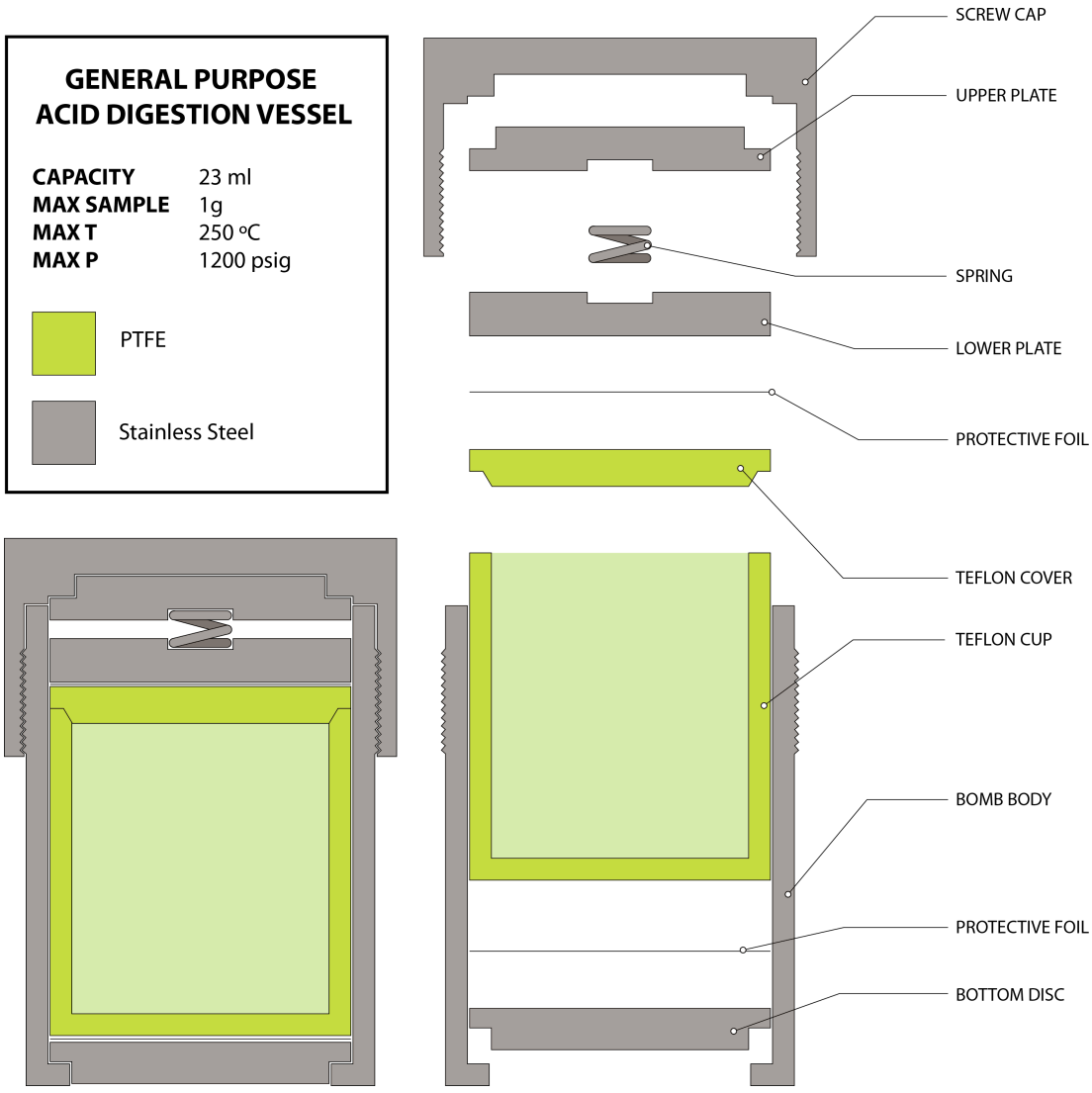

Figure 2.1: Schematic diagram of the general purpose acid digestion vessel used in the HPTS method. The exploded view shows the separate components in the assembly. Image adapted from Parr Instruments user documentation.

2.4 Analytical Techniques

At total of 36 trace elements were measured (Table 2.2) for each eclogite. Dissolved samples were analysed using an Agilent 7500ce series ICP-MS system at the NERC and SUERC East Kilbride, Scotland. BCR-2 was prepared as a calibration standard using the LPTS method, and measured after every 5 samples, whereas an internal standard of In was introduced into each sample solution. More information can be found in Appendix A.2 (pg. 282).

Separated rutile grains for some eclogite samples were analysed by Laser Ablation ICP-MS at the School of Earth and Environmental Sciences (SEES), University of Portsmouth. Details of the acquisition of those data can be found in Chapter 4 (pg. 147).

Whole-rock XRF analyses were conducted at the School of GeoSciences, University of Edinburgh, using a Panalytical Pw2404 X-ray spectrometer. Details of the analytical procedure can be found in Appendix A.1 (pg. 281).

2.5 Comments on Laboratory Procedures

2.5.1 Obvious Digestion Failures using LPTS

Incomplete rutile dissolution in many LPTS samples was clearly indicated by dark red and black sediment in the bottom of beakers at the end of the dissolution procedure. We recovered and photographed some of this material from one sample, in order to assess the mineralogy and level of corrosion. Figure 2.2 shows that all major minerals were completely dissolved, except for rutile. The grains lack the rounded or convoluted outlines one might expect of crystals being attacked by acids, especially on smaller grains which have a higher surface to volume ratio. Given the small mass of sample used in the experiment, and seemingly large amount of residual material, we infer that a negligible volume of rutile was dissolved.

Table 2.2: List of elements analysed in each analytical technique, ordered by atomic number

		ICP-MS			
At. No.	**Element**	**LPTS**	**HPTS**	**LA**	**XRF**
21	Sc	○	○	○	●
23	V	●	●	●	●
24	Cr	●	●	●	●
28	Ni	○	○	○	●
29	Cu	○	○	○	●
30	Zn	○	○	●	●
31	Ga	○	○	●	○
37	Rb	○	○	○	●
38	Sr	○	○	●	●
39	Y	○	○	○	●
40	Zr	○	○	●	●
41	Nb	●	●	●	●
42	Mo	●	●	●	○
50	Sn	●	●	●	○
50	Sn	○	○	●	○
56	Ba	○	○	○	●
57	La	●	●	○	●
58	Ce	●	●	○	●
59	Pr	●	●	○	○
60	Nd	●	●	○	●
62	Sm	●	●	○	○
63	Eu	●	●	○	○
64	Gd	●	●	○	○
65	Tb	●	●	○	○
66	Dy	●	●	○	○
67	Ho	●	●	○	○
68	Er	●	●	○	○
69	Tm	●	●	○	○
70	Yb	●	●	○	○
71	Lu	●	●	○	○
72	Hf	●	●	●	○
73	Ta	●	●	●	○
74	W	○	○	●	○
82	Pb	●	●	●	●
90	Th	●	●	○	○
92	U	●	●	●	●

● - Analysed, ○ - Not analysed

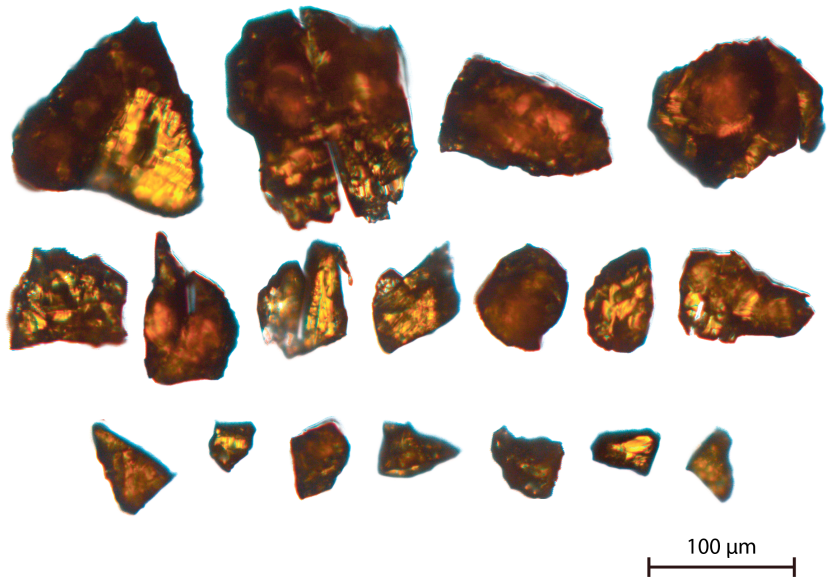

Figure 2.2: Photomicrograph of rutile grains left after subjecting an eclogite sample to the standard dissolution procedure for rock powders. Crystals of all sizes have similar angularities suggesting that very little or no digestion took place.

2.5.2 HPTS Pressure Vessel Failures

We observed wetness on the outside of the beaker and corrosion products on the pressure vessels in a small number experiments. Such failures of the seal were accompanied by a lack of a negative pressure in the PTFE beaker. In these instances, much of the solution was lost, and the experiment had to be repeated. Three samples (41, Geg, Lef2) failed on their first run, yet the contents of the beaker were largely recoverable. We analysed the solutions from these three failed runs along with successful duplicates in order to assess the effect of loss of a good seal on the data. Data from the original and duplicate samples are highlighted in table 2.3.

Table 2.3 shows some elements (i.e. Nb, Ta, Mo, Pb, Cr) can exhibit significant variation between HPTS duplicates (lowest value up to 60% lower than highest), while V and Hf do not. Where significant variations in concentration are found between duplicates, the lowest measured concentration of Nb, Ta, and Mo is generally equal to or greater than the corresponding element concentration for the LPTS data. Where $X_{HPTS} < X_{LTPS}$ (Ta, Cr, Pb and U only), capsules in each case lacked a good seal prior

to opening.

2.5.3 HPTS BCR-2 Standard

Due to very long preparation times (approximately 4 days, in batches of 4), it was not practical to prepare many BCR-2 powders in the pressure vessels. However, one BCR-2 standard was prepared using the HPTS method in order to investigate any element loss. Table 2.4 shows that HPTS concentrations of Sn and Pb are significantly lower than accepted standard values. Sn in particular clearly indicates losses on the order of 35% when prepared using HPTS.

2.5.4 Blank HPTS Control

Since the HPTS method employs highly corrosive acid mixes at a temperature very close to the melting temperature of the PTFE capsule (ca. 250^oC), it was thought that some volatile elements could escape into the PTFE capsule. If this occurred, these volatiles may accumulate and contaminate subsequent samples. Although no data collected prior to the running of a blank directly suggested contamination, it was nonetheless prudent to run a blank bomb sample to check. Analysis of the blank sample yielded no measurable concentrations of any of the selected elements.

Table 2.3: Measured concentrations (in ppm) of selected trace elements for samples prepared using LPTS (L) and HPTS (H) techniques.

	Nb		Ta		Mo		Hf		Sn		U		V		Cr		Pb	
Sample	L	H	L	H	L	H	L	H	L	H	L	H	L	H	L	H	L	H
1	1.37	2.35	0.105	0.12	0.262	0.82	0.787	0.988	2.088	1.562	0.367	0.923	64.65	73.01	171.9	122.7	6.89	16.54
8	0.191	0.82	0.055	0.051	0.271	0.544	0.786	1.08	1.485	0.851	0.375	0.309	135.6	140.6	344.5	370.2	5.68	3.48
14	1.02	3.5	0.072	0.153	0.387	0.687	1.18	2.11	1.768	1.273	0.483	0.565	188.7	191.2	149	151.3	6.54	2.65
22	9.42	22.46	0.23	1.22	0.389	0.796	0.622	4.13	2.382	2.042	1.31	1.25	268.7	274.3	117.5	120.4	8.27	7.68
30	1.12	2.47	0.075	0.149	0.64	0.749	0.456	3.19	1.697	1.351	0.199	0.191	343.9	342.3	220.2	230.5	3.1	5.61
30d	-	2.506	-	0.147	-	0.803	-	3.17	-	1.378	-	0.189	-	345.3	-	231.8	-	3.196
32	7.33	8.55	0.174	0.436	0.344	0.427	0.832	3.35	1.996	1.561	0.311	0.061	403.7	405.6	85.8	91.4	7.54	8.71
37	0.684	1.15	0.065	b.d.	0.219	0.445	0.365	2.12	1.494	1.102	0.077	b.d	186.4	192.7	889.4	1017.4	2.79	3
41’	0.423	1.19	0.055	b.d.	0.189	0.523	0.394	b.d	1.308	1.087	0.176	b.d	34.7	37.86	27.92	18.39	7.42	5.45
41”	-	0.413	-	0.034	-	0.227	-	0.472	-	0.665	-	0.129	-	35.99	-	27.66	-	3.31
46	3.31	4.8	0.098	0.237	1.46	1.68	0.417	1.87	1.533	1.119	0.099	0.121	163.5	163.6	100.8	115	4.32	4.37
47	1.19	6.88	0.072	0.247	0.169	0.672	0.371	2.05	2.064	1.353	0.034	0.056	137	137.2	142.5	145.8	3.42	2.14
51	4.98	7.91	0.162	0.496	1.29	1.41	0.513	5.93	2.479	1.783	0.726	0.885	217.4	228.3	33.55	35.43	5.12	3.68
53	10.07	16.39	0.209	0.864	1.01	1.76	0.542	4.53	1.682	1.743	0.742	1.04	365.6	372	503.5	505	23.36	23.58
Geg’	0.383	2.13	0.059	0.016	0.165	0.548	0.72	0.97	1.423	0.902	0.154	b.d	277.2	275.5	657.2	576.7	3.52	3.83
Geg”	-	2.17	-	0.025	-	0.587	-	0.972	-	0.959	-	b.d	-	289.5	-	581.1	-	1.47
kval	0.95	2.19	0.071	0.086	0.232	0.503	0.424	3.44	1.613	0.982	0.14	b.d	358.2	371.6	198.2	226.4	6.15	4.04
Lef1	0.851	3.41	0.06	0.145	0.361	0.445	0.73	2.03	1.574	0.955	0.056	0.032	220.6	232.8	383.3	465.2	3.76	2.59
Lef2’	1.83	5.33	0.059	0.102	0.23	0.425	0.607	2.29	1.21	1.187	0.033	b.d	201.1	205.5	621.8	708.1	9.35	8.59
Lef2”	-	5.17	-	0.153	-	0.436	-	2.22	-	0.649	-	0.034	-	204.7	-	698	-	10.45
Lef2’	-	5.22	-	0.1	-	0.507	-	2.2	-	1.01	-	b.d	-	204.6	-	575.8	-	9.46

[d] - Duplicate sample; ’-’ Sample not duplicated in standard procedure;

b.d. - Below detection limits; S - Standard preparation technique; B - Bomb-digested sample

2.6 Results

2.6.1 Model HPTS Concentrations

Assuming LPTS results in negligible dissolution of rutile, we may use measured trace element concentrations of separated rutiles to model the element concentrations in a sample where rutile has been completely dissolved (i.e. samples prepared by HPTS). Trace elements used in this way are those present in relatively high abundance in rutile (i.e. Nb, Ta, Mo, Hf, V, Cr, Pb and U). If HPTS does indeed dissolve all rutile, both model and measured HPTS concentrations should be well correlated.

The model HPTS concentration is calculated using the mass balance equation

$$C_e = X_r.C_r + (1 - X_r).C_{rest} \tag{2.1}$$

where C_e is the model whole-rock concentration, C_r is the concentration measured in a separated rutile by LA-ICP-MS, X_r is the mass fraction of rutile, and C_{rest} is the LPTS concentration.

The value of X_r in Equation 2.1 is calculated by converting the volume abundance of rutile as determined by scanning electron microscope (SEM) phase mapping (see Chapter 4), into a mass fraction using the equation

$$X_r = \frac{V_r \times \rho_r}{\rho_{wr}} \tag{2.2}$$

where V_r is the measured volume fraction of rutile, ρ_r is the density of rutile (4.25 g c^{-3}), and ρ_{wr} is the total density of the sample (given as 3.35 g c^{-3}).

2.6.2 HTPS vs. LPTS

Figure 2.3 shows that for most samples, important rutile-hosted trace elements show near ubiquitous and significant increases in concentration from LPTS to HPTS techniques. Absolute differences between HPTS and LPTS concentrations for each analysed element may be described here by a value of δX, where X is the element in

Table 2.4: HPTS and accepted standard trace element compositions for BCR-2. Powdered BCR-2 was dissolved using HPTS using the same technique as eclogites in this chapter. The data show significant variations only occur for Sn (0.65) and Pb (0.88).

Element	BCR-2 Concentrations		
	Bomb	Standard Values	Ratio
La	24.38	25.0	0.98
Ce	53.05	53.0	1.00
Pr	6.59	6.76	0.98
Nd	28.37	28.0	1.01
Sm	6.47	6.7	0.97
Eu	1.89	2.00	0.95
Gd	6.53	6.8	0.96
Tb	1.04	1.07	0.97
Dy	6.3	6.55	0.96
Ho	1.25	1.33	0.94
Er	3.63	3.63	1.00
Tm	0.56	0.54	1.04
Yb	3.4	3.5	0.97
Lu	0.51	0.51	1.00
Hf	5.00	5.00	1.00
Ta	0.732	0.738	0.99
Pb*	**9.64**	**11.0**	**0.88**
Th	6.07	6.2	0.98
U	1.64	1.69	0.97
V	409.8	416	0.99
Cr	17.49	18.0	0.97
Nb	13.06	13.1	1.00
Mo	0.26	0.248	1.03
Sn*	**1.37**	**2.1**	**0.65**

* - Elements with significantly lower values in bomb-digested samples compared with accepted BCR-2 values.

question. The value of δX is calculated using the following equation:

$$\delta X = X_{HPTS} - X_{LPTS} \tag{2.3}$$

Niobium and Tantalum

Unsurprisingly, every sample has positive δX_{Nb}. Similarly, most samples have positive δTa ($Ta_{HPTS} > Ta_{LPTS}$), with the exception of samples 41 and 08 which have negative δTa. During LA-ICP-MS we encountered no inclusions that could explain such low Ta concentrations, and data calibration sheets for raw ICP-MS data have been checked and no errors found.

Molybdenum

Mo_{HPTS} is always greater than Mo_{LPTS} and thus δMo is always positive. Mo in rutile is typically 5-10 ppm, i.e. only slightly less abundant than Ta.

Hafnium

Hf_{HPTS} also is always greater than Hf_{LPTS} (i.e. $\delta Hf > 0$). Over half of the eclogite samples (7 out of 11) show significantly higher relative increases in Hf than in Nb. Since Nb is far more abundant in rutile, it is likely much of this Hf is derived from zircon, either as undissolved matrix grains or inclusions in rutile.

Thorium

δTh is consistently negative in all but one eclogite sample. Th is highly incompatible in rutile, and therefore its concentration in it is assumed to be negligible. Addition of rutile into the total digested material would therefore effectively dilute the Th concentration. A line of best fit through the data reveals reveals a trend that has a slope of 1, and intercept of -0.3. This line of best fit suggests the mechanism by which the Th concentration is reduced is independent of the Th concentration itself. Using simple mixing equations (equations 2.4-2.6), and ignoring the effect of zircon, one can estimate the minimum modal proportion of rutile necessary to achieve the amount of dilution needed to explain these observations. In this particular example, digested

sample excluding rutile (V_1 and X_1) is mixed with an unknown quantity of dissolved rutile (V_2 and X_2) to produce a diluted solution (X_T). If we assume that Th = 0 ppm ($X_2 = 0$) and that total dissolution is achieved ($V_T = 100\%$), the equation may be simplified to:

$$X_T = \frac{V_1.X_1}{100} \tag{2.4}$$

The modal volume of rutile is calculated by:

$$V_2 = 100 - V_1 \tag{2.5}$$

We combine and rearrange equations 2.4 and 2.5 to produce:

$$V_2 = \frac{100.X_T}{X_1} - 100 \tag{2.6}$$

To achieve a dilution of 0.3 ppm, approximately 0.5 wt. % of rutile must be added. Such a modal abundance of rutile is typical of many of these samples that have around 0.64 $\pm$ 0.43 vol.% (see Chapter 4, page 147).

Pb and U

Pb and U in data are mildly inconsistent. HTPS values may be slightly higher, largely the same, or slightly lower than corresponding LPTS values. The BCR-2 standard prepared using HPTS showed that Pb may be around 12 % lower in HPTS data than expected, thus potentially explaining some of the anomalously low HPTS Pb values. Figure 2.4 shows U has lower variability, and that the data may be loosely described by a 1:1 relationship.

Chromium

Although Cr is often present in very high abundances in rutile (often >1000 ppm), only small increases in Cr (around 10 %) for all except two samples (01 and 41) are observed. Samples 01 and 41 show 29 % and 26 % reductions in Cr concentrations respectively, and unfortunately no data are available for the composition of their rutile grains. Coincidentally sample 41 had Ta_{HPTS}/Ta_{LPTS} <1. Only relatively small increases in Cr are typically observed because the estimated partition coefficient of Cr ($\approx$ 4.0) into rutile is significantly lower than that for elements such as Nb ($\approx$ 300) and Ta ($\approx$ 230).

Vanadium

The concentration of V in rutile is often significantly higher than many other commonly analysed trace elements, however δV is typically around +5 %, within what may be regarded as reasonable analytical error. Reported mean partition coefficients between rutile and a basaltic mineral assemblage are fairly similar: 2.34, 1.48 and 1.8 (Jenner et al., 1994; Hauri et al., 1994; Pertermann and Hirshmann, 2002, respectively), whereas our data suggest a slightly higher partition coefficient in an eclogite assemblage (5.37 $\pm$ 1.2)). Such relatively low partition coefficients are not expected to yield significantly high δV above expected error, and hence V_{HPTS} and V_{LPTS} are highly correlated.

2.6.3 HPTS vs. XRF

The same nine elements (Nb, Cr, V, U, Th, Pb, La, Ce, and Nd) were analysed using both XRF and HPTS-ICP-MS techniques. If total dissolution is achieved via the HPTS method, these two datasets are expected to exhibit strong correlations for each element. We can see in Figure 2.6 that XRF and HPTS data for three elements correlate very well (Nb, Cr, and V: $R^2 > 0.99$) , two moderately well (Ce and Nd: $R^2 > 0.95$), and two not particuarly well (Th and Pb: $R^2 < 0.9$).

Where R^2 is greater than 0.95, slopes of best fit lines are very close to 1, i.e. measured concentrations from each technique yield highly statistically similar results. XRF data

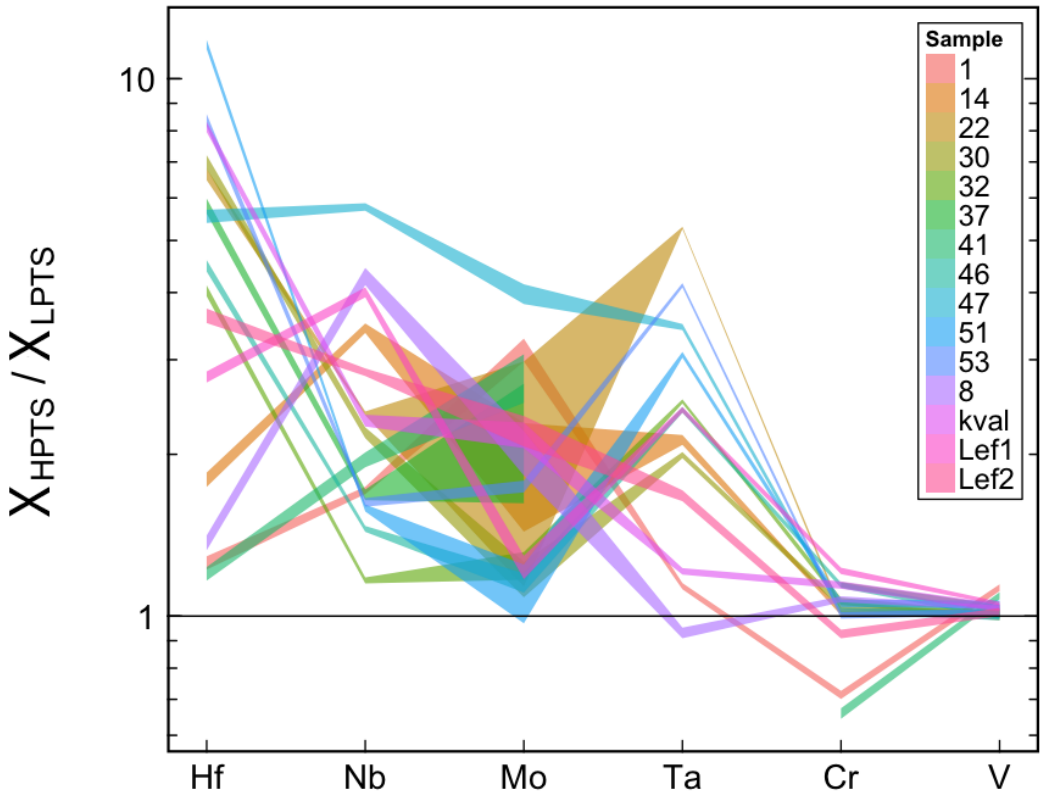

Figure 2.3: Comparison of concentrations (C) measured by HPTS and LPTS techniques for elements particuarly abundant in rutile and zircon. Most elements show significant increases in measured concentrations of up to an order of magnitude. A number of samples show curiously low concentrations Ta and Cr. Ribbons represent the combined relative analytical error.

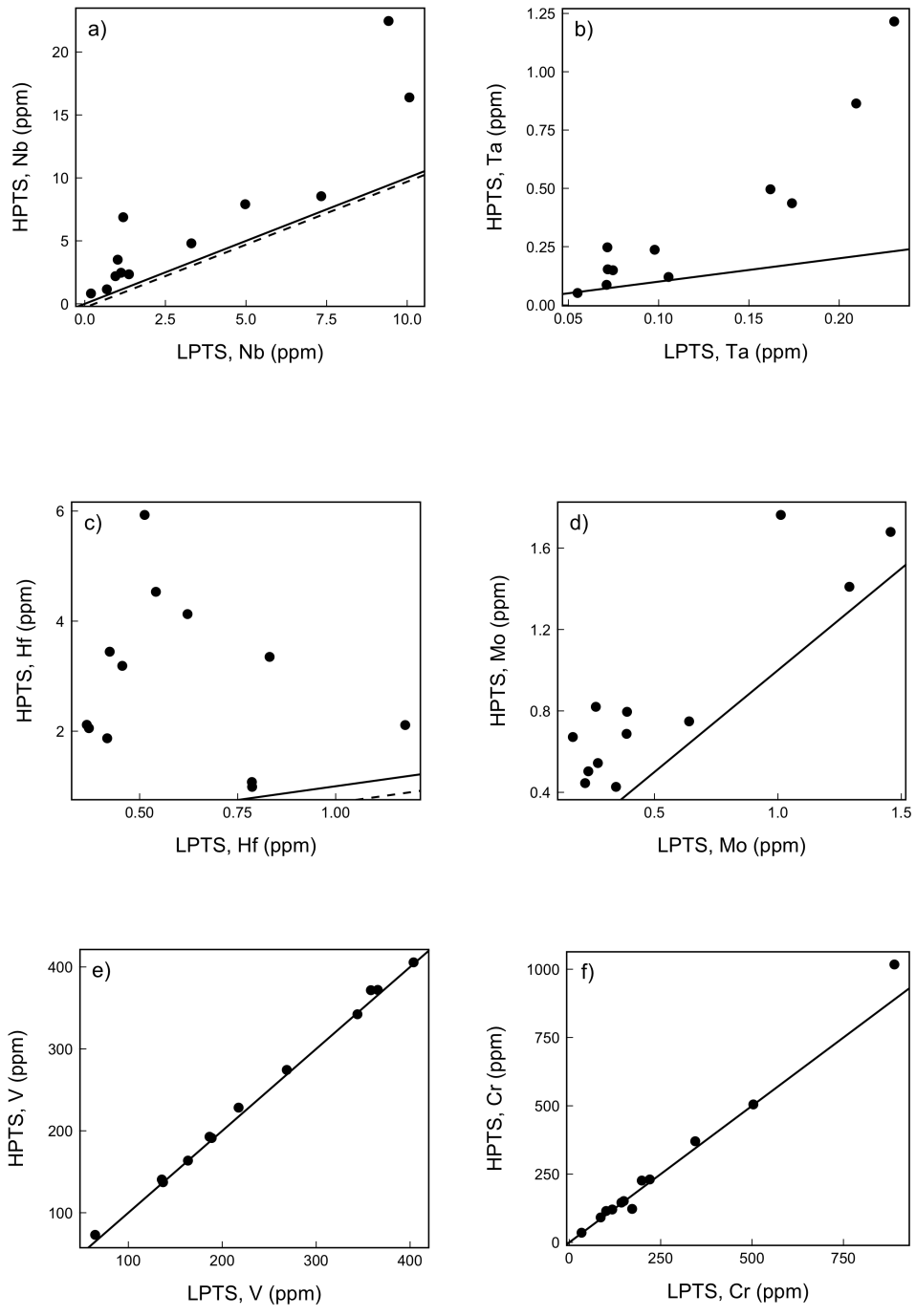

Figure 2.4: (Continued on following page.)

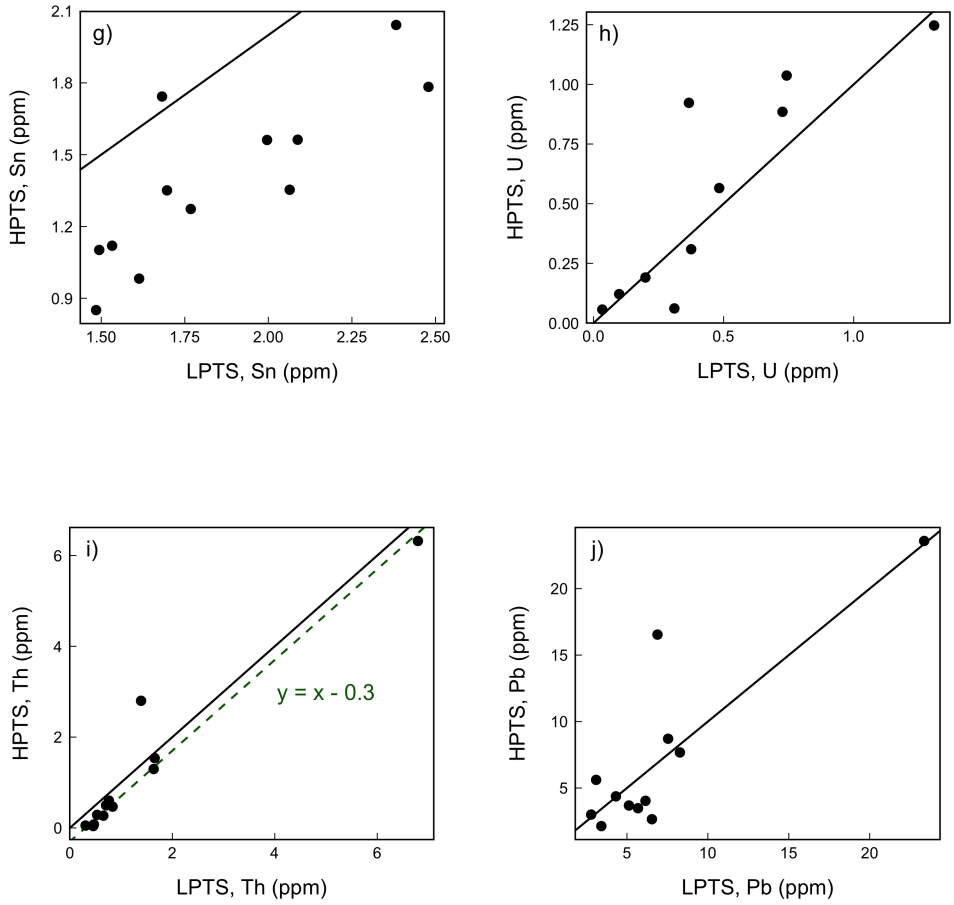

Figure 2.4: Comparisons of measured trace element concentrations for HPTS and LPTS data. Solid line has a slope of 1 and intercept of 0. Dashed lines are lines of best fit.

for Nb are well correlated with HPTS and not LPTS data. The slopes of best-fit lines for V and Cr also noticeably shallower for XRF vs. LPTS than XRF vs HPTS (Figures 2.6c-2.6b and Figures 2.6c-2.6b).

Concentrations of Th and U are often much closer to detection limits for XRF spectrometry (0.35 $\pm$ 0.5 and 0.45 $\pm$ 0.5 respectively) than for ICP-MS (0.04 and 0.05 respectively), which could help explain poor correlation of the data. Since the Th, and to a lesser extent U, HPTS and LPTS are well correlated (Figures 2.4i and 2.4h respectively), the corresponding lack of correlation with XRF data likely reflects relatively large XRF error.

2.7 Discussion

2.7.1 Element Sensitivities

As expected, δX for elements present in rutile in high abundances are always as high. Although V and Cr are often the most abundant trace elements in rutile, δV and δCr are typically less than 10 %. This is due to their relatively low partition coefficients for rutile. The elements shown to be most sensitive to rutile dissolution are Nb and Ta, followed by Mo.

2.7.2 Element Losses and Data Reliability

HTPS data for Sn and Pb are not always wholly reliable, since in some samples δX is negative. This cannot be explained by dilution by an unknown accessory phase, and therefore it is thought that Sn and Pb form volatile complexes with ions in the acidic solutions which, at some point in the sample preparation procedure, may escape.

Model Sn concentrations are typically 40-70% lower than observed HPTS concentrations, yet less than 10 % higher than LPTS data. Indeed the BCR-2 HPTS standard showed 35 % less Sn than the standard actually contains. Since BCR-2contains no rutile, dilution by rutile-hosted Sn-poor phases is not a valid explanation. Instead, we argue that the HPTS technique greatly increases the potential

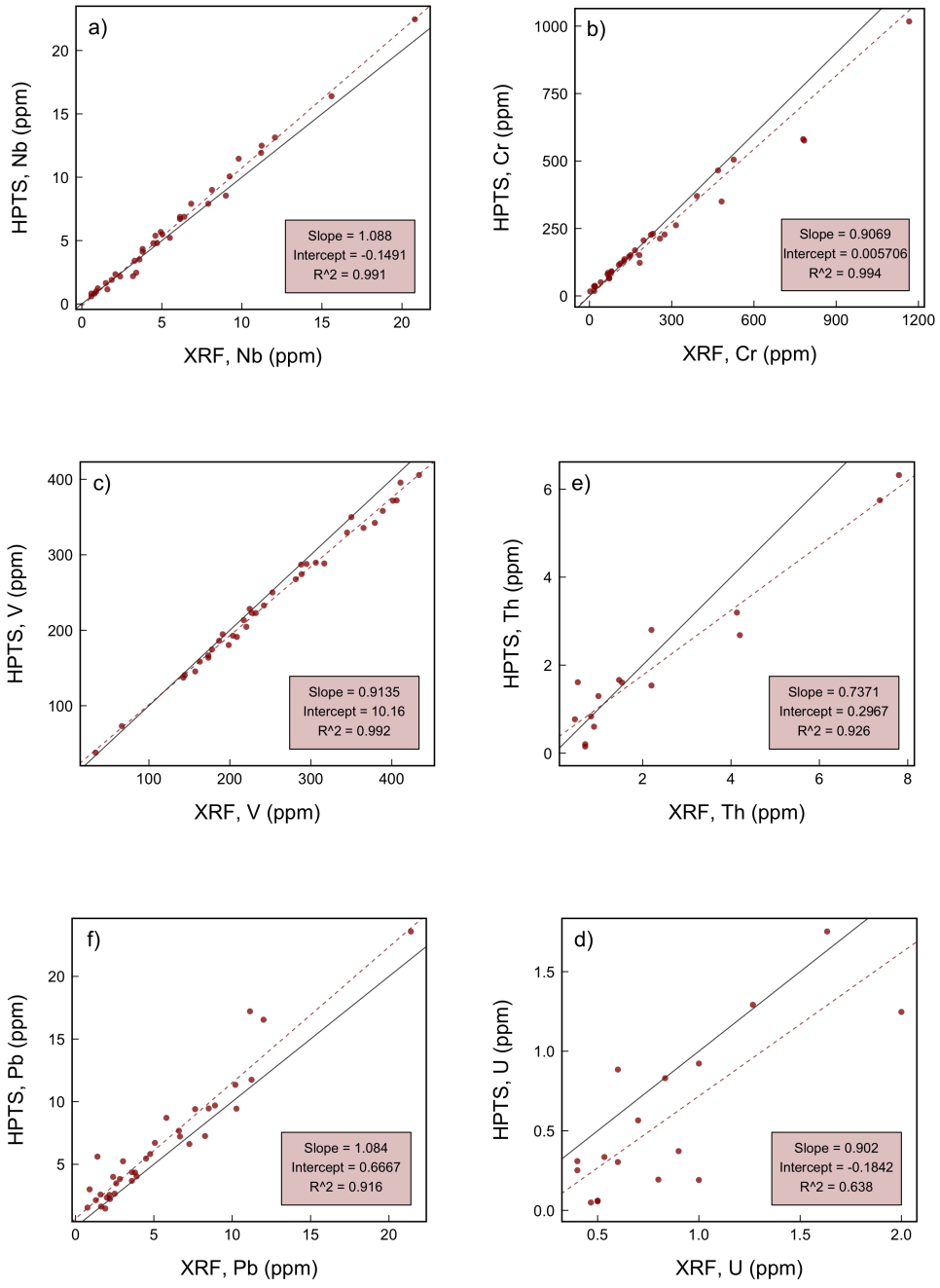

Figure 2.5: Comparisons of measured trace element concentrations for HPTS and XRF data. Solid line has a slope of 1 and intercept of 0. Dashed lines are lines of best fit.

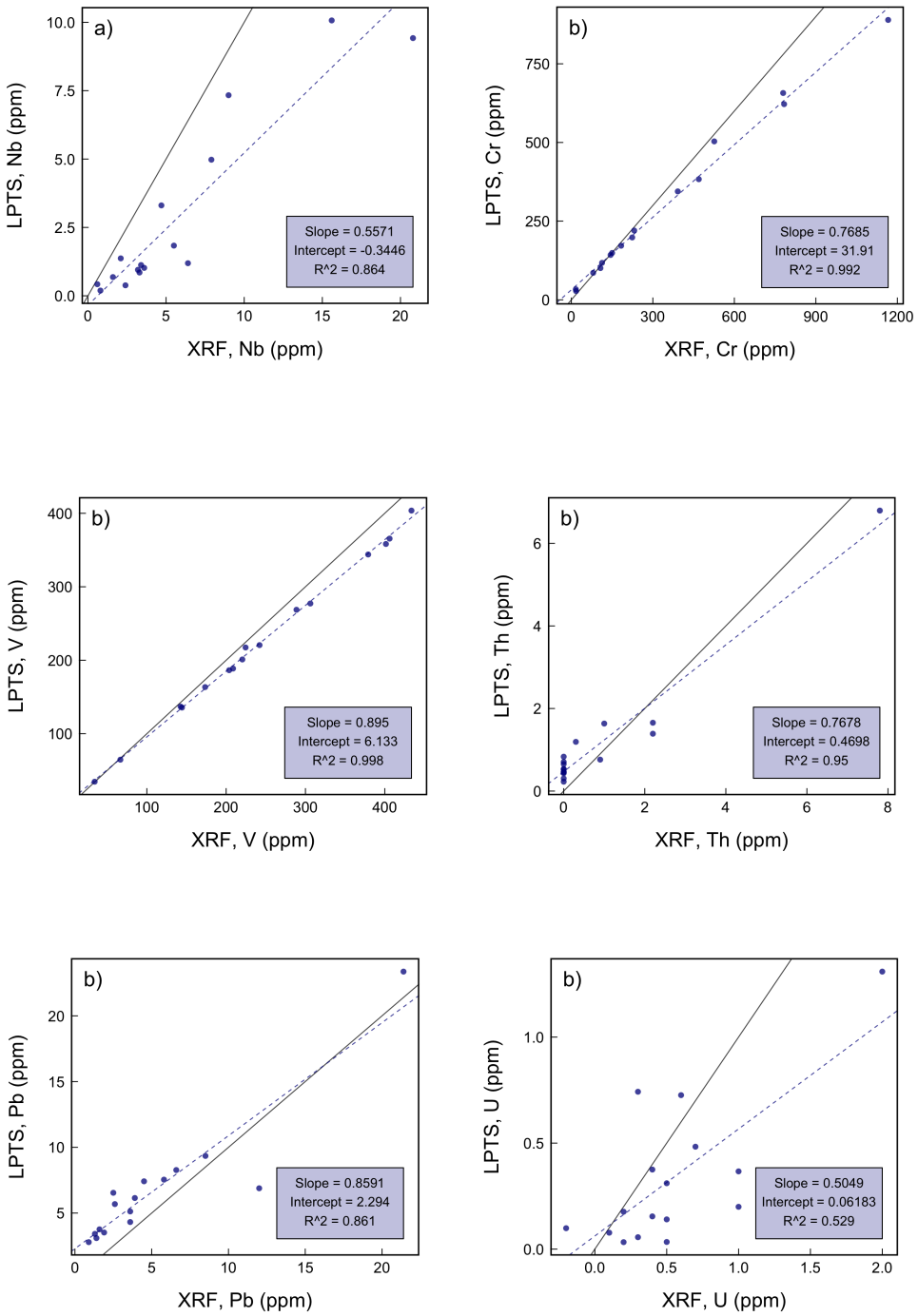

Figure 2.6: Comparisons of measured trace element concentrations for LPTS and XRF data. Solid line has a slope of 1 and intercept of 0. Dashed lines are lines of best fit.

for volatility of Sn in almost all samples. Furthermore, as Sn is reduced in almost all samples, it is not thought that this volatile loss is related to leakage from digestion vessels.

Pb concentrations are often so low in rutile (<0.1 ppm) that model HPTS Pb concentrations are not significantly higher (0.02-0.03 ppm) than measured LTPS or indeed XRF concentrations for the whole-rock. Observed HPTS concentrations, however, can be much lower (-8 to -146 %) than predicted and even lower than concentrations in LPTS data. The BCR-2 HPTS standard indicated a 12 % loss of Pb, and therefore it is believed losses of the same magnitude are likely contributing to these differences. Despite this, both Pb_{LPTS} and Pb_{HPTS} are usually greater than Pb_{XRF}. suggesting Pb_{XRF} is generally underestimated. During both LPTS and HPTS, exposed fragments of zircon should be dissolved, whereas rutile-hosted zircons are shielded. Increased Pb volatilisation attributed to HTPS could counteract expected increases in Pb liberated from rutile-hosted zircon, generating a spurious correlation between XRF and HTPS data.

It is already known that Ta is particularly unstable in hydrofluoric acid, and therefore one should subject Ta data with extra scrutiny. Yet for most samples in this study, predicted Ta_{HPTS} is broadly in agreement with observed Ta_{HPTS}, suggesting that our data are reasonable. This is corroborated by the HPTS BCR-2 sample that showed no evidence of Ta loss. Only one sample (41^{d}) showed Ta loss (δTa = -0.021ppm, -38 %), and this happens to also be a failed seal experiment. In this case the volatile Ta compounds likely escaped in a vapor. One must therefore always confirm the integrity of the seal has been maintained during HPTS.

2.7.3 Effectiveness of HPTS

The vast majority of data indicate that LTPS dissolves little or no rutile, whereas HTPS dissolves all of it. HPTS concentrations for elements with high partition coefficients for rutile are in the majority of cases higher, and closely match the concentrations predicted using known rutile compositions and modal abundances. Furthermore, important elements such as Cr, Pb, V, and particularly Nb, are better correlated with

XRF analyses when HTPS data are used, and in the case of Nb, this strongly indicates total rutile dissolution is achieved.

2.8 Conclusions

- Standard LPTS acid digestion procedures do not achieve complete digestion of rutile and zircon-bearing powdered samples.
- Analyses of solutions prepared using LPTS techniques in which as little as 0.5 wt.% rutile is not dissolved, may yield erroneous concentrations for a number of important trace elements (Nb, Ta, Hf, Mo and Th).
- Undissolved rutile may contain a mass of other accessory minerals (e.g. zircon) which also have significant trace element compositions that contain an important amount of the whole-rock trace element inventory for a number of trace elements (e.g. Zr and Hf).
- The efficacy of acid digestion of acid resistant minerals such as rutile and zircon is greatly increased when the temperature is increased from 100^oC to 220^oC. The higher temperature increases the mobility of ions and reduces viscosity. The significance of higher pressures attained in digestion vessels (estimated to be around 1000 psi) is thought to be limited to the role of increasing the boiling point of acids used, thereby allowing them to remain liquid and in contact with the sample at the necessary temperature.
- Pb and Sn concentrations measured in samples prepared by HPTS are likely too low, owing to the high volatility consistently exhibited by these elements.
- In the eclogites studied, approximately 0.49 $\pm$ 0.13 % of all available TiO_2 is rutile.

2.9 Future Work

The scope of this study was restricted by both time and resources, leaving much more to be investigated. For instance, a better understanding of volatile element loss must be gained in order to assess the reliability of the HPTS technique. Ensuring Ta in

particular is properly retained and measured throughout the HPTS procedure is vital, as accurate measurements of whole-rock Nb/Ta ratios are essential not only for this study, but in general when preparing rutile-bearing lithologies for ICP-MS analysis.

Future investigative work should aim to achieve the following:

- Compare more LTPS and HTPS standards which are rich in Sn, Pb and Ta.
- Increase the number of eclogite samples as both LPTS and HTPS duplicates.
- Conduct HPTS experiments at a range of intermediate temperatures to investigate whether this reduces the incidence of bomb failures and volatile loss.

Chapter 3

Whole-Rock Geochemistry of Norwegian Eclogites: Protolith identification and estimates of element flux during subduction*

Abstract

High pressure (HP and ultra-high pressure (UHP) orogenic eclogites in the Western Gneiss Region (WGR) of Norway are amongst the best exposed and most studied eclogites in the world, yet surprisingly few authors have published data on their whole-rock trace element composition. The data that do exist (e.g. Griffin and Brueckner, 1985) are scarce, restricted in element availability, and are of relatively low precision. To address this shortfall, we present high precision measurements of a comprehensive selection of major and trace elements for over 30 classic Norwegian eclogites. Our data show that a significant number of samples have preserved their protolith rare earth element (REE) and high field strength element (HFSE) abundances and ratios. Discriminant analysis of these samples revealed most have mid-ocean ridge basalt (MORB) or arc basalt geochemical affinities (Group A and B respectively). Interpretation of Group B eclogites is complicated by the so-called 'metasomatic problem', in which it is difficult to determine whether arc-like geochemical signatures are inherited from the protolith, metasomatism of the protolith during metamorphism, or a combination of both. The coherence of geochemical signatures, lack of evidence of infiltration of partial melts or Sr enrichment, as well as arc-like Pb/Zr and Pb/Nd suggest that Group B eclogites are indeed derived from arc-like basalts. These findings are in agreement with models of Early Caledonian plate configurations which involve the accretion of island arcs onto the Baltican continental margin shortly before

*Co-authors: Godfrey Fitton - *The University of Edinburgh*; Simon Harley *The University of Edinburgh*

subduction of the margin under Laurasia. We suggest that Group A eclogites represent MORB-like intrusions in or near the pre-Caledonian Continent-Ocean Transition (COT) of Baltica.

3.1 Introduction

Eclogites in the WGR of Norway have been at the centre of several important geological discoveries. For instance, in the early 1920s the Finnish geologist Pentti Eskola used eclogites from western Norway to define the eclogite facies of metamorphism (Eskola, 1920, 1921). Just over half a century later, Smith (1984) reported the mineral coesite in some Norwegian eclogites, with which he helped define a new type of metamorphism: ultra-high pressure (UHP) metamorphism.

Subsequent investigations on Norwegian eclogites have largely dealt with their prograde and retrograde mineralogical evolution (e.g. Mørk, 1986; Krogh, 1980, 1982; Cuthbert et al., 1983; Cuthbert, 1985; Mørk and Mearns, 1986; Griffin et al., 1985; Griffin, 1987; Mysen and Heier, 1972; Carswell and Harvey, 1985), pressure-temperature-time (PTt) histories (Griffin and Brueckner, 1985; Mearns, 1986; Mørk and Mearns, 1986; Krogh et al., 1974; Gebauer et al., 1985; Harrison, 1981; Cuthbert et al., 1983; Jamtveit, 1987; Griffin, 1987; Mørk et al., 1988; Dallmeyer and Gee, 1986a; Dallmeyer, 1988), and mechanisms of their somewhat enigmatic occurrence in apparently lower grade basement gneisses (e.g. Krogh, 1977; Lappin and Smith, 1978; Smith, 1980; Cuthbert et al., 1983; Griffin et al., 1985; Carswell and Cuthbert, 1986; Jamtveit, 1987; Smith, 1988; Cuthbert and Carswell, 1990; Andersen et al., 1991; Austrheim, 1991; Krogh and Carswell, 1995; Smith et al., 1995).

Most of the aforementioned studies have concentrated on understanding Norwegian eclogites in the context of the Caledonian Orogeny, however many protoliths to eclogites in the WGR were probably formed >1 Ga and not recrystallised to eclogite until the Caledonian Orogeny (e.g. Walsh et al., 2007). Figure 3.1 shows that eclogites in the WGR had a long and probably complex history before the Caledonian that remains largely unexplored. In particular, there still exists a significant gap in available geochemical data for these classic eclogites. Major element compositions of rocks

and minerals are available for some prominant localities (e.g. Binns, 1967; Smith, 1968; Bryhni et al., 1969; Green, 1969; Mysen and Heier, 1972; Lappin, 1974; Smith, 1976; Kechid, 1984; Svensen et al., 2001), but reliable and useful trace element data for whole-rocks is restricted to a hand full of individual localities (e.g. Griffin and Brueckner, 1985).

In this study we provide analysis of the major and trace element composition of a suite of over 30 Norwegian eclogites. Using these data, we can: suggest likely protolith types, and therefore increase our understanding of the pre-Caledonian margins of Baltica and Laurentia; as well as to quantitatively assess the likely element fluxes in and out of these eclogites during their P-T-t evolution.

3.1.1 Sample Information

Figure 3.2 shows the locations of eclogite exposures sampled in this study. Samples and localities were chosen to reflect the wide petrological variability and geographical spread observed in the Norwegian eclogite population. For instance, included in the sample set are quartz eclogites, amphibole eclogites, kyanite eclogites, and orthopyroxene eclogites. Additionally, we collected samples of eclogite that cover a range in retrogressive overprint, in order to assess the extent to which common retrogressive amphibolitisation may affect the trace element geochemistry of eclogites. Petrographic descriptions of our eclogite samples are given in Appendix B (page 285).

3.1.2 Analytical Methods

The preparation of whole-rock powders for geochemical analysis was already detailed in Chapter 2 (pg. 53), and is not repeated here. Concentrations for 10 major elements (Si, Al, Fe, Mg, Ca, Na, K, Ti, Mn and P) and 17 trace elements (Ba, Ce, Cr, Cu, La, Nb, Ni, Pb, Rb, Sc, Sr, Th, U, Y, Zr and Zn) were measured using X-ray fluorescence (XRF) spectrometry at The University of Edinburgh (see Appendix A.1, page 281 for details). A further 14 trace elements (Cr, Hf, Nb, Mo, Pb, REEs, Sn, Ta, Th, U and V) were measured using High Pressure and Temperature Solution Inductively-Coupled Plasma Mass Spectrometry (HPTS-ICP-MS) at SUERC in East Kilbride, of which full details are given in Chapter 2 (page 53).

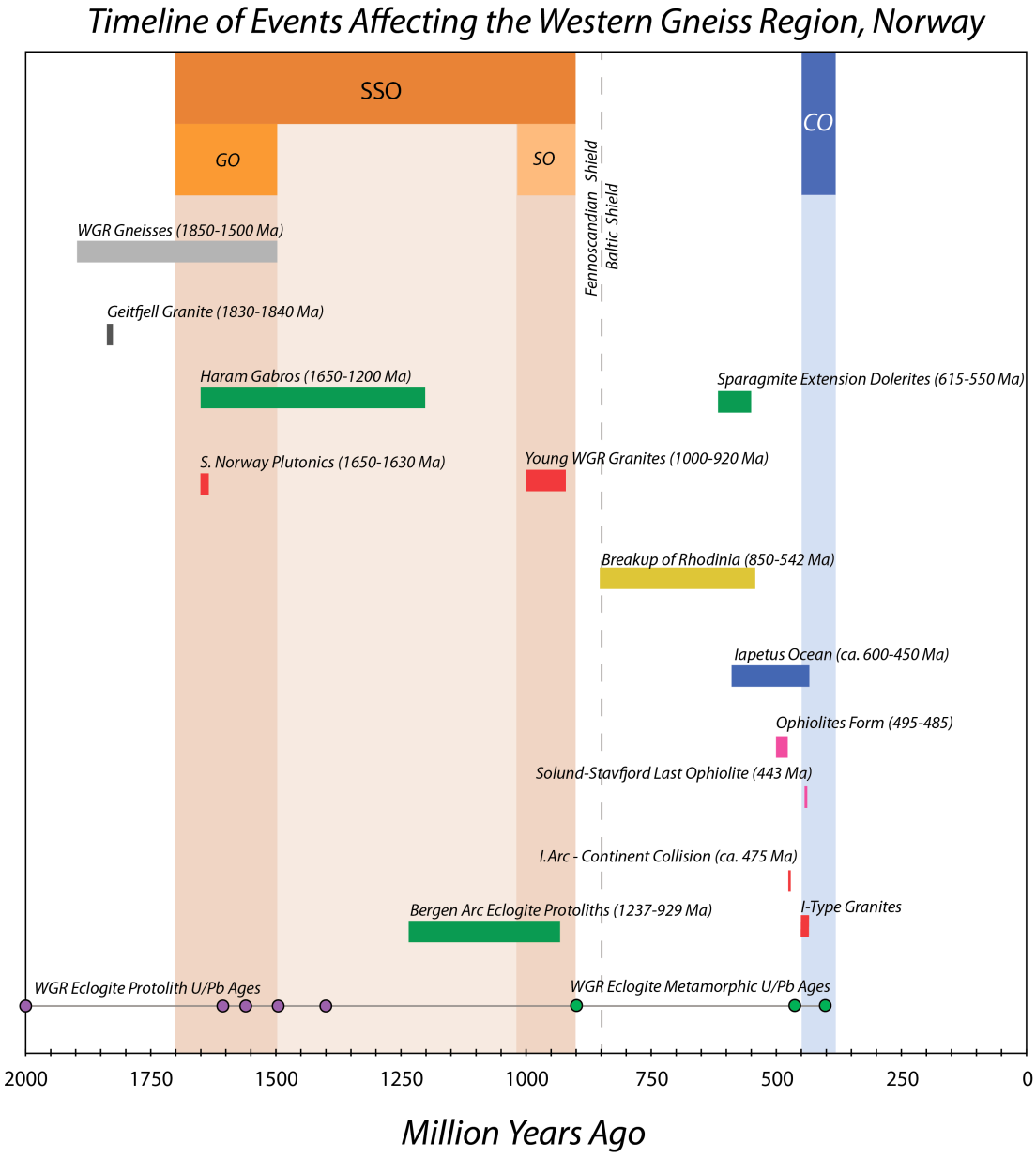

Figure 3.1: Timeline of events affecting the WGR basement from 2.0 Ga to present. The timeline covers the two main orogenic events that affected the region: the Southwest Scandinavian Orogen (SSO) including the Gothain (GO) and Sveconorwegian (SO), and the Caledonian Orogen (CO).

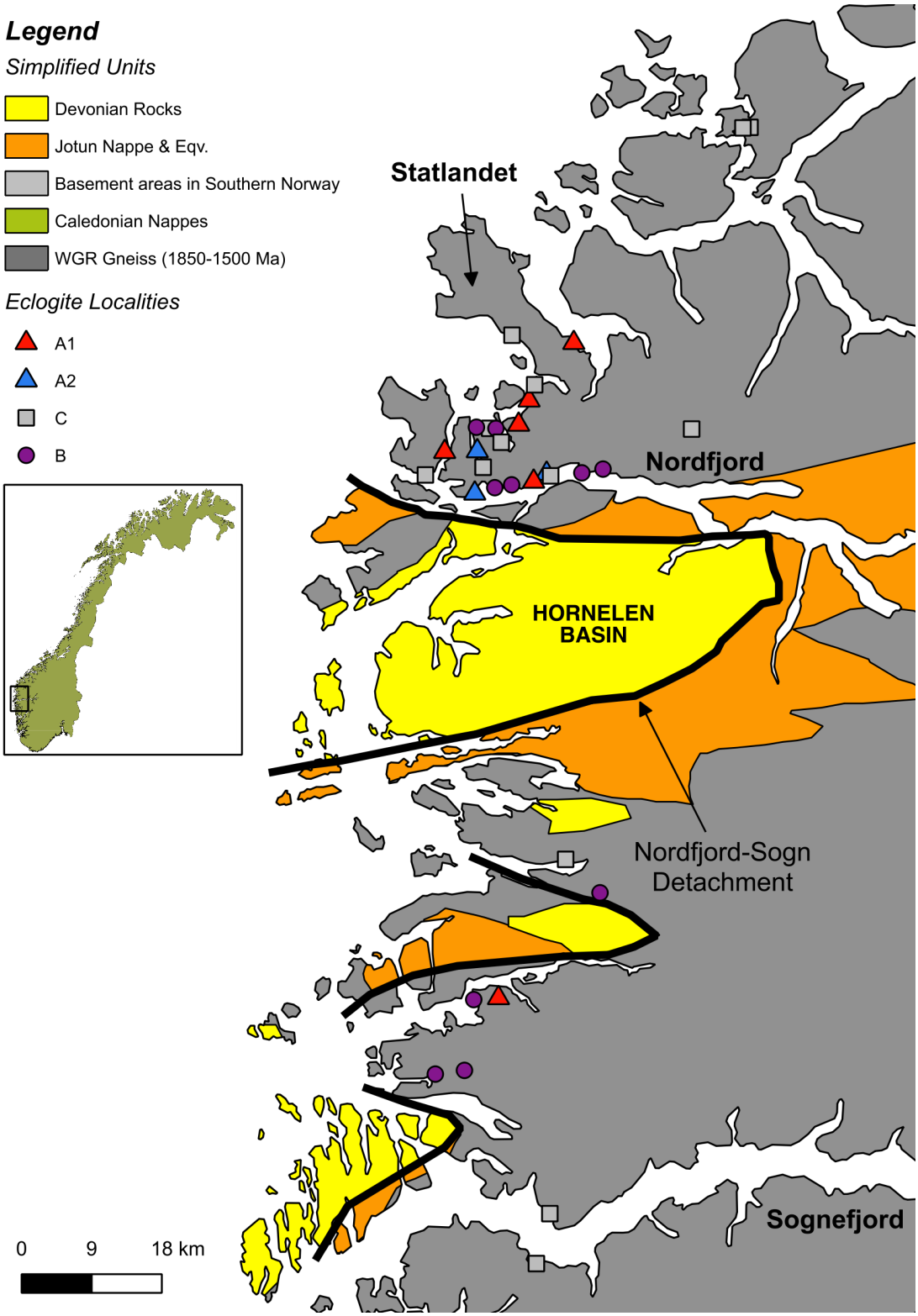

Figure 3.2: Map showing sample locations and assigned groups of collected Norwegian eclogites projected onto a simplified geological map of Western Norway. Eclogite symbols represent groupings based on trace element geochemical characteristics, discussed in the next section.

3.2 Results

Concentrations of all measured major and trace elements are available in Appendix C.2.1 to C.2.4, page 305-310. In this section, major element oxides are explored largely as a preamble to the more useful trace element data, which are in turn only used in this section to characterise broadly coherent geochemical signatures within the sample population in order to provide a starting point for protolith identification.

3.2.1 Major Elements

Figure 3.3 is a total alkali silica (TAS) plot that shows the majority of eclogites are basaltic (SiO_2 of 45-52 wt.%) and $Na_2O+K_2O<5$ wt.%). Around half of the eclogites have $SiO_2<48$ wt.%, the typical minimum silica content of both tholeiitic and calc-alkaline basalts generated in most magma-generating tectonic settings. Eight samples plot outside the basalt field: three of these have $SiO_2<45$ wt.% (WGR-64, -65, -78), and a further three have $SiO_2>55$ wt.% (WGR-70, -76, -80); the remaining two have Na_2O+K_2O 5.0-5.5 wt.% (WGR-22 and WGR-60).

The remaining oxides are displayed in a series of Harker diagrams (Figure 3.4), albeit mostly without significant correlations. Fe_2O_3 is mostly between 10 and 16 wt.% but may be as low as 4 wt.% or as high as 22.3 wt.%, and defines a loose negative correlation with silica. Most samples have 0.6-2.5 wt.% TiO_2, yet four samples (WGR-51, -64, -65, -78) have 3.0-6.0 wt.% TiO_2. Al_2O_3 is typically 13-19 wt.%, however may be as low as 6.6 wt.% (WGR-76) or as high as 25.5 wt.% (WGR-41). MgO for most samples is ca. 5-10 wt.%, with a minimum of 3.2 wt.% (WGR-60) and maximum of 16.3 wt.% (WGR-76). Eclogites are generally Mg-poor and Fe-rich, plotting as high-Fe tholeiitic basalts on Al-(Fe + Ti)-Mg and Al-Fe-Ti diagrams (Figures 3.5 and 3.6). Most samples have CaO 7.0-12, however WGR-76 again stands out with CaO = 15.9 wt.%. Alkalis are often typical of fresh MORBs or significantly elevated (up to 1.25 wt.% K_2O, WGR-70; and up to 4.6 wt.% Na_2O, WGR-22). loss on ignition (LOI) corrected for Fe-oxidation is typically between 0.9 and 1.2wt.%.

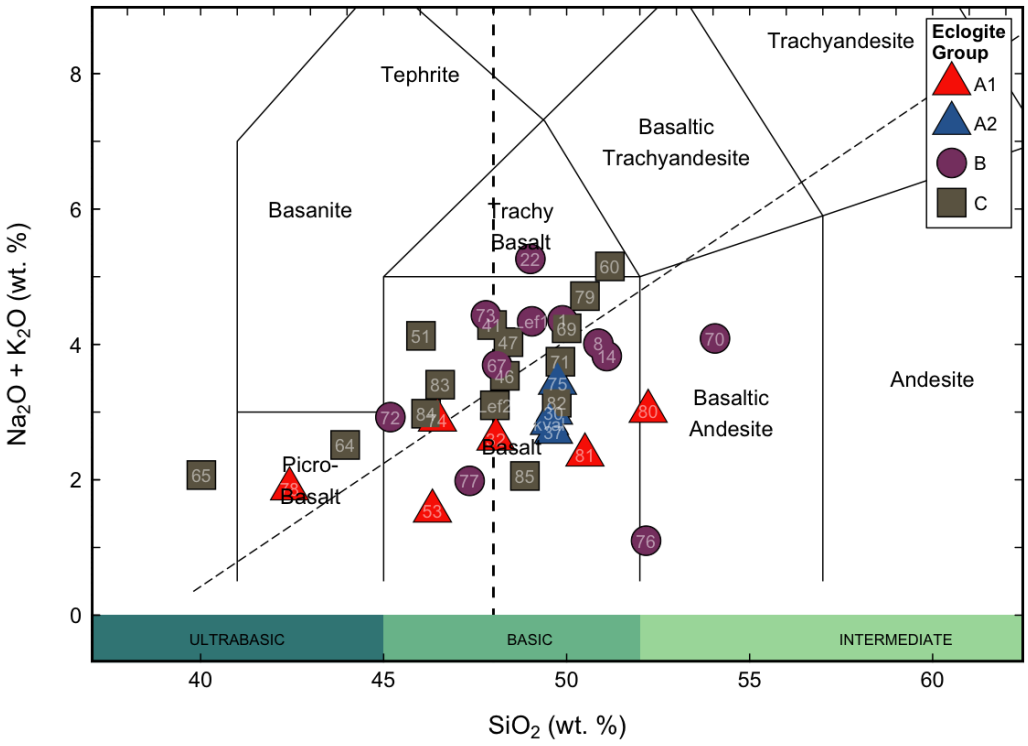

Figure 3.3: Norwegian eclogite compositions plotted on a total alkali silica (TAS) diagram (after Le Maitre et al., 1989). Symbols and colours represent eclogite groups defined later in this chapter. The vertical dashed line at SiO_2 = 48 wt.% is the typical minimum for most basalts formed in magma-generating tectonic settings. The sloping dashed line divides alkaline and subalkaline volcanic rocks (above and below respectively) and is taken from MacDonald (1968). The plot shows that most eclogites fall within the basalt field either side of the alkaline-subalkaline divide, with group A eclogites mostly plotting as subalkaline.

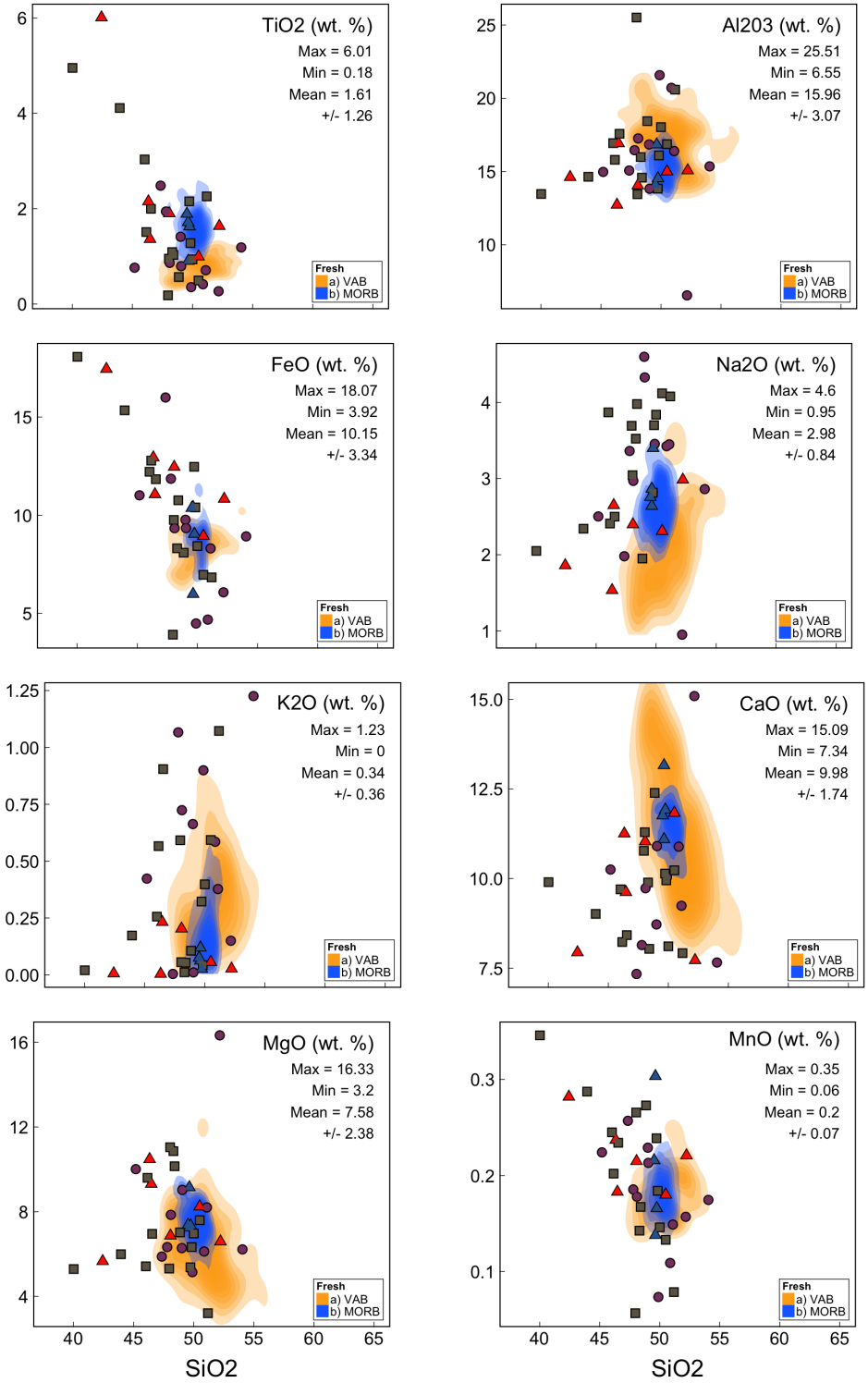

Figure 3.4: Harker diagrams showing the major-element compositions of Norwegian eclogites compared with fresh MORB (blue) and arc basalt (yellow). Data for MORB and VAB extracted from PetDB. Note that major elements for most eclogites remain largely in range of fresh MORBs and arc basalts. Furthermore, note that group A2 plot almost exclusively within the field of MORB.

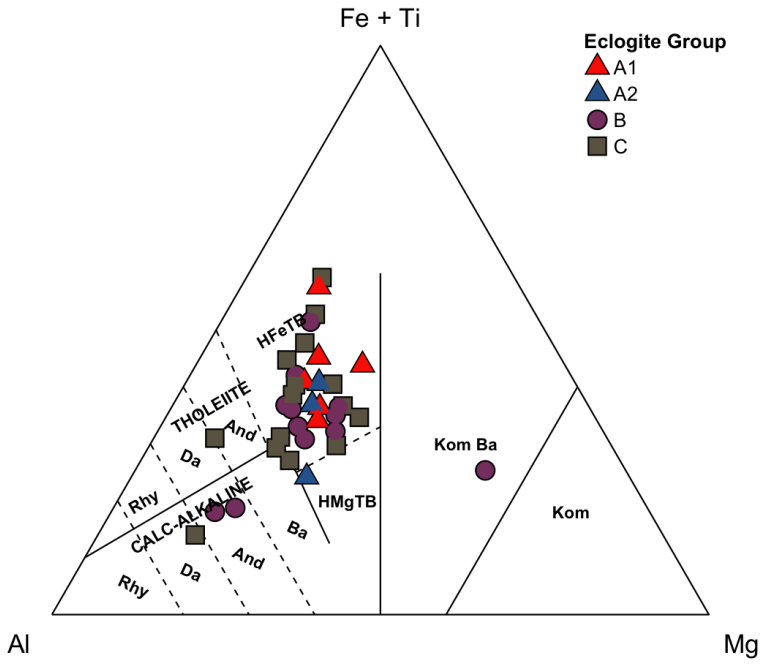

Figure 3.5: AFM diagram using Al, ($Fe_{(total)}$ + Ti) and Mg showing the fields of tholeiite, calc-alkaline basalt and komatiite. Rhy: rhyolite; Da: dacite; And: andesite; Ba: basalt; HFeTB: high-Fe tholeiitic basalt; HMgTB: high-Mg tholeiitic basalt; Kom: komattiite/komatiitic. All but one eclogite have Al>Mg, and plot mostly in the field of high-Fe tholeiites. After Rickwood (1989).

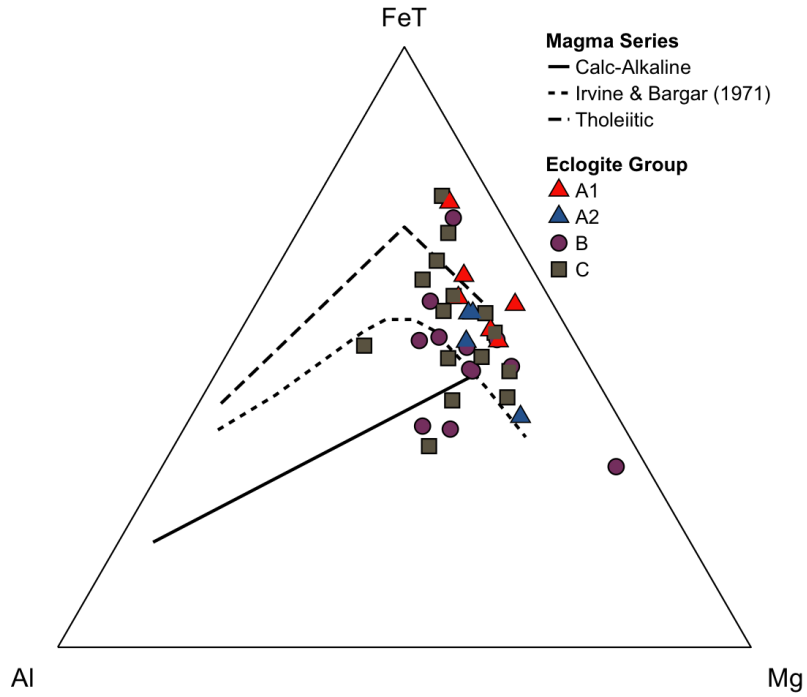

Figure 3.6: An AFM diagram showing Irvine and Bargars's (1971) boundary between-, and trends of calc-alkaline (Cascades lavas) and tholeiitic (Thingmuli Volcano, Iceland) magma series. This diagram also suggests that the majority of samples have tholeiitic protoliths with a tendency for the high-Fe variety. (After Rickwood, 1989, and references therein.)

3.2.2 Trace Elements

Multi-element plots provide a good starting point for the broad characterisation of our sample population. We selected elements that we expected to be least sensitive to metamorphism: i.e. the REEs La to Lu, and a selection of HFSEs (e.g. Th, Nb, Ta, Zr, and Hf). Our starting hypothesis was that many eclogites would have protoliths derived from MORB-like crust, and so we normalised each element to recently published values for average normal mid-ocean ridge basalt (N-MORB) given by Gale et al. (2013). N-MORB-normalised concentrations are denoted with the subscript letter 'n' (e.g. Nb_n).

Figures 3.7 to 3.10 are multi-element plots of four groups of eclogites that we were able to identify based on similar geochemical features. Details of these features in each group are as follows:

Group A1

Generally smooth patterns with mild enrichment in LREEs (i.e. $(La/Sm)_n \geq 1$). The highly incompatible HFSEs Th, Nb and Ta are enriched over the more compatible HSFEs Zr, Hf, Ti and Y, but are not necessarily enriched over N-MORB. The exceptions are Nb and Ta, which are *always* enriched over N-MORB. Although generally greater than N-MORB, Th is often strongly depleted relative to Nb (i.e. $(Th/Nb)_n < 1$). Heavy rare earth elements (HREEs) are flat and scatter closely around 0.5-2. The multi-element signature is typical of MORB, specifically Transitional MORB (T-MORB) and enriched mid-ocean ridge basalt (E-MORB).

Group A2

Flat and smooth REE patterns lack LREE enrichment (i.e. $(La/Sm)_n \approx 1$). Samples differ from A1 in that they also lack noteable enrichment in Nb, Ta, and Th. These elements are also typically depleted relative to N-MORB and similarly compatible elements (e.g. $(Nb/La)_n \leq 1$).

Group B

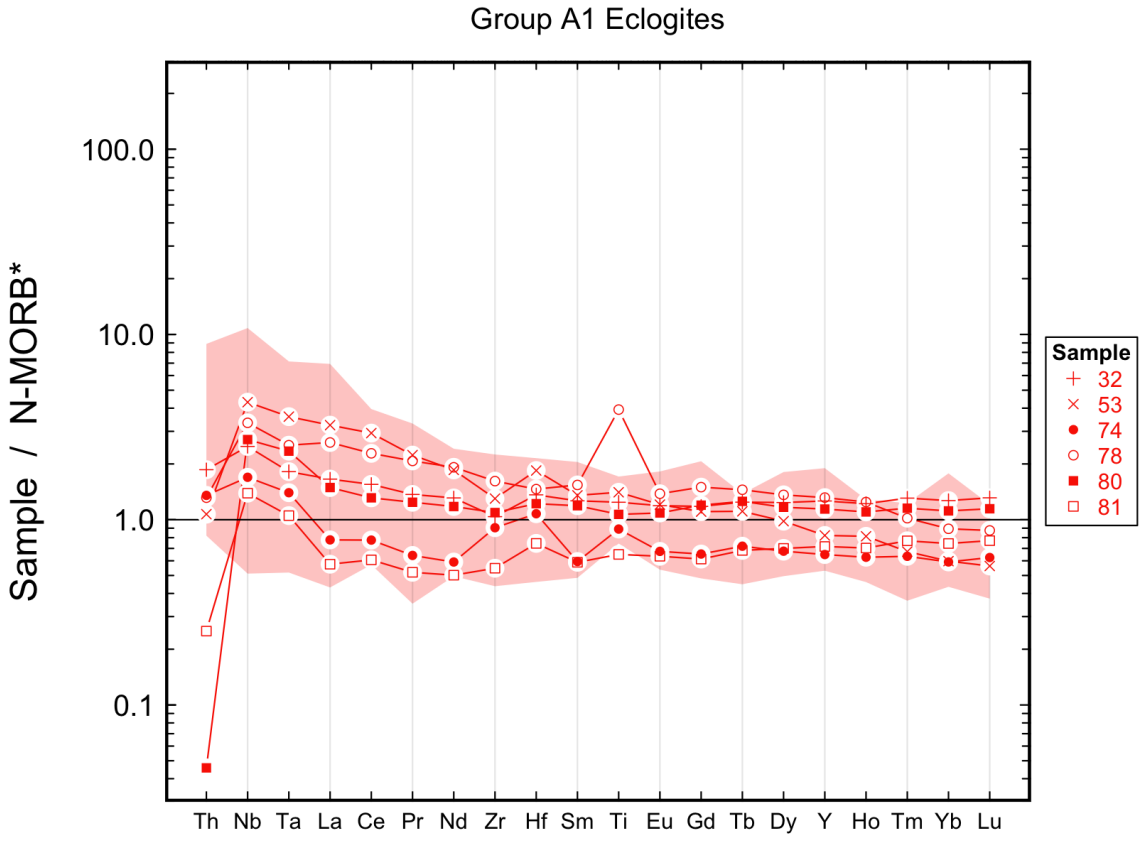

Figure 3.7: A multi-element diagram for group A1 eclogites normalised to N-MORB (Gale et al., 2013). Shaded area is 2σ range of fresh MORBs from PetDB. Elements arranged in order of increasing compatibility during mantle melting from left to right.

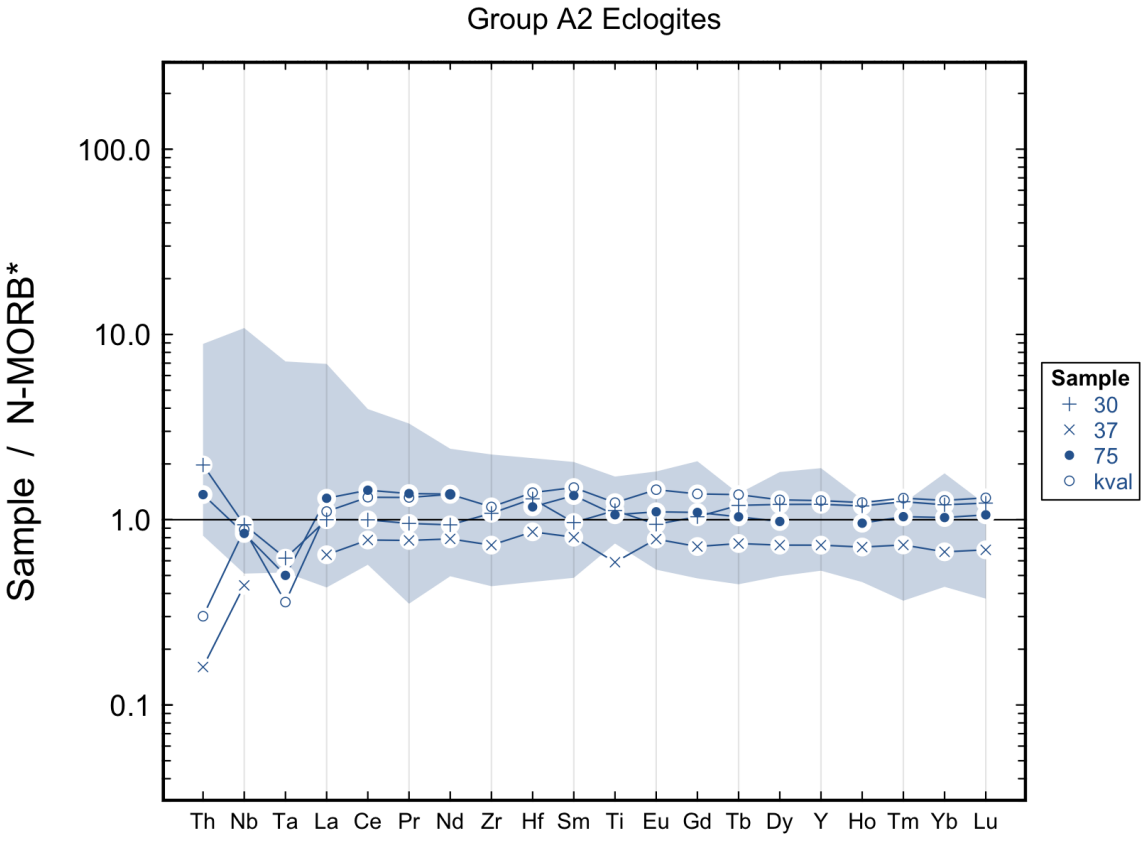

Figure 3.8: A multi-element diagram for group A2 eclogites normalised to N-MORB (Gale et al., 2013). Shaded area is 2σ range of fresh MORBs from PetDB. Elements arranged in order of increasing compatibility during mantle melting from left to right.

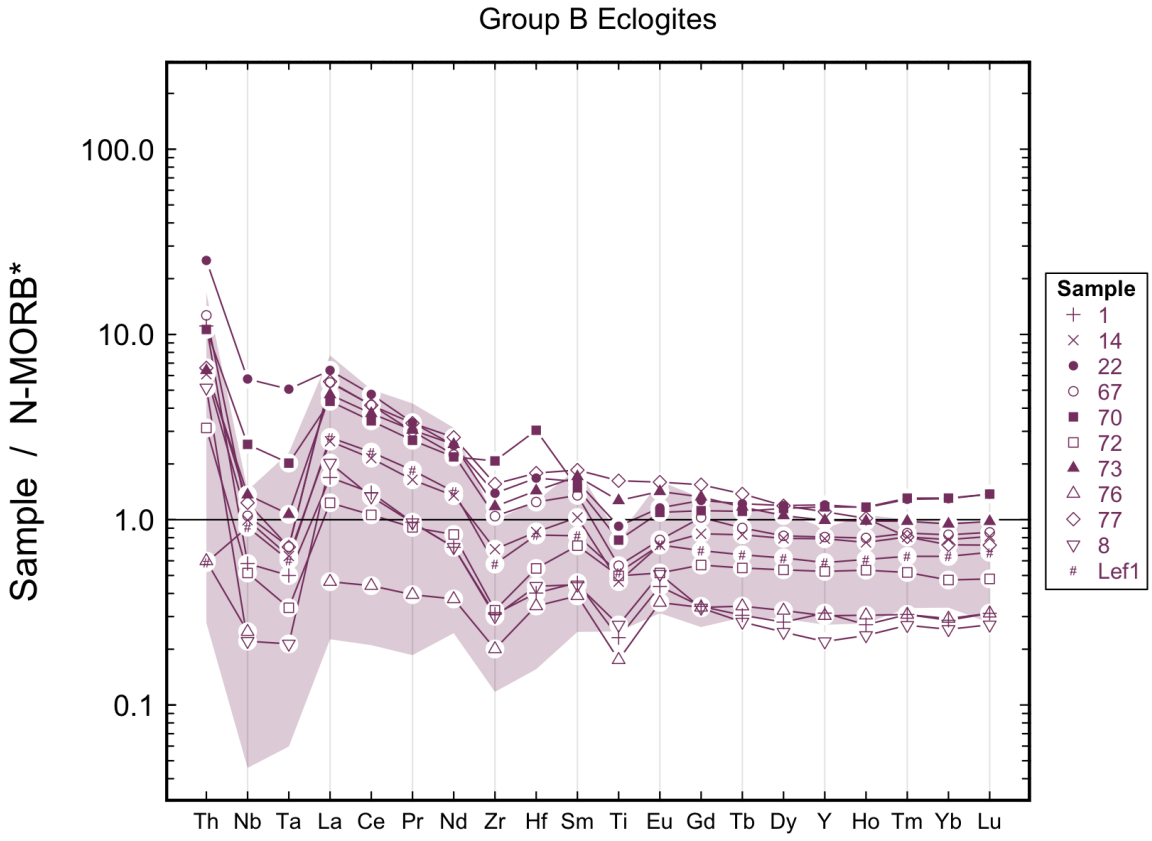

Figure 3.9: A multi-element diagram for group B eclogites normalised to N-MORB (Gale et al., 2013). Shaded area is 2σ range of fresh VABs from PetDB. Elements arranged in order of increasing compatibility during mantle melting from left to right.

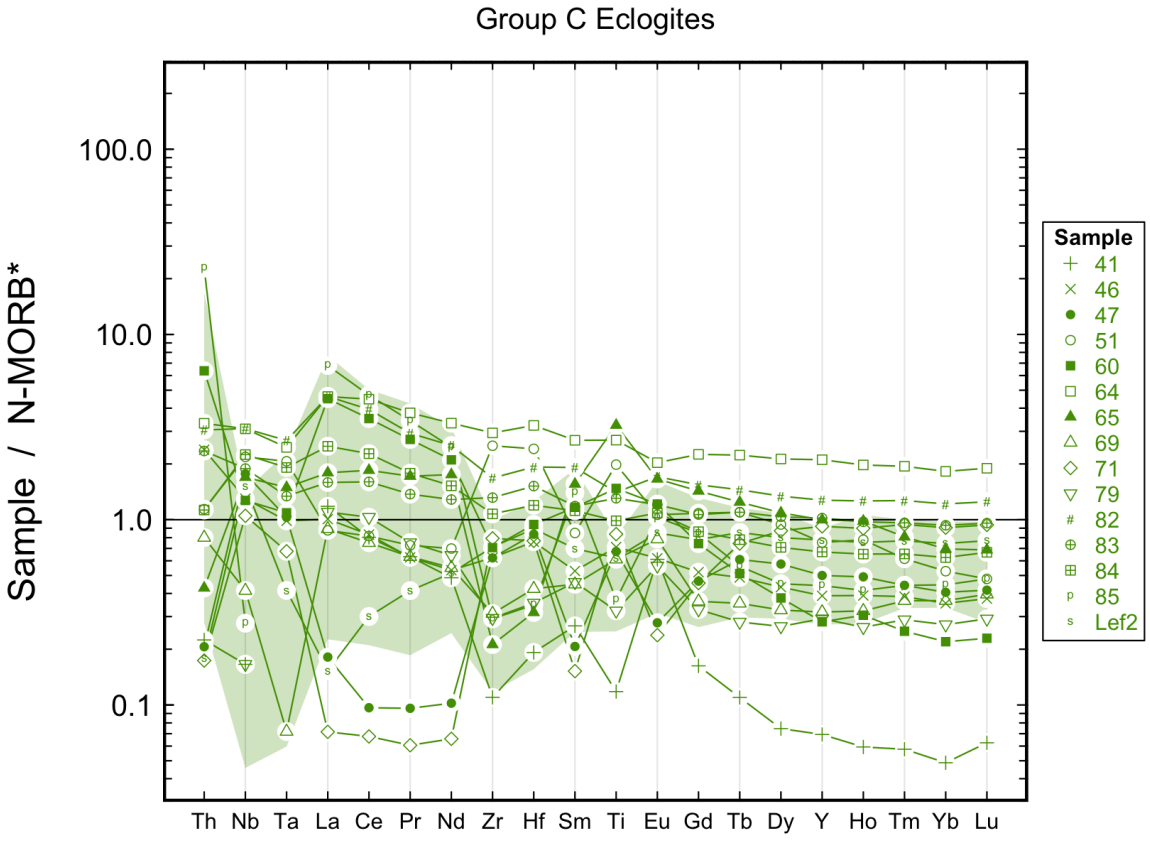

Figure 3.10: A multi-element diagram for group B eclogites normalised to N-MORB (Gale et al., 2013). Shaded area is 2σ range of fresh VABs from PetDB. Elements arranged in order of increasing compatibility during mantle melting from left to right.

The majority of samples with coherent trace element signatures fall into group B. Samples in this group are characterised by incompatible element enrichment (i.e. $(La/Sm)_n > 1$) with prominent negative anomalies in Nb, Ta, Zr, and Ti. Thorium is enriched over N-MORB ($Th_n \gg 1$) and La ($[Th/La]_n > 1$) but not anomalously so relative to the slope defined by LREE enrichment. Nb and Ta have strong negative anomalies, with absolute concentrations mostly equal to or less than N-MORB. Other HFSE anomalies (e.g. Zr and Ti) are less pronounced, however concentrations are often less than N-MORB. HREEs (including Y) are smooth and generally depleted relative to N-MORB. Signatures and abundances appear similar to those of many island arc basalts (IABs).

Group C

A significant number of often extensively retrogressed samples have irregular and seemingly non-systematic multi-element signatures. Irregular abundances for trace elements appears to mostly affect the REEs and not HFSEs. Group C samples are therefore not included in discrimination diagrams that employ REEs. Indeed, we must also be more skeptical of HFSE concentrations for samples in this group.

The concentrations of large ion lithophile elements (LILEs) (e.g. Ba, Rb, K, and Sr) along with Pb and U, are considered to be relatively mobile during metamorphism. As such, these elements are best discussed in the context of the quantative assessment of element mobility (section 3.3.3, page 125).

3.3 Discussion

3.3.1 Correlation Analysis: Identifying immobile trace elements

The overall mobility of any element during subduction is sensitive to four main variables: phase stabilities of important controlling minerals; physical and geochemical properties of vector fluids; fluid/rock ratios; and fluid flow dynamics (e.g. Xiao et al., 2013). Given the complex dependency of element mobility, there has understandably been ongoing debate surrounding the behavior of both major and trace elements elements during subduction. Although the debate is far from settled,

recent studies have found that both HFSEs and REEs may be considered largely immobile during metamorphism up until the eclogite facies (e.g. Xiao et al., 2013, 2012; EL Korh et al., 2009; Volkova et al., 2009; Spandler et al., 2007; Munker et al., 2004; Spandler et al., 2004, 2003; Tribuzio et al., 1996). It is also becoming apparent that elements found to be enriched over MORB in arc magmas (e.g. Ba, Th, Cs, LREEs) may be mostly derived from subducted sediments (e.g. Plank, 2005) and not from the underlying basaltic slab. Regardless of one's opinion on the specific sources of mobilised elements, it is clear that element mobility is highly dependent on local geological conditions, and therefore we must treat suites of samples on a case-by-case basis.

One of the most effective ways of investigating element behavior in a suite of samples is to conduct a correlation coefficient analysis. Highly correlated pairs of elements suggest similar geochemical behavior during a variety of magmatic and metamorphic processes. We may quantitatively assess likely element fluid mobilities in metamorphosed samples by comparing elements often cited as having very low mobility (e.g. HFSEs) with subject elements of similar compatibility in magma genesis yet of unknown fluid mobility (e.g. Nui, 2004; Xiao et al., 2012). On the assumption that chosen HFSEs are indeed immobile, a statistically significant correlation with a subject element therefore indicates both have experienced limited mobility. A more conservative conclusion would be that both have experienced *similar* mobility.

There is evidence to support these inferred mobilites with respect to the transition of mafic rocks to eclogite. Mørk and Brunfelt (1988) published some of the earliest support for country rocks being the protoliths for some Norwegian eclogites, by showing that olivine gabbros on Flemsøy had transformed into eclogite without significant changes to their LREE inventory. In the more recent literature, there is now relatively strong evidence that argues against the significant liberation of LREEs, LILEs, and many other trace elements during the subduction related transformation of many mafic rocks into eclogite (Miller et al., 2007, e.g.). Specifically, several key minerals common to elcogite mineral assemblages have been shown to host and preserve many of these elements during and after the crystallisation of eclogite. For example, zoisite and clinozoisite (Sr, Pb, U, Th and LREEs), apatite (Sr, Pb, REEs),

phengite (Cs, Rb, Ba), garnet (Y, HREEsm Sc), rutile (Nb, Ta, Ti) and Zircon (Zr, Hf) (e.g. Miller et al., 2007; Messiga et al., 1995; Spandler et al., 2003, 2004; Zack et al., 2002b, 2001; Tribuzio et al., 1996, amongst others).
To test this type of analysis we used the HFSEs Nb, Zr and Y as proxies for a range of other trace elements with varying degrees of compatibility in mantle melting. Figure 3.11 shows calculated correlation coefficients plotted as lines on a multi-element style plots. From these plots we can suggest the following:

- Nb, Ta, Zr, Hf, Ti, Y, REEs and U in group A samples are immobile, whereas Th, Rb, Ba, K, Sr and Pb are mobile.
- Ba, Th, U, and REEs are immobile and Rb, K, Pb, and Sr appear to be mobile in group B eclogites.
- HFSEs (excluding Th) and heavy rare earth elements (HREEs) seem immobile, and LILEs, Th and LREEs mobile in group C eclogites.

We can study relative mobilities further by constructing correlation coefficent matrices (Figure 3.12). These matrices identify coherent behavior amongst immobile (Nb-Ta, Zr-Hf and Zr-Y) and mobile (Rb, Ba and K) elements. Furthermore, they highlight interesting differences between element correlations in each eclogite group. For instance, Mo has been suggested as an immobile element similar to Nb (Fitton, 1995) due to its similar ionic radius (Mo^{4+} = 0.65 Å and Nb^{5+} = 0.64 Å, Shannon, 1976). Unsurprisingly, Mo and Nb are significantly correlated in group A (r = 0.77) and C (r = 0.6). However, Figure 3.12 shows that in group B eclogites Mo correlates significantly with the *mobile* elements Rb, K and Ba as well as supposedly *immobile* Th and U, but not with Nb as one might expect. Similarly, strong correlations between Mo and U are not surprising when one considers that Mo and U often combine to form a variety of oxidised and non-oxidised compounds which may be stable to ultra-high grade conditions (Okamoto, 2012; Effenberg and Ilyenko, 2007). Furthermore, in group B samples U correlates significantly with both HFSEs *and* the LILEs Ba and Rb. This might indeed suggest that the mobilisation of these elements may be rather limited.

The evidence from the correlation analyses above suggest that the majority of HFSEs may be reliably used in discriminant analysis, with the exception of Th which only

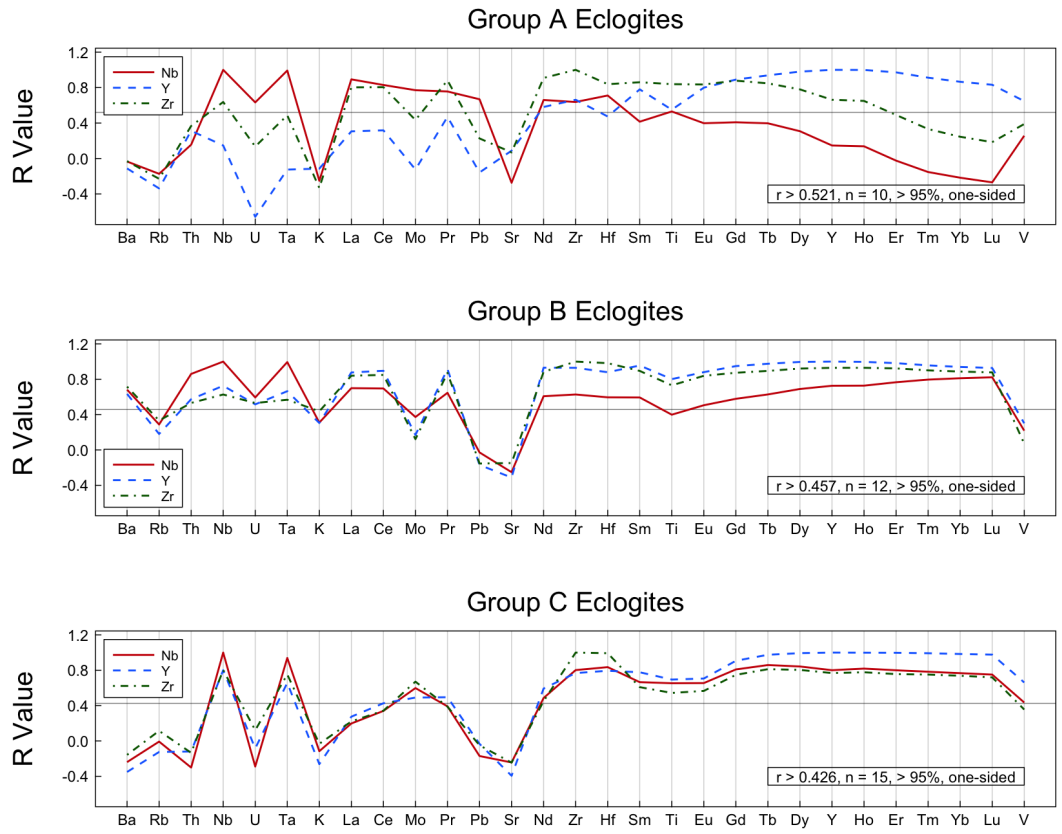

Figure 3.11: Correlation coefficient diagrams of Nb, Zr and Y with other trace elements for Norwegian eclogites. Methodology from Nui (2004); Xiao et al. (2012). Elements ordered from left to right in order of increasing compatibility during mantle melting. The HFSEs Nb, Zr and Y are chosen to represent different incompatibilities and are assumed to be immobile during even high grade metamorphism. The horizontal line represents the minimum Pearson product-moment correlation coefficient (r) above which correlations are considered statistically significant at the 95 % level. Those elements that plot above the line are considered immobile, and those below it mobile.

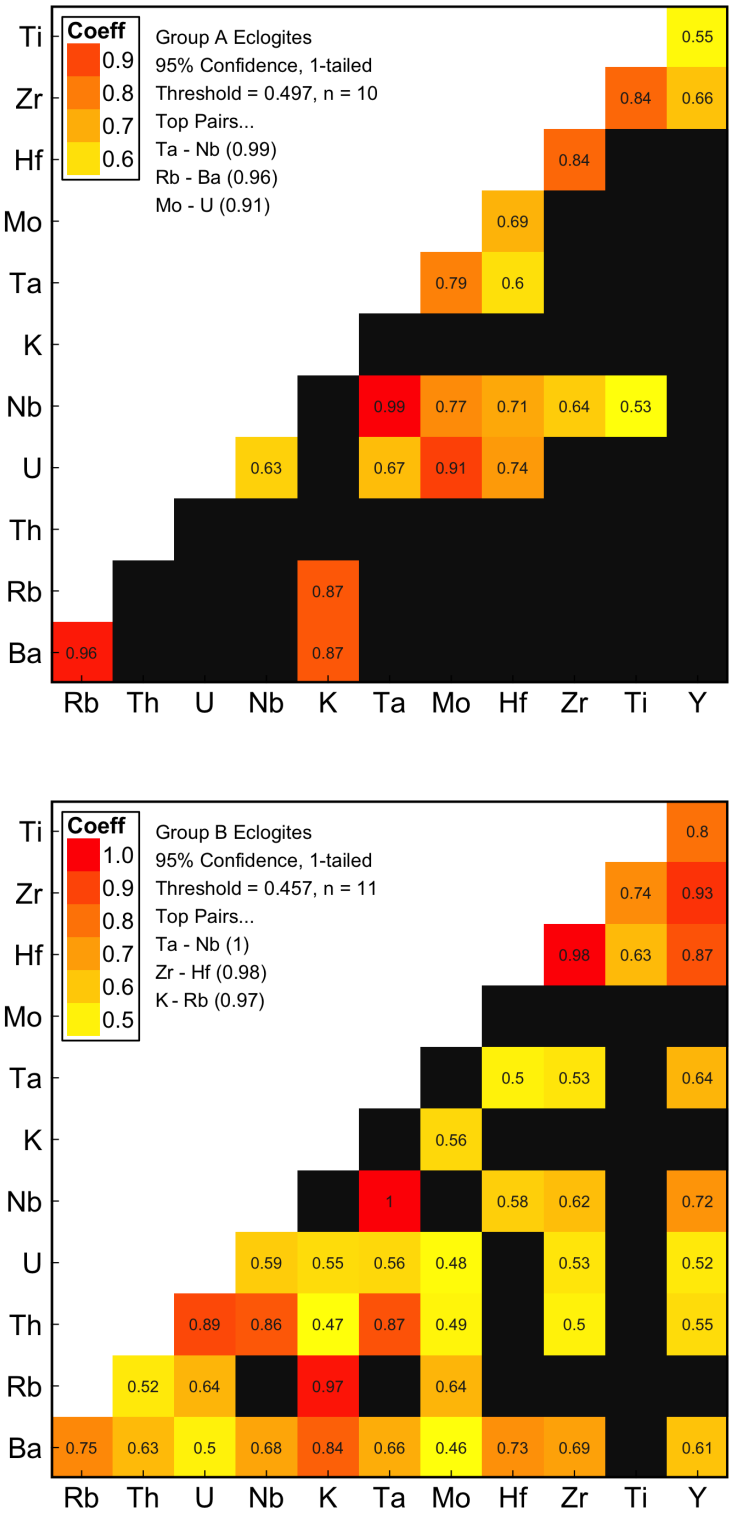

Figure 3.12: Continued...

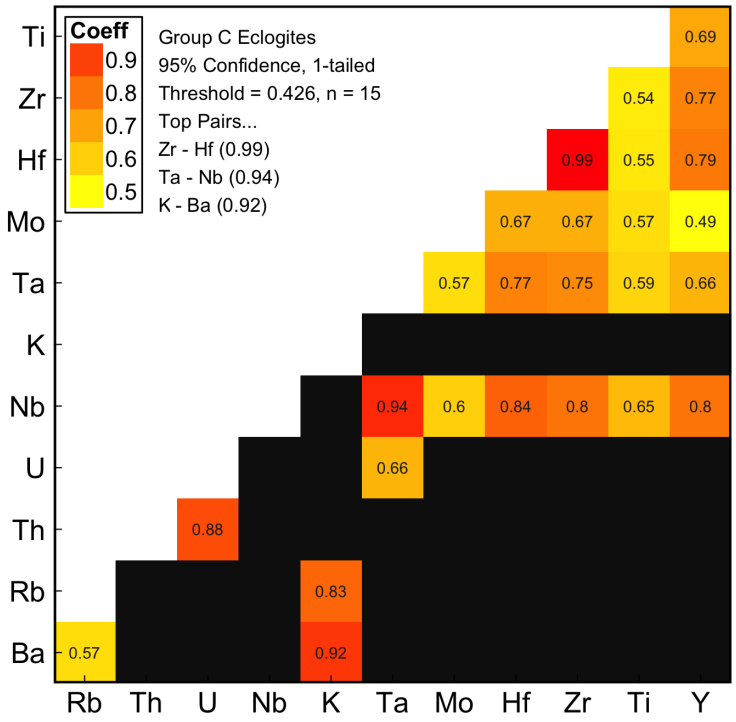

Figure 3.12: Correlation coefficient grids for a selection of trace elements: a) group A eclogites; b) group B eclogites; c) group C eclogites. Coloured tiles indicate significantly correlated, and black tiles not significantly correlated pairs respectively, based on 95% confidence one sided test.

appears to be reliable with respect to group B eclogites. LREEs appear largely immobile, with the exception of the majority of group C eclogites where their concentrations have clearly been perturbed. HREEs are consistently and significantly correlated with Zr and Y suggesting that they too are also largely immobile.

3.3.2 Discriminant Analysis

This study uses trace element discriminant analysis to deduce the likely tectonic setting in which protolith magmas were generated. In order to do so, we must assume that the elements used in the discriminant analysis have remained largely immobile, as indicated by the correlation analysis described above.

Linear Discrimination Diagrams of Agrawal et al. (2008)

The linear discrimination diagrams of Agrawal et al. (2008) employ logarithmic transformations of the elemental ratios La/Th, Sm/Th, Yb/Th and Nb/Th into several so-called Discrimination Factors (DFs) which have been shown to be capable of effectively identifying tectono-geochemical associations of even highly metamorphosed rocks including eclogites. Since the correlation analysis above suggests Th in group A and C eclogites might be relatively mobile, we must remain cautious when interpreting these discrimination diagrams. Nonetheless, in Figures 3.13-3.16 all but two group B samples are identified as IABs. Group B samples WGR-76 and WGR-LEF1 consistently plot away from the rest in the group, always closer to mean N- and E-MORB compositions. The remaining samples and groups are generally identified as being MORB-like, where the samples appear to define linear trends involving N-MORB, E-MORB, and VAB. Agrawal et al. (2008) suggests that such linearities are indicative of mixing of magma types. Figures. 3.13-3.16 therefore suggest that eclogite protolith magmas may have been formed in a back-arc setting where island arc magmas and MORB-type magmas were created in close temporal and physical proximity.

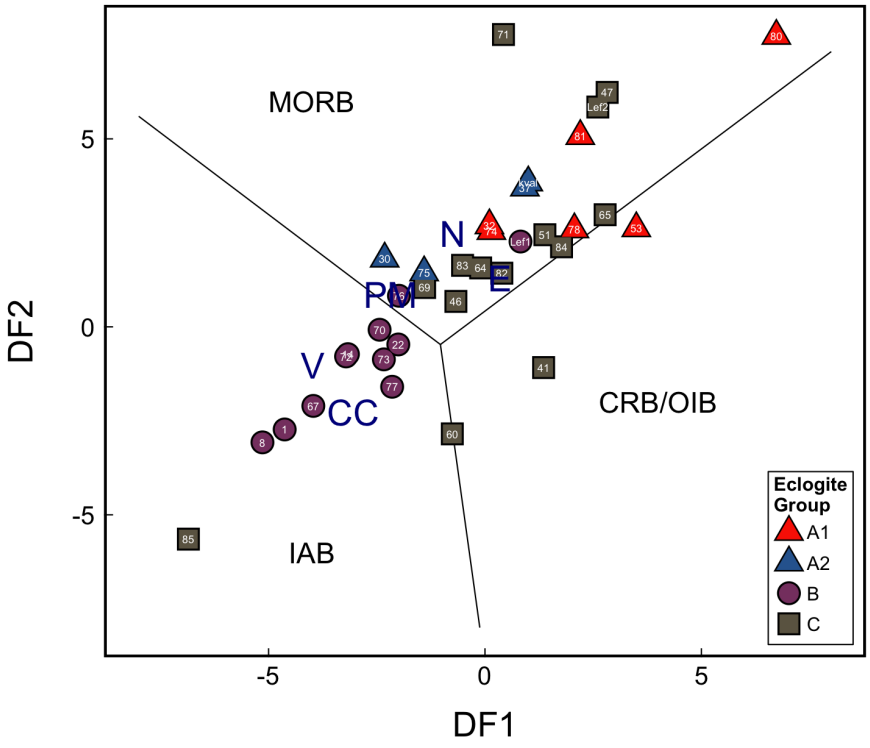

Figure 3.13: Linear discrimination diagram of (Agrawal et al., 2008, Figure 1) with fields for mid-ocean ridge basalt (MORB), island arc basalt (IAB), continental rift basalt (CRB), and ocean island basalt (OIB). Abbreviations: CC, continental crust; E, E-MORB; IAB, Island Arc Basalt; N, N-MORB, PM, primitive mantle; V, volcanic arc basalt. DF1 = 0.3518 $\log_e$(La/Th) + 0.6013 $\log_e$(Sm/Th) – 1.3450 $\log_e$(Yb/Th) + 2.1056 $\log_e$(Nb/Th) – 5.4763; DF2 = –0.3050 $\log_e$(La/Th) – 1.1801 $\log_e$(Sm/Th) + 1.6189 $\log_e$(Yb/Th) + 1.2260 $\log_e$(Nb/Th) – 0.9944. The data suggest that group A and C eclogites are mostly of MORB-affinity, whilst group B eclogites are mostly of IAB affinity.

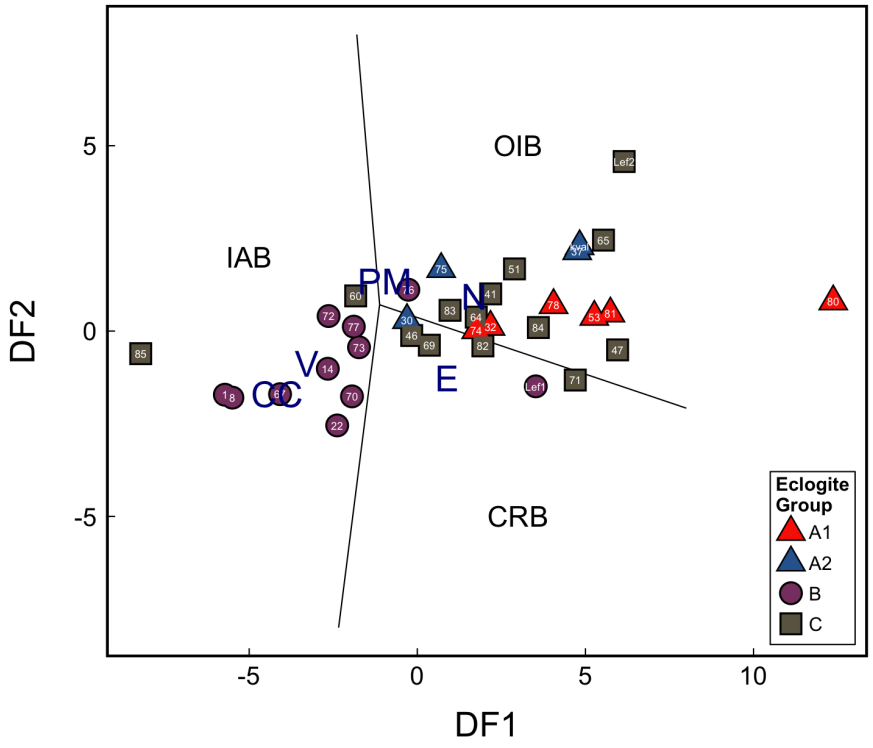

Figure 3.14: Linear discrimination diagram of (Agrawal et al., 2008, Figure 2a) with fields for island arc basalt (IAB), continental rift basalt (CRB) and ocean island basalt (OIB). Abbreviations: CC, continental crust; E,E-MORB; IAB, Island Arc Basalt; N, N-MORB, PM, primitive mantle; V, volcanic arc basalt. DF1 = 0.5533 $\log_e$(La/Th) + 0.2173 $\log_e$(Sm/Th) – 0.0969 $\log_e$(Yb/Th) + 2.0454 $\log_e$(Nb/Th) – 5.6305; DF2 = –2.4498 $\log_e$(La/Th) + 4.8562 $\log_e$(Sm/Th) – 2.1240 $\log_e$(Yb/Th) – 0.1567 $\log_e$(Nb/Th) + 0.94. Since MORB is lacking in this diagram, group A and C eclogites plot in the fields of OIB and CRB, whereas group B eclogites again mostly plot within the field of IAB

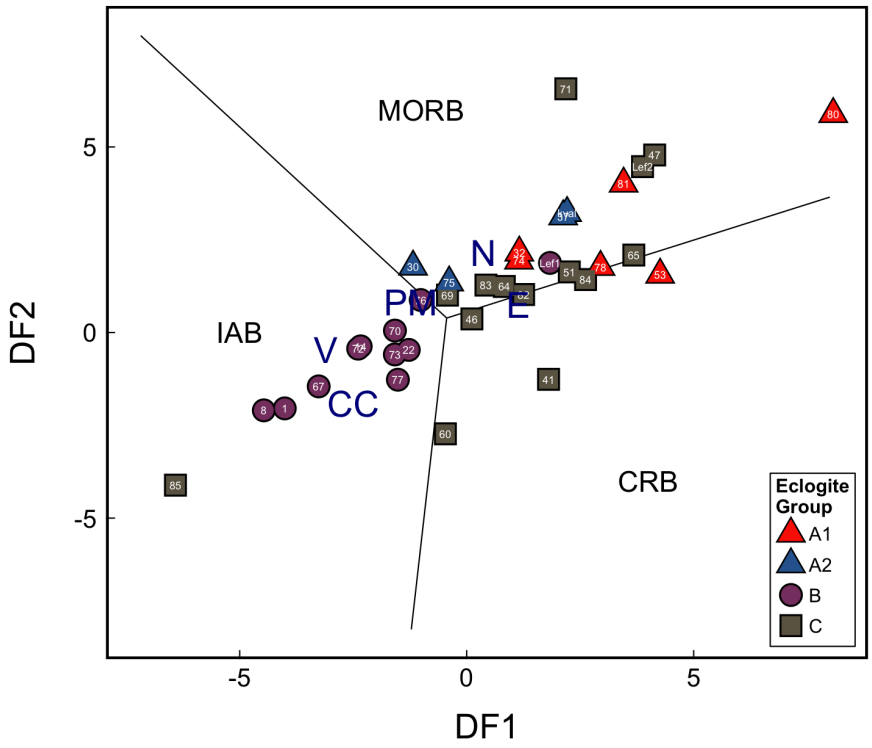

Figure 3.15: Linear discrimination diagram of (Agrawal et al., 2008, Figure. 2b) with fields for IAB, MORB and CRB. Abbreviations: CC, continental crust; E,E-MORB; IAB, Island Arc Basalt; N, N-MORB, PM, primitive mantle; V, volcanic arc basalt. DF1 = 0.3305 $\log_e$(La/Th) + 0.3484 $\log_e$(Sm/Th) – 0.9562 $\log_e$(Yb/Th) + 2.0777 $\log_e$(Nb/Th) – 4.5628; DF2 = –0.1928 $\log_e$(La/Th) – 1.1989 $\log_e$(Sm/Th) + 1.7531 $\log_e$(Yb/Th) + 0.6607 $\log_e$(Nb/Th) – 0.4384. Group B eclogites have indicated IAB affinities whilst group A and C eclogites are mostly in the field of MORB. The data appear to form a rough linear trend with a slope parallel to the MORBCRB boundary.

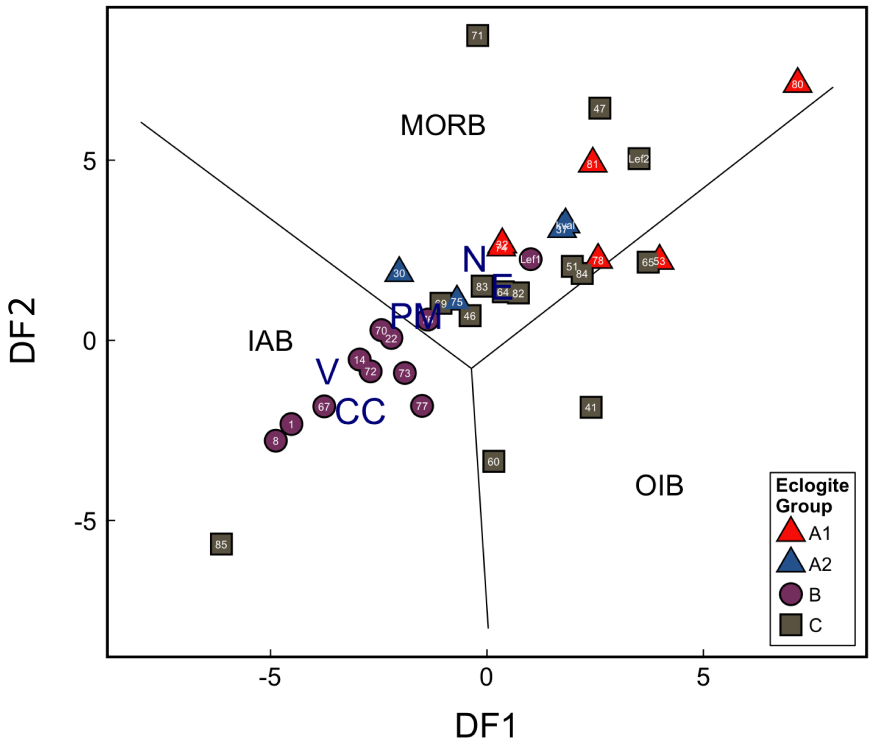

Figure 3.16: Linear discrimination diagram of (Agrawal et al., 2008, Figure 2c) with fields for IAB, MORB and OIB. Abbreviations: CC, continental crust; E,E-MORB; IAB, Island Arc Basalt; N, N-MORB, PM, primitive mantle; V, volcanic arc basalt. DF1 = 1.7517 $\log_e$(Sm/Th) – 1.9508 $\log_e$(Yb/Th) + 1.9573 $\log_e$(Nb/Th) – 5.0928; DF2 = –2.2412 $\log_e$(Sm/Th) + 2.2060 $\log_e$(Yb/Th) + 1.2481 $\log_e$(Nb/Th) – 0.8243. As in Figures 3.13-3.15, group A and C eclogites have apparent MORB-like protoliths, and group B have apparent IAB protoliths.

Nb-Zr-Y

Nb and Zr are widely thought to be amongst the most immobile HFSEs (e.g. Pearce, 1983; Brenan et al., 1994; Staudigel et al., 1996), and thus can remain insensitive to even high grade metamorphism. Both Nb and Zr appear in three discrimination diagrams: Zr/Y vs. Nb/Y (Figure 3.17); a Nb-Y-Zr ternary (Figure 3.18); and bivariate plot of Nb vs. Zr (Figure 3.19).

In Figure 3.17, Nb and Zr are both normalised to the immobile element Y which removes the effects of any fractional crystallisation. This diagram is particularly suited to distinguishing N- and E-MORB using the discriminant Δ Nb (Fitton et al., 1997), but is not suited to differentiating MORB from VAB. Group A1 samples fall mostly within the E-MORB field, and A2 samples plot in a tight cluster in the centre of the N-MORB field. The compositional range of group B samples is large: ΔNb can be both greater and less than 1 such that samples fall well within the field of common VABs as well as E-MORBs and some N-MORBs. Most of group C fall inside the common compositional fields of MORBs and IABs, except for those which have on other plots exhibited anomalously high (WGR-51) or low (WGR-65) Zr concentrations (e.g. Figures 3.18 and 3.24).

In a Zr-Y-Nb ternary (Figure 3.18, after Meschede, 1986) group A1 samples may be classified as so-called transitional MORBs (T-MORBs), whereas group A2 samples plot almost in the centre of the field of N-MORB/IAB. The majority of group B samples plot as IABs with the exception of one sample with high Nb which plots in the field of E-MORB. Group C samples scatter across the MORB, IAT and within-plate basalt (WPB) fields.

On a plot of Nb vs. Zr (Figure 3.19) group A1 plot in the field of E-MORB as represented by Icelandic basalts (i.e. the iceland array (ICE)), with some overlap with the field of OIB. A2 samples again plot in a reasonably tight cluster in the field of N-MORB. As with Figure 3.17, VABs plot over both N- and E-MORBs, and therefore group B samples plot as N- and E-MORBs. Group C eclogites plot in the same area as group A and B eclogites. Within group B and C there exists a clear low Zr population (Zr$<$40 ppm, Group B: WGR-1, -8, -72, -76; Group C: WGR-41, -65, -69, -79 and

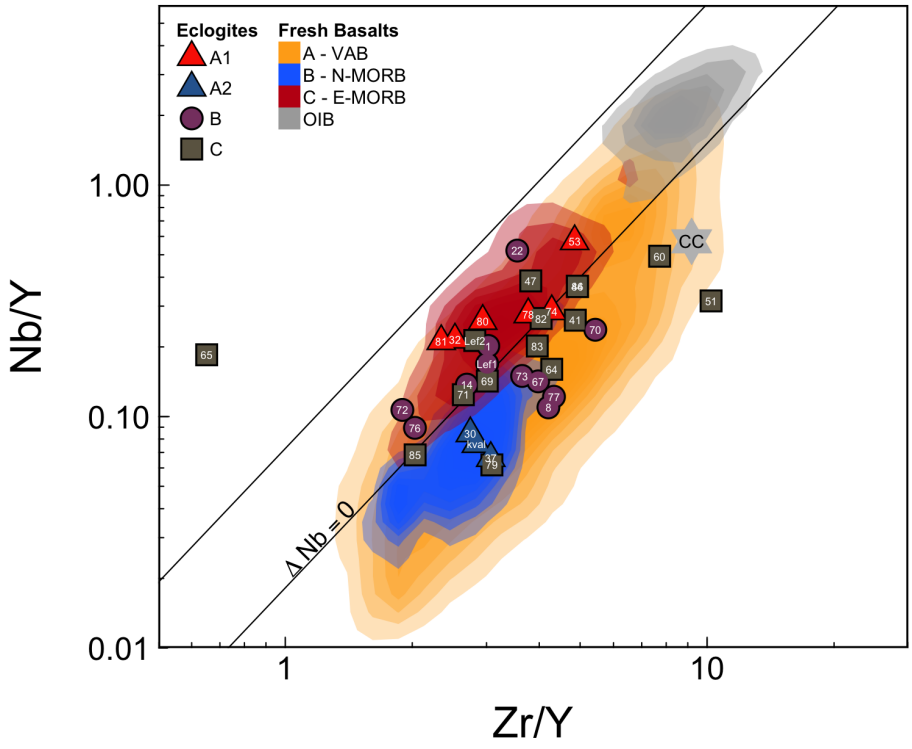

Figure 3.17: Nb/Y vs. Zr/Y variation diagram for Norwegian Eclogite samples (points) and reference basalts (fields). Fields represent calculated Gaussian probabilities and at their edges define 80% probability of the reference data, and are contoured to indicate the spread of data within that probability range. Reference data were taken from PetDB. The lower line represents the parameter ΔNb = 0 which is calculated by ΔNb = 1.74 + log(Nb/Y) - 1.92 log(Zr/Y) as set out by Fitton et al. (1997). The upper line represents the ΔNb limit of most Icelandic Basalts (neovolcanics) (Fitton et al., 1997, 2003). The star represents the bulk continental crust (CC) and is based on values in Rudnick and Fountain (1995) and Barth et al. (2000). Group A1 eclogites are distinctly enriched compared to group A2 samples. All of group A samples and most of group C samples plot in the fields of common MORBs. Note that this diagram is unable to distinguish between MORB and IAB.

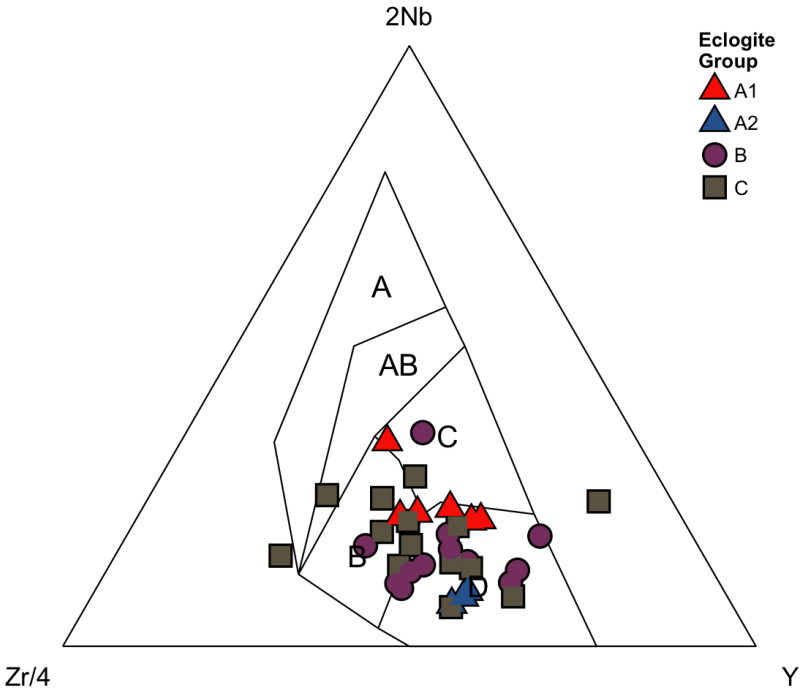

Figure 3.18: The Zr-Nb-Y tectonic discrimination diagram after Meschede (1986). Fields are labelled as: A, within-plate alkali basalts (WPABs); AB, WPABs and within-plate tholeiites (WPTs); B, WPTs; and volcanic arc basalts (VABs); C, E-MORB; D, N-MORB and volcanic arc basalt (VAB). Group A1 eclogites plot with moderately enriched E-MORBs, otherwise known as T-MORB, with slight overlap into the field of within-plate tholeiites (WPTs) and volcanic arc basalts (VABs). The position of most group B samples in this plot is consistent with a VAB origin.

-85) which also tend to have lower Nb (most have Nb<3 ppm).

Zr - Y

Pearce and Norry (1979) showed that Zr/Y was an effective discriminant between IAB, MORB and WPB. Figure 3.20 shows that A1 and A2 eclogites have typical MORB compositions. Group B samples plot as either VAB or, with moderately elevated Zr/Y and Zr, as WPBs. Figure 3.21 uses the same axes to use reference fields constructed from basalts in the PetDB.org geochemical database. It was found, however, that Zr/Y did not discriminate between oceanic basalts and WPBs well. Figure 3.21 does show that the combined field of N- and E-MORBs extends over a grater range of Zr/Y than does the field of MORB in Figure 3.20. As such, group A1 and A2 eclogites plot within the fields of E- and N-MORB respectively. Most Group B eclogites can be said to have E-MORB-like Zr/Y, however one must note that several group B samples do have Zr outside the range of most MORBs. Similarly, most group C samples have MORB-like Zr/Y albeit with Zr often lower than most MORBs.

ΔNb - La/Sm

ΔNb (see Fitton et al., 1997) and primitive mantle normalised La/Sm (i.e. La/Sm_n) provide two different effective ways of measuring enrichment of MORB-like rocks, but are not effective at discriminating other basalt types. Figure 3.22 shows ΔNb versus La/Sm_n for eclogite groups A and B. Group A1 samples plot largely within the field of most E-MORBs and group A2 samples plot inside the field of fresh N-MORB. Most group B samples have La/Sm_n higher than MORB and more typical of continental crust, yet have ΔNb within the range of N- and E-MORBs. Group C samples are omitted from Figure 3.22 since their La concentrations are assumed to have been significantly altered during metamorphism.

La-Y-Nb

The La-Y-Nb discrimination diagram of Cabanis and Lecolle (1989) shown in Figure 3.23, is effective at discriminating between IATs and MORBs (i.e. La/Y), as well as degrees of MORB enrichment (i.e. Nb/Y). A1 samples plot in the field of moderately enriched MORBs, whereas group A2 samples with their notably lower Nb/Y plot inside the field of N-MORB. Group B samples plot mostly within the field

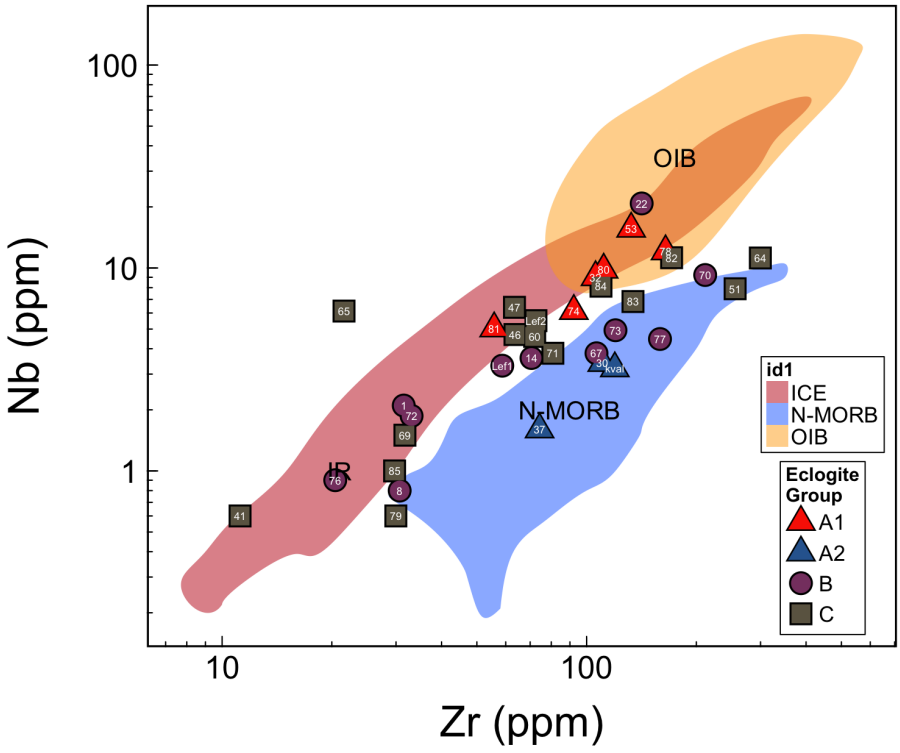

Figure 3.19: Nb vs. Zr with data fields for fresh N-MORB, E-MORB/iceland array (ICE) and OIB compiled by Fitton and Godard (2004) using data from the literature. Group A1 eclogites unsurprisingly fall in the E-MORB/ICE field, whilst group A2 samples plot well within the field of N-MORB. Group B eclogites show a somewhat bimodal distribution of samples observed elsewhere (see figures: 3.20, pg. 110; 3.22, pg. 112; and 3.30, pg. 124): one group plots between group A1 and A2 samples in the N-MORB and E-MORB fields; the other has lower Nb and Zr plotting towards the lower end of the iceland array (ICE). Group C eclogites also appear to mimic this slight bimodality, particularly pronounced in Zr concentrations.

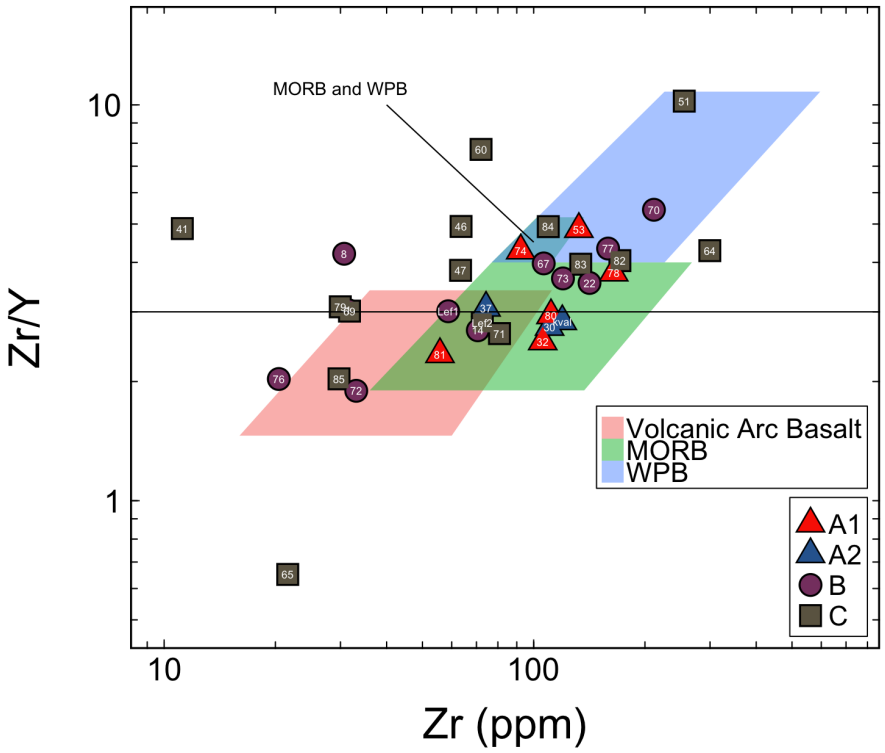

Figure 3.20: Zr/Y vs. Zr discrimination diagram (after Pearce and Norry, 1979). Group A eclogites plot largely in the field or MORBs. Group B eclogites plot both in the field of VABs suggesting arcs involving only oceanic crust, and WPBs suggesting continental arcs. Group C eclogites again have a highly variable distribution which does not suggest a clear common protolith.

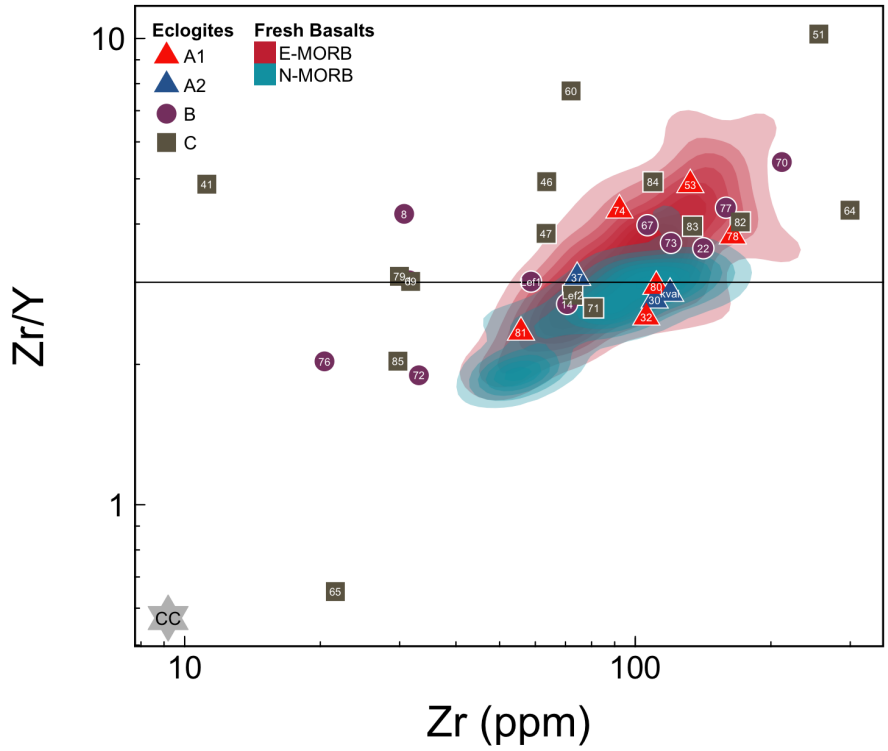

Figure 3.21: Zr/Y vs. Zr variation diagram. Coloured fields are plotted from data from the PetDB database, showing the field of 80 % confidence based on Gaussian density for N- and E-MORB. The field of VABs largely coincides with MORB and is therefore not shown. Unlike Figure 3.20 MORBs cover a much greater range in Zr/Y and Zr. Group A1 and A2 eclogites plot within the fields of N-MORB and E-MORB respectively.

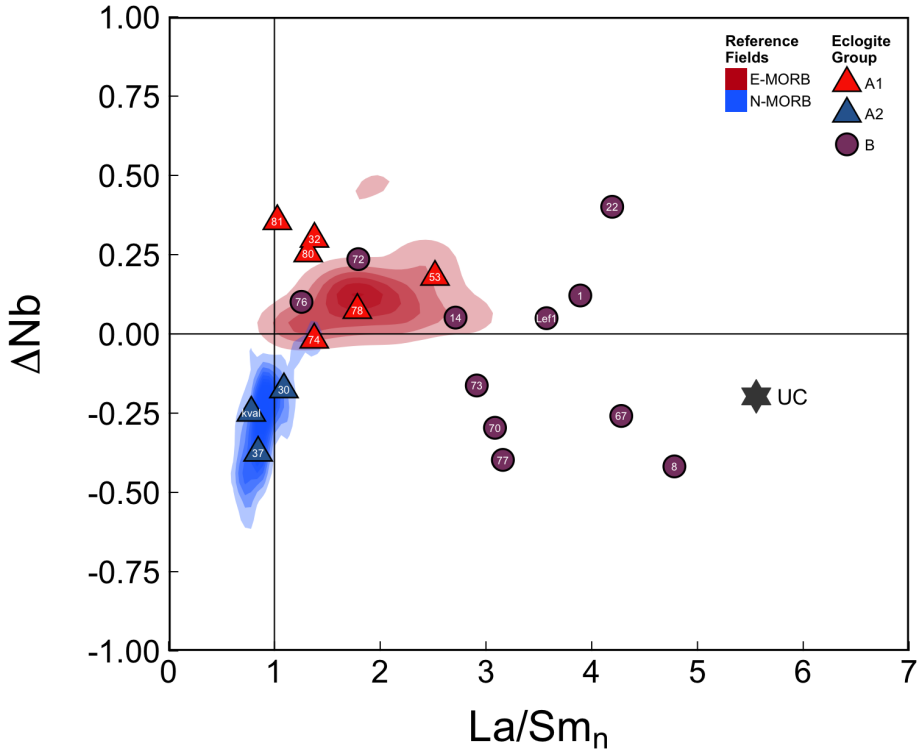

Figure 3.22: ΔNb plotted against $(La/Sm)_n$ for Norwegian eclogites, with reference fields for fresh E-MORB and N-MORB constructed using data from PetDB and Fitton (2007). ΔNb is a parameter defined by Fitton et al. (1997) and is calculated as 1.74 + log(Nb/Y) - 1.92 log(Zr/Y). $(La/Sm)_n$ is the primitive mantle normalised La/Sm (using values of McDonough and Sun (1995)). The vertical line at $(La/Sm)_n$ = 1 separates LREE-enriched samples ($(La/Sm)_n>1$) and LREE-depleted samples ($(La/Sm)_n<1$). Group A1 eclogites mostly have clearly *positive* ΔNb and $(La/Sm)_n>1$, whereas group A2 eclogites have clearly *negative* ΔNb and $(La/Sm)_n<1$. Most group B eclogites have $(La/Sm)_n>2.5$, outside of the range of both N- and E-MORB. Group C are not plotted since their La concentrations are thought to have been significantly altered during metamorphism.

of calc-alkaline and transitional IATs. As with Figures 3.13-3.16, Figure 3.23 also appears to suggest mixing between a calc-alkaline island arc magma, N-MORB and T-MORB magmas. Groups C samples are omitted since their La concentrations are thought to have been significantly peturbed during metamorphism.

Zr/La - Nb/La

The ratios Zr/La and Nb/La provide alternatives to ΔNb as a measure of MORB enrichment. Unlike ΔNb, however, Nb/La is also capable of making some distinction between arc basalts and MORBs. This is because arc basalts are generally depleted in Nb relative to La. A plot of these two ratios (Figure 3.24) therefore provides effective discrimination of the eclogite groups which have so far indicated MORB- and arc-like protoliths. A1 samples plot largely in the field of E-MORB, and A2 samples plot in a tight cluster in the field of N-MORB. Group B samples have significantly lower Nb/La and Zr/La and therefore plot together with common fresh arc volcanic rocks (VABs). Once again, groups C samples are omitted since La concentrations in them are not considered reliable.

Nb/Hf vs. Nb

A plot of Nb/Hf vs Nb (Figure 3.25, pg. 116) can discriminate between MORBs and VABs, and highlights some interesting properties of our samples. A1 rocks have high Nb/Hf and plot in a field occupied by MORBs and VABs. A2 samples have much lower Nb/Hf (0.8-1.1) than do fresh N-MORBs (Nb/Hf$>$2). Nb in A2 samples has elsewhere been shown to be remarkably N-MORB-like (e.g. Figures 3.17-3.19, pg. 106-109) and therefore elevated Hf concentrations appear to be responsible for the low Nb/Hf. Unusually high Hf could also explain the positions of A2 eclogites in the Th-Hf-Ta ternary (Figure 3.28, pg. 121) discussed below, as well as lower than expected Zr/Hf (Figure 3.27, pg. 119). Group B also have low Zr/Hf which are almost exclusively subchondritic.

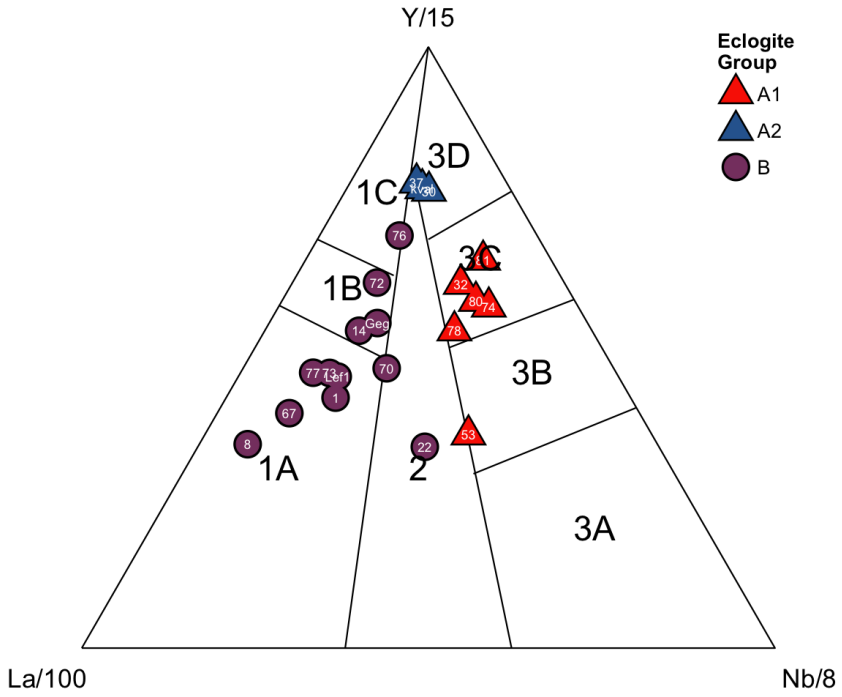

Figure 3.23: Norwegian eclogites plotted on top of a La-Y-Nb ternary (Cabanis and Lecolle, 1989, after). Fields are: 1A, calc-alkali volcanic arc basalts; 1B transitional island arc basalts; 1C, tholeiitic island arc basalts; 2, continental basalts and back-arc basin basalts (poorly defined); 3A intercontinental alkali basalts; 3B, E-MORB; 3C, T-MORB; 3D, N-MORB. As indicated in a variety of other diagrams, group A1 samples are T-/E-MORB like, group A2 samples are N-MORB like, group B samples are (calc-alkaline) IAB-like. Groups C samples are omitted since their La concentrations are thought to have been significantly peturbed during metamorphism.

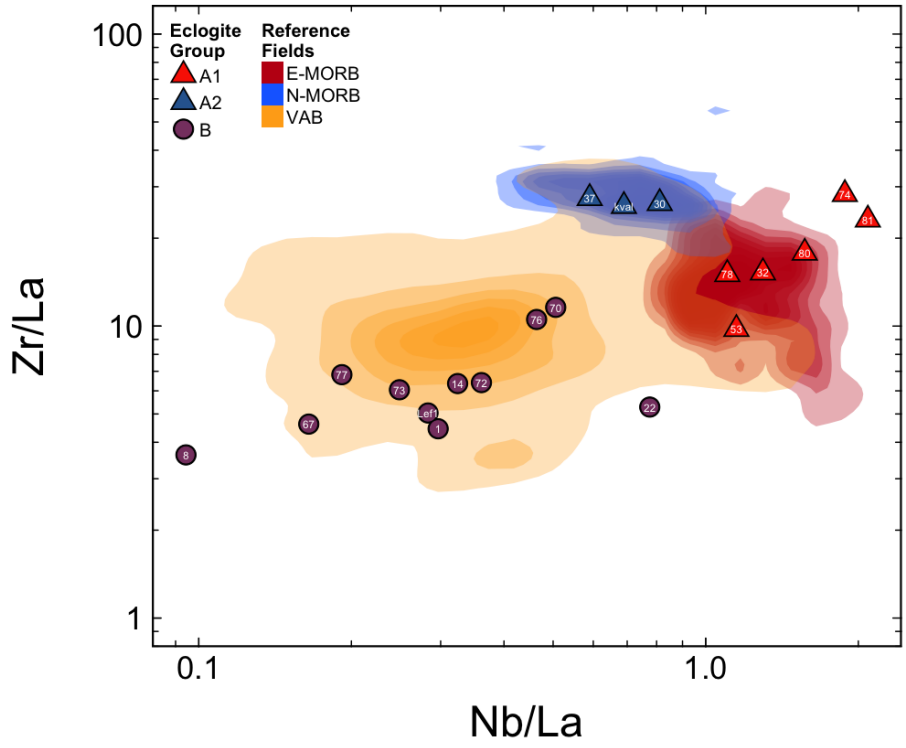

Figure 3.24: Zr/La-Nb/La discrimination diagram for VAB, E-MORB and N-MORB. The coloured fields represent kernel density estimates for fresh basalts from the literature (PetDB.org). This discrimination diagram separates the eclogite groups well since Nb/La and Zr/La reflect the features of the multi-element patterns used to define them. The distinctive negative Nb anomaly of VABs separates IAB from MORB, whereas Zr/La separates N-MORB from the more enriched E-MORB and of course VAB. Group A1 eclogites conform relatively well with a E-MORB protolith, whilst group A2 eclogites plot in a tight cluser in the centre of a field of fresh N-MORB. Group B eclogites have a larger scatter, as do VABs which define a similar field.

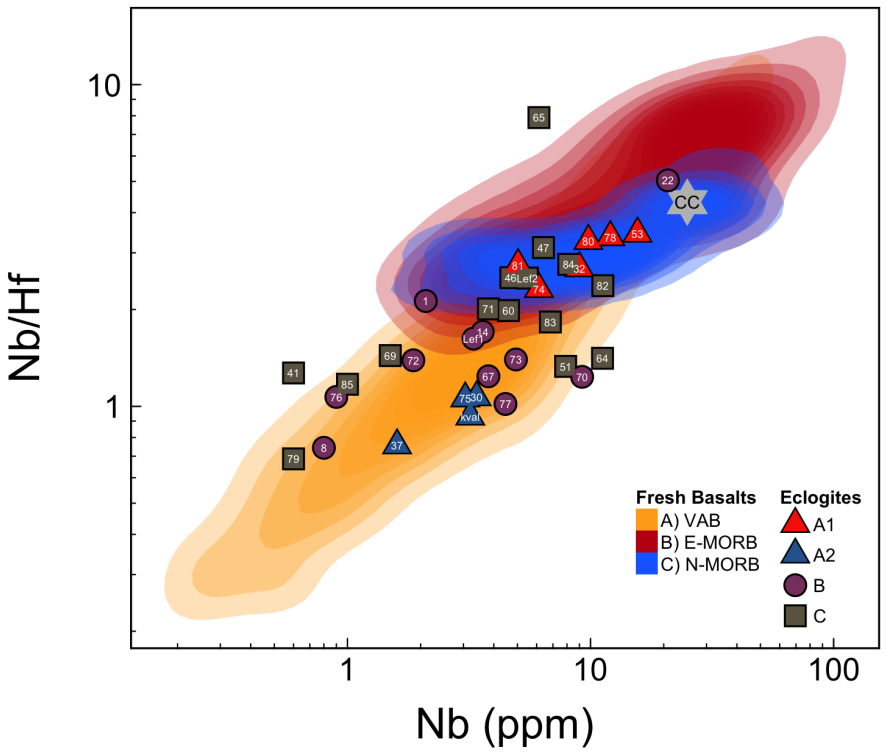

Figure 3.25: Bivariate plot of the immobile elements Hf and Nb in the plot configuration of Nb/Hf vs. Nb. Coloured fields for E-MORB, N-MORB and VAB were constructed using data downloaded form the online PetDB archive. This diagram is capable of a moderate distinction between VABs and MORBs. Some overlap between the MORB and VAB does occur, but the plot still shows several important features in the data. A MORB-like protolith for A1 eclogites is appropriate here, since A1 eclogites plot in a relatively tight cluster in the MORB field. Group A2 eclogites plot outside the MORB field, despite being elsewhere identified as likely having MORB-like protoliths. Group B eclogites stray from the field of MORB alone, and can be consistently explained as having IAB-like protoliths.

Nb and Ta

A plot of Nb/Ta against Nb (Figure 3.26) is a not particularly useful discrimination diagram, but it does highlight the important trace element ratio Nb/Ta. A1 samples have chondritic to slightly subchondritic Nb/Ta. Concentration of Ta in group A2 samples is low, and was only above detection limits for two A2 samples. Those A2 samples unsurprisingly have relatively high (suprachondritic) Nb/Ta, however the lack of data makes it hard to characterise A2 Nb/Ta in general. Group B have mildly subchondritic to mildly suprachondritic Nb/Ta which may be considered largely chrondritic on average. An important feature of this diagram is that none of the eclogites has Nb/Ta in the range of average continental crust. This is particularly important for group B samples as it provides good evidence that continental crust has not contaminated the samples during either magma genesis, or infiltration of crustally-derived partial melts during metamorphism.

Zr and Hf

A plot of Zr/Hf versus Zr (Figure 3.27) is also not a particularly useful tectonic setting discrimination diagram, but this too illustrates some important features in the data. A1 samples have highly variable Zr/Hf (28-46), whereas A2 samples are almost exactly chondritic. Group B Zr/Hf is chondritic to significantly subchrondritic, but largely coherent with the large range in Zr/Hf exhibited by fresh VABs. Group C mimic the scatter of group A and B combined.

Low Zr/Hf ratios may be explained by high concentrations of Hf in some samples as highlighted in Figure 3.25, particuarly in A2 eclogites. However, multi-element plots (e.g. Figure 3.7) show that Zr appears to be slightly depleted relative to similary compatible elements. Furthermore, the Zr/Hf ratio as seen on such multi-element diagrams shows that Zr/Hf tends to decrease along with total REE concentrations (ΣREE). This trend is seen most clearly in group B samples, but is also clear in group C eclogites, despite their irregular signatures.

Contamination of the primary magma with continental crust either during mamga genesis or metamorphism would be expected to *raise* the Zr/Hf, however Figure 3.26 shows this not to be the case.

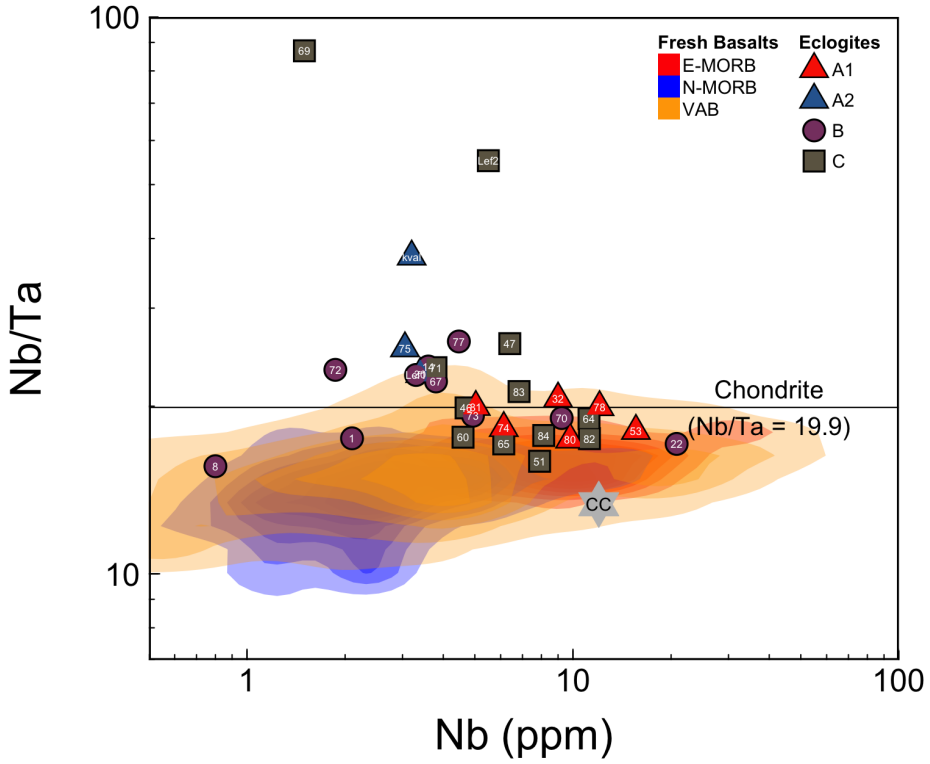

Figure 3.26: Nb/Ta vs. Nb for Norwegian eclogites. Most eclogites in this study have moderately sub-chondritic to moderately supra-chondritic Nb/Ta, with a median (19.9) that is exactly chondritic. As seen elsewhere, Nb appears to be largely typical of expected protoliths, and therefore it appears likely that unusually low Ta concentrations more strongly control the observed deviations in Nb/Ta.

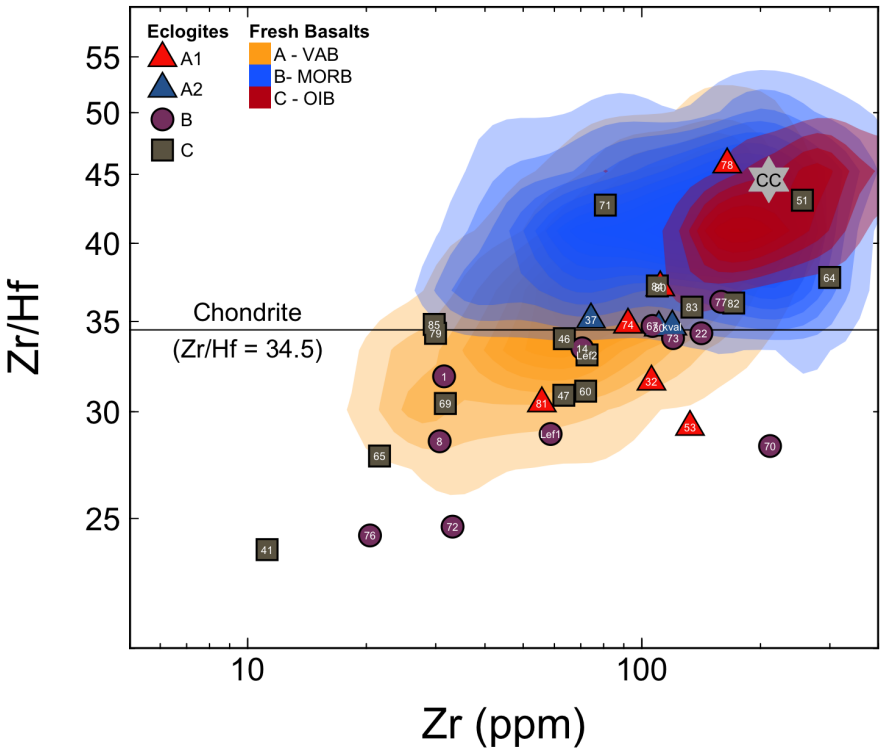

Figure 3.27: Zr/Hf vs. Zr for Norwegian eclogites with reference fields of fresh MORBs and VAB. Group A1 eclogites have a relatively large scatter in Zr/Hf from 29-47, whilst A2 eclogites have largely chrondritic (34.5) Zr/Hf. Group B eclogites have a wide range of mostly subchrondritic Zr/Hf. Group C eclogites have the largest spread in Zr/Hf not conforming to any other eclogite group in particular.

Th-Hf-Ta

The elements Hf and Ta are considered to be highly immobile during metamorphism, whilst the mobility of Th is remains contested. For instance, the correlation analysis presented above suggested that Th may only be considered immobile in group B samples. Therefore, we must be more cautious of discriminant analyses that involve Th.

The Th-Hf-Ta simplex of Wood (1980) (Figure 3.28) is a relatively well established discrimination diagram particularly adept at identifying VABs by their elevated Th/Hf ratio.

Figure 3.28 shows that all except one group B sample (WGR-LEF1) plot well within the field of IAT. Many group B samples have Hf/Th <3 indicating calc-alkaline affinity. Group A1 samples have notably lower Hf/Ta than group A2 samples, and plot on the boundary between N- and E-MORB fields. Group A2 samples, plot close to but not inside the field of N-MORB. Group C samples generally lie between A1 and A2 samples in the field of N-MORB. There is little indication in group A samples that Th has been significantly mobilised, despite the correlation analysis above suggesting that Th in group A samples can not be considered immobile.

Th/Yb vs. Nb/Yb

Figure 3.29 is a plot of Th/Yb and Nb/Yb, and is often used to detect different types of enrichment and depletion in basaltic or metabasaltic rocks. As expected, group B eclogites have high Th/Yb and therefore plot above the mantle array (Pearce, 1982, 1983). Many group A samples, however, plot slightly below the MORB array. Since Nb/Yb of such samples is still largely MORB-like, relatively low Th is the most likely control on Th/Yb. The correlation analysis conducted above suggested that Th in group A samples may be mobile, and thus the low Th/Yb may represent metasomatic depletion of these samples. Group C samples also plot in or significantly below the manlte array, suggesting they may too have experienced some loss of Th during metamorphism.

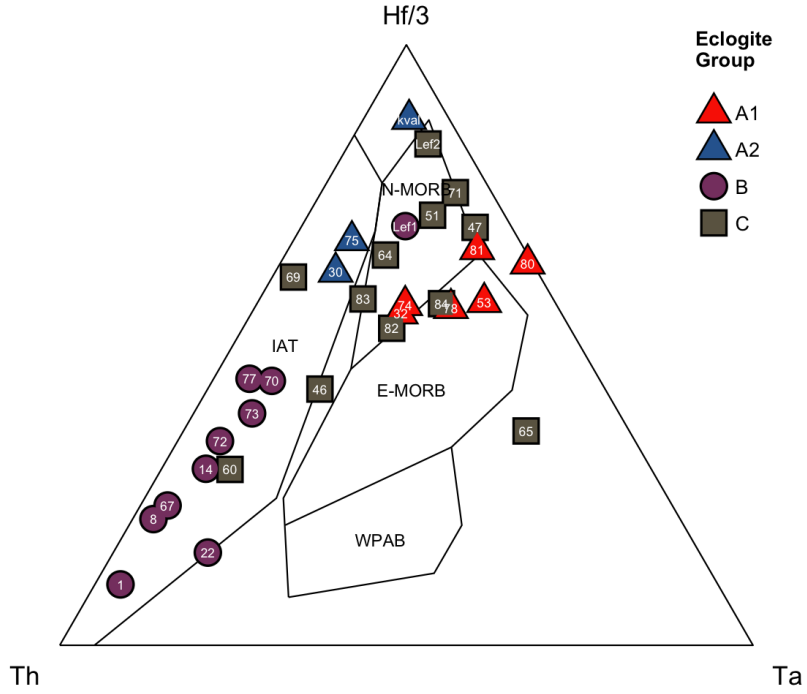

Figure 3.28: The immobile-element Th-Hf-Ta discrimination diagram after Wood (1980), known for being particuarly useful for identifying VABs or IATs. Fields are labeled as island arc tholeiite (IAT), normal mid-ocean ridge basalt (N-MORB), enriched mid-ocean ridge basalt (E-MORB) and within-plate alkali basalt (WPAB). Th is presumed immobile. Group A1 samples may be best described as transitional mid-ocean ridge basalts (T-MORBs). Group A2 eclogites plot just outside the field of N-MORB., most likely due to a depletion in Hf (see Fig. 3.25, pg. 116) for an otherwise N-MORB-like composition. Most group B eclogites have Hf/Th$<$3 meaning they may be better described in this diagram as CABs.

.

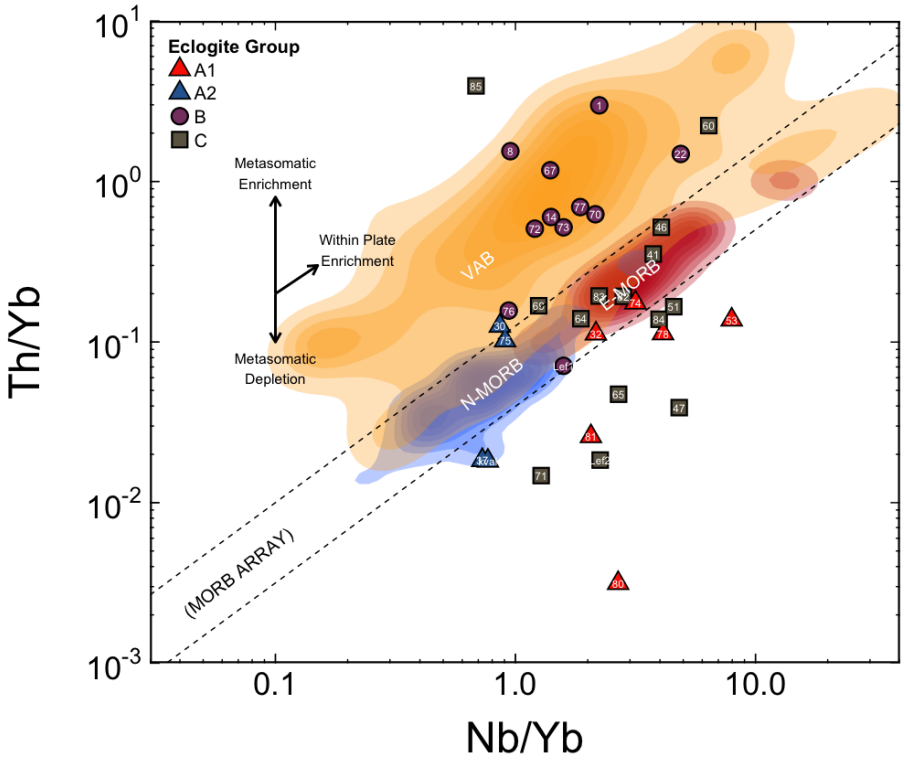

Figure 3.29: Th/Yb vs. Nb/Yb discrimination diagram after Pearce (1982, 1983). Few eclogite samples plot in the mantle array: group A1 eclogites are either within or below the MORB array, whilst A2 eclogites are either above or below but not within the MORB array. Group B eclogites plot consistently above the mantle array, however their elevated Th/Yb cannot differentiate between metamorphic enrichment of the protolith's magmatic source or metamorphic enrichement of a basalt with an otherwise different tectonic affinity. Group C eclogites (those with irregular, often depleted REE signatures) in general plot around or below the MORB array, suggesting metamorphic depletion.

Ti-V-Sm

Vermeesch (2006) proposed the Ti-V-Sm ternary (Figure 3.30, pg. 124) as a discrimination diagram after finding it was highly effective at discriminating basaltic samples from a range of tectonic environments. Although not particularly sensitive to differences between MORBs and arc basalts, the diagram appears to provide good discrimination of eclogite samples: most A1 samples and all A2 samples plot in the relatively small field of MORB, whilst group B samples with their lower Ti/(Sm+V) plot almost exclusively in the field of IAB. Group C samples are omitted since their Sm concentrations are thought to have been significantly altered during metamorphism.

Overview of Discriminant Analysis

REE and immobile trace element discriminant analyses provide strong evidence that Norwegian eclogites are derived from a mixture of MORB-like and VAB-like protoliths. Group A samples record N-type, T-type to E-MORB compositions, whereas group B eclogites are most likely to have arc basalt protoliths. A large number of samples that show evidence of significant alteration (including group C eclogites) appear to retain HFSE compositions largely analogous to group A and B eclogites, suggesting not only that they also have MORB and arc basalt protoliths, but that most HFSEs do indeed remain immobile up to the eclogite facies. We suggest that Th is the HFSE with the greatest potential for mobility, however in most cases the protolith Th composition appears to experience only minor perturbation. It is clear that HFSEs alone are not effective at discriminating between MORB and arc-basalt, thus so far it has been difficult to suggest meaningful protoliths for group C samples.

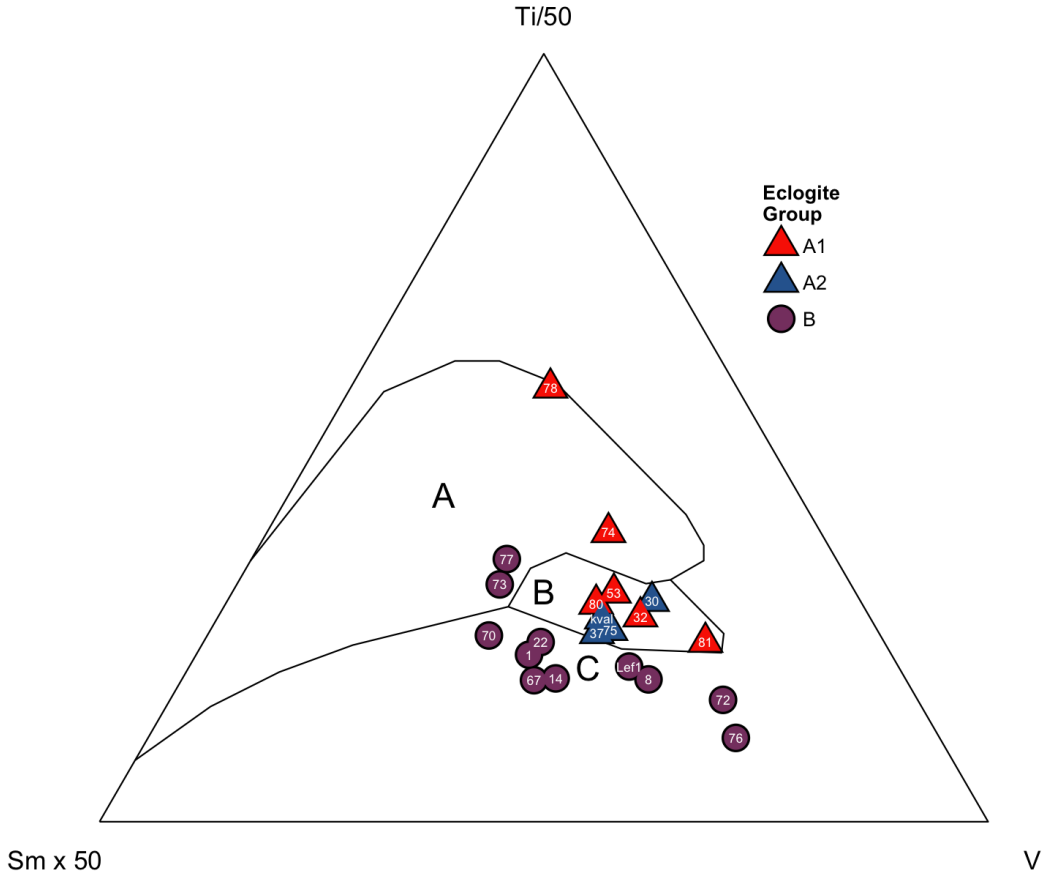

Figure 3.30: Ternary discrimination diagram involving Ti, V, and Sm in ternary space. Field labels are: A, OIB; B, MORB; C, IAB. After Vermeesch (2006). All group A2 and several A1 eclogites plot in the field of MORB. Only two group A1 eclogites plot outside the MORB field due to relatively high concentrations of Ti. As seen in many other discrimination diagrams, group B eclogites plot here in the field of IAB, as indicated by relatively low Ti/(50.Sm+V). Group C eclogites are well scattered, with mostly relatively high Ti concentrations.

3.3.3 Element Mobility Assessment

Direct comparisons of absolute trace element abundances between eclogites and their expected protoliths in order to quantify element gains and losses is not likely to be very important, since this approach does not account for the natural compositional variation expected in different protolith magmas. In order to quantitatively assess element mobility, we must first account for these variations.

At least for fresh MORBs, elements with similar compatibilities ought to, and indeed often do, correlate well with each other. Therefore, ratios of elements with similar incompatibilities are able to effectively filter out the effects of different degrees of partial melting and fractional crystallisation. If suspected *mobile* trace elements are normalised to similarly compatible yet *immobile* trace elements, and this ratio compared to the spread in values for the same ratio in a model protolith composition, it is possible to quantitatively estimate the net element flux.

Becker et al. (2000) quantified element flux from eclogites in a similar way, but only compared eclogites to an average MORB composition. This does not take into consideration the natural variation in both element concentrations and elemental ratios in MORB. By using 2σ distributions of real data in our calculations to define 'normal' ranges in element concentrations and ratios, we believe a more accurate estimation of element flux may be achieved. The work-flow for our mobility assessment is as follows:

- A preliminary mobility assessment (i.e. section 3.3.1, page 94) suggested which elements may be treated as mobile and immobile in the sample set.

- Likely protoliths are determined using a thorough immobile-element discriminant analysis (i.e. section 3.3.2, page 100).

- Appropriate trace element ratios are chosen to highlight mobility: the highly incompatible and potentially mobile elements Ba, Rb and K are normalised to Nb and Th; whereas the moderately incompatible elements Pb and Sr are normalised to Zr and Nd.

- The typical range in values for each ratio in *fresh* protoliths is defined by -2σ and +2σ percentiles.
- The estimated minimum mobility (EMM) is then calculated as follows:
  - If the whole rock ratio (a) is greater than -2σ and less than +2σ (i.e. within range of the values in fresh protolith basalts), then the EMM is assumed to be zero.
  - Otherwise, the EMM is calculated using the following equation:

$$EMM = \frac{a - b}{b} \times 100 \tag{3.1}$$

where a is the whole rock ratio, and b is the closest 2σ value (i.e. if a is lower than the range of fresh protoliths, then b = -2σ, and if it is above the range of fresh protoliths b = +2σ). The value for EMM is given as a vector percentage, in that it can be positive or negative for gains and losses respectively.

The minimum, median and maximum EMM for each eclogite group are presented in Table 3.1.

Potassium

Table 3.1 and Figure 3.31 show that only a small number of samples have experienced substantial depletion in K (up to 98-99%, 66% median). This maximum mobility is in general agreement with the findings of Becker et al. (2000) who infered up to 95-98 % mobility of K from a suite of orogenic eclogites. However, most samples have K/Nb within the range shown by their protoliths. This suggests that for many eclogites, K may be relatively immobile on scales greater than a few centimeters.

Barium

Figure 3.31 also shows that K-depleted samples typically record losses in Ba on the order of 50-80 %, lower than the value of 95-98% calculated by Becker et al. (2000).

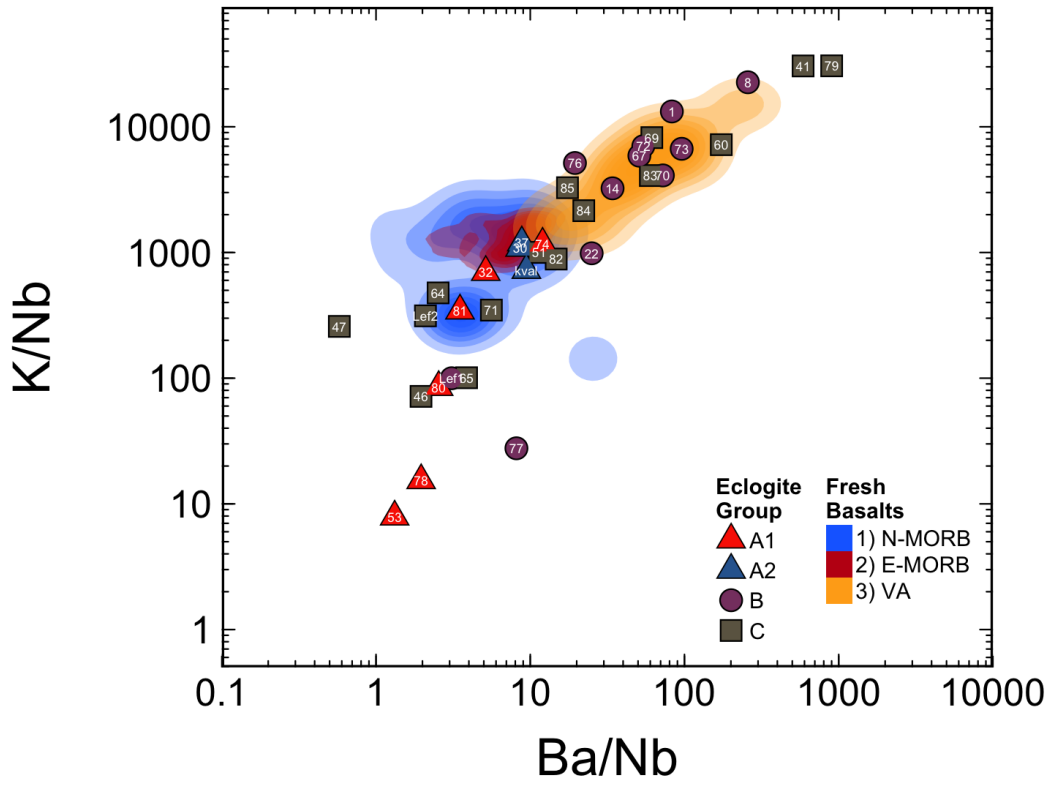

Figure 3.31: K/Nb vs. Ba/Nb diagram for Norwegian eclogites with reference fields for normal mid-ocean ridge basalt (N-MORB), enriched mid-ocean ridge basalt (E-MORB) and volcanic arc basalt (VAB) constructed using data from PetDB. Abbreviations are: CC, Continental Crust; E, E-MORB; N, N-MORB; PM, Primitive Mantle. The data suggest that K is more mobile than Ba, however neither are exclusively mobile. Depletion of K is most significant in group A1 eclogites which record up to two orders of magnitude depletion.

Table 3.1: Table of mobile-immobile trace element ratios with corresponding $\pm 2\sigma$ values for fresh protoliths (data from PetDB.org) alongside the minimum, median and maximum estimated minimum mobility (EMM) for all eclogites in each eclogite group.

	N-MORB		E-MORB		VAB		Group A1 (%)			Group A2 (%)			Group B (%)		
	-2σ	$+2\sigma$	-2σ	$+2\sigma$	-2σ	$+2\sigma$	Min	Med	Max	Min	Med	Max	Min	Med	Max
Ba/Nb	1.60	13.16	2.86	14.57	16.50	268.96	-50	-5	0	0	0	0	-81	0	0
K/Nb	164.82	2639.07	631.01	1956.09	1390.88	14986.17	-99	-66	0	0	0	0	-98	0	51
Th/Nb	0.03	0.58	0.05	0.10	0.17	1.18	-94	-55	0	-20	-8	0	-74	0	37
U/Nb	0.01	5.36	0.02	0.03	0.07	0.58	-62	-1	119	0	0	0	-86	0	0
Rb/Nb	0.19	1.30	0.27	1.18	1	19.22	-86	-17	89	0	0	0	-89	0	23
Sr/Zr	0.38	2.26	0.53	3.03	2.92	16.94	0	0	0	0	0	42	-85	-24	0
Sr/Nd	3.34	21.10	5.02	21.57	18.51	67.53	0	0	0	0	0	35	-83	-47	0
Pb/Zr	0	0.04	0	0.01	0.02	0.12	139	547	1607	0	1	26	-26	0	338
Pb/Nd	0.02	0.27	0.03	0.10	0.08	0.64	120	420	1226	5	48	104	-1	0	271

Once again, however, most samples record no detectable loss. This is supported by Becker et al. (2000) who suggests that eclogites may only contribute less than 20 % of the Ba found in arc magmas, the majority being derived from subducted sediments. Thus it appears that hand specimens and outcrops for many of our eclogites may be considered relatively closed systems, even to elements generally considered highly mobile.

Strontium

Figure 3.32 shows that there is a stark contrast in the apparent mobility of Sr in group A and B eclogites: group A samples indicate largely unchanged Sr, whereas group B eclogites can have Sr depletions on the order of 25-50%, reaching as high as 85% for the most depleted. Becker et al. (2000) calculated that Sr mobility in eclogites is $<$10 %, again in agreement with observations for group A eclogites. The very low Sr concentration in group B samples suggests either Sr has been highly mobilised from these samples, or that the concentration of Sr in the protolith was originally much lower than that in most IABs. The lack of enrichment in Sr for group B eclogites argues against significant contamination of the eclogite via melts or fluids derived from sediments or continental crustal rocks either during magma genesis or metamorphism.

Lead

Figure 3.33 shows that Pb is strongly enriched over MORB in almost every single sample. Group A samples have the greatest relative enrichment from their supposed protoliths with most samples having 420-550% greater Pb. Group A2 samples have less obvious Pb enrichment, at around 50 %. Just over half of group B samples have VAB-like Pb/Zr and Pb/Nd, a further three have significantly *elevated* Pb, and the remaining two have Pb between MORB and VAB. When present, Pb enrichment in group B can up to around 300 %. The majority of group C samples plot either in or above the field of VABs. The apparent enrichment of Pb in group A but not group B eclogites is intriguing: Pb enrichment is a common feature of seafloor/seawater alteration, whereas moderate Pb *loss* would be expected during

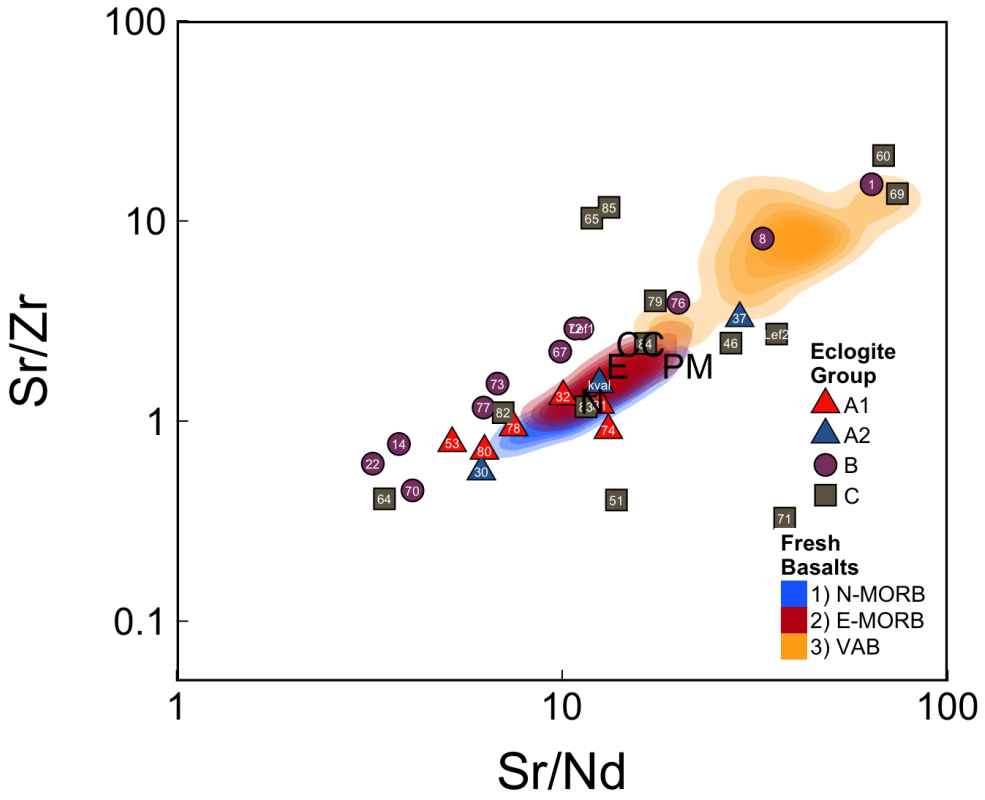

Figure 3.32: Sr/Zr vs. Sr/Nd variation diagram for Norwegian eclogites with reference fields for normal mid-ocean ridge basalt (N-MORB), enriched mid-ocean ridge basalt (E-MORB) and volcanic arc basalt (VAB) constructed using data from PetDB. Abbreviations are: CC, Continental Crust; E, E-MORB; N, N-MORB; PM, Primitive Mantle. The strong correlation supports the assumption that Sr is significantly more mobile than the denominators Zr and Nd. Depletion in Sr affects most samples, but greater depletion is suggested for group B eclogites.

metamorphic dehydration. The additional Pb observed in group A eclogites is not expect to have been sourced from adjacent crustal rocks, since there is no evidence of coupled Pb and Sr enrichment over MORB. The disparity in Pb enrichments between group A and B eclogites suggests that the Pb enrichment in group A eclogites was imparted by a process not experienced by group B eclogites. This can be used to support an argument for a MORB origin for group A eclogites, but not for group B.

Rubidium

Figure 3.34 shows two thirds of group A1 samples, together with a small number of group B (WGR-77, LEF1) and group C samples (WGR-46, -47, -65, -71, and LEF2) have low Rb/Nb equivalent to a 20-90% decrease in Rb. These samples define a linear trend which shows Rb exerts a greater control than Nb on Rb/Nb. Group A2 samples appear to have largely N-MORB-like Rb/Nb, whilst group B and the remainder of group C samples have high Rb/Nb more typical of VABs.

Uranium and Thorium

The correlation analysis at the beginning of this section led to the suggestion that U and Th may be considered immobile in group B samples, but mobile in A and C samples. Figure 3.35 is a plot of Th/Nb versus U/Nb, which also suggests U and Th are only immobile in group B samples. Compared with fresh MORBs, group A and C eclogites exhibit coupled U and Th enrichment or depletion.

When we compare Figures 3.35 and 3.36, we can show that the effect of Th mobilisation in MORB-like samples (i.e. group A) is very small compared with the compositional range of Th in both fresh VABs and group B eclogites. Therefore, although Th was not identified as an immobile element in group A samples, Th concentrations may be considered largely unchanged. Furthermore, in Figure 3.36 there are no linear trends between fresh MORB and values for upper continental crust (UCC) or globally subducted sediment (GLOSS). This indicates that neither were significantly involved in the enrichment of group B eclogites.

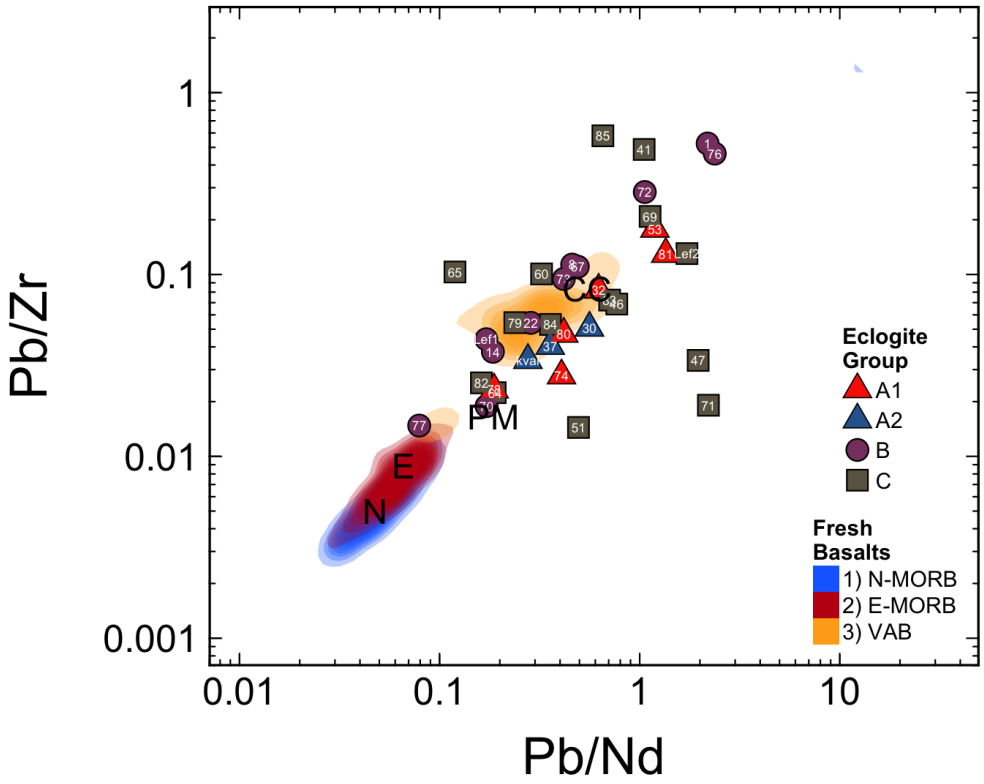

Figure 3.33: Pb/Zr vs. Pb/Nd variation diagram for Norwegian eclogites with reference fields for normal mid-ocean ridge basalt (N-MORB), enriched mid-ocean ridge basalt (E-MORB) and volcanic arc basalt (VAB) constructed using data from PetDB. Abbreviations are: CC, Continental Crust; E, E-MORB; N, N-MORB; PM, Primitive Mantle. Almost every sample has higher Pb/Zr and Pb/Nd than MORB, however group B eclogites show apparently less relative Pb-enrichement than group A eclogites. With the exception of group C eclogites, Pb/Zr and Pb/Nd are well correlated suggesting that Pb mobility dominates each ratio.

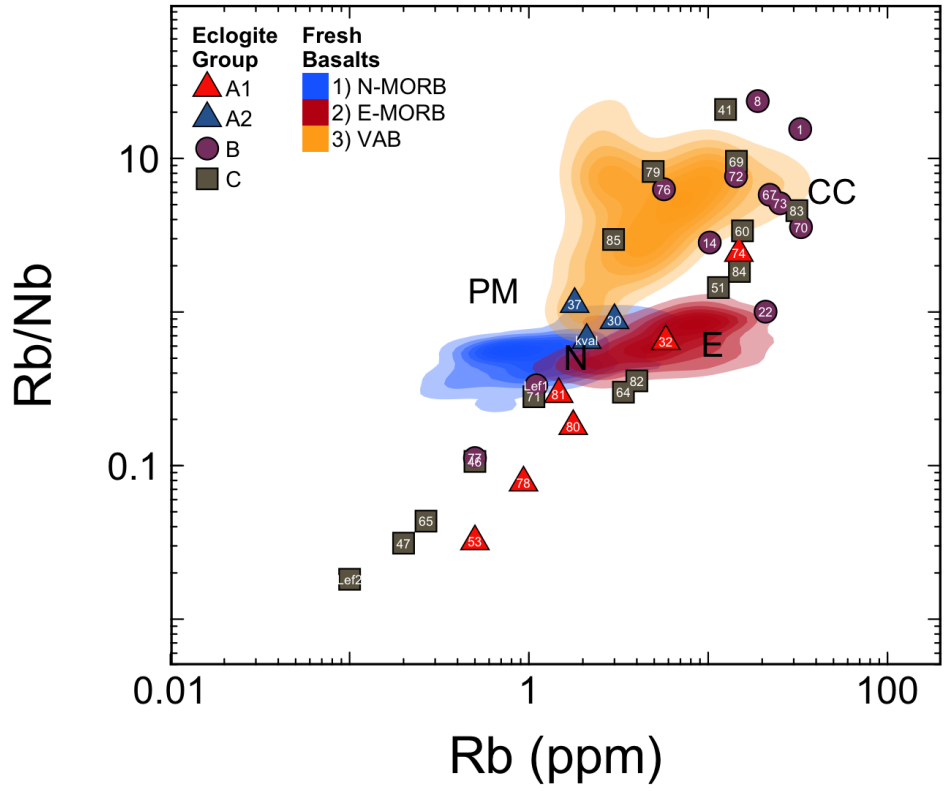

Figure 3.34: Rb/Nb vs. Rb diagram for Norwegian eclogites with reference fields for normal mid-ocean ridge basalt (N-MORB), enriched mid-ocean ridge basalt (E-MORB) and volcanic arc basalt (VAB) constructed using data from PetDB. Abbreviations are: CC, Continental Crust; E, E-MORB; N, N-MORB; PM, Primitive Mantle. The figure highlights the apparent Rb mobility in group A eclogites but not in group B. Depletion of Rb in group A eclogites is restricted to group A1. Group B eclogites don't show the correlation that one might expect if their high Rb/Nb was a result of metasomatic enrichment of a MORB-like eclogite. Instead, the lack of correlation suggests that the high Rb/Nb is primary.

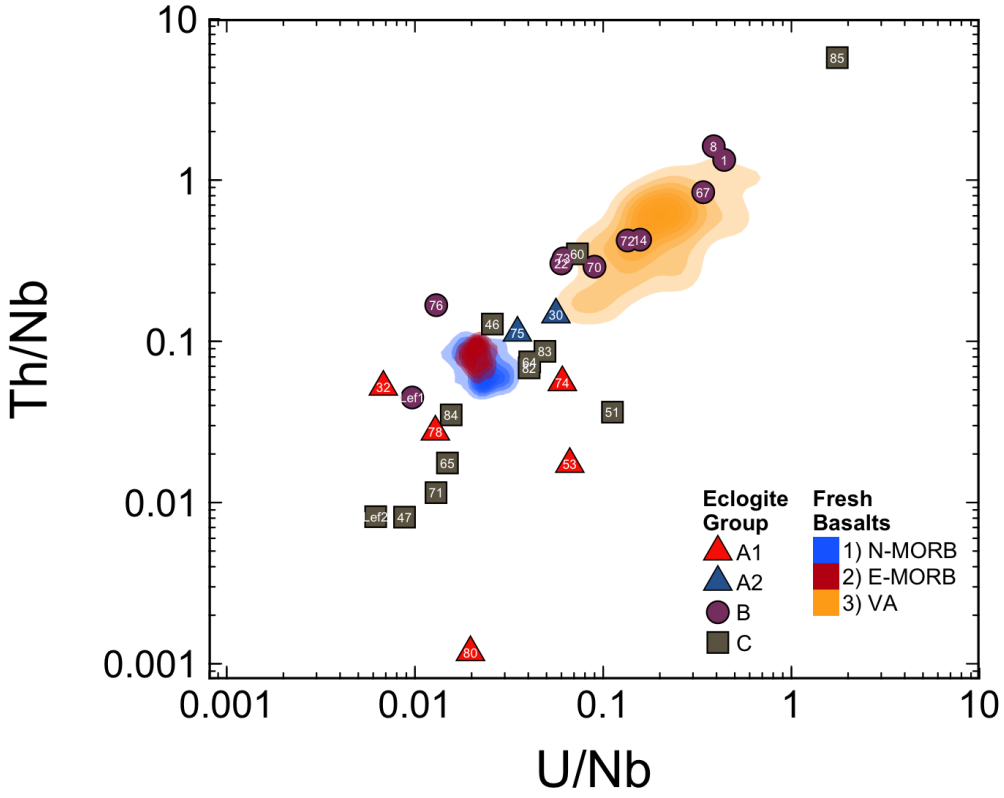

Figure 3.35: Th/Nb vs. U/Nb diagram for Norwegian eclogites with reference fields for normal mid-ocean ridge basalt (N-MORB), enriched mid-ocean ridge basalt (E-MORB) and volcanic arc basalt (VAB) constructed using data from PetDB. The figure shows that group A eclogites have significantly perturbed U and Th, while group B eclogites seem to have unchanged U and Th.

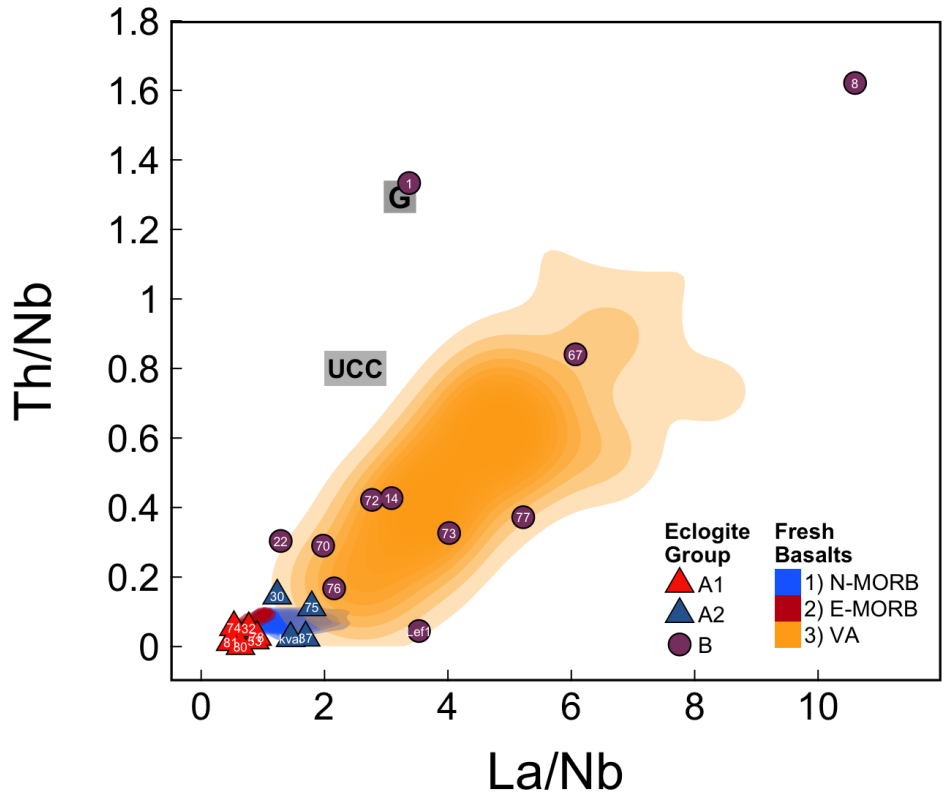

Figure 3.36: Th/Nb vs. La/Nb. Abbreviations: G, Globally Subducted Sediment (GLOSS); UCC, upper continental crust. Although Figure 3.35 shows that Th/Nb in group A eclogites has been altered, this diagram suggests this deviation may be relatively small when compared with much higher Th/Nb found in VABs. There appear to be no linear trends involving UCC or GLOSS, suggesting that neither has been responsible for contaminating the composition of samples. Fields of N-MORB, E-MORB and VAB from PetDB.org; UCC from Plank (2005).

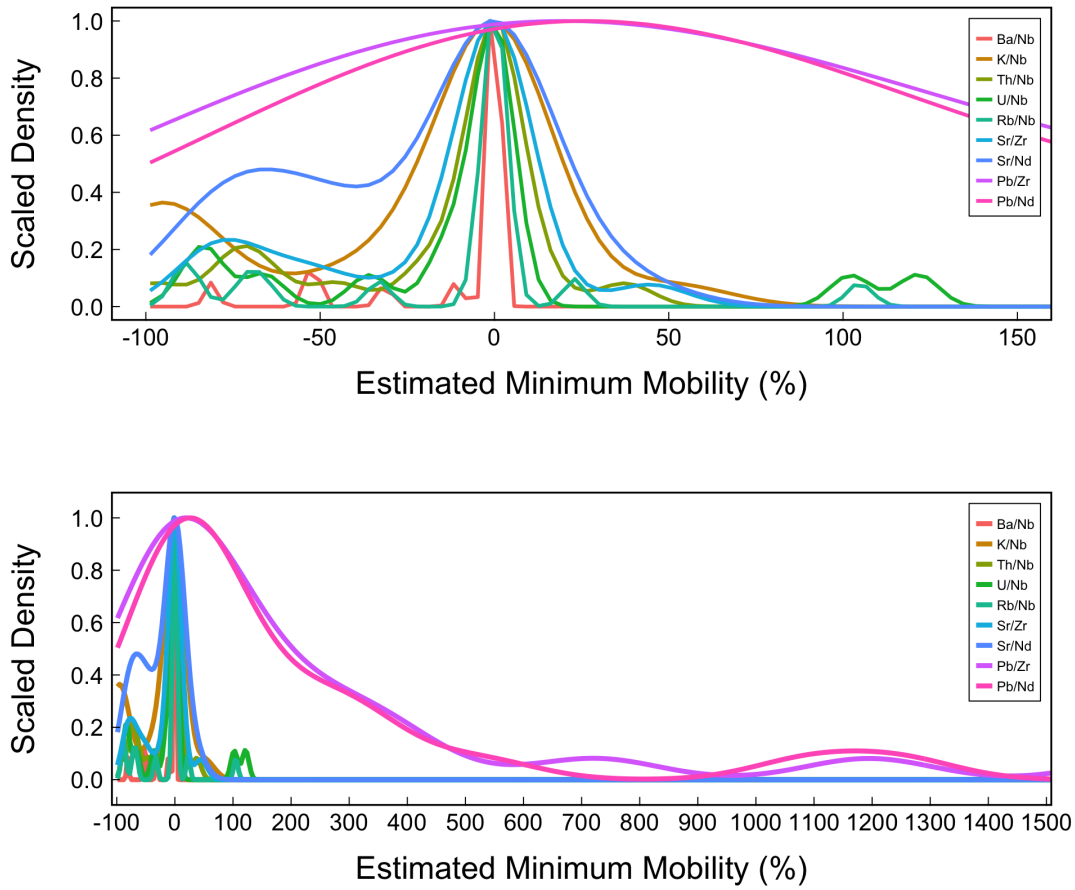

Figure 3.37: Gaussian density distribution curves (scaled to 1.0) for EMMs for apparently mobile elements in Norwegian eclogites. The diagram is produced twice with different ranges in x-values in order to highlight the difference in apparent Pb mobility compared with the other mobile elements. The density curves suggests relative mobility of the elements is Ba<Rb<U<Th<Sr≈K≪Pb.

Relative Mobilities

Figure 3.37 shows Gaussian density estimates for the EMMs for each supposedly mobile element, expressed as ratios to similarly compatible immobile elements. The model density distributions allow for gaps in the data to be interpolated across, and for the relative mobilities of elements to be highlighted. The curves show that the relative element mobilities is Ba<Rb<U<Th<Sr≈K≪Pb. With the exception of Pb, element gains rarely exceed 50%, and element losses of Ba to Th on the relative mobility scale appear to be mostly less than 50%.

3.3.4 The Metasomatic Problem

A problem exists with respect to the interpretation of metabasaltic rocks with subduction zones geochemical signatures (i.e. group B samples). These signatures could reflect the setting in which the primary magma was generated, but could also be caused by infiltration of metasomatic fluids and/or melts during HP- to UHP metamorphism. Interpretation of samples such as those in group B is complicated further because many HFSEs alone are not capable of distinguishing between MORB and VAB. In light of such a problem, two end-member hypothesis must be evaluated:

Hypothesis 1

HFSEs and REEs have remained largely immobile on both the prograde and retrograde path, and as such these elements may be used with confidence to characterise the tectonic setting in which the protolith was generated.

Hypothesis 2

Metasomatic fluids or melts either leaving or entering the sample in an open system have corrupted the original trace element characteristics of the protolith, making it almost impossible to infer the composition of the protolith from trace element composition alone.

Presented below are several lines of evidence that favor hypothesis 1; that group B eclogites in this study truly represent basalts generated in a subduction zone setting.

REE and HFSE Mobility in the Literature

It is becoming increasingly apparent in the literature that the fluid-mobility of REEs and HFSEs during subduction is highly complex, and a number of conditions can effectively mobilise and fractionate these elements (e.g. Zack and John, 2007). However it seems that for whole-rock compositions and trace element signatures of rocks metamorphosed away from zones of major fluid flow, REEs and HFSEs may be considered largely immobile up to and including the eclogite facies (e.g. Tribuzio et al., 1996; Arculus et al., 1999; Spandler et al., 2003; Usui et al., 2007; EL Korh

et al., 2009; Xiao et al., 2012).

During the prograde metamorphism of basaltic rocks, the minerals lawsonite, epidote, titanite, garnet, rutile and phengite control most of the trace element inventory of the whole-rock from early prograde through to peak metamorphism. This is facilitated not only by their collective affinity for trace elements, but also by the large stability range of, in particular, phengite, epidote, apatite, titanite and rutile (EL Korh et al., 2009). Many of the eclogites in this study preserve prograde epidote, apatite, phengite and rutile that have likely been responsible for preserving much of the protolith trace element signature. To investigate this further, one may use a simple Rayleigh-distillation equation (Equation 3.2) to calculate the relative loss for a particular element on the whole rock inventory:

$$C_s = C_0(1 - F)^{(1/D)-1} \tag{3.2}$$

Where C_0 is the starting concentration, C_s is the concentration in the remaining solid, F is the fraction of fluid extracted, and D is the partition coefficient. Equation 3.2 was used to construct Figure 3.38 which shows that even a loss of as much as 3 wt% of fluid from a sample (F=0.03), in which any element is enriched 10$\times$ (D=0.1) compared with the whole-rock, still leaves 75% of the original inventory of that element in the rock residue (Zack and John, 2007). Such a loss would be expected to be within scatter expected in the protolith composition (e.g. Spandler et al., 2004), suggesting that REEs and HFSEs in many samples are reliable indicators of protolith composition. This further supports the idea that high fluid-rock ratios are required to significantly affect trace element compositions of even UHP lithologies (e.g. Spandler et al., 2003; John et al., 2007).

Coherence of Geochemical Signatures

The trace element characteristics of arc magmas represent the sum of many complex geochemical processes in both the slab and the mantle wedge above. It therefore seems unlikely that the local remobilisation of slab fluids or partial melts during subduction would impart arc signatures onto otherwise MORB-like rocks, such that they would be almost indistinguishable from fresh arc basalts. This means that the arc signatures

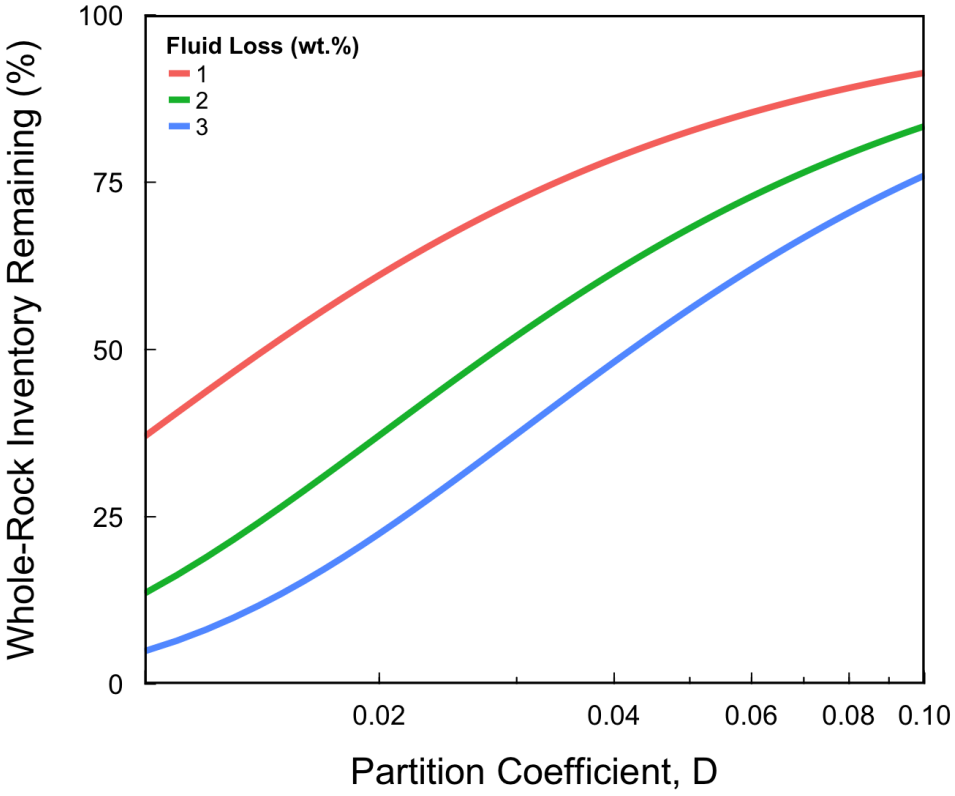

Figure 3.38: Models of the remaining inventory of an element in a soild after extraction of different mass fraction of fluid, in which the element can be enriched from 10 (D = 0.1) to 100 (D = 0.01) times, calculated using the Rayleigh distillation equation (Equation 3.2). The graph shows that even for a loss of 3 wt.% fluid in which an element is enriched over 10 times that of the whole rock, over 75 % of the original inventory remains in the depleted solid.

in group B eclogites are likely to be a result of the composition of protoliths, rather than alteration during metamorphism. Furthermore, the remarkably coherent trace element characteristics of group B eclogites, for both mobile and immobile elements over such a large geographical area also invites further scepticism. It is hard to envisage a metasomatic process operating in an open system by which such coherent enrichment of samples could occur over great distances. Rather, it seems more likely that the arc-signature is in fact a result of magma generation in a volcanic arc setting. Indeed, the collision of island arc crust onto the Baltican margin is very much a ubiquitous feature along the Caledonian suture in Norway.

Infiltration of Partial Melts

One possible explanation for group B VAB-like geochemical signatures is the infiltration of partial melts. The Zr/Y and Zr/Hf of average continental crust is around 8-12 and 45 respectively (e.g. Weaver and Tarney, 1984; Taylor and McLennan, 1985; Wedepohl, 1995), ratios that are much higher than almost all eclogites in this study which have Zr/Y of 2-6 (Figure 3.17) and Zr/Hf 24-37. Similarly, continental crust has Nb/Ta = 11.4 (Barth et al., 2000), lower than every single eclogite in this study (i.e. Nb/Ta of 12-100, Figure 3.26). For each of these elemental ratios, any deviation from expected protolith values move *away* from all continental crust values, suggesting that crustal melts are not responsible for contaminating any group of eclogite in Norway. Furthermore, Plank (2005) and Xiao et al. (2012) showed that Th/Nb and La/Nb are important tracers in MORB, arc magmas and the continental crust, and that Th is only significantly mobilised during partial melting. High Th in group B samples therefore represents either original composition or infiltration of partial melts of continental crust or subducting sediment. Aside from the fact that no petrographic evidence for partial melts is observed in the samples, Figure 3.36 shows it is unlikely that melts derived from continental crust or subducting oceanic sediment have contributed to the enriched composition of group B eclogites.

Pb and Sr

There exists unusual differences in the apparent behavior of Pb and Sr in group A versus group B eclogites given their likely protoliths. EMMs for Sr are 24-50% greater (i.e. depleted) in group B samples than in group A. It is possible that the original

concentration of Sr in group B protoliths was much lower than typical arc basalt, or that more Sr was indeed lost from group B samples than group A. If the former is the case, one may argue that group B eclogites could be MORBs that have been enriched during subduction by sediment or continental crust derived fluids. This, however does not stand up to scrutiny: Sr mobility in eclogite is considered to be $<$10 % (Becker et al., 2000; EL Korh et al., 2009), and most Sr enrichment observed in arc basalts appears to be derived from subducted sediments (Becker et al., 2000). Therefore, metasomatic enrichment of a MORB during subduction would be expected to result in a Sr enrichment that is largely retained even through retrogression. The very opposite is the case for group B eclogites suggesting they are in fact arc basalts.

Pb also shows contrasting enrichment styles in group A and B eclogites. All eclogites have much higher concentrations of Pb than fresh MORB. Hydrothermal alteration of MORBs in close proximity to pelagic sediments often results in significant transfer of Pb from sediments to basalts (German, 1993), whereas Pb intrinsic to the protolith is typically *lost* during hydrothermal alteration (on the order of 60 %) at moderate- to high-grades of metamorphism (Becker et al., 2000). Thus it appears that *all* eclogites have some Pb enrichment process in their history, be that during magma genesis or hydrothermal alteration.

Group A eclogites have clear MORB protoliths, and therefore their Pb enrichment is most likely due to infiltration of fluids sourced from sediments. Despite this, group A samples show little other evidence of hydrothermal enrichment, suggesting that Pb may have remained largely immobile during subsequent metamorphism, or that enriching fluids were likely compositionally simple with a trace element inventory dominated by Pb.

Most group B eclogites have Pb/Zr and Pb/Nd typical of arc basalts. The high Pb in arc basalts is attributed to enrichment of the mantle source with sediment-scavenged Pb (e.g. Becker et al., 2000; Plank, 2005; Xiao et al., 2013). Arc basalts are expected to have relatively little association with pelagic sediments, and therefore be expected to show little to moderate *loss* of Pb during subduction, unless subsequently infiltrated by fluids or melts originating from subducting sediments. With the exception of three samples (WGR-01, -72 and -76) group B eclogites show Pb/Zr and Pb/Nd typical of arc

basalt. Enrichment of MORB by sediment sourced hydrothermal fluids may explain elevated K, Ba and Pb, but lack of K and Ba enrichment in group A samples suggest that the Pb enrichment of group B is linked to the protolith composition.

HREEs

Basaltic magmas formed in island arc settings generally have chondrite-normalised HREEs patterns that are lower than yet parallel to those of N-MORB, reflecting potentially greater degrees of partial melting than in the case of MORB, largely driven by high water contents. During subsequent metamorphism of basalt, HREEs are considered largely immobile, particularly given their affinity for sequestration in the almost ubiquitous and abundant phase garnet. Manning (2004) reports that Cl-free supercritical fluids, thought to be one of the most significant vectors of trace element transport in subduction zones, also have HREEs depleted relative to N-MORB, but their N-MORB normalised HREE slope is steep and negative. One might therefore expect that metasomatic alteration at eclogite facies would result in a steepening of the HREEs on a N-MORB normalised plot. Lack of such a feature in our data suggests that greater degrees of partial melting are likely to be responsible for the total HREE inventory (Σ_{HREE}).

3.3.5 Potential Cumulates Eclogites

There is little decisive geochemical evidence observed that strongly suggests cumulate origins for sampled eclogites. Eclogites from Vengen (78), Sandvollen (64) and Naustdal (65) have low silica contents (i.e. less than 45 wt.%). Vengen has unusually high Ti (6 wt.%) but has an otherwise N-MORB-like geochemical signature. The Naustdal eclogite has a rather chaotic Group C signature, however has relatively low Zr (21 ppm) and high Sm (5.4 ppm). The Sandvollen eclogite on the other hand is typically significantly enriched in all trace elements over N-MORB. Hollocher et al. (2007) show that cumulate eclogites in the region are typified by Zr $<$10 ppm and Sm $>$4 pmm. For those samples we have been able to assign to groups A and B, the vast majority have geochemical compositions and signatures expected in a non-cumulate mafic rocks.

3.3.6 Felsic Gneisses and Eclogite Paragenesis

The vast majority of Norwegian eclogites are found within masses of felsic gneisses. We have already discussed the extent to which these gneisses may have affected the geochemistry of eclogites *after* eclogite crystallisation, but what about before and during prograde crystallisation? The evidence presented here suggest that the role of any gneiss-derived fluids on the geochemistry of the crystallising eclogite must also have been, in most cases insignificant. Many of the eclogites may well have transformed to such under relatively dry conditions. The general rarity of zoisite in most samples, apparent crystallisation of garnet before omphacite, and the inability for one to link trace element enrichments to crustally-derived fluids supports the idea that the involvement of the surrounding gneisses on the geochemistry of the prograde crystallisation of many Norwegian eclogites was not significant. Transition to eclogite through amphibolite may have involved several weight percent of water native to the eclogite body, which during dehydration, could have provided fluids that could have catalysed prograde eclogite mineral reactions.

3.3.7 Implications for Understanding Pre-Caledonian Norway

As discussed in Chapter 1, the basement gneisses of western Norway have their origins as far back as 1.85 Ga or more, a time of significant crustal growth that included the Southwest Scandinavian Orogen (SSO). Protolith age determinations (mostly Zircon U/Pb) are only available for a handful of WGR eclogites (e.g. Walsh et al., 2007), and show that the majority formed during the Gothian (1.7-1.5 Ga) or Sveconorwegian (1.2-0.9 Ga) orogenies, although a small number have been shown to have formed much more recently (e.g. 459 Ma, Walsh et al., 2007), probably belonging to Early Silurian Iapetus allochthons.

It was unfortunately beyond the scope of our study to date more of the WGR eclogite population, however it seems reasonable to assume that the majority of WGR eclogites may have been generated long before the formation and closure of Iapetus. Regardless of exact timing of formation, our analysis suggests that many of the eclogites in the Precambrian basement of western Norway were generated in volcanic arcs which were

accreted onto the continent during one of several orogenic events. A smaller number of eclogites, which have MORB-like protoliths, could have been closely associated with such island arcs, and thus could represent adjacent oceanic crust that was caught up in accretion. Such a simple model can explain why IAB-type eclogites dominante the population, but also why otherwise subduction-prone MORB-like rocks were accreted.

Furthermore, it is more than likely that the continental crust has grown mostly via the progressive accretion of island arc material (e.g. Barth et al., 2000), and therefore the indicated origins of Norwegian eclogites agree with what would be expected in the basement of a mature continent. With further age-determinations of eclogite protoliths, we may improve significantly our understanding of the formation of the basement in western Norway.

3.4 Conclusions

One of the main objectives of this study was to identify the likely tectonic settings in which the protoliths for a representative suite of eclogites from Western Norway were formed. It is clear that most of the eclogites in Western Norway have very complex histories, yet we were able to identify with confidence the likely protoliths for a significant number of important eclogite localities:

- Around 10 Norwegian eclogites appear to have been generated by melting a metasomatically enriched mantle (group B), either in a subduction zone or continental setting. It is hard to say which, because Western Norway has experienced several discrete episodes of oceanic arc accretion, as well as significant continental volcanism.

- A total of 9 eclogites were formed with compositions in the range of N- to E-MORB (group A), and were therefore probably generated from a distinctly different mantle to that of group B eclogites. It is suggested that their protoliths may have been formed in an oceanic setting and subsequently accreted onto the continental margin.

- More than half of the samples have trace element signatures that appear to have been significantly altered during metamorphism (group C), therefore making it

difficult to assign likely protoliths. However, several key trace elements (e.g. Nb, Ta, Zr, Hf, and Y) have remained largely immobile in these samples, and allow us to show that their protoliths are likely to be similar to either group A or group B samples.

- Both REEs and HFSEs can remain largely immobile during subduction to eclogite facies conditions, and thus allow confident protolith determinations.
- Smooth REE patterns in eclogites that are similar to potential fresh protoliths suggest negligible REE mobility, and as such may be used to suggest protolith types. In particular, high similarities with fresh arc volcanic rocks likely reflects original protolith composition rather than metasomatic enrichment.
- REE are clearly mobilised in *some* samples, indicated by irregular and spikey REE signatures. However, HFSEs in such samples appear to remain largely immobile, suggesting that even eclogites altered in open systems may preserve some aspects of their protolith's composition in HFSEs.

Chapter 4

The Geochemistry of Rutiles from HP and UHP Eclogites, Western Norway*

Abstract

Rutile (TiO_2) is common accessory phase in HP and UHP metabasites that is resistant to partial melting, dissolution by metamorphic fluids, and both physical and chemical weathering. Even when present at concentrations <2 wt. % rutile can dominate the whole-rock budgets for a number of highly charged trace elements (e.g. Nb, Ta, Mo and Sn). Our understanding of the role rutile plays in controlling geochemical processes in a variety of geological settings is still in its infancy, and so there remains much to be learned. Over 400 high precision LA-ICP-MS trace element analyses of rutile crystals have been acquired from 28 classic HP-UHP eclogites from the Western Gneiss Region (WGR) of Norway. These data are combined with new high-precision HPTS-ICP-MS and XRF data for corresponding whole rocks. Our analysis shows that significant proportions of the whole-rock inventories for Ti (50-100 % of all TiO_2), Ta (50-98%), Nb (43-90%), Sn (8-30%), and Mo (5-26%), along with small amounts of V (2-7%), Cr (<7%), Hf (<5%) and Zr (<1%) in Norwegian eclogites are found in rutile. Model partition coefficients between whole rock and rutile provide the first evidence from natural samples that Ta is 5-15 % more compatible in rutile than Nb, whilst Hf can be just as or twice as compatible in rutile than Zr, in mineral-fluid settings. Despite their ionic similarities, Nb and Mo are not strongly coupled in rutile, because Mo is relatively fluid mobile under oxidising conditions. Eclogites containing rutiles with Mo $>$10-15 ppm are likely to have undergone infiltration of oxygenated fluids rich in Mo yet poor in other highly charged elements such as Sn. Rutiles from any one sample often have highly heterogeneous composition, reflecting limited macroscopic diffusion of important trace elements. This indicates that great caution should be exercised in

*Co-authors: Godfrey Fitton - *The University of Edinburgh*; Simon Harley *The University of Edinburgh*; Craig Storey - *The University of Portsmouth*

interpreting sediment provenance from the trace element signatures of small (e.g. n <100) populations of detrital rutile. Relatively high whole rock Nb/Ta ratios are used to suggest that Norwegian eclogites experienced loss of Ta during dehydration in the lower- to middle-amphibolite facies before the onset of rutile crystallisation.

4.1 Introduction

Titanium is the ninth most abundant element in the continental crust ($\approx$ 0.7 wt.% TiO_2, Rudnick and Fountain, 1995), and is mostly held within the minerals rutile (TiO_2), ilmenite ($FeTiO_3$), and titanite ($CaTiSiO_5$). Rutile may form in igneous rocks (e.g. granites, pegmatites, kimberlites, and mantle xenoliths), medium- to high-grade metamorphic rocks (e.g. amphibolites and eclogites), or in hydrothermal ore deposits (often associated with quartz veins). Wherever it is formed it is an important host for several highly charged elements (e.g. V, Cr, Fe, Al, Mo, Nb, Sn, Sb, Ta, W) that are useful in studying geochemical processes (Deer et al., 1962; Graham and Morris, 1973; Haggerty, 1991; Deer et al., 1992; Hassan, 1994; Fett, 1995; Murad et al., 1995; Smith and Perseil, 1997; Rice et al., 1998; Zack et al., 2002b, 2004; Bromiley et al., 2004; Scott, 2005; Carruzzo et al., 2006). Studies on the geochemistry of rutile have demonstrated its value in the fields of geothermometry (Zack et al., 2004; Watson et al., 2006; Ewing et al., 2013), geochronology (e.g. Taylor, 2008; Vry and Baker, 2006; Richards et al., 1988; Corfu and Andrews, 1986), sediment provenance analysis (e.g. Zack et al., 2004; Stendal et al., 2006; Triebold et al., 2007; Meinhold et al., 2008; Morton and Chenery, 2009), subduction zone geochemistry (e.g. Rudnick et al., 2000; Klemme et al., 2005) and igneous petrogenesis (e.g. Dawson and Smith, 1977; Deer et al., 1992; Rudnick et al., 2000; Von Quadt et al., 2005; Ripp et al., 2006, and many others). Rutile is also both highly resistant to physical and chemical weathering, diageneis, high-grade metamorphism and partial melting. It is clear that, when present in a rock or sediment, rutile represents a highly valuable information resource for geologists.

In the next two chapters the geochemistry of rutile in Norwegian eclogites is exploited to address several important questions related not only to local geology, but also to a broader understanding of geochemical processes involving eclogites and rutile.

Specifically, we aim to address the following questions:

1. What is the trace element composition of eclogite-hosted rutiles from western Norway, and to what extent do these rutiles control the trace element inventory of their whole-rocks?

2. Can we use the composition of rutiles to learn more about the partitioning behaviour of trace elements into rutile?

3. To what extent can rutile geochemistry reflect important geochemical characteristics of its whole rock?

4. What do rutiles in Norwegian eclogites tell us about the thermal histories of their host rocks, and how does this better our understanding of the evolution of the Scandinavian Caledonides?

This chapter deals with questions 1-3, and the following chapter deals with rutile geothermometry.

4.2 Method

4.2.1 Sample Selection & Preparation

In response to constraints on time and funds, it was decided to only separate out and analyse rutiles from a representative suite of our whole-rock eclogite sample. Eclogites were chosen to reflect a range of features present in the sample set: whole rock trace element signature, petrographic texture (including modal abundance of rutile), geographical location, and the amount of remaining material available for further analysis. A summary of the chosen eclogites is shown in Table 4.1.

Rutile Modal Abundance

It is important to accurately determine the abundances of rutile in each sample in order to make reliable connections between the concentrations of elements in rutiles and their corresponding whole-rocks. Petrographic point counting of minor phases is neither efficient enough, nor accurate enough for this purpose. Rather, a scanning

Table 4.1: Overview of samples included in this study. The table includes information on the mass proportion of rutile (calculated from phase maps), the number of rutiles sampled, and the total number of rutile analyses per whole-rock sample.

Sample	Locality	wt.% Rutile	No. Rutiles	No. Analyses
08	Drøsdal	-	7	11
14	Åsnes	-	7	20
30	Kvalneset	0.38	8	16
32	Krokaberg	-	7	13
37	Angelshaug	0.59	6	13
46	Nybø	-	10	16
51	Flatraket	1.97	9	9
53	Årsheimneset	1.18	10	15
63	Sandvollen	3.53	9	16
65	Naustdal	1.31	10	12
67	Fossheim	0.55	10	14
69	Engebøfjellet	0.75	9	11
70	Åsneset	1.01	6	11
71	Holmane	0.97	8	9
72	Raudegga	-	8	12
73	Almenningen	-	10	32
74	Måløy	1.13	7	15
75	Straumen	1.23	7	10
76	Gangeskaret	-	11	41
77	Seljeneset	-	8	12
78	Vengen	7.23	10	16
79	Havik	-	8	17
80	Flister	1.05	12	15
81	Runderheim	1.02	11	13
82	Salt	-	7	8
83	Årdalen	1.18	7	13
85	Hareidland	0.55	5	5
Lef	Lefdal	0.55	9	11

electron microscope was used to produce backscattered electron (BSE) phase maps of polished sections of eclogite from which the volume and mass abundances of rutile in each sample could be calculated with an acceptable level of accuracy. The disadvantage of this technique is that without automated software to image the whole slide, acquisition of phase maps was a time-consuming process. Regardless, the procedure used to acquire BSE images is described below.

Carbon-coated polished sections of eclogites were loaded into a Phillips XL30CP SEM at the School of GeoSciences, The University of Edinburgh. For each sample, the first step was to locate a grain of rutile. Rutile is rich in heavy elements that produce more BSEs, and therefore appears brighter than other phases in the image. The brightness and contrast settings were then adjusted to isolate rutile backscatter from other major minerals (Fig. 4.1). Ilmenite, which produces even more backscatter than rutile, often occurs in close proximity to rutile and therefore further adjustments ensured sufficient greyscale contrast between between the two.

Since the mean size of rutile grains varies from sample to sample, appropriate magnification settings could also vary, and as such so could the number of images required to make a satisfactory phase map of the sample. For most samples, approximately 50-100 images were acquired across the section surface. Acquired images were corrected for pixel shape to accurately reflect the true proportions of rutile.

BSE images for each sample were then batch processed in ImageJ, a free and open source Java-based image processing and analysis program originally developed by the National Institute of Health. A range of greyscale values that isolated rutile were applied to the batch, and a percentage volume computed, which was then converted into wt.%. using the densities of the main phases observed in the eclogites.

Table 4.1 and Figure B.1 show that most samples have between 0 and 1.5 wt.% rutile, which for most samples accounts for around 40-70 % of the whole rock TiO_2, assuming rutile contains 98 wt.% TiO_2. The remaining TiO_2 is probably mostly ilmenite, along with some Ti substituted into major minerals, most likely to be garnet.

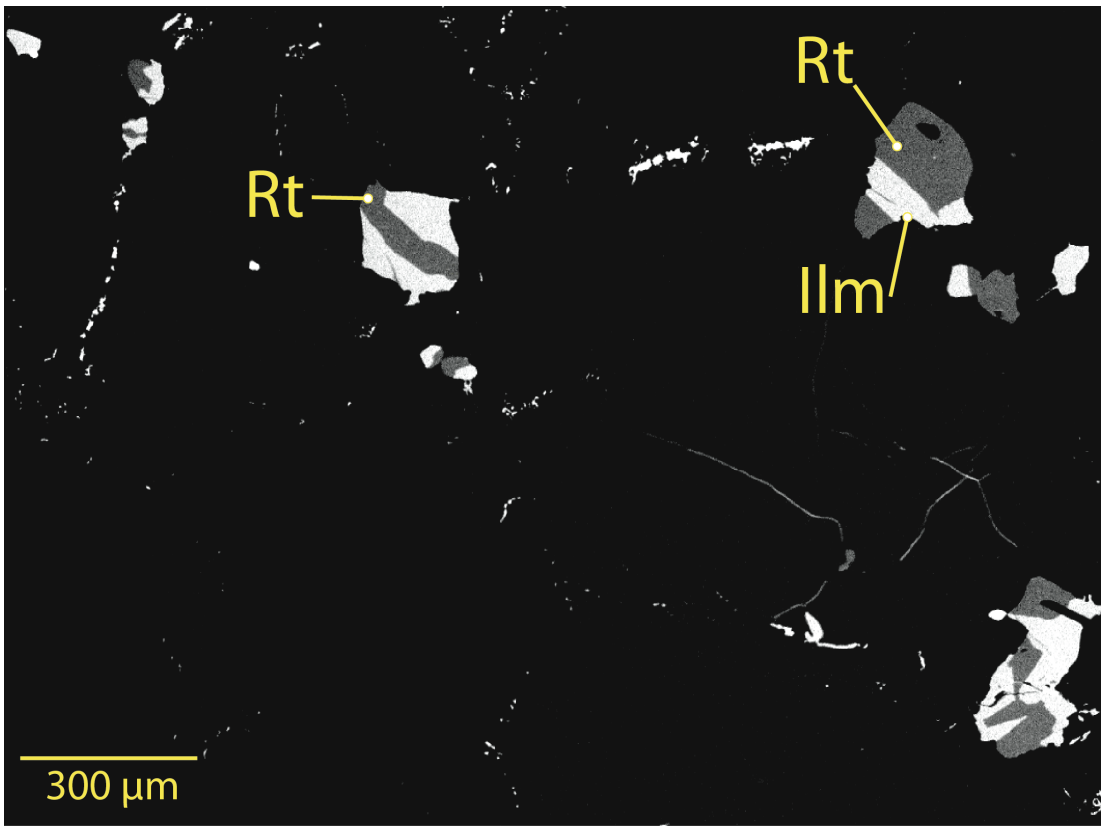

Figure 4.1: Example BSE image of rutile-bearing eclogite from Norway (Sample WGR-22, image 22-008). Rutile (Rt) is 50% grey and ilmenite (Ilm) is white. Modal proportions of rutile were determined by calculating the surface area of rutile from many BSE images using the free image processing software ImageJ.

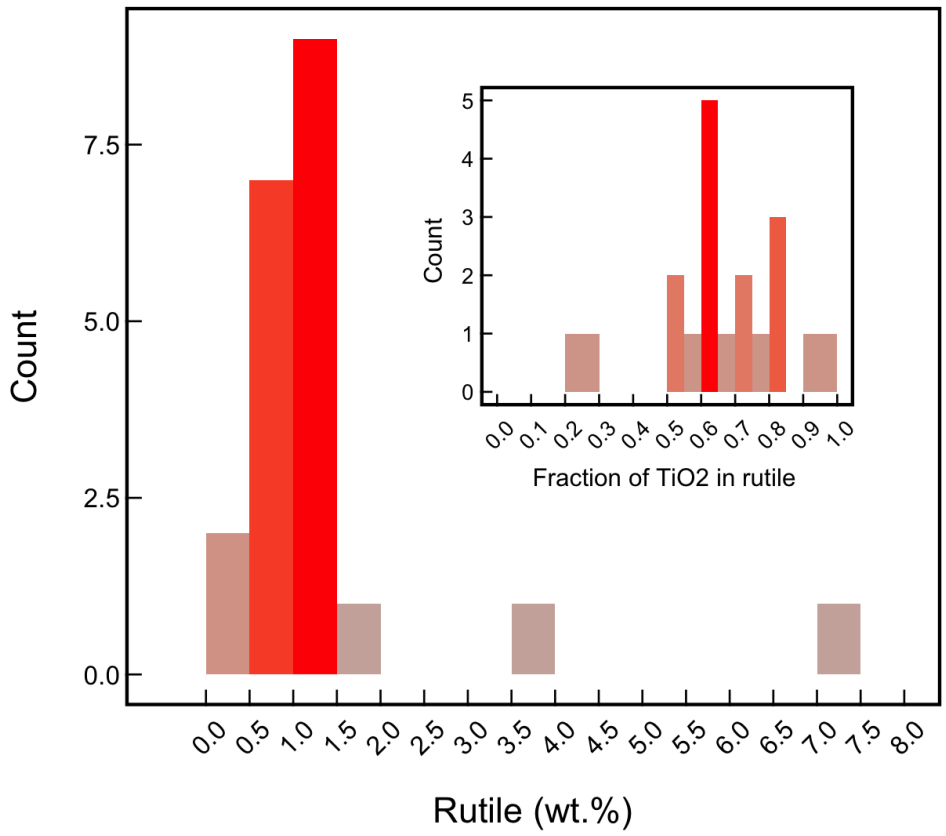

Figure 4.2: Histogram showing the distribution of rutile modal abundances (expressed as fractions, F) in selected Norwegian eclogites. The data show that most samples have up to 1.0-1.5 wt.% rutile, accounting for mostly 50-100% of all available TiO_2.

Crushing and Sieving

Approximately 1.0-1.5 kg of unweathered eclogite was split into fragments of approximately 2-3 cm maximum width using a hand-operated hydraulic rock splitter. The fragments were then loaded into a tungsten carbide jaw crusher and crushed into chips of ca. 0.5 cm diameter or less. The chips were then sieved into three fractions: A $<$120 μm; B=120-212 μm; and C$>$212 μm. Any material with a grain size of $>$ 212 μm was ground in 50 ml batches inside a tungsten carbide grinding barrel for no more than 5 seconds. After each grinding for 5 seconds, the contents were sieved to recover fractions A-C. Any remaining material in the coarse fraction was ground again for no more than 5 seconds until none remained in fraction C. This cyclical grind-remove-grind procedure reduced the amount of material ground into fraction A, most of which would be too fine to analyse.

Fraction B was then placed into a large glass bowl and cleaned using deionised water to remove any fine material (i.e. fraction A) stuck electro-statically or otherwise to the outside of larger grains. The wet sample was transferred to a laboratory tray, covered with tissue and dried for a period of 2 days in a oven at 28^{o}C.

Once dry, a neodymium magnet (2.5cm x 1.5 cm x 0.5 cm) wrapped in a sample bag was passed over the sample in the tray to remove any highly magnetic grains which could later clog the magnetic mineral separator.

Mineral Separation and Mounting

Separation of rutile from the rest of the sample was achieved with a Frantz magnetic mineral separator. The slope and tilt of the slide were set to 20° and 25° respectively. Sieved fraction B (120-212 μm) for each sample was then fed slowly though the machine at 1 A of current, where both the magnetic and non-magnetic fractions were collected and labelled. The 1 A non-magnetic fraction was then fed back into the separator, with the current set to 1.5 A. Once again, both the magnetic and non-magnetic fractions were collected and labelled. The 1.5 A non-magnetic fraction was, in most cases, dominated by grains of quartz and rutile. This final non-magnetic fraction was cleaned one last time using a small amount of acetone.

A surface on which to hold the selected grains for mounting was prepared using a small sheet of glass, a layer of flat silicone sheet, and up-turned brown packaging tape. Using a binocular microscope, grains of rutile were carefully extracted from a Petri dish using fine tweasers and placed into tight grid patterns on the tape adhesive, all within a 10 mm diameter circle. A 25 mm round former was then placed with its center over the grains onto the tape, and approximately 3 ml of epoxy resin poured carefully into the mould using a pipette. The resin was then allowed to set in a pressure chamber in order to reduce the amount and volume of any bubbles that may have formed.

Once the resin was set, the discs were removed and the meniscus on their bottom side ground away to produce a flat surface parallel with the top. Around 5-10 μm of the top surface was ground away carefully to expose flat areas of the embedded rutile grains.

Backscatter electron images (BSEs) of the discs were obtained using the same SEM that was used to create phase maps of eclogite polished sections. The samples were carbon-coated and imaged using the following settings: 20 kV beam potential, 10.0 mm working distance, 72.5 contrast, 42.4 brightness, and 200$\times$ magnification.

4.2.2 LA-ICP-MS

Separated rutile grains were analysed using LA-ICP-MS at the School of Earth and Environmental Sciences (SEES), University of Portsmouth using a New Wave (ESI) UP-213 Laser Ablation System and an Agilent 7500LE Series ICP-MS. The samples were loaded into the vacuum chamber of the laser ablater, and the pressure reduced to 4.9-5.3 $\times 10^{-6}\ Pa$. A laser beam (spot: 40-50 μm; fluence: 4 $J\ cm^{-2}$; energy: 43-44.5 $\%$; frequency: 10 Hz) was used to ablate the sample into a He and Ar gas (He flow rate - 0.75 $l\ min^{-1}$; Ar flow rate - 1.20 $l\ min^{-1}$) which was then fed into the mass spectrometer. The analytical procedure is described in more detail below.

Standards

The standards used to calibrate LA-ICP-MS data were National Institute of Standards and Technology (NIST) Glass standard reference material (SRM) 610 and rutile

standard R10. SRM 610 is a synthetic glass which was first developed in the 1970s by the NIST, Corning Glass Works, and the American Society for Testing and Materials (ASTM) for calibration and control during the bulk analysis of glass only. SRM 610 has since become a popular standard in a variety of micro-analytical applications (Kane, 1998) and its composition is well studied. Preferred values for 610 are taken shown in Table 4.2 and are taken from Pearce et al. (1997) and Rocholl et al. (2000). Rutile R10 is a relatively homogeneous natural sample from Gjerstad, Southern Norway. Provisional values for the composition of R10 were determined by Luvizotto et al. (2009) using a variety of techniques (EMP, SIMS, ID-MC-ICP-MS, LA-ICP-MS). Those provisional values are given in Table 4.3.

Analytical Procedure

Care was taken to choose sensible sites for analysis on each grain: backscatter maps (e.g. Figure 4.3) were used to identify and avoid inclusions or areas of alteration. Where suitable surface area permitted it, a minimum of one core and and one rim analysis were obtained for as many grains as possible per sample. It must be recognised that the designation 'core' can be misleading, as such analyses do not necessarily correspond with the geometric core of the analysed grain (see Figure 4.4).

For each analysis, data acquisition time was $60s$. The time line of events within each acquisition was as follows:

$0s$ - Acquisition starts, recording of background counts per second (CPS)

$10s$ - Laser is fired with the aperture closed

$20s$ - Laser aperture is opened and sample ablation begins

$60s$ - Acquisition ceases, the laser is turned off and ablation stops

The laser was fired $10s$ before ablation begins to enable the beam to reach a stable intensity. A ramp in CPS observed after the ablation begins at $20s$ (see Figure 4.5) is likely to be the result of a number of processes acting throughout the equipment: heating of the sample surface by the laser; evacuation of the vaporised material through

Table 4.2: Preferred values for NIST SRM 610 glass used by the program signal integration for laboratory laser systems (SILLS), obtained from the end-user documentation (Guillong et al., 2008). Only elements analysed are shown here.

NIST SRM 610 Glass		
Element	**wt. ppm**	**Reference**
Al	10791.4	Pearce et al. (1997)
Si	327090.7	Pearce et al. (1997)
Sc	441.1	Pearce et al. (1997)
Ti	434.0	Pearce et al. (1997)
V	441.7	Pearce et al. (1997)
Cr	405.2	Pearce et al. (1997)
Mn	433.3	Pearce et al. (1997)
Zn	456.3	Pearce et al. (1997)
Ga	438.1	Pearce et al. (1997)
Sr	516.0	Rocholl et al. (2000)
Zr	437.0	Rocholl et al. (2000)
Nb	419.4	Pearce et al. (1997)
Mo	376.8	Pearce et al. (1997)
Sn	396.3	Pearce et al. (1997)
Sb	368.5	Pearce et al. (1997)
Hf	421.0	Pearce et al. (1997)
Ta	376.6	Pearce et al. (1997)
W	445.3	Pearce et al. (1997)
Pb	426.0	Rocholl et al. (2000)
U	461.5	Rocholl et al. (2000)

Table 4.3: Provisional prefered values for rutile R10 from Luvizotto et al. (2009). Confidence in values for other elements reported in Luvizotto et al. (2009) are too low to report as standard values.

Rutile R10 Provisional Values	
Element	**Concentration (ppm)**
Zr	789 ± 13
Nb	2633 ± 280
Sb	2.02 ± 0.17
Hf	38.8 ± 1.5
Ta	504 ± 63

tubing into the ICP-MS unit; and the ionization and acceleration of ions towards the detectors. Only readings after CPS become stable may be used to determine the composition of the sample.

Even though care was taken to avoid obvious inclusions and defects in each grain, some analyses show evidence that they were contaminated by inclusions. Contaminated analyses can be identified by steepening or fluctuating CPS data for elements that dominate the composition of expected inclusions. For instance, Figure 4.6 shows undulating and steep lines for Zr and Hf persisting from $22s$ onwards, strongly suggesting that a zircon inclusion was being uncovered and vaporised by the ablation process. One may identify alumino-silicate inclusions in the same manner (e.g. Figure 4.7). Such acquisitions (listed in Table 4.4) were discarded.

Data files from each acquisition were processed using the open source program SILLS (signal integration for laboratory laser systems) developed by Guillong et al. (2008). Acquisition data were loaded into the program in batches of 20, at which point the time ranges of background and sample analysis count data to be used were manually selected on plots similar to Figure 4.5. Analyses 1, 2, 19, and 20 in every batch were of standard 610 (glass), and in every other batch analysis 18 was of rutile standard R10. The internal standard was assumed to be $TiO_2 = 98wt.\%$. SILLS uses all these standards as well as time stamps of each analysis to calculate the composition and

Table 4.4: List of analyses discarded due to corruption of acquisition data by an inclusion. Example of the evidence used is seen in Figures 4.6 and 4.7. For reference, the analysis number format is sample-grain-spot.

Discarded Analyses	
Lab No	**Analysis No**
SE17F03	76-20-02
SE18B05	74-01-02
SE18B10	74-11-01
SE18C07	37-04-03
SE18C16	37-05-01
SE18C17	37-05-02
SE18D05	37-19-01
SE18D06	37-19-02
SE18D16	30-22-01
SE18F13	75-10-01
SE18H08	83-09-02
SE18I03	32-09-01
SE18I04	32-09-02
SE18I09	32-20-03
SE18I10	32-19-01
SE19B04	53-01-02
SE19C16	Lef-02-01
SE19D04	Lef-03-02
SE19D09	Lef-06-02
SE19E16	65-04-01
SE19E17	65-07-01
SE20B08	71-11-01

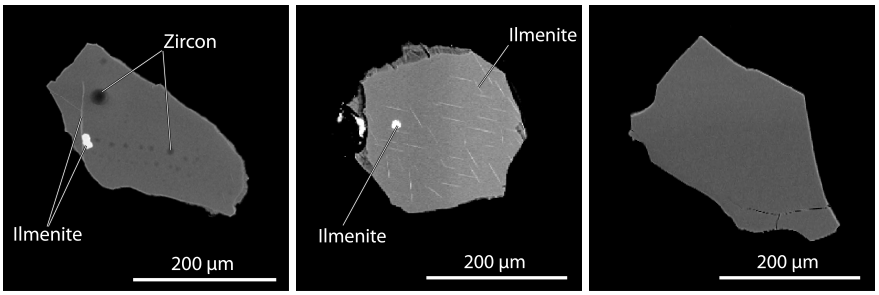

(a) Grain R83-01 (b) Grain R70-08 (c) Grain R79-15

Figure 4.3: Example backscatter images of rutile grains showing features taken into consideration when choosing a site of analysis. Grain R83-01 contains dark circular spots which are interpreted to be radiation halos around zircon: zircon grains would have a white colour if exposed. Light grey-white areas in R83-01 and R70-08 are ilmenite. Ilmenite often occurs as granular inclusions or more commonly as alteration along cracks and cleavage planes. Grains such as R79-15 showed no obvious inclusions, but sometimes the analysis revealed an inclusion had been hit.

accompanying statistical attributes for each analysis.

After conversion to concentration format by the program SILLS, the analyses of the rutile standard R10 were checked for consistency. It can be seen in Figure 4.8 that significant variation in the analysis of R10 only occurs for Pb. This is not thought to be due to instrument drift, but rather because concentration of Pb is around the limit of detection. The negligible variation in the concentrations of the other trace elements is interpreted to mostly reflect minor heterogeneity in the R10 grain, and thus no further correction based on R10 analyses is applied.

4.3 Results

Data on the composition of eclogite-hosted rutiles is presented under headings that help us address the research questions identified in the introduction to this chapter:

- The Trace Element Inventory of Rutile
- Analogous Trace Elements in Rutile
- Comparisons of Rutile and Whole-Rock Composition

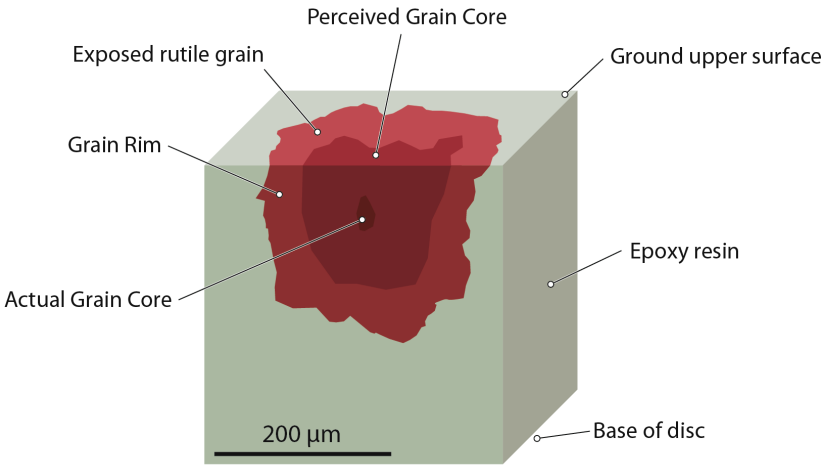

Figure 4.4: Schematic cross section of a mounted rutile grain. The geometric core of the mineral grain is unlikely to coincide with the apparent core as viewed from the 2D exposed section. Similarly, crystals may be broken, in which case even the geometric core will not correspond to the true core of the original crystal. Caution must therefore be used when affixing *core* and *rim* designations to grain analyses.

A statistical summary of the rutile trace element composition within each eclogite is provided in Table 4.5 (pages 166-173), whereas the complete data table is presented in Appendix C (page 333).

4.3.1 The Trace Element Inventory of Rutile

There are two main questions concerning the trace element inventory of rutiles that we wish to address: which elements are found in significant concentrations in eclogite-hosted rutiles; and to what extent does rutile control the budget for these elements in the whole-rock?

Trace Element Inventories of Rutile

Rutile compositions were calculated assuming TiO_2 = 98 wt. %. Figure 4.9 shows most rutiles have a total inventory of analysed trace elements of between 2000 and 4000 ppm, dominated by V, Cr, Nb, Si, Zr, Al and W. The remaining 1.6 to 1.8 wt.% of unallocated composition is assumed to be mostly Fe^{3+} and possibly H^{+}.

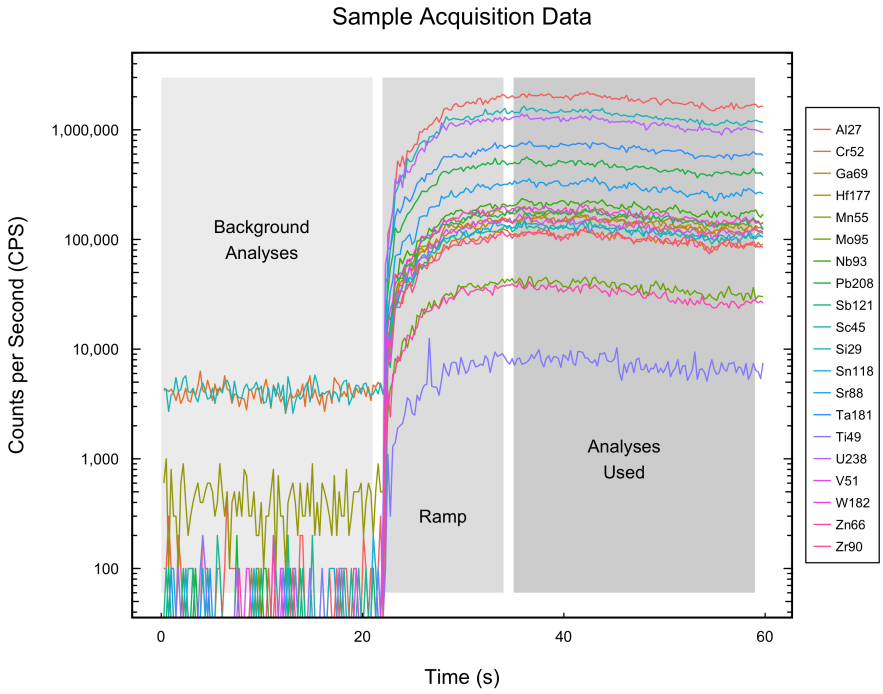

Figure 4.5: Sample acquisition data for a rutile grain in this study. The data may be split temporally into three parts. First, background analyses are collected from $1-20\ s$. The laser aperture is then opened and the ablation commences. It takes approximately $10-15\ s$ for the stream of ions hitting the detector to become stable, at which point the number of counts per second remains reasonably stable. It is only the data within this last part of the acquisition process which are used to calculate the sample composition.

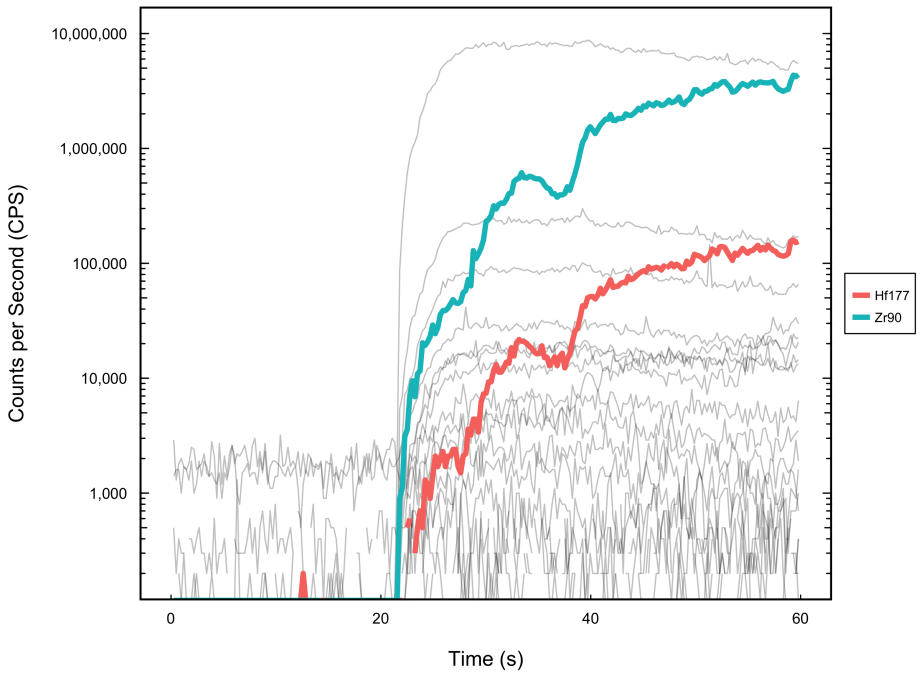

Figure 4.6: Acquisition data for rutile R83-09 spot 02 (lab number 83-09-02). The steep gradients of Zr and Hf indicate that a zircon was being progressively uncovered and ablated together with the surrounding rutile matrix. Since a zircon was clearly included in most of the ablation, this analysis cannot be used to reliably reflect the geochemistry of the host rutile, and thus must be discounted.

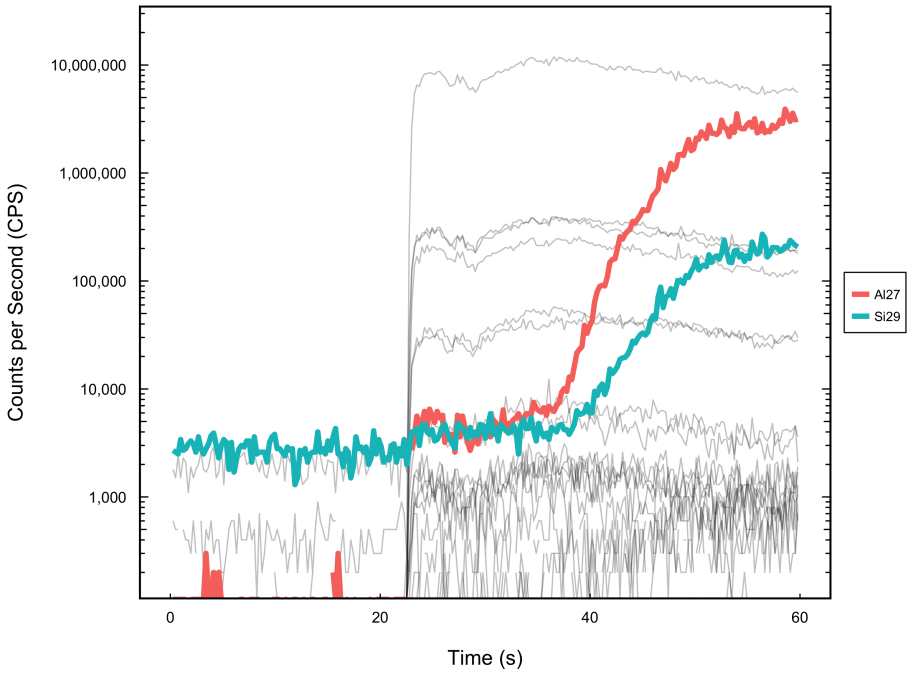

Figure 4.7: Acquisition data for rutile R74-11 spot 01 (lab number 74-11-01). The elements Al and Si appear to indicate that an aluminosilicate inclusion is being progressively ablated together with the surrounding rutile matrix. As with Figure 4.6, such obvious contaminations of the analysis meant the acquisition was disregarded.

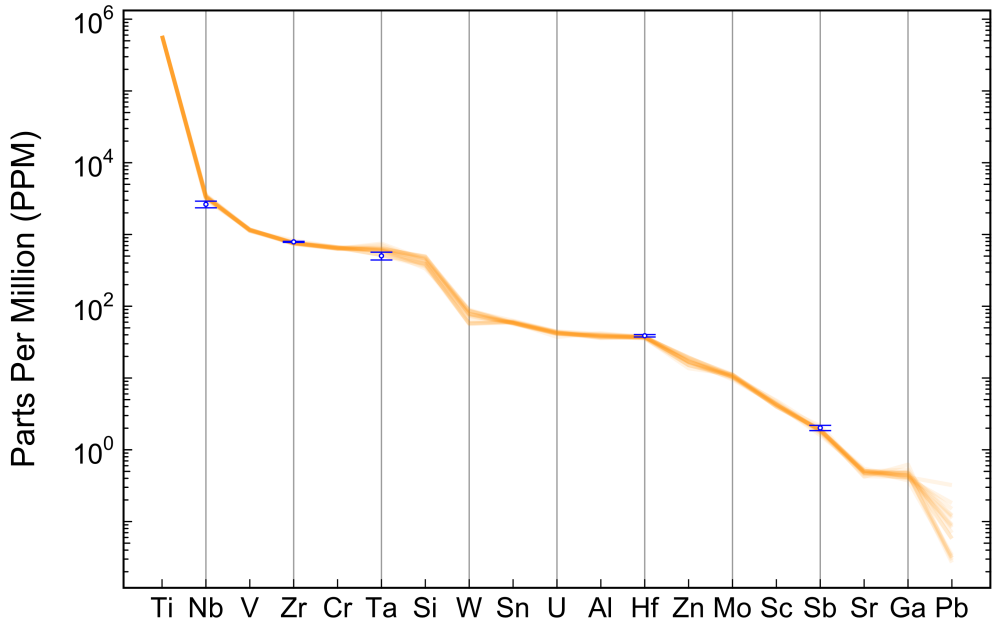

Figure 4.8: Multi-element diagram for R10 analyses. Orange lines represent analyses of R10 from this study, measured as a control at regular intervals alongside unknown rutiles. Blue points and associated error bars represent the accepted values and associated errors for a selection of trace elements from Luvizotto et al. (2009) (see Table 4.3). The diagram shows that most elements have very limited variation, with the exception of Pb which appears to vary in concentration over at least an order of magnitude. Furthermore, measured R10 concentrations appear to largely agree with the values of Luvizotto et al. (2009), perhaps with the exception of Nb, which is slightly higher in our analyses. It was not deemed necessary to apply a dynamic correction to data in this study.

Table 4.5: Summary of LA-ICP-MS data for rutiles analysed in this study. All concentrations are given in ppm.

Sample		14	30	32	37	46	51	53
n_a		20	16	13	13	16	9	15
n_g		7	8	7	6	10	9	10
Al	Min	26.8	58.2	25.1	43.2	27.5	71	45.4
	Max	102.5	160.2	150.2	150.6	244.5	106.5	301.4
	Mean	60.4	91.1	93.5	89.6	101.2	86.7	162.8
	SD	23.7	28.8	44.2	33.3	68.2	11.5	78.6
	Median	61.5	78.1	114.5	82.3	90.9	86.9	165.8
Si	Min	325.4	353.9	340.9	373.2	341.2	331.6	305.1
	Max	479.1	643.9	449.5	476.5	428.6	470.5	913.9
	Mean	422.7	442.8	392.2	420.5	388.8	403.7	474.7
	SD	42.1	63.5	30.7	29	27.4	49.1	188
	Median	428.8	428.5	389.1	423	393.3	401.1	394.4
Sc	Min	1.1	1.3	1.4	1.3	0.4	0.4	0.6
	Max	5.5	3	6.1	4.6	1.8	2.6	1.5
	Mean	2.4	1.9	2.5	2.7	1.2	1.2	1
	SD	1.3	0.5	1.2	0.9	0.5	0.6	0.3
	Median	1.9	1.9	2.2	2.7	1.1	1.1	0.9
V	Min	702.4	1557.5	772.1	957	971.4	824.8	1859.2
	Max	1847.4	2028	2375	1656.9	1134.6	1108.8	2272.8
	Mean	951.4	1752.1	1737	1313.4	1067.9	975.3	2055.5
	SD	399.5	144.2	505.2	239.5	42.9	86.5	130.9
	Median	793.4	1748.7	1868.7	1395.9	1058.7	956.5	2028.2
Cr	Min	823.9	582.1	109.2	13.5	276.6	57	880.8
	Max	2160.4	1399.3	1268.8	4433.7	830.2	75.2	1301
	Mean	1435	1014.9	668	1066.9	401.2	66.4	1164.6
	SD	437.7	275.2	431.9	1529.2	141.1	6	102.8
	Median	1329.6	1066.2	732.2	783.1	389.8	67.4	1205.8
Zn	Min	14.9	13.7	16.2	12.4	10.9	13.6	13.5
	Max	22.2	17.5	19.8	17.2	15.2	20	22.9
	Mean	17.2	15.9	17.1	15	13.3	15.8	16.6
	SD	2.2	0.9	1.1	1.4	1.5	1.9	2
	Median	16.4	16	16.8	14.9	13.3	15.2	16.4
Zr	Min	68.4	146.2	95.7	89.7	175.6	114.3	234.8
	Max	224.7	250.3	222.2	339.4	213.6	152.1	300.7
	Mean	109.9	201.5	160.9	164.6	197.2	141.1	255.3
	SD	50.1	25.8	47.2	75.4	10.6	12.7	15.4
	Median	91.8	201.7	173.4	145.5	197.5	147.5	252.9

n_a - Number of analyses
n_g - Number of grains analysed

Continues on next page...

Table 4.6: Continued...

Sample		14	30	32	37	46	51	53
n_a		20	16	13	13	16	9	15
n_g		7	8	7	6	10	9	10
Nb	Min	128.6	113.2	93.3	87.7	444.7	228.5	700.1
	Max	486.7	192.2	1619.1	127.5	504.2	302.2	802.2
	Mean	361.8	129.5	642.7	103.2	472.7	257.2	751.9
	SD	124.4	18.8	486.4	14.8	15.6	23.6	26
	Median	412.1	127.4	583.5	98	470.1	260.6	758
Mo	Min	4.9	4.5	3.9	3.4	10.4	18.1	52
	Max	9.7	11.3	10.6	4.5	15.5	21	57.5
	Mean	6.2	9.6	7.2	4.1	12.4	19.7	54.7
	SD	1.3	1.6	2.6	0.3	1.6	0.8	1.5
	Median	5.8	10.1	7.5	4.2	11.7	19.9	54.3
Sn	Min	10.6	26.6	8	15.5	22.8	37.3	42.5
	Max	29.8	38.7	48.7	31.7	28.4	41.3	48
	Mean	15.3	29.3	25.2	21.6	26.3	39.5	46.4
	SD	6	3.2	12.9	5.1	1.5	1.6	1.5
	Median	13.5	28.1	21.4	21.1	26.1	40.2	46.5
Sb	Min	2.1	1.8	0.9	0.4	1.4	1.7	13.5
	Max	5.9	2.6	19.1	1.4	2.3	2.5	16.1
	Mean	4.8	2	8.3	0.9	1.9	2.2	14.9
	SD	1.2	0.2	6.7	0.3	0.3	0.2	0.6
	Median	5.3	2	5.7	0.9	2	2.3	15
Hf	Min	3.5	5.7	3.9	3.7	5.6	3.9	8.3
	Max	9.2	9.5	9	15.5	7.6	5.9	11.8
	Mean	4.7	7.8	6.2	7.4	7.1	5.2	9.3
	SD	1.9	1.1	1.6	3.5	0.6	0.7	0.8
	Median	4	8	6.3	6.5	7.2	5.6	9.2
Ta	Min	4.6	7	8.7	4.2	24	11.9	29.7
	Max	35.8	10.4	130.4	14.4	31.1	23.5	59.6
	Mean	22.4	8.6	40.6	7.8	27.6	18.9	42.6
	SD	9.1	1	39.8	3.5	1.8	3.7	8
	Median	24.4	8.5	28.6	6.9	27.5	18.1	43.4
W	Min	1.8	1.3	3.5	2.7	29.7	40.8	50
	Max	2972.1	2	2200.3	5.8	39.2	54.3	167.3
	Mean	2169.8	1.5	301.9	4.1	35	48.5	95
	SD	1018.7	0.2	685	0.9	2.3	5.6	39.8
	Median	2509.5	1.5	38.1	4	35.3	50.9	90.3

Continues on next page...

Table 4.7: Continued...

Sample		63	65	67	69	70	71	72
n_a		16	12	14	11	11	9	12
n_g		9	10	10	9	6	8	8
Al	Min	15.9	100.3	68.2	42.2	31.4	53.3	1.5
	Max	171.5	305.8	230.9	148.7	114.8	244.5	185.9
	Mean	88.6	169	127.3	83.1	65.8	128.2	84.4
	SD	44.4	78.5	50.1	38.2	27.2	57.7	50.4
	Median	86.6	136.9	121.3	78.5	58.8	116.9	78
Si	Min	351.5	367.2	347.3	297.7	370	336.8	319.9
	Max	569.8	485.8	476.9	463.9	592.6	403.9	496
	Mean	410.5	415.5	423.8	381.5	409.4	369.6	391.8
	SD	47.5	39.3	45.4	46.8	62.8	27.9	57.1
	Median	407.2	398	435.5	371.1	390.1	351.1	375.3
Sc	Min	0.8	1.2	1	0.8	1	0.3	0.8
	Max	3	2.9	3.7	6.1	17.1	3.3	18
	Mean	1.5	1.7	1.8	3	3.1	1.4	3.5
	SD	0.5	0.4	0.7	2.2	4.7	0.9	4.8
	Median	1.5	1.7	1.7	1.8	1.7	1.3	2
V	Min	1119.7	1106.3	872.5	838.1	547.5	699	1281.3
	Max	1353.7	1350.6	1145.2	1918.2	1320.4	1863.8	2219.8
	Mean	1268.1	1252.8	997.2	1298.3	1152.9	972.9	1921.3
	SD	77.7	77.1	84.8	499.6	236	497.6	313.4
	Median	1273.3	1276.2	998.4	972.5	1237.7	717.9	2025.3
Cr	Min	158.3	23.1	494.3	177.7	156.9	218.2	262.5
	Max	409.1	73.5	959.7	5277.9	574.1	2109.4	13438.5
	Mean	240.8	48.3	701.5	1642.9	238	1223.2	1412.7
	SD	81.4	18	151.9	1791.4	121.2	665.7	3787.3
	Median	231.3	47.1	662.9	1099.7	201.6	1281.1	333.6
Zn	Min	12.3	15.5	18.3	13.3	10.3	13.6	12.2
	Max	15.8	20.8	21.2	16	13.3	15.1	25.4
	Mean	14	17.4	19.7	14.4	11.6	14.2	16.3
	SD	1.2	1.5	1	0.9	0.7	0.4	4.9
	Median	14.2	17.1	19.7	14.4	11.5	14.2	14.3
Zr	Min	77	74.1	62.7	72.4	107.8	113	96.7
	Max	144.4	97.8	92.7	281.8	186	193.6	243.5
	Mean	115.1	85	77.9	159.6	138.6	144.1	145.1
	SD	20.8	7	9.4	96.6	21.7	26.6	36.3
	Median	118.9	84.6	77.5	83.9	135.7	135.6	139.8

Continues on next page...

Table 4.8: Continued...

Sample		63	65	67	69	70	71	72
n_a		16	12	14	11	11	9	12
n_g		9	10	10	9	6	8	8
Nb	Min	217.4	104.2	443.4	117.1	260.3	458.2	169.5
	Max	325.2	168.5	616.7	637	1164.6	941.4	560.3
	Mean	269.3	137.8	514.5	355.4	440.2	722.1	273.2
	SD	26.4	18.3	50.8	216.3	319.1	168	99.4
	Median	269.1	136.2	507.5	232.4	304.3	749.8	255
Mo	Min	19.7	7.1	7.3	2.2	9.1	4.9	16.5
	Max	28.3	8.9	9.4	22	24.5	19.8	32.5
	Mean	24	8.1	8.5	10.5	20.9	14.9	20.9
	SD	1.8	0.4	0.7	9.1	5.2	5.6	4.3
	Median	24	8	8.2	3.4	22.9	17.3	19.6
Sn	Min	32.4	1.9	20	5.2	35.2	22.3	34.3
	Max	40.8	2.6	34.6	39.9	44.6	50.5	49.5
	Mean	37.2	2.2	29.3	18.3	38.6	29.9	40.4
	SD	2.5	0.2	4.9	14.3	2.9	11.7	4.9
	Median	37.6	2.3	32.5	7.9	37.8	24.2	38.4
Sb	Min	0.2	1.8	9.9	1.6	0.2	2.2	8.4
	Max	0.3	2.5	12.5	22.8	11	10	26.5
	Mean	0.2	2.2	11.2	10	2	5	21.4
	SD	0	0.2	0.8	8.3	3.9	2.8	4.9
	Median	0.2	2.2	11.2	13.5	0.3	4.4	22.8
Hf	Min	3.9	3.6	3.5	3.1	4.4	4.3	7.2
	Max	6.5	4.3	4.5	10	7.3	6.9	11.3
	Mean	5.3	3.8	4.1	6.5	5.8	5.4	8
	SD	0.7	0.2	0.3	2.3	0.8	1	1.1
	Median	5.5	3.8	4.1	6.9	5.6	5.3	7.7
Ta	Min	11.6	5.3	11.8	5.6	12.8	22.3	8.3
	Max	20.3	12.9	46	39	48.2	38	19.1
	Mean	16.8	9.5	30.2	21.4	21.8	29.1	12.1
	SD	2.7	2.5	9.6	12.7	12.5	5.6	2.7
	Median	17.7	9.8	29	16.3	16.7	26.8	11.5
W	Min	1.9	0.8	23.8	2.2	8.3	11.8	41.5
	Max	10.3	1.1	33	6.5	31.4	21.3	117.1
	Mean	7.1	0.9	28.3	3.9	13.1	15.5	62.9
	SD	2.5	0.1	2.5	1.4	7.6	3.2	21.1
	Median	8	0.9	28.9	3.8	10.3	14.8	56.3

Continues on next page...

Table 4.9: Continued...

Sample		73	74	75	76	77	78	79
n_a		32	15	10	41	12	16	17
n_g		10	7	7	11	8	10	8
Al	Min	24.1	68	56.2	0.5	17.7	51.4	0.6
	Max	118.8	213.9	158	1042.4	180.3	285.3	148.1
	Mean	64.9	135.1	92.1	29.9	82.4	120.3	68.2
	SD	29.4	43.6	33.9	162.7	44.3	56.4	34.5
	Median	63.7	151.9	91.2	1.6	78.8	104	70.3
Si	Min	357.2	335.1	360.7	335.9	341.5	259.9	346.7
	Max	554.8	697.8	454.4	1955	401.4	431	453.5
	Mean	452.2	457.3	392.5	502.9	374.9	379.6	404.4
	SD	45.9	84.4	31.1	321.9	19.3	45.9	29.6
	Median	446.9	456	383.7	428.3	376	389	404.4
Sc	Min	0.4	0.6	1	0.8	0.9	0.6	1.2
	Max	6.3	0.9	2.1	2.5	2	1.8	4.8
	Mean	2.6	0.8	1.5	1.4	1.3	1.1	2.6
	SD	1.8	0.1	0.4	0.3	0.3	0.4	1
	Median	1.9	0.8	1.4	1.4	1.2	1	2.4
V	Min	810.9	916.5	955.1	1035.3	1335.8	1141	1190.3
	Max	1246.3	1104.3	1415	1450	1686.4	1386.3	1684.9
	Mean	1028.4	1013.1	1249.3	1262.9	1482.3	1283	1441.7
	SD	127.1	57.2	147	103.1	111.2	71	184.9
	Median	1018.5	1016.9	1286.4	1268.8	1478.4	1291.3	1485.4
Cr	Min	41.7	152.7	168.3	9553.9	6.4	12.9	234.5
	Max	391.1	423.3	450.4	13713.8	87	24.1	1529.2
	Mean	201.8	269.7	323	11228.5	30.4	18.7	950.2
	SD	115.6	93.1	98.4	1198	33	3	329.9
	Median	166.9	235.2	314.1	11085.8	14.6	18.1	950.3
Zn	Min	14.7	11.7	16.8	17.8	15.1	16.8	11.6
	Max	47.1	19.8	18.1	21.9	18.1	18.9	16.8
	Mean	20.2	14.5	17.6	20	16.2	17.9	14.4
	SD	7.3	2.2	0.4	1	0.9	0.6	1.6
	Median	18.2	13.9	17.6	19.9	16.1	18.1	13.9
Zr	Min	135	151	147.7	157.3	129.1	116.6	103.5
	Max	271.7	212.5	169.7	194.8	166.6	161	203.2
	Mean	164.4	176.8	159.1	170.8	143.8	128.2	159.5
	SD	26.2	18.8	8.6	9.1	9.1	11.9	28.7
	Median	159.6	170.8	162.1	169.3	142.2	123.2	160.2

Continues on next page...

Table 4.10: Continued...

Sample		73	74	75	76	77	78	79
n_a		32	15	10	41	12	16	17
n_g		10	7	7	11	8	10	8
Nb	Min	253	468.5	42.9	246.8	157.1	126.8	87
	Max	333	567.6	97.3	593	270.2	233.5	336.2
	Mean	296.7	511.4	64.6	329.9	230	187	132.4
	SD	21.7	24.6	21.8	111.3	32.6	24.6	65.8
	Median	300.6	504.8	62.4	271.9	240.3	185.3	111.7
Mo	Min	7.5	15.3	0.8	20.9	6.3	4.9	8
	Max	10.5	17.7	1.3	28.5	7	6.5	25.9
	Mean	9.1	16.5	1.1	24.3	6.6	5.5	10.7
	SD	0.7	0.8	0.2	1.5	0.3	0.5	5.4
	Median	9.2	16.3	1.1	24.2	6.6	5.5	8.7
Sn	Min	23	33.6	16	25.9	17.3	12.8	23
	Max	33	38.2	21.1	47.5	20.3	15.4	40.3
	Mean	26.9	35.5	17.5	36.4	18.9	14	28.8
	SD	2.3	1.3	1.5	6	1	0.7	4
	Median	26.3	35	17	36.6	19	14	28.3
Sb	Min	2.3	3.3	1.2	7.2	0.2	0.4	0.2
	Max	3.3	6.8	2	11.3	0.3	0.7	5
	Mean	2.9	4.4	1.4	8.8	0.2	0.5	4
	SD	0.2	1.3	0.2	0.7	0	0.1	1.5
	Median	2.9	3.8	1.4	8.8	0.2	0.5	4.5
Hf	Min	4.7	6.6	8.2	6.4	6	4.9	4.6
	Max	9.7	9.1	10	8.2	7.7	6.7	8.7
	Mean	6.2	7.7	9.1	7.4	6.9	5.6	6.4
	SD	1	0.8	0.7	0.4	0.5	0.5	1.3
	Median	6.3	7.5	9	7.3	6.9	5.7	6.3
Ta	Min	9.9	23	2.5	11.4	6	2.1	6.2
	Max	21.7	47.9	5.6	19.8	15.8	20.5	18.3
	Mean	15.1	33.7	3.9	15.6	10.7	10.5	8.4
	SD	2.8	6.2	1.2	1.7	3.3	4	3.2
	Median	15.1	33.7	3.7	15.2	10.6	10.3	7.3
W	Min	5.6	34.4	1.2	45.3	1.4	0.9	6.5
	Max	9.5	52.2	2.6	59.5	1.8	1.7	25.9
	Mean	7.9	40.4	1.9	50.4	1.6	1.2	17
	SD	1	6.5	0.5	3.1	0.2	0.2	4.9
	Median	8	37.1	1.8	49.7	1.7	1.2	16.7

Continues on next page...

Table 4.11: Continued...

Sample		8	80	81	82	83	85	Lef
n_a		11	15	13	8	13	5	11
n_g		7	12	11	7	7	5	9
Al	Min	31.2	24.7	16.9	82	20.1	79.2	61.3
	Max	296.7	757.9	192.3	136.8	305.5	338.4	207
	Mean	105.7	193.8	74.1	105.1	86.4	164.3	134.2
	SD	97.8	235.8	44.9	16.8	76.3	113.7	46.7
	Median	49.9	78.5	66.6	105.9	73.6	95.8	132.7
Si	Min	296.1	351.5	340.4	331	359	364	359.9
	Max	427	1565.8	399.7	448.3	968.2	983.6	433.5
	Mean	368.4	549.7	377.6	379.8	453.4	538.1	397.6
	SD	36.5	329.4	17.1	44.1	158.1	257.1	23
	Median	371.7	399.3	377.2	374.6	409	446.5	403.5
Sc	Min	1.1	0.4	1.4	1.5	0.4	1.2	0.8
	Max	3	7.4	5.1	10.1	6.5	9.7	2
	Mean	1.8	2.8	2.3	3.8	1.5	3.7	1.4
	SD	0.7	1.9	1	2.8	2.2	3.4	0.4
	Median	1.8	2	2.1	3	0.6	2.7	1.5
V	Min	600.6	1247.9	1232.1	1621	618.6	2066.4	787
	Max	1172.8	1772.4	1755.7	2545	1104.7	2693.8	984.8
	Mean	913.7	1584.7	1459.4	1932.3	913	2360.5	912.3
	SD	213.9	187.6	178.6	306.1	181.7	255	70.4
	Median	863.8	1681.7	1422.4	1878	969.7	2331.9	933.4
Cr	Min	332.6	41.5	650.9	99.8	119.3	168.3	948.4
	Max	2350.3	614.6	1525	275	286	1466.2	2108.6
	Mean	1439.6	460.9	1050.6	193.6	201.9	732.4	1196.1
	SD	676.5	145.5	253.6	66.6	49.2	502	320.5
	Median	1477.3	496	1055.4	182.5	200.5	528.2	1144.5
Zn	Min	10.7	9.9	13.1	14	13.6	14.6	11.8
	Max	13.7	24.1	15.8	16.7	18.9	17.2	14.8
	Mean	12.6	13.9	14.2	15.7	15.4	15.7	12.8
	SD	0.8	4.1	0.8	0.9	1.6	1.1	0.9
	Median	12.7	12	14.1	15.7	14.9	15.6	12.5
Zr	Min	80.9	96.8	184.1	257.3	238.3	347.3	182.3
	Max	219.8	242.6	240.3	277.2	329.9	500	220.8
	Mean	117.2	209.6	218.1	265.9	279	407.4	209.4
	SD	49.2	36.3	16.9	7.2	26.5	67.3	10.7
	Median	100.7	216.8	218.7	264.3	282	381.9	212.8

Continues on next page...

Table 4.12: Continued...

Sample		8	80	81	82	83	85	Lef
n_a		11	15	13	8	13	5	11
n_g		7	12	11	7	7	5	9
Nb	Min	73.8	171.9	387.6	488.1	264.5	228.4	410
	Max	582.1	1004	651	680.3	432.8	256.5	836.6
	Mean	227.6	753	567.4	583.1	346.9	237.1	508.3
	SD	174.9	221.2	63.5	62.8	40.9	12.1	120.9
	Median	173.2	719.8	571.2	587.5	352.6	230.3	481.1
Mo	Min	4	8.5	6.2	15.3	20.7	23.4	2.6
	Max	12.9	12.8	7.8	21.8	43.5	25.8	3.8
	Mean	5.8	11.2	7	18.8	25.1	24.4	3.2
	SD	3.5	1.2	0.5	2.3	7.2	1.2	0.3
	Median	4.3	11.4	7	19.7	22.3	23.7	3.2
Sn	Min	5.7	1.9	17.8	26.2	25.9	25.2	13.7
	Max	27.3	45	24.6	35.8	53.4	41.6	16.6
	Mean	10.9	34.1	21	31.8	32.2	31.3	15.4
	SD	7.8	10	2.1	4	8.9	6.7	0.8
	Median	7.6	35.7	20.5	33.9	29.3	27.8	15.6
Sb	Min	1.8	2	1	1.5	7.5	1.3	1
	Max	5.6	3.9	2.2	1.9	8.4	1.9	1.7
	Mean	4.1	2.5	1.7	1.7	8	1.5	1.3
	SD	1.3	0.4	0.3	0.1	0.3	0.2	0.2
	Median	4.5	2.4	1.7	1.7	8.1	1.5	1.3
Hf	Min	3.8	4	6.7	8.8	7.1	12.6	5.3
	Max	7.8	9.8	9.2	10.4	10.3	17.4	9.7
	Mean	5	7.9	7.9	9.6	9	14.2	8.6
	SD	1.4	1.6	0.7	0.5	1.1	1.9	1.2
	Median	4.6	8.1	7.8	9.7	9.3	13.6	8.8
Ta	Min	2.9	13.2	31	32.9	16.4	8.2	16.1
	Max	30.3	140.3	34.4	38.2	19.2	12.6	23.8
	Mean	13.9	61.9	32.9	36	17.8	10.1	20.9
	SD	10.3	37	0.9	1.8	0.8	1.7	2.3
	Median	12.6	45.6	32.8	35.9	17.8	10.2	21.5
W	Min	35.6	1	5	3.7	15.7	139.8	7.2
	Max	120.5	45.1	13.4	4.6	29.3	175.4	27.5
	Mean	91.3	35.3	9.6	4	18.7	156.7	14
	SD	30.9	10.1	2.6	0.3	3.6	12.8	6.3
	Median	108.8	37.7	9.5	3.9	17.3	155	13.3

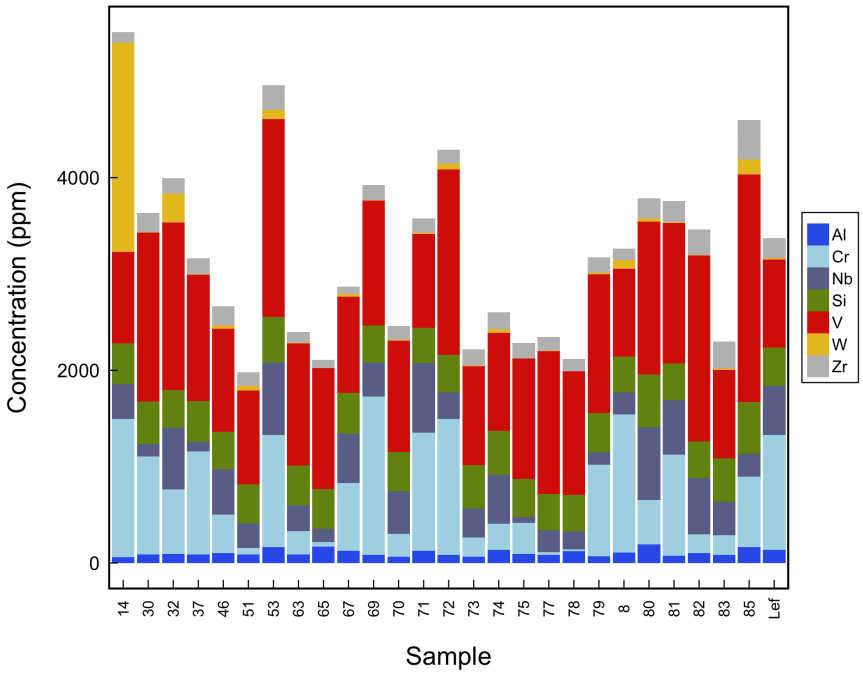

Figure 4.9: Cumulative bar plot of selected trace element compositions in analysed rutiles. The plot shows that V is the dominant trace-element, followed by Cr, Nb, Si, Zr and W. Sample 76 has been omitted due to unusually high concentration of Cr (11229 ppm).

Histograms for each analysed element in all rutiles are presented in Figure 4.10. The elements Si, Al, Zn, V, and Sc exhibit normal distributions, whereas Mo, Sb, Nb, and Ta show varying degrees of bimodality.

Rutile's Control on Whole-Rock Inventories

The mass balance equation below (equation 4.1) describes the relative contributions of two components of known mass fraction and concentration to the concentration of the combined mass.

$$C_{total} = (X_1.C_1) + (X_2.C_2) \tag{4.1}$$

Where C is the concentration and X is the mass fraction of component 1, component 2, and the total. We may adapt equation 4.1 to calculate the proportions of the whole-rock inventory for a chosen element present in rutile:

$$\%\ Inventory\ in\ Rutile = \frac{X_r.C_r}{C_{total}} \times 100 \tag{4.2}$$

Where C_r is the concentration measured in rutile, X_r is the mass fraction of rutile, and C_{rest} is concentration stored in all other phases.

Equation 4.2 was applied to our samples using corresponding rutile and whole-rock data (Appendix C.2, page 305). Figure 4.11 shows the typical percentages of whole rock inventories stored in rutile for a number of trace elements, calculated from the mean compositions of analysed rutile grains. The plot shows that rutiles from Norwegian eclogites mostly contain 50-98% and 43-90% of whole rock Nb and Ta respectively, along with significant amounts of whole rock Sn (8-30 %) and Mo (2-26%). The concentrations of other elements in rutile (i.e. V, Zr and Hf) each account for less than 5-7% of the whole rock inventory. Less than 1% of the total inventory for all other analysed trace elements are stored in rutile, and were not plotted in Figure 4.11.

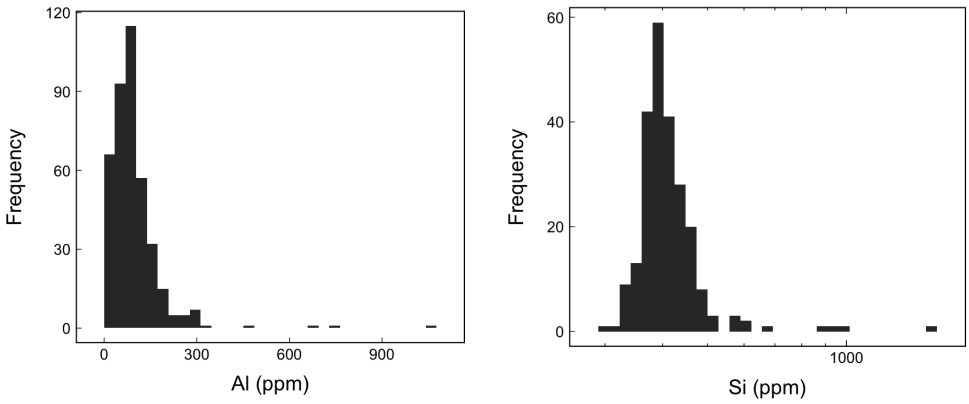

(a)

(b)

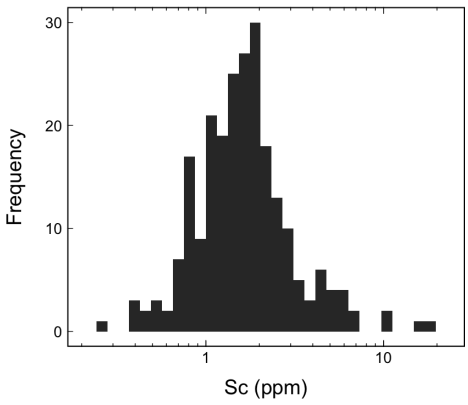

(c)

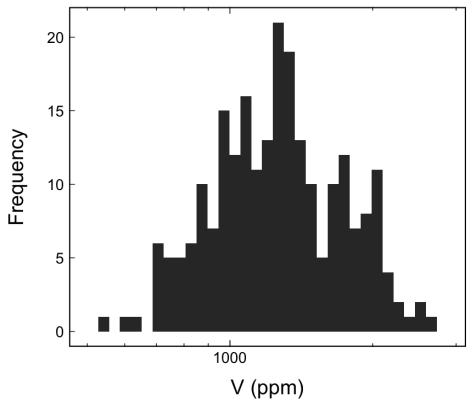

(d)

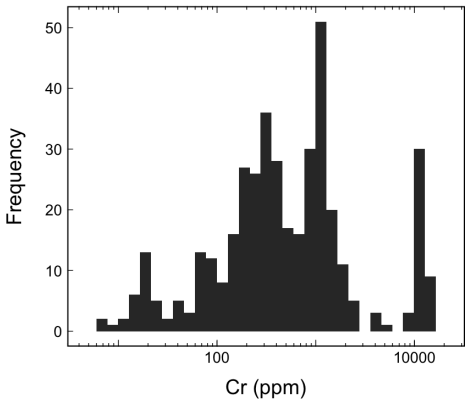

(e)

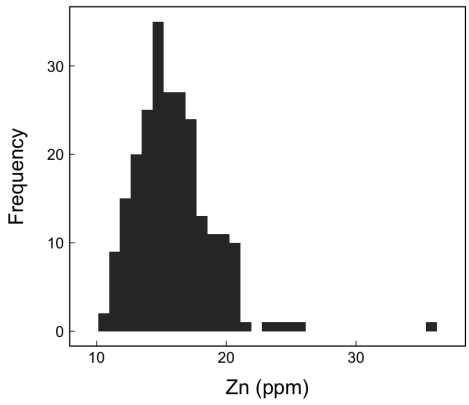

(f)

Figure 4.10: Continued...

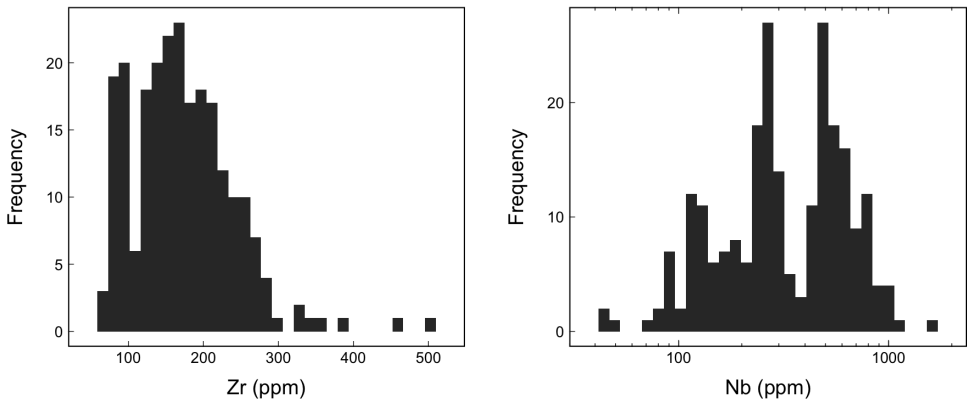

(g)

(h)

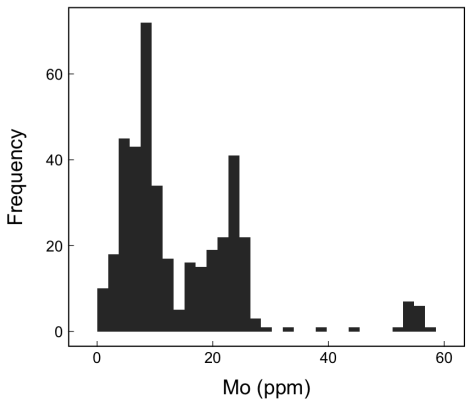

(i)

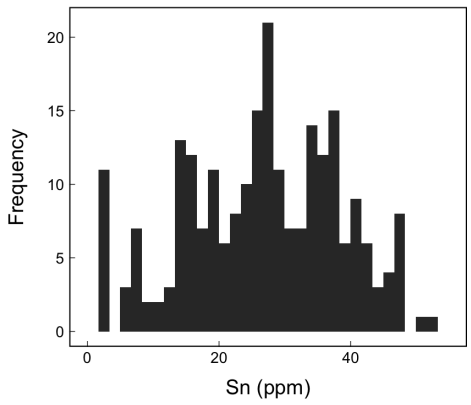

(j)

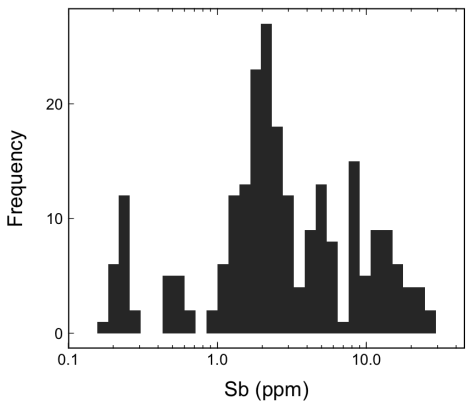

(k)

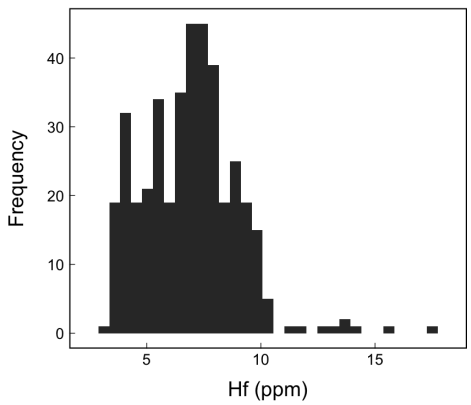

(l)

Figure 4.10: Continued...

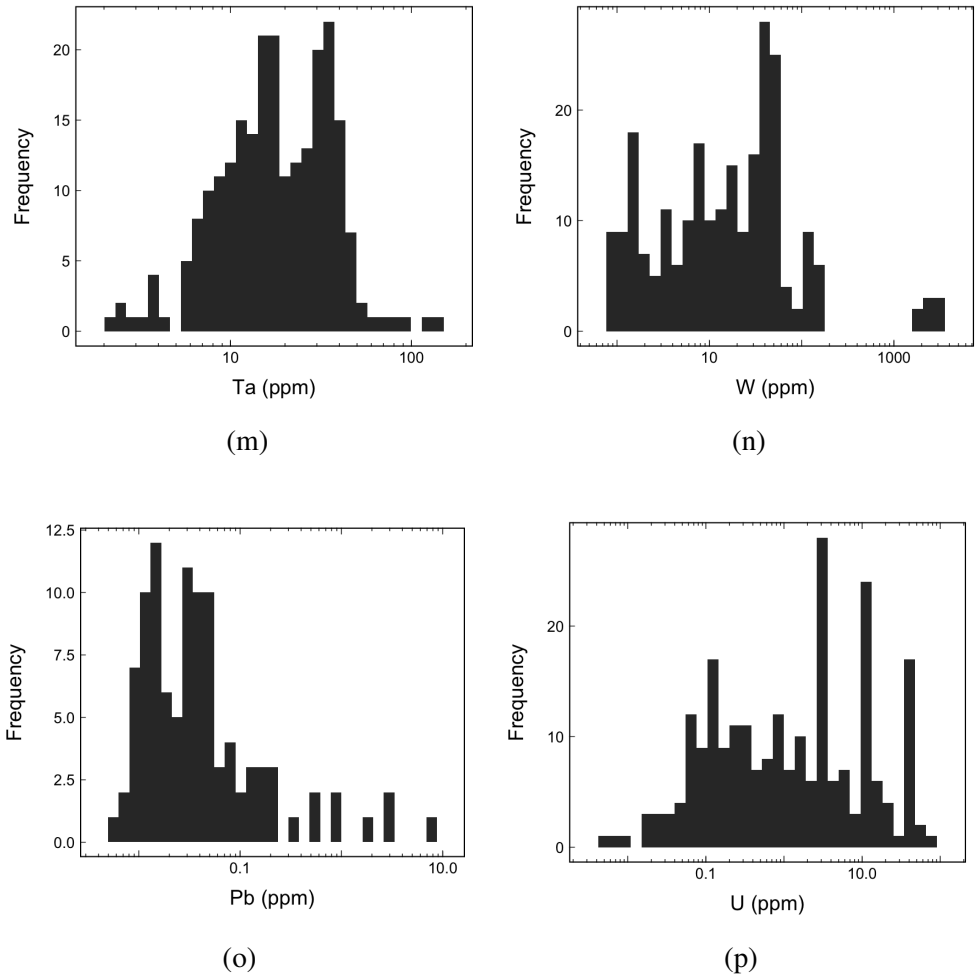

Figure 4.10: Density distribution plots for element concentration of weighted mean rutile compositions. Normal distributions are observed in Si, Al, Zn, V and Sc. Bimodal distributions are present in Mo, Sb, Nb and Ta.

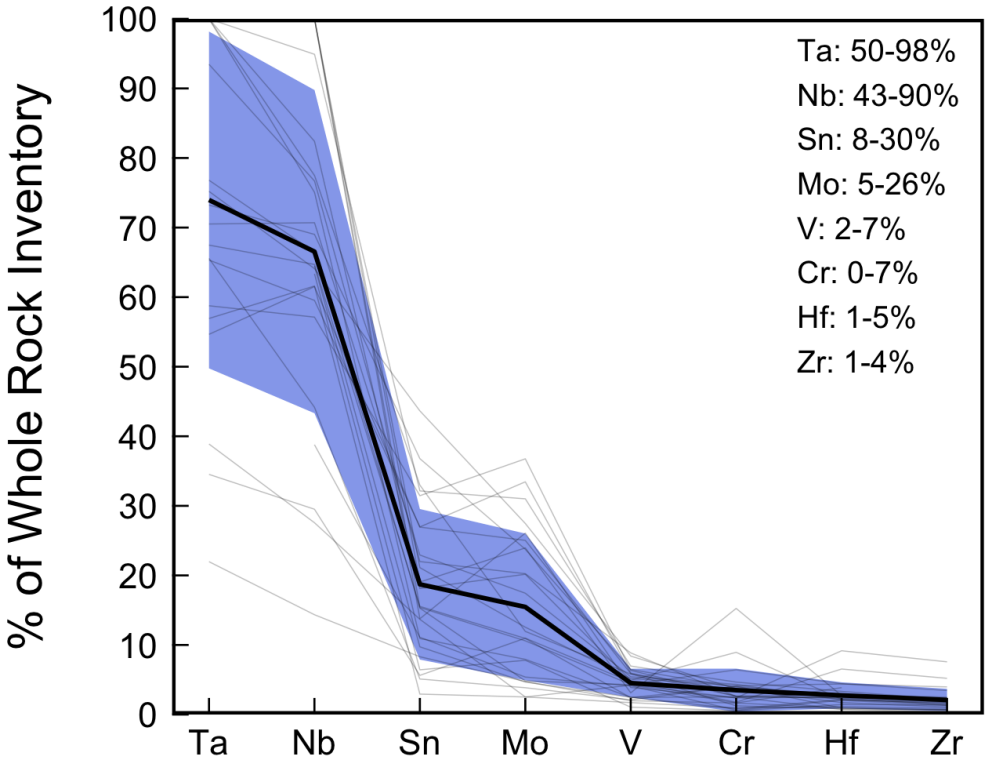

Figure 4.11: Diagram showing the calculated inventories of whole rock trace elements stored in rutile, expressed as a percentage of the whole rock total. Thin lines represent individual samples, whereas the thick line and accompanying blue band represent the mean and 2σ spread of the entire dataset respectively. The figure confirms the observations of others that whole rock Ta and Nb are often dominantly controlled by rutile.

4.3.2 Analogous Trace Elements

Coupled substitutions in rutile occur due to the need to maintain charge neutrality (e.g. Bromiley et al., 2004). For instance, the pentavalent cations Nb^{5+} and Ta^{5+} are thought to enter rutile coupled to a trivalent cation such as Fe^{3+}, Al^{3+} or Cr^{3+}, replacing two Ti^{4+} cations. Bromiley et al. (2004) show that H^{+} ions may frequently be coupled to Fe^{3+}, potentially making rutile a rather hydrous rather than a nominally anhydrous mineral (NAM).

However, there are also elements that show analogous partitioning into rutile, the best known being Nb and Ta. Their partitioning into rutile is not coupled in sense of charge balance, but are analogous due to their similar affinities for substituting into the rutile lattice. Elements whose concentrations are seemingly linked in rutile are identified below.

Correlation Matrices

Correlation coefficient matrices can identify potentially significant relationships in a dataset that warrant further investigation, and are calculated as Pearson product-moment correlation coefficients. Figure 4.12 is a correlation matrix for all rutile analyses obtained in this study, whereas Figure 4.13 shows several correlation matrices based on the groups assigned to the host eclogite in the previous chapter.

Figure 4.12 identifies many statistically correlated element pairs in the total rutile population. Not all the element pairs identified as being statistically correlated necessarily represent geochemically analogous substitutions into rutile. However, the particularly strong correlations between Nb and Ta (ρ = 0.99), Zr and Hf (ρ = 0.9), and U and Cr (ρ = 0.79) suggest that these elements may indeed be geochemically coupled. Other generally highly correlated element pairs include Pb and Sr (ρ = 0.79), and Sn and Mo (ρ = 0.63 to 0.81).

Figure 4.13 shows that although strong correlations remain between Nb and Ta, and Zr and Hf in all eclogite groups, the strength and significance of correlation between many other element pairs can vary significantly between host eclogite groups. For instance, Nb and Mo are significantly correlated in group A and C eclogites ($\rho = 0.36$

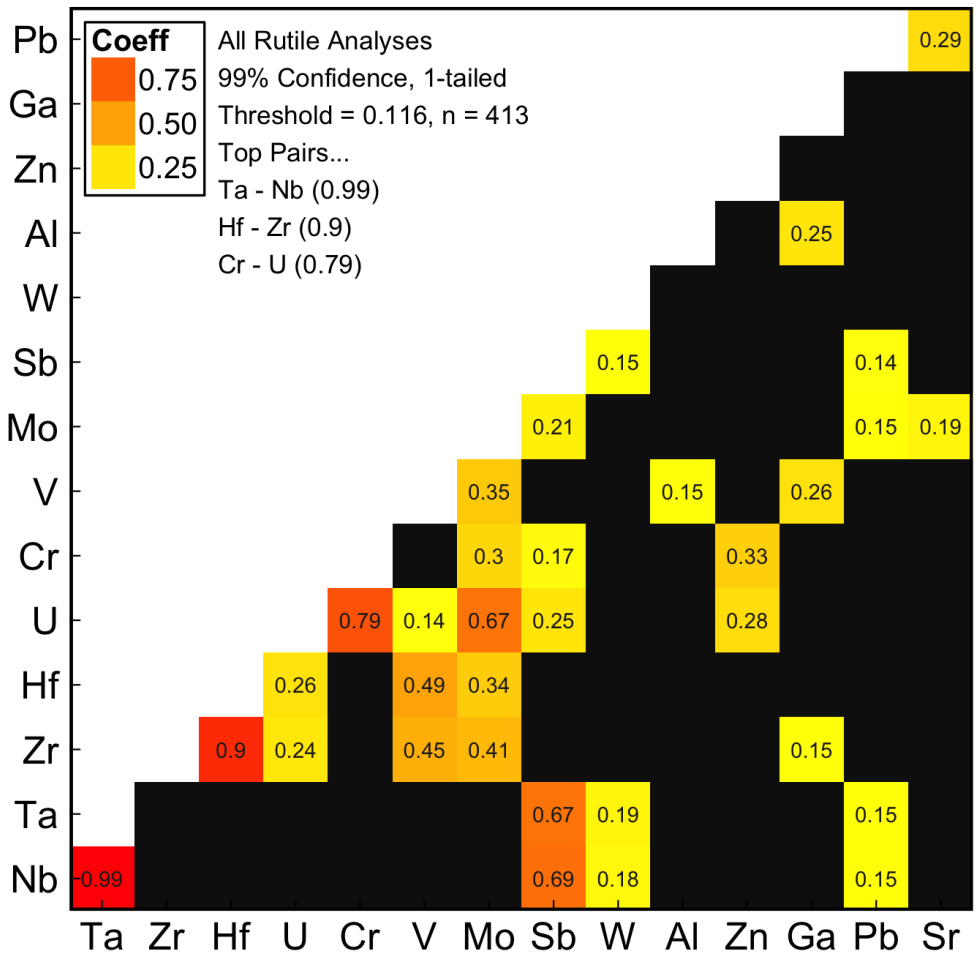

Figure 4.12: A correlation coefficient matrix for elements analysed in rutiles from Norwegian eclogites. Coloured squares represent statistically significant correlations that exist between elemental abundances in analysed grains. Above the threshold, the relative significance is highlighted using a yellow-red colour scale. The figure shows that Nb-Ta and Zr-Hf are the most significantly correlated element pairs in the analysed rutiles.

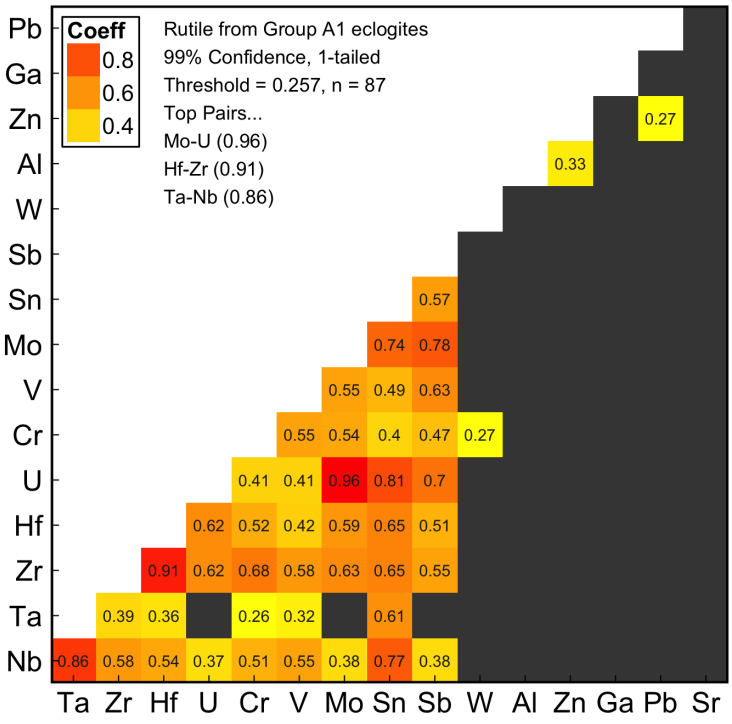

(a)

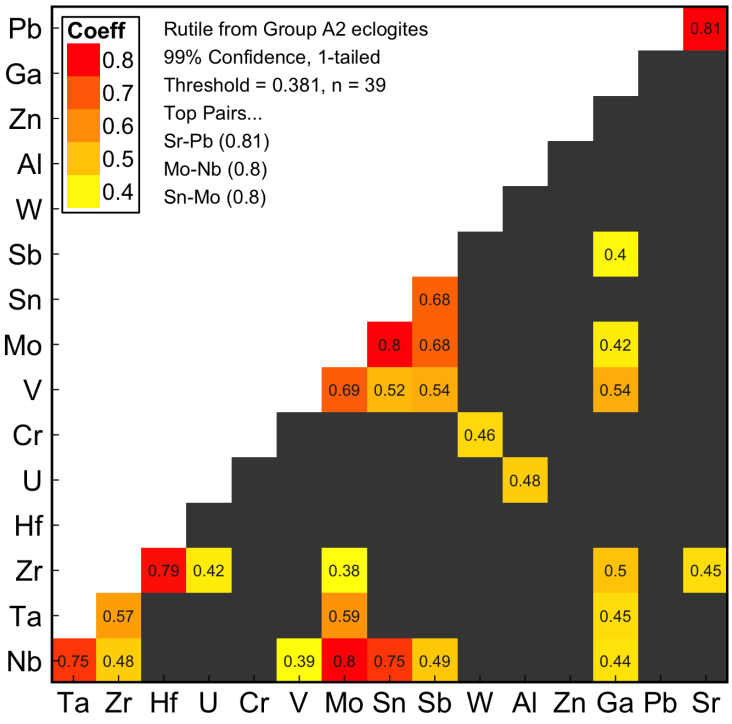

(b)

Figure 4.13: Continued... (1/2)

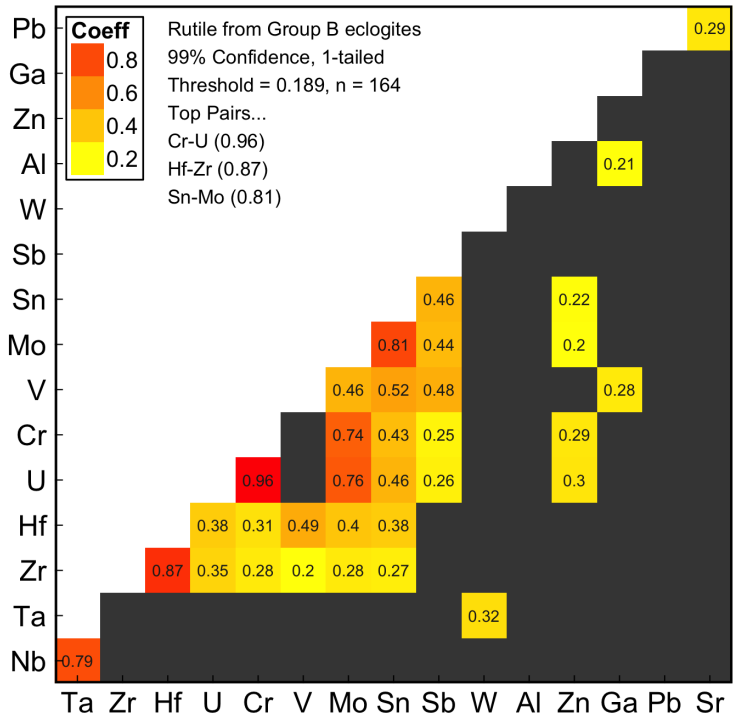

(c)

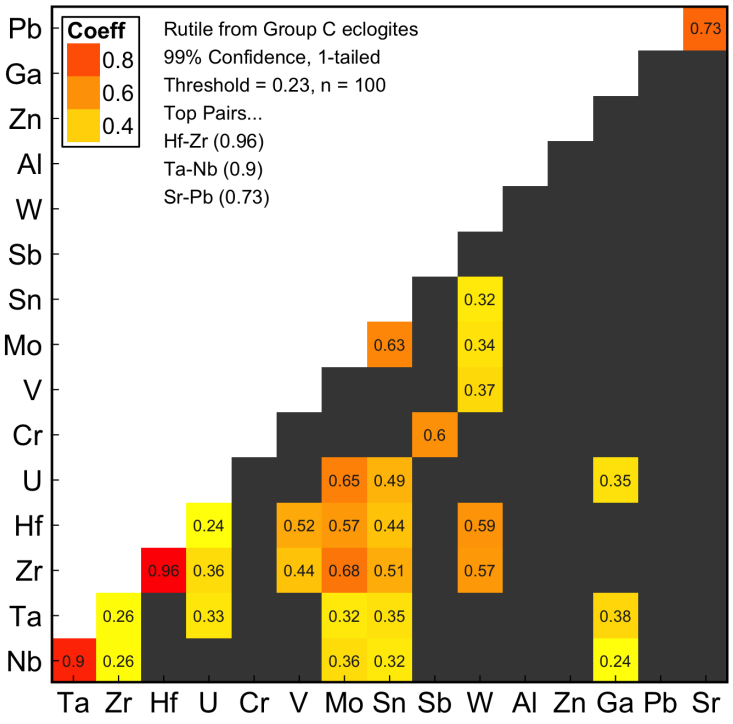

(d)

Figure 4.13: A correlation coefficient matrix for elements analysed in rutiles from Norwegian eclogites. Coloured squares represent statistically significant correlations which exist between elemental abundances in analysed grains. Above the threshold, the relative significance is highlighted using a yellow-red colour scale. The figure shows that Nb-Ta and Zr-Hf are the most significantly correlated element pairs in the analysed rutiles.

to 0.8 respectively), but not in group B ($\rho < 0.189$).

Nb and Ta

The mean Nb and Ta composition of individual rutiles are generally highly correlated ($\rho_{Nb/Ta} = 0.99$, Figure 4.12), as are the average rutile compositions for each whole-rock (Figure 4.14). Table 4.13 and error bars in Figure 4.14 show the standard deviation of Nb and Ta concentrations for all analyses within each whole-rock. They show that Nb and Ta concentrations within the rutile population of each whole-rock sample are highly variable. Most rutile populations have a standard deviation in Ta of 10-30 ppm, and a range in Nb of often in excess of 100 ppm. Despite the huge scatter within and amongst rutiles in any whole-rock, Figure 4.14 shows that the mean Nb and Ta composition of all rutiles in each whole-rock consistently show a chondritic Nb/Ta of around 19.9.

Zr and Hf

Zr and Hf concentrations in rutile are generally well correlated (ρ = 0.9, Figure 4.12; R^2 = 0.799, Figure 4.15). Figure 4.15 shows that rutiles have almost exclusively subchondritic Zr/Hf of around 30 (R^2 = 0.86). There appears to be no systematic difference in the correlation of Zr with Hf between rutiles hosted in eclogites from different whole-rock groups. Error bars plotted in Figure 4.15 show the standard deviation in Zr and Hf for all measured rutiles in each whole-rock. Those standard deviations are relatively low compared with those observed for Nb and Ta, showing only variations of <10 ppm.

U and Cr

Figure 4.12 indicates that U and Cr are strongly correlated in the whole rutile dataset (ρ = 0.79). However, Figures 4.13a-4.13d show that this correlation doesn't hold within eclogite groups. Cr in rutile can vary from not much more than a few ppm to over 3000 ppm, whilst U is generally only 0-2 ppm. Consequently, the data are well described by a line with a near-zero gradient. The identification of this statistically significant, yet geologically insignificant relationship highlights why correlation

Table 4.13: Summary of Nb and Ta variation in analysed rutiles. Abbreviations: SD, standard deviation; RSE, relative standard deviation.

Sample	Mean Nb (ppm)	Mean Ta (ppm)	Nb/Ta	SD Nb (ppm)	SD Ta (ppm)	RSD Nb (%)	RSD Ta (%)
08	196.8	11.66	16.9	171	10.297	87	88
14	381	23.88	16	122	8.863	32	37
30	126.8	8.5	14.9	13	0.922	10	11
32	644.7	40.64	15.9	486	39.644	75	98
37	104.4	8.41	12.4	15	3.939	15	47
46	474.2	27.59	17.2	13	1.72	3	6
51	257.2	18.95	13.6	24	3.661	9	19
53	758.5	43.21	17.6	24	8.453	3	20
63	270.8	16.55	16.4	21	2.076	8	13
65	138.1	9.44	14.6	16	2.357	11	25
67	522.8	31.94	16.4	50	8.622	10	27
69	325.1	19.23	16.9	210	11.787	65	61
70	558.8	26.07	21.4	407	16.196	73	62
71	755.1	29.81	25.3	145	5.463	19	18
72	262	11.76	22.3	81	2.405	31	21
73	296.9	15.41	19.3	21	2.32	7	15
74	512.3	33.34	15.4	17	4.703	3	14
75	68.6	3.81	18.00	23	1.256	33	33
76	351.6	15.77	22.3	135	2.203	38	14
77	228.1	10.63	21.5	37	3.149	16	30
78	186.3	10.29	18.1	27	4.165	14	41
79	129.7	8.17	15.9	42	2.258	33	28
80	721.4	55.55	13	229	33.851	32	61
81	560.8	32.75	17.1	64	0.869	11	3
82	594.9	36.1	16.5	57	1.851	10	5
83	343.8	17.75	19.4	55	0.893	16	5
85	237.1	10.13	23.4	12	1.679	5	17
Lef	527.5	20.71	25.5	126	2.406	24	11

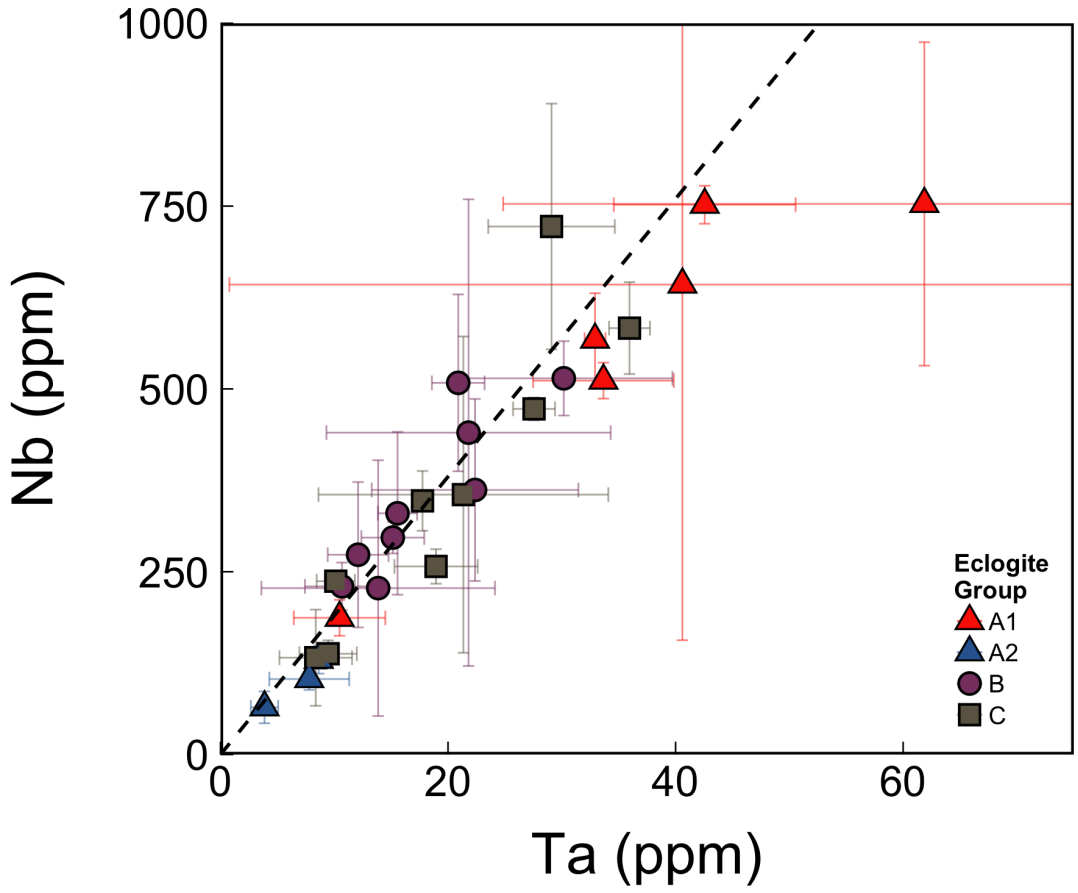

Figure 4.14: Nb vs. Ta variation diagram for rutiles in Norwegian eclogites. Points show the average rutile composition for each whole rock, with symbols indicating the whole-rock eclogite group. Error bars represent the standard deviation of Nb and Ta in all rutile analyses for each whole-rock. The dashed line has a slope of Nb/Ta = 19.9, i.e. chondritic.

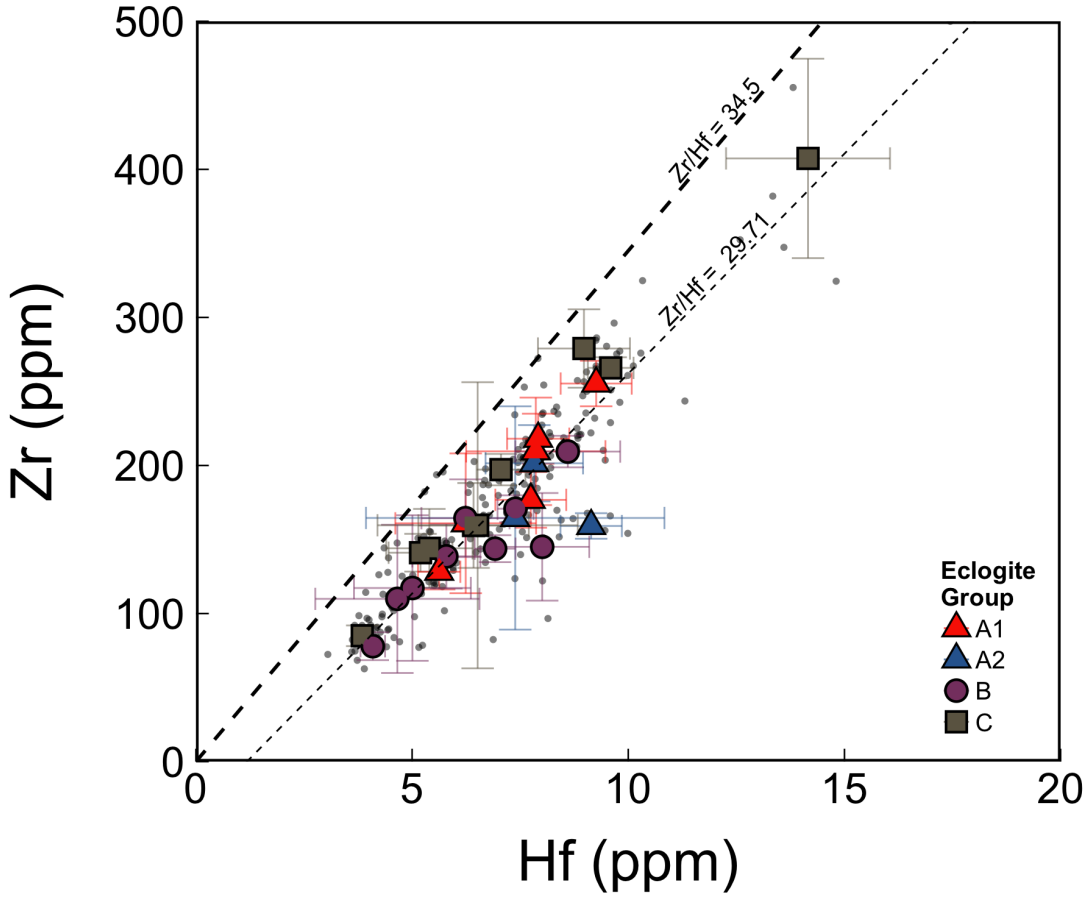

Figure 4.15: Zr vs. Hf variation diagram for rutiles from Norwegian eclogites. Points show the average rutile composition for each whole rock, with symbols indicating the whole-rock eclogite group. Error bars represent the standard deviation of Zr and Hf in all rutile analyses for each whole-rock. The thick dashed line has a slope of Zr/Hf = 34.5, i.e. chondritic. The thin dashed line is a line of best fit, which has a slope of Zr/Hf approximately equal to 30.

coefficient matrices are useful only as a tool to suggest relationships for further investigation.

Sn and Mo

Many rutiles in this study exhibit very strong correlations between Sn and Mo (e.g. ρ_{A1} = 0.74, ρ_{A2} = 0.8, ρ_{A2} = 0.81, ρ_{C} = 0.63, Figures 4.13a-4.13d and 4.16). Figure 4.16 shows in more detail that Sn and Mo for many samples are indeed highly correlated, fitting well to a line where Sn/Mo = 5. However, it is clear from Figure 4.16 that there is a significant population of rutiles in which Sn and Mo are not correlated. Samples that deviate from the a line of Sn/Mo = 5 tend to have higher Mo (>15 ppm) yet similar or only slightly elevated Sn (24-50 ppm). Figure 4.17 illustrates in more detail the distribution of Mo concentrations in rutiles from different eclogite groups, showing in particular that group B and C eclogites possess the highest populations of these high-Mo rutiles, whereas group A show very few high-Mo rutiles. The relatively high number of high-Mo rutiles in group C eclogites can help explain the much lower correlation coefficient for Sn and Mo shown in Figure 4.13d. Interestingly, group C eclogites were classified as such because whole rock N-MORB-normalised multi-element signatures were highly chaotic, and as such were interpreted to be characteristic of significant hydrothermal alteration. The significance of the relationship between Sn and Mo is described in more detail in the discussion, where the other annotations in Figure 4.16 are explained.

Nb and Mo

Figures 4.13a - 4.13d (pg. 182) show that Nb and Mo are only strongly correlated in rutiles from group A2 eclogites (ρ_{A2} = 0.8), weakly correlated in rutiles belonging to group A1 and C eclogites (e.g. ρ_{A1} = 0.38, ρ_{C} = 0.35) and not at all within the entire rutile population (Figure 4.12). Figure 4.18 shows a variation diagram for Nb and Mo. Note that those samples with rutiles that contain Mo >15 ppm may represent a group of eclogites with a different geochemical or metamorphic history (Figure 4.16). There is no obvious significant correlation between Nb and Mo for any group of samples, particularly when one considers those with with Mo <15 ppm separately.

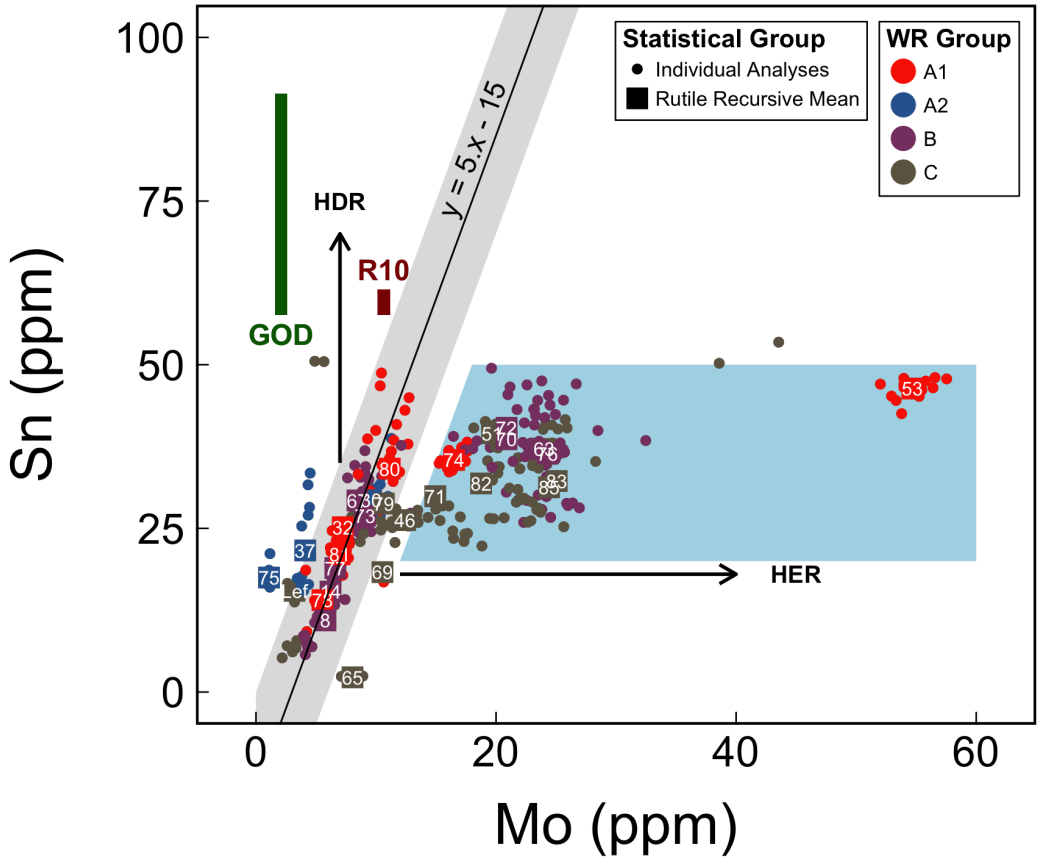

Figure 4.16: Variation diagram for Sn and Mo. The diagram shows that samples with relatively low Mo (<15 ppm) typically have correlated Sn and Mo. Samples with higher Mo show no correlation between Sn and Mo. GOD and R10 are hydrothermally deposited rutiles (HDRs) whereas those with high Mo and low Sn are thought to be hydrothermally enriched rutiles (HERs).

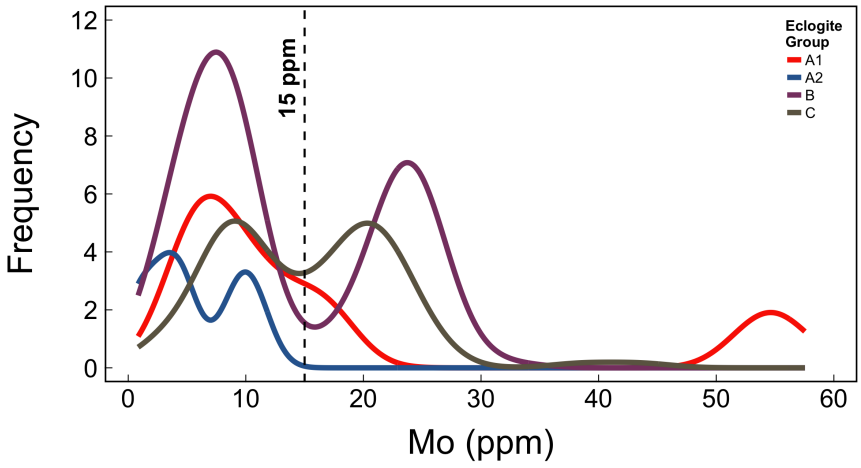

Figure 4.17: Density distributions of Mo in rutile for the four eclogite groups. Dashed vertical line at Mo = 15 ppm indicates the approximate trough between bimodal peaks. Group B and C eclogites have the most pronounced bimodal distributions, with the largest proportions of rutiles with more than 15 ppm Mo.

4.3.3 Comparisons of Rutile and Whole-Rock Composition

It is obvious so far that significant proportions of the whole-rock HFSE budget may be sequestered in rutile. For those elements with the highest affinity for rutile (i.e. Ta, Nb, Sn and Mo), strong correlations should exist between rutile and the host rock concentrations. Furthermore, important relationships between rutile and whole rock concentrations appear to exist, and may yield potentially useful information about the connections between rutile and whole-rock geochemistry.

Nb and Ta

Figure 4.14 above (page 186) shows that the greater the concentration of Nb and Ta in the whole rock, the greater the concentration of Nb and Ta in rutile. For instance, rutiles from eclogites that have low Nb (group A1) have Nb $<$150 ppm, whereas those from more enriched eclogites (group A2) tend to have rutiles with Nb $>$400 ppm. This simply illustrates that the concentration of Nb and Ta in rutile must be largely controlled by the availability of Nb and Ta in the whole-rock.

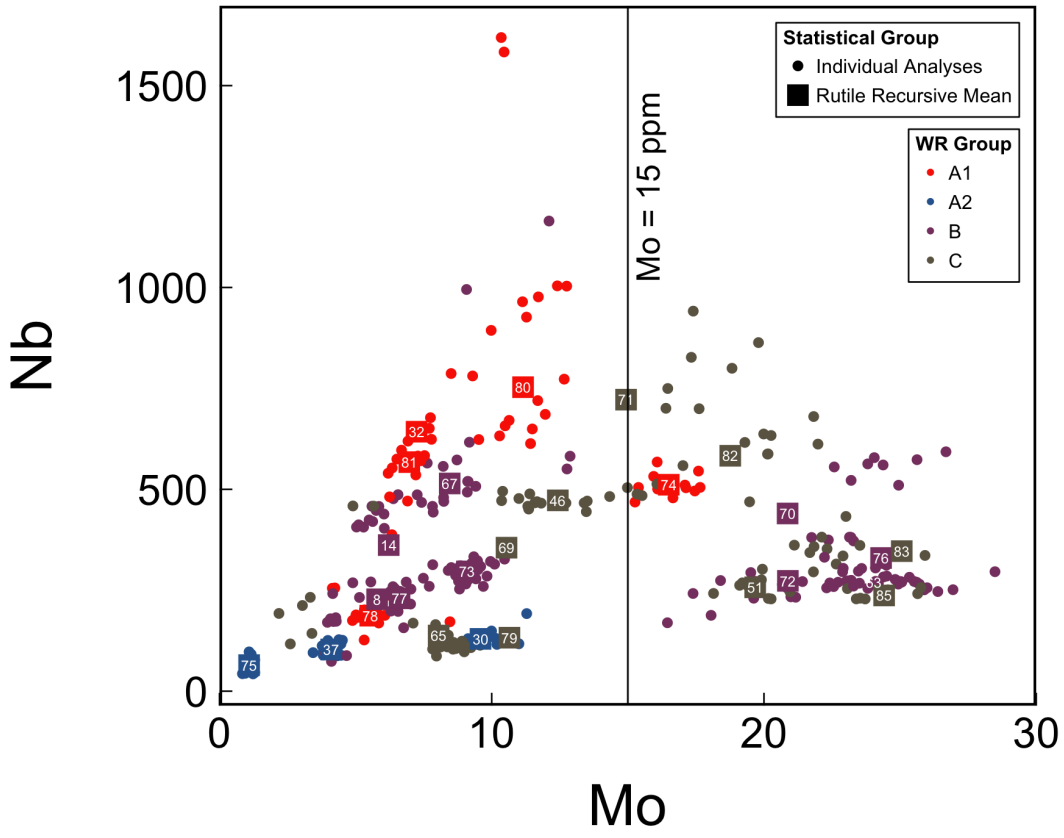

Figure 4.18: Nb vs. Mo variation diagram for rutiles from Norwegian eclogites. Round points represent individual rutile analyses, squares represent mean rutile composition for each whole rock, and colours indicate the eclogite group to which the whole-rock belongs. A vertical line at Mo = 15 separates out so-called 'high Mo' rutiles that have a potentially different geochemical or metamorphic history.

Figure 4.19 is a plot of Nb/Ta in rutiles plotted against the Nb/Ta of their host whole-rock. As with Figure 4.14, it highlights the large spread in Nb/Ta recorded in rutiles from each sample. Even though rutile controls approximately 50-100 % of the whole-rock Nb and Ta in most of these samples, there is no statistically significant correlation between whole-rock and rutile Nb/Ta. Despite the lack of such a correlation, Figure 4.19 does show that for over two thirds of the eclogites studied, the mean rutile Nb/Ta ratio of rutiles is less than the whole rock. This is illustrated further in Figure 4.20 where we see that the relatively normal distribution of Nb/Ta in the entire rutile data set has a median Nb/Ta approximately 2.5 less than that the whole-rocks.

To investigate the discrepancy between the affinities of Nb and Ta for rutile, we may use rutile versus whole rock Nb/Ta to suggest relative partition coefficients of Nb and Ta. This is achieved by adapting an equation that describes the relationship between the concentrations of Nb and Ta in rutile and the whole rock:

$$\frac{Nb_{rt}}{Ta_{rt}} = \frac{D_{rt}^{Nb}.Nb_{wr}}{D_{rt}^{Ta}.Ta_{wr}} \tag{4.3}$$

Where D_{rt}^{Nb} and D_{rt}^{Ta} are the partition coefficients of Nb and Ta for rutile relative to the whole-rock composition, rt denotes the concentration in rutile, and wr the concentration in the whole-rock.

We can rearrange equation 4.3 to quantify the relative difference between D_{rt}^{Nb} and D_{rt}^{Ta}, assuming $D_{rt}^{Ta} > D_{rt}^{Ta}$:

$$\frac{D_{rt}^{Ta}}{D_{rt}^{Nb}} = \frac{\left({}^{Nb}/_{Ta}\right)_{wr}}{\left({}^{Nb}/_{Ta}\right)_{rt}} \tag{4.4}$$

Figure 4.21 shows this relative difference in estimated partition coefficients for Nb and Ta substitutions into rutile (i.e. D_{rt}^{Ta}/D_{rt}^{Ta}), calculated using equation 4.4. The figure shows that D_{rt}^{Ta}/D_{rt}^{Ta} can vary from 0.76 to 0.9 (-25 % and +90% respectively), probably because the distribution of Nb and Ta between rutile grains in each rock is not even. Despite the large spread in relative partition coefficients, the median

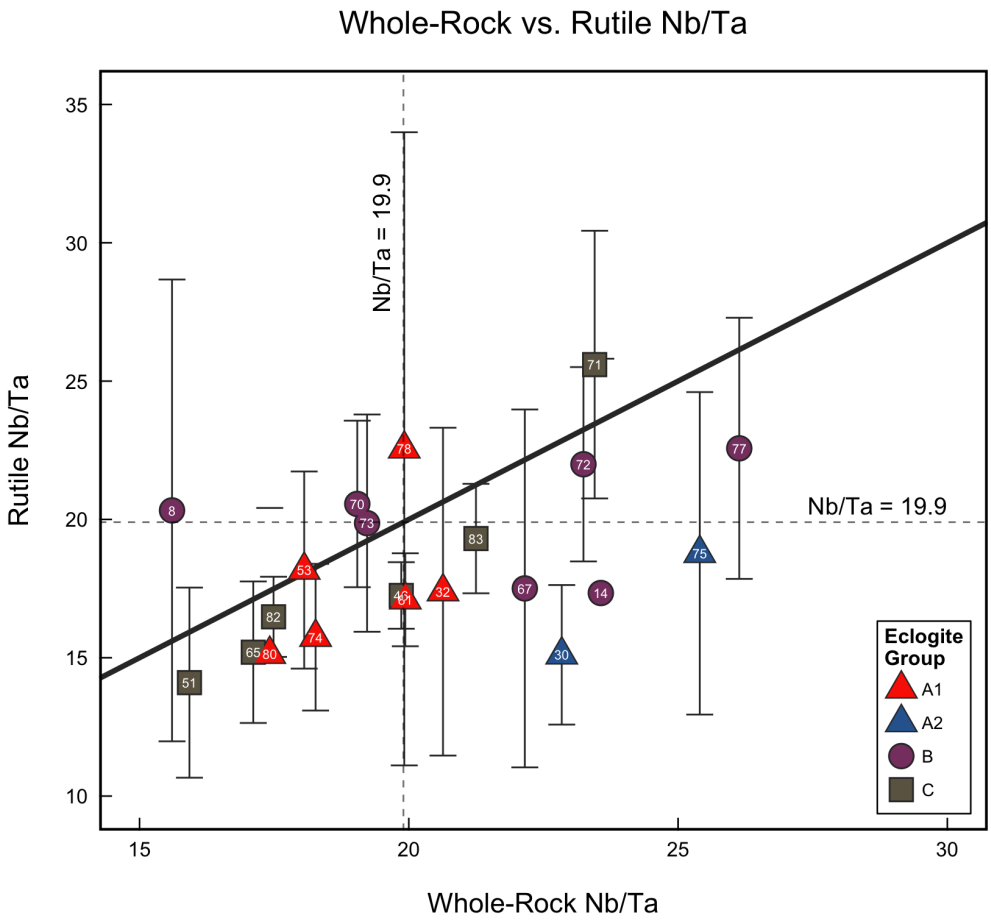

Figure 4.19: Comparison of whole-rock and rutile Nb/Ta. Rutile Nb/Ta is expressed as the mean of rutile means (red square) with accompanying standard deviation. Vertical and horizontal lines represent chondritic Nb/Ta of around 19.9, and the thick solid line represents a gradient equal to one. The figure shows the relatively large spread in measured rutile Nb/Ta within each eclogite sample compared with the whole-rock. Note also that more than two thirds of eclogites have whole-rock Nb/Ta greater than of their mean rutile composition.

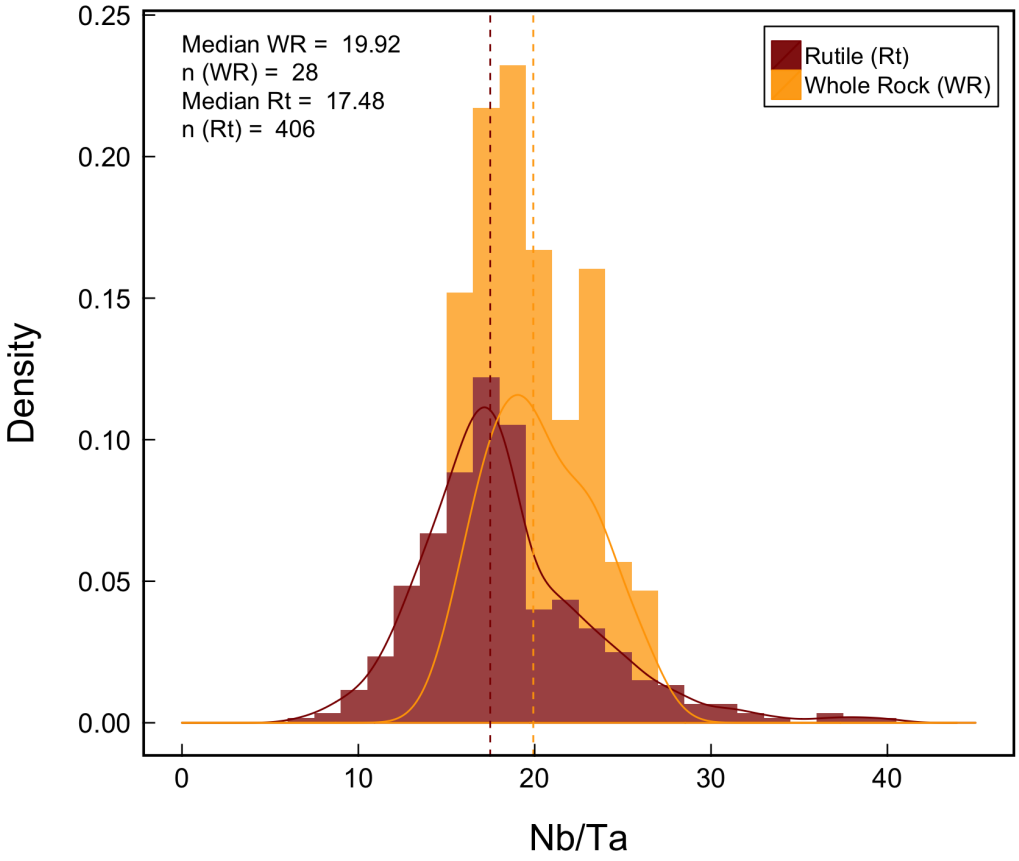

Figure 4.20: Histogram of rutile (dark red) and whole-rock (yellow-orange) Nb/Ta ratios. Rutile data are computed mean compositions of individually analysed rutile grains. Density is calculated using a linear model that employs a Fourier transform. Solid lines represent a linear approximation of the calculated density, vertical dashed lines represent median values. Median rather than mean values are used as they more accurately represent the distribution of values in the data.

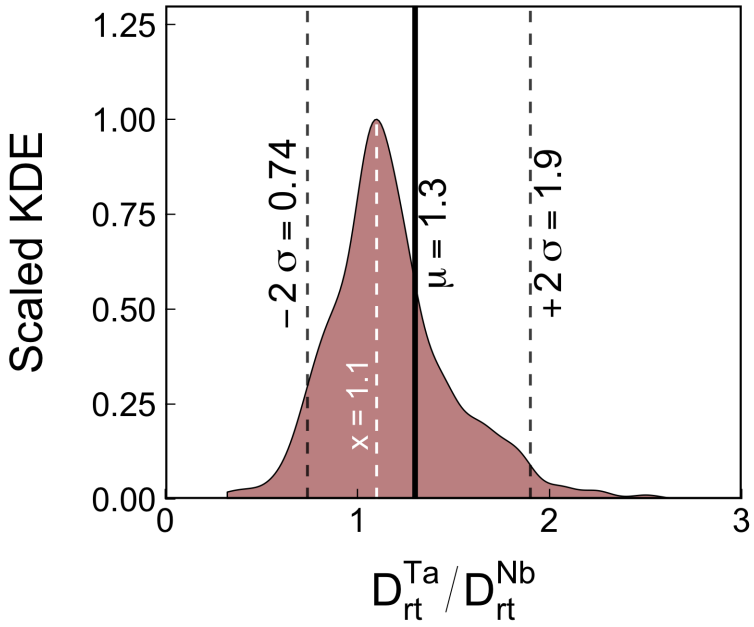

Figure 4.21: Histogram showing the density distribution (scaled kernel density estimates) of relative the difference between D_{rt}^{Nb} and D_{rt}^{Ta} expressed as rD_{rt}^{Ta}/D_{rt}^{Ta} using equation 4.4. Dashed black vertical lines indicate 2σ spread in the data, the white dashed line is the peak density, and the solid black line is the mean (μ). The plot shows that Ta can be 26 % less to 90 % more compatible in rutile than Nb, with a peak density at 10 % greater compatibility and a mean (μ) of 30 % greater compatibility.

value suggests Ta is around 10 % more compatible than Nb in rutile, and the average suggests Ta is 30% more compatible in rutile than Nb. If we use median Nb/Ta values from Figure 4.20in equation 4.4 we find that Ta is typically 13% more compatible than Nb in rutile. We may therefore conservatively estimate is that Ta is typically around 10 % more compatible than Nb in rutile.

Nb and Cr

It has been suggested by some authors (e.g. Zack et al., 2002b, 2004; Meinhold et al., 2008; Triebold et al., 2012) that Nb and Cr in rutile may be used to distinguish between metabasaltic and metapelitic host rocks. Rutiles in metapelites tend to have low Cr but high Nb, whereas metabasites have lower Nb and higher Cr. Several discrimination diagrams exist, but the exact parameters, if any, of distinct metabasaltic versus metapelitic host rock fields are yet to be robustly determined. Since the eclogites in this study are believed to be metabasites, we may test current discrimination diagrams with these new data.

Most rutiles in this study have Nb $<$800 ppm and Cr $\leq$ 2500 ppm (Figure 4.22). Using the discrimination fields of Zack et al. (2004), Meinhold et al. (2008), and Triebold et al. (2007), most eclogites therefore plot in the field of rutiles from metabasites, as expected. Some individual rutile compositions plot significantly outside the metabasite host field with very high Nb. However, in all cases the mean rutile composition of rutile for each whole-rock falls within the field of rutiles from metabasites. This highlights the scatter in the composition of rutile from any one sample, particularly with respect to Nb. Furthermore, it shows that one must proceed with care when interpreting analyses in a small rutile population.

Zr and Hf

Figure 4.23 shows that, although the Zr/Hf ratio of rutile within any one eclogite sample is highly variable, it is almost always less than that of the host whole-rock. However, Figure 4.23 shows that there is only a weak correlation between whole-rock and rutile Zr/Hf, whether for all samples or within eclogite groups. Rutiles in

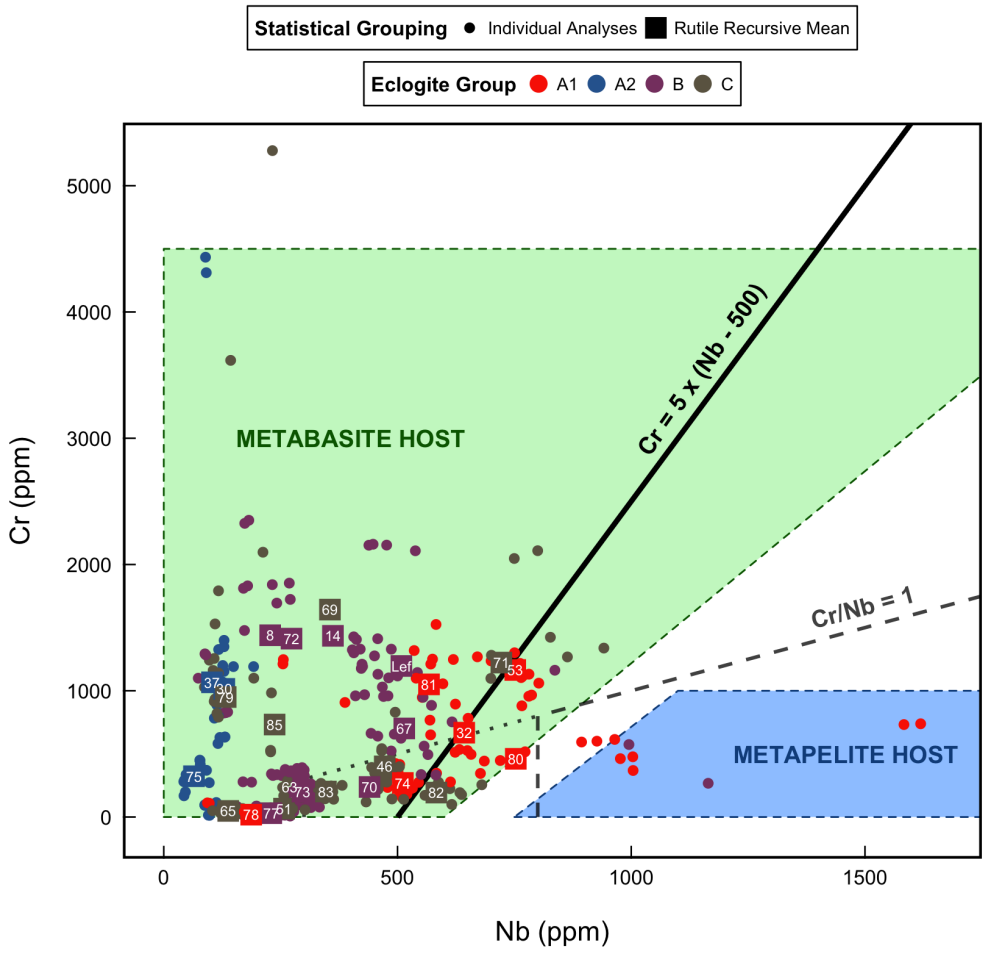

Figure 4.22: Cr vs. Nb diagram for eclogite-hosted rutiles, Western Norway. Green and blue fields are taken from Zack et al. (2004). Solid line (from Triebold et al., 2012) supposedly separates rutiles from metabasites and metapelites above and below respectively. The dashed line represents a combined discrimination between the Nb = 800 ppm cutoff of Meinhold et al. (2008) and the Cr/Nb = 1 line of Triebold et al. (2007) and again purportedly separates metabasic and metapelitic hosts to the top left and bottom right respectively. The diagram shows that rutiles from Norwegian eclogites indeed reflect metabasaltic hosts. Some scatter into metapelitic fields is shown, but the mean compositions of samples remain within the metabasite host field.

whole-rocks with significantly elevated Zr/Hf (WGR-51, WGR-71 and WGR-78) do not show elevated Zr/Hf compared with eclogites with chondritic or sub-chondritic Zr/Hf.

As shown with Nb and Ta, we can estimate the relative difference between Zr and Hf by calculating D_{rt}^{Hf}/D_{rt}^{Zr} using equation 4.4 (page 192) above. Since Zr and Hf are highly correlated in rutile, the temperature dependence of Zr in rutile is not expected to exert significant scatter into the results of this calculation. Figure 4.24 shows that whilst Hf compatibility in rutile relative to Zr is highly variable, but Hf is nonetheless almost always just as or up to 90 % more compatible than Zr in rutile, with an average around 25-36 % greater affinity for rutile than Zr in rutile. The difference in partitioning behaviour of Zr and Hf in rutile is not expected to significantly effect the whole rock Zr/Hf since rutile typically contains less than 5 % of the whole-rock Zr and Hf inventory (Figure 4.11).

4.4 Discussion

4.4.1 The Trace Element Inventory of Rutile

It is clear from Figure 4.9 that the trace element inventory of rutile is dominated by V, Cr and to some extent, Nb. However, by comparing the trace element inventories of rutiles with corresponding whole-rocks (Figure 4.11), we showed that it is in fact Ta and Nb, and to a lesser extent Sn and Mo, that are the most 'important' trace elements in rutile with respect to the whole-rock trace element budget.

The affinity of Nb and Ta for rutile is perhaps one of the best known geochemical features of rutile. Several recent publications (e.g. Zack et al., 2002a; Aulbach et al., 2008; Marschall et al., 2013) have gone further to suggest that Nb and Ta in eclogites is stored almost exclusively in rutile. However, until now there has been little empirical evidence from natural samples to support the claim. Our data show that although rutile may significantly dominate whole-rock Nb and Ta budgets, as much as around 50 % of the whole rock budget for both Nb and Ta may well be stored in other phases. Importantly, this means that one cannot always assume that the mobility

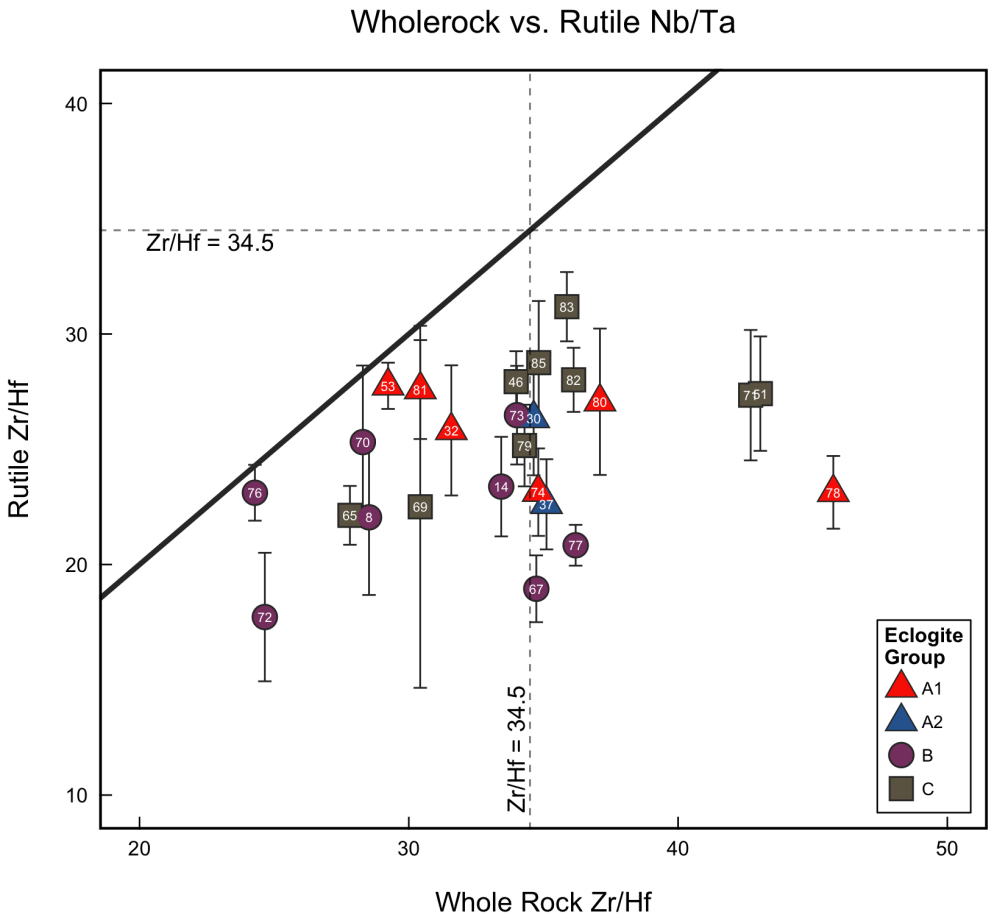

Figure 4.23: Histogram showing the density distribution (scaled kernel density estimates) of relative the difference between D_{rt}^{Zr} and D_{rt}^{Hf} expressed as D_{rt}^{Hf}/D_{rt}^{Zr} using equation 4.4. Dashed black vertical lines indicate 2σ spread in the data and the solid black line is the mean (μ). The plot shows that for most rutiles Hf is just as or up to 90 % more compatible in rutile than Zr, with a mean (μ) and peak density at around 25-36% higher compatibility for Hf over Zr.

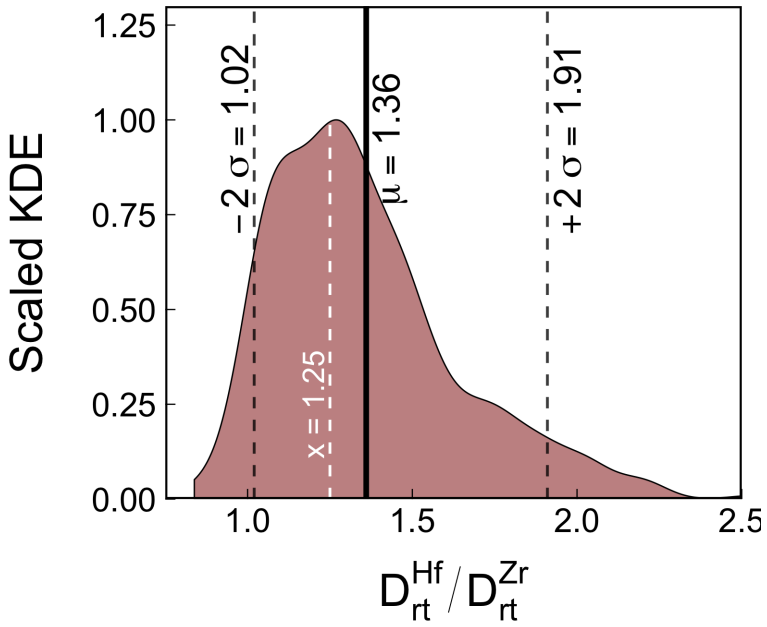

Figure 4.24: Relative difference between ${}^{rt}D_{Hf}$ and ${}^{rt}D_{Zr}$ assuming ${}^{rt}D_{Zr} = 1$ calculated using equation 4.4. The data show that although the relative partition coefficients of Zr and Hf into rutile can be highly variable, Hf is in most cases clearly just as or significantly more compatible in rutile than Zr.

of Nb and Ta during either partial melting or dissolution are controlled exclusively by rutile. Furthermore, this means that one must consider the possibility that significant amounts of Nb and Ta may be partitioned into other potentially less resistant phases, and thus may be more readily mobilised than previously thought.

Figure 4.11 also reveals a large difference in the apparent partitioning behaviour of Nb and Mo into rutile. Nb^{5+} and Mo^{4+} have similar ionic radii (0.64 and 0.65 Å respectively) and thus one might expect them to behave in a geochemically coherent manner. Indeed, Fitton (1995) reported coupled Nb-Mo depletion in some Late Cenozoic continental basalts from the Western United States, and suggested that both were largely retained in rutile in the subducting slab. Our data do indeed show that significant amounts of both Nb and Mo may be retained in rutile. However, Figure 4.11 also reveals that there exists a large difference in the amount of whole rock Nb and Mo stored in rutile, suggesting that along with being an important host for Nb and Mo, rutile may also cause significant fractionation of Nb from Mo. The systematics of Nb and Mo are discussed in more detail below.

4.4.2 Trace Element Systematics in Eclogitic Rutiles

Nb and Ta

Niobium and Tantalum in geological systems have near identical ionic radii and charge (Nb^{5+} = 0.69 Å and Ta^{5+} = 0.68 Å), and so their behaviour in geochemical systems is generally strongly coupled. However, despite the chemical similarities between Nb and Ta there are significant differences in the Nb/Ta ratios observed in the accessible parts of the Earth compared with those observed in chondrites, as well as there being significant differences between the Nb/Ta observed in various components within the crust-mantle system. Studies on the behaviour of Nb and Ta within the crust-mantle system in particular, are clearly important in increasing our understanding of crust formation processes.

Rutile is often cited as a dominant, possibly exclusive host for Nb and Ta in metabasic rocks such as eclogites (e.g. Zack et al., 2002a; Aulbach et al., 2008; Marschall et al.,

2013). Indeed, we have shown that although rutile may not always be considered an exclusive Nb and Ta host, it nonetheless dominates its host rock Nb and Ta inventory. Since a significant proportion of the slab in subduction zones is likely to be made of rutile-bearing metabasaltic rocks, it is therefore reasonable to assume that rutile exerts a significant control on the behaviour of Nb and Ta in subduction zones, and in the crust-mantle system as a whole.

Unsurprisingly, Nb and Ta measured in rutiles in this study are highly correlated, indicating overall analogous behaviour. The concentrations of Nb and Ta in rutile appear to be controlled mostly by the availability of Nb and Ta in the whole rock, along with their partition coefficients for rutile. However, relatively minor yet important differences in the the behaviour of Nb and Ta with respect to rutile have been identified.

For instance, we have shown that Ta may be 10 % more compatible in rutile than Nb, an observation also made by Green and Pearson (1987), Schmidt et al. (2004), Klemme et al. (2005), and Xiong et al. (2011). The reason for this is probably the smaller ionic radius of Ta^{5+}. Melts and/or fluids in equilibrium with rutile may therefore be expected to have Nb/Ta approximately equal to or slightly higher than that of the original rutile population. Significant scatter within and amongst rutile crystals in each sample suggests that microscopic to macroscopic homogenisation, and therefore diffusion, of Nb and Ta within eclogites is a relatively slow process. Furthermore, scatter within the Nb/Ta ratios of rutiles suggests that there may also be significant differences in the diffusivity of Nb and Ta both within and between rutile grains. This is supported by Marschall et al. (2013) who found that Nb diffusion in rutile is approximately 1.6-18 times faster than that of Ta.

The largely chondritic Nb/Ta of eclogites reported here (Figure 4.20) are typically significantly higher than the Nb/Ta expected in their corresponding protoliths. For example, basalts from the PetDB database have the following Nb/Ta ratios: N-MORB = 13.82 $\pm$ 3.1, n = 408; E-MORB = 16.1 $\pm$ 1.6, n = 240; VAB = 14.6 $\pm$ 0.4, n = 4226. This suggests that significant fractionation of Nb from Ta, and an overall increase in Nb/Ta has occurred at some point in the eclogite's metamorphic history. Since Ta appears to be 10% more compatible than Nb in rutile, which in turn controls the majority of the Nb and Ta inventory of its host rock, one might expect that the whole

rock Nb/Ta would be in-fact *lowered* during metamorphic alteration.

According to the experimental findings of Marschall et al. (2013) an elevated Nb/Ta could suggest a partial melt, produced in equilibration with rutile, was extracted from the whole rock. However, we have found no field, petrographic or geochemical evidence to suggest that partial melting has occurred in our samples, or that partial melts infiltrated them. Furthermore, the conditions necessary to partially melt these Norwegian eclogites (T>900 ^{o}C at 2.5-3.5 GPa, Skjerlie and Patiño Douce, 2002) were not attained by our samples.

The simplest explanation appears to be one in which Nb/Ta may have been elevated prior to the growth of rutile. Rutile is absent until the upper amphibolite facies (ca. 1.5 GPa Liou et al., 1998; Xiong et al., 2005), before which most of the Nb and Ta is held in titanite and amphibole (Liang et al., 2009). Nb is much more compatible in amphibole than Ta (Ionov and Hofmann, 1995; Foley et al., 2000), and amphibole may persist well into the eclogite facies without dehydrating. It is possible that significant quantities of Ta are lost in fluids produced by the dehydration of other hydrous phases before the onset of rutile crystallisation and the breakdown of amphibole. Loss of relatively more Ta from the whole rock could therefore raise the whole-rock Nb/Ta. Indeed, whole rock compositions for many eclogites show Nb concentrations typical of expected protoliths, yet rather low Ta. This supports the idea that some Ta may have been lost in early dehydration fluids before the onset of prograde rutile crystallisation. That the mean Nb/Ta of these eclogites is 19.98 is therefore perhaps only coincidental, and may even be considered suprachondritic if chondritic Nb/Ta is around 17-18 (e.g. Thompson, 1982).

Nb and Cr

It was first suggested by Zack et al. (2002b) that the growth of rutile from ilmenite in metapelites led to a minimum concentration of Nb of around 800-900 ppm. However more recent data from Luvizotto et al. (2009) and Triebold et al. (2007) suggest that metapelitic rutiles may equilibrate with as little as 300-500 ppm Nb. This creates an area of increased uncertainty on the Cr-Nb rutile discrimination diagram where

Nb = 300-800 and Cr/Nb <1. Several rutiles and corresponding mean compositions from Western Norway plot within this area of uncertainty, yet all other available evidence suggests these eclogites are metabasic. Taken individually, these high-Nb rutile grains might suggest the involvement of pelitic meterial. Given that the mean Nb-in-rutile concentration for such samples is arguably mafic, it is difficult to support the argument that such high-Nb rutiles suggest mingling of pelitic material with the protolith magma, as one would expect the high-Nb signature to affect the majority of rutiles. These high-Nb rutiles are found in rocks that show moderate to significant retrograde alteration, and thus the most likely explanation for such out-lying high-Nb rutiles is that they probably inherited their signature during fluid-related alteration during metamorphism *after* the crystallisation of the initial prograde rutile population.

The most recent attempt to improve the rutile Nb-Cr discrimination diagram by Triebold et al. (2007) led the authors to suggest a line with equation Cr = 5 $\times$ (Nb-500) could correctly classify up to around 90 % of their data set. The parameters of this line are based on a larger data set than that of Zack et al. (2004), however this discrimination was only determined by visual means. Our data agree better with the relatively older classification fields of Zack et al. (2002b), Zack et al. (2004), Meinhold et al. (2008), and Triebold et al. (2007).

As has already been made clear, rutile compositions within any one whole rock can be highly variable, especially with respect to Nb. Therefore one must exercise extreme caution when using small populations (e.g. n $<$ 100) of rutile in provenance studies, particularly those where little or nothing is known about the host rocks.

Zr and Hf

Zr and Hf often exhibit analogous behaviour in a wide variety of geochemical processes, so strong correlations between them in rutile suggest that partitioning of Zr and Hf into rutile is also rather analogous. Indeed, the experimental observations of Klemme et al. (2002, 2005) suggest this is the case. However, our data have shown that Hf can be just as or much more compatible in rutile than Zr. The reason for the variability in the relative partition coefficients is probably the added temperature dependence of Zr in rutile. Indeed, the relatively high observed scatter not only in

Zr concentrations, but also the Zr/Hf ratios (e.g. Figure 4.15) of rutiles supports the idea that the temperature dependence of Zr in rutile probably plays a significant role in introducing much of the scatter into Zr/Hf ratios. However, it is also likely that diffusion of Hf and Zr within and between rutile grains is also a significant contributing factor to the spread of observed Zr/Hf ratios.

The temperature dependence of Zr in rutile is relatively well understood (e.g. Zack et al., 2004; Watson et al., 2006), and therefore in light of the observations one might suggest that Hf in rutile must also be somewhat temperature-dependent. However, the concentration of Zr in rutile is only temperature dependent when it is buffered by coexisting zircon and possibly quartz. In the absence of zircon, the concentration of Zr in rutile must be controlled predominantly by the whole rock inventory of Zr, its diffusivity in the rock, and the abundance of- and partition coefficient for rutile. The concentration of Hf is not buffered by zircon, and so as with Zr in a zircon-absent assemblage, the concentration of Hf in rutile, regardless of the presence or absence of zircon, must also be controlled by the whole rock inventory, its diffusivity, and the abundance of- and partition coefficient for rutile. Despite these differences, the persistence of a correlation between Zr and Hf in a population of rutiles grown in a mostly zircon-buffered environment, shows that the effect of temperature on the absolute Zr concentration must be relatively small.

Sn and Mo

Sn and Mo have have very similar ionic radii (Sn^{4+} = 0.69 Å, Mo^{4+} = 0.65 Å, Mo^{3+} 0.69 Å) and thus often behave similarly in geochemical processes. Indeed, we have shown that both Sn and Mo have similarly high compatibilities in rutile (i.e. rutile contains 8-30% and 5-26% of whole rock Sn and Mo respectively, Figure 4.11). However, the data have shown that the concentrations of Sn and Mo are not always analogous in rutile.

Hydrothermally deposited rutiles typically have high (>50 ppm) Sn (e.g. Clark and Willkiams-Jones, 2004; Zack et al., 2004; Luvizotto et al., 2009). Rutile standard R10 (from Norway) and rutile GOD (from Scotland) analysed in this study were both

hydrothermally deposited, and both do indeed have Sn >50 ppm. However, the Mo concentration in both R10 and GOD does not exceed 15 ppm (Figure 4.16), and is comparable with the Mo concentration of many rutiles in Norwegian eclogites. This suggests Sn and Mo could be fractionated from one another in certain hydrothermal fluids.

High-Mo rutiles in our study are not significantly enriched in Sn when compared with the rest of the population. Given the otherwise analogous behaviour of Sn and Mo, this also suggests that significant fractionation of of these elements has affected some component of a system in which these high-Mo rutiles either grew or re-equilibrated.

If the observed high-Mo rutiles were grown from a high-Mo yet low-Sn hydrothermal fluid, one might expect a bimodal distribution of rutile Mo concentrations within each eclogite: a population of relatively low-Mo metamorphic rutiles in which Sn and Mo are correlated; and a second high-Mo population that grew from the fluid itself. However, we can see from Figure 4.16 that the concentration of Mo in rutiles from the same sample are actually rather similar, suggesting instead that all rutiles in each eclogite sample have similar histories.

Rutile vs. whole-rock Mo inventories provide further clues to the origins of high-Mo rutiles. In samples where Sn and Mo are correlated, rutile controls 7.7 $\pm$ 5 % of the whole rock Mo. By contrast, in samples with high-Mo, rutile controls an average of 20.3 $\pm$ 7.4 % of whole rock Mo. If the rock was infiltrated by a fluid with externally derived Mo, one might expect the proportional dominance of all Mo-bearing phases to remain fairly constant, whilst the whole-rock Mo concentration was increased. This might be especially true for eclogites, since garnet and clinopyroxene are particularity important hosts for Mo (e.g. Zack et al., 2002b). If, however, high-Mo rutiles gained their Mo by redistribution of Mo already within the whole rock, the percentage of Mo controlled by rutile would increase, whilst whole rock Mo would be unchanged. The mean whole rock Mo concentration for eclogites that have rutiles with Mo $<$ 15 ppm is 0.75$\pm$0.3 ppm, whereas those eclogites with high-Mo rutiles have Mo of 0.84$\pm$0.4 ppm, which is approximately 11% higher. Furthermore, rutiles in sample WRG-53 have by far the highest Mo concentrations of all rutiles (>50 ppm), as well as having a whole-rock concentration significantly above the mean (Mo = 1.76 ppm). We can

therefore infer that eclogites with high-Mo rutiles probably gained additional Mo from an external source. We can also suggest that, since the percentage of whole rock Mo is also higher in high-Mo rutiles, the partitioning of fluid-derived Mo into rutile was probably more efficient than into garnet or clinopyroxene.

Bali et al. (2012) show that Mo may be highly mobile in moderately to highly saline fluids with high fO_2. We may therefore speculate that eclogites with high-Mo rutiles have at some point in their metamorphic histories, after the prograde growth of rutile, experienced infiltration of Mo-Rich, Sn-poor, high fO_2 and possibly saline fluid. In this case, most if not all rutiles within the whole-rock appear to have equilibrated with this fluid. Since a significant number of group C eclogites contain high-Mo rutiles, compared with other groups, it can be further suggested that such a fluid could also be responsible for destroying the protolith's trace element signature, otherwise preserved in many eclogites. Similarly, several group B eclogites also have rutiles that belong to the high-Mo group, prompting us to consider the possibility that the whole-rock signatures of some group B eclogites may too have been somewhat corrupted by metamorphic fluids.

It is very difficult to ascertain with the information we have when the infiltration of such fluids might have taken place. However, the apparent ubiquitous equilibration of rutile grains with respect to Mo at least suggests it may have occurred at relatively high temperatures that promoted higher rates of diffusion, i.e. somewhere around the time of peak metamorphism. Similarly, the question as to the origins of this fluid-derived Mo, and why it is not associated with equally significant amounts Sn would be a logical next step for further study.

Nb and Mo

Nb^{5+} and Mo^{4+} have similar ionic radii (0.64 Å and 0.65 Å respectively) and thus might be expected to behave in an analogous manner in geochemical systems. Our data do indeed show that there is a very general positive correlation between Nb and Mo in rutile. Both may be described as compatible in rutile, however Mo much less so than Nb. For instance, an average of 5-26% of whole rock Mo in our samples is stored in eclogite-hosted rutile compared with 50-98% for Nb (Figure 4.11). Furthermore,

eclogites in which rutiles have more 'normal' concentrations of Mo (i.e. <15 ppm), rutile contains on average only 7.7 ± 5 % of whole-rock Mo.

Beyond the very broad positive correlation between Nb and Mo, there is no immediately identifiable and explainable systematic correlation between the concentration of Nb and Mo in rutiles in eclogites. That said, the data do to some extent support the inference made by Fitton (1995) that rutile is important in controlling Mo flux during subduction, and that rutile may be responsible for some coupled Nb and Mo depletions in arc magmas.

As shown above, it appears that Mo can be highly mobile in some hydrothermal fluids (Noll et al., 1996; Bali et al., 2012), and that rutile might scavenge significant amounts of any Mo from those fluids. This means that the magnitude and strength of correlation of Nb and Mo depletions observed in arc magmas may have potential to be used as a proxy for the composition and extent of the interaction of hydrothermal fluids with rutile-bearing parts of the slab. Further to this point, since Mo appears to be both fluid mobile and relatively compatible in rutile (e.g. Figure 4.11), bimodal distributions in-, and/or significantly elevated concentrations of Mo in rutile may be a good indicator of the hydrothermal history of a sample. Once again, these are speculative statements that could be lines of further investigation.

4.5 Conclusions

The main conclusions drawn from this study relate directly to the geochemistry of eclogite-hosted rutiles, and the way in which the composition of rutile may be linked to geochemical features of its host whole-rock.

- In the analysed eclogites, approximately 40-70 % of all available TiO_2 in the whole rock is present as rutile.

- The trace element geochemistry of most eclogitic rutiles appears to be dominated by V, Cr, Nb, Si, Zr and W.

- Rutile typically controls significant proportions of the whole-rock budget for Ta (40-90%), Nb (35-85%), Sn (7-24%) and Mo (4-22%).
- Rutile is not always the exclusive host for Nb and Ta. As much as 50% of whole rock Nb and Ta may be partitioned into other minerals.
- Several inferences about compatibility of trace elements in rutile can be made. Since eclogites in this study are not considered to have undergone partial melting, these compatibilities are thus assumed to be reflecting relative compatibilities in the presence of fluid.
- Ta is approximately 10 % or more compatible in rutile than Nb, supporting the experimental observations of (e.g. Marschall et al., 2013).
- Hf is almost always just as or up to 90 % more compatible than Zr in rutile, and is in most instances Hf can be said to be around 25-36 % more compatible in rutile.
- Ta concentrations and Nb/Ta ratios suggest that many eclogites in this study may have lost Ta in fluids expelled during dehydration in the lower- to middle amphibolite facies before the onset of rutile crystallisation.
- Rutile in subducted eclogites has the capacity to play an important role in controlling the Mo flux to the overlying mantle wedge, as first suggested by Fitton (1995).
- Despite its similarity to Nb, Mo substitution into rutile does not appear to be analogous with Nb, probably because unlike Nb, Mo can be significantly fluid mobile.
- Any Mo in eclogite-hosted rutiles present in concentrations over 10-15 ppm was probably scavenged from an external source. The metamorphic fluids responsible for delivering this Mo to the eclogite were probably high fO_2 and saline in composition (Bali et al., 2012).

Broader Implications

This study has identified several issues and implications that are particularly applicable to others investigating the trace element geochemistry of rutile.

- Important elemental ratios (e.g. Nb/Ta, Nb/Cr and Zr/Hf) in rutile from any one sample can he highly variable, such that small populations of rutile analyses cannot be used to accurately infer the trace element characteristics of their protoliths.
- The Nb/Cr ratio of rutile is an effective way of distinguishing between rutiles from metabasites and rutiles from metapelites. Our data are best classified by the Nb/Cr discrimination criteria of Zack et al. (2004).

4.6 Further Work

4.6.1 Fluid Compositions

The apparent decoupling of analogous concentrations of Sn and Mo in eclogitic rutiles in cases where there appears to have been infiltration of high fO_2 and possibly saline fluids, needs more detailed investigation. Specifically, this would involve an in-depth look at any fluid inclusions within eclogites that have high-Mo rutile populations, to see whether or not-, and possibly when fluids of the anticipated composition infiltrated the eclogite.

4.6.2 Rutile and Whole-Rock Geochemistry

Our comparisons of the geochemistry of rutile with that of its host whole-rock have been by no means exhaustive. There are many geochemical and petrographic features of whole rock geochemistry that have not been compared with the compositions of accessory rutile. Since the data already exist, further investigations in this direction will likely need to implement data mining techniques to recommend potentially geologically significant relationships worth further investigation.

Chapter 5

Zr-in-Rutile Thermometry of HP and UHP Eclogites, Western Norway*

Abstract

The Zr-in-rutile thermometer (ZRT) is a powerful single mineral geothermometer particularly useful for eclogites in which rutile is a common accessory phase. Since rutile is generally highly resistant to dissolution, partial melting, and trace element re-equilibration, rutile has the potential to store and protect valuable information about the temperature histories of its host rock. We analysed the Zr concentrations and Zr-in-Rutile temperatures recorded by over 230 rutile crystals from 28 samples of HP to UHP eclogite from the WGR. Norwegian eclogites are shown to be medium temperature (MT) eclogites, with minimum estimates of T_{max} in the range of 600-750 ^{o}C. Much of this range reflects a regional eclogite facies thermal gradient increasing from the south-southwest to the north-northwest of the WGR. Individual rutiles crystals record temperatures that are typically within $\pm$0-15 ^{o}C of the mean, whereas the mean temperatures of rutiles within eclogite samples typically fall within a range of mostly $<\pm$20-40 ^{o}C. We show that the majority of rutile crystals probably underwent significant internal homogenisation before reaching T_{max}, destroying much of the thermal zonation. Inter-rutile homogenisation was limited due to slow diffusion rates, and shows that rutiles probably crystallised over a temperature range of approximately 100 ^{o}C or less. Burial around peak metamorphism indicates a supercool gradient of around 2 ^{o}C/km. Exhumation rates after T_{max} to $T < 600$ ^{o}C were rapid ($<$2 Ma), and probably aided the preservation of eclogite assemblages. We present a high-resolution thermal map of the Nordfjord-Statlandet region which shows that the thermal gradient preserved in the WGR basement was subjected to deformation during collapse of the orogen. Our findings support and add resolution to other

*Co-authors: Godfrey Fitton - *The University of Edinburgh*; Simon Harley *The University of Edinburgh*; Craig Storey - *The University of Portsmouth*

geothermometry studies in the area (e.g. Griffin et al., 1985; Cuthbert et al., 2000).

5.1 Introduction

Fett (1995) was the first to suggest that the concentration of Zr in rutile was sensitive to temperature after observing a discrepancy between the Zr concentration in rutile in medium-temperature (MT) eclogites and high-temperature (HT) granulites. Five years later, Harley and Motoyoshi (2000) reported the apparently temperature-dependent exsolution of zircon in rutile in a UHT sapphirine quartzite from the Napier Complex, Eastern Antarctica. Subsequent experimental studies on the system $ZrO_2 - TiO_2$ conducted by Troitzsch and Ellis (2004) confirmed suspicions that Zr in rutile could indeed be used to develop a single mineral geothermometer.

It is now well known that partitioning of Zr into rutile, grown in equilibrium with zircon and quartz, is highly dependent upon temperature. As a consequence, several authors (Zack et al., 2004; Watson et al., 2006; Ferry and Watson, 2007; Tomkins et al., 2007) have developed the so-called Zr-in-rutile thermometer (ZRT) using both natural and experimental samples. Zack et al. (2004) published the first ZRT (equation 5.1 below) based on 31 natural metamorphic samples with 'known' peak temperatures of 430-1100 ^{o}C. This empirical derivation relied on temperatures reported in a number of other publications that were calculated using a variety of different mineral thermometers. As such, this thermometer is not generally considered to be robust.

$$T \pm 50(^{o}C) = 127.8 \times ln(Zr_{ppm}) - 10 \tag{5.1}$$

Using both experimental and natural samples, Watson et al. (2006) published a revised ZRT (equation 5.2). Both the experimental and natural data conformed to a log-linear relationship (Figure 5.1). Their thermometer was calibrated for rutiles equilibrated at

10 kbar, but does not include a variable for pressure in the ZRT itself.

$$T \pm 20(^oC) = \frac{4470}{7.36 - log(Zr)} - 273 \tag{5.2}$$

Ferry and Watson (2007) revised the thermometer of Watson et al. (2006) using more rutiles from whole-rocks with a greater range of α_{SiO_2}:

$$T(^oC) = \frac{7.420 \pm 0.105 + 4530 \pm 111}{log(Zr) + log(\alpha_{SiO_2})} - 273 \tag{5.3}$$

In their paper, Ferry and Watson (2007) provide guidance on how equation 5.4 can be adapted for rutiles for which the activities of zircon and quartz are not known.

Whilst no integration of pressure into the ZRTs of Watson et al. (2006) or Ferry and Watson (2007) was made, both papers acknowledged a pressure dependence that required further study. Tomkins et al. (2007) was the first to account for pressure dependence by building a thermometer with data gathered from experiments ran over the range of both pressures and temperatures within which rutile grows in nature. They proposed three new ZRTs applicable to rutile stabilised in the fields of the SiO_2 polymorphs α-quartz, β-quartz, and coesite (equations 5.4, 5.5, and 5.6 respectively):

$$T(^oC) = \frac{83.9 + 0.410 \times P}{0.1428 - R \times ln(Zr_{ppm})} - 273 \tag{5.4}$$

$$T(^oC) = \frac{85.7 + 0.473 \times P}{0.1453 - R \times ln(Zr_{ppm})} - 273 \tag{5.5}$$

$$T(^oC) = \frac{88.1 + 0.206 \times P}{0.1412 - R \times ln(Zr_{ppm})} - 273 \quad (5.6)$$

Figure 5.1 compares the ZRTs of Zack et al. (2004), Watson et al. (2006), Ferry and Watson (2007), and Tomkins et al. (2007). Lines representing the ZRTs of Watson et al. (2006), Ferry and Watson (2007), and Tomkins et al. (2007) are all largely parallel to one another, with the magnitude of their separation largely representing the effect of pressure. The thermometer of Zack et al. (2004) is dissimilar in shape to the other ZRTs, resulting in significant differences in temperature estimates for most Zr concentrations, except for where the thermometers intersect. At the time of writing, the thermometer of Tomkins et al. (2007) is the best calibration available, and is shown to consistently calculate temperatures in agreement with other geothermometry techniques (e.g. Zhang et al., 2009; Ewing et al., 2013).

Several characteristics of the ZRT as it currently exists make it appealing for use in a variety of geological settings, for instance:

- The ZRT can applied to single crystals, such that it may be employed in sediment provenance studies where detrital rutiles are disassociated from their former host rocks.
- Zr in rutile is often present in concentrations of >100 ppm, enough to be reliably measured using relatively simple and cheap analytical tools (e.g. electron microprobes).
- Rutile commonly grows in a variety of igneous and high grade metamorphic conditions, meaning it can be used on UHP and UHT lithologies (e.g. Zack and Luvizotto, 2006; Chen et al., 2007; Chen and L., 2008; Baldwin and Brown, 2008; Vaggelli et al., 2008; Chen et al., 2009; Luvizotto and Zack, 2009; Zhang et al., 2009, 2010; Gao et al., 2010; Jiao et al., 2011; Meyer et al., 2011; Chen et al., 2013; Zheng et al., 2011, this study) as well as a range of igneous rocks.
- Rutile is highly resistant to melting, dissolution by most metamorphic fluids,

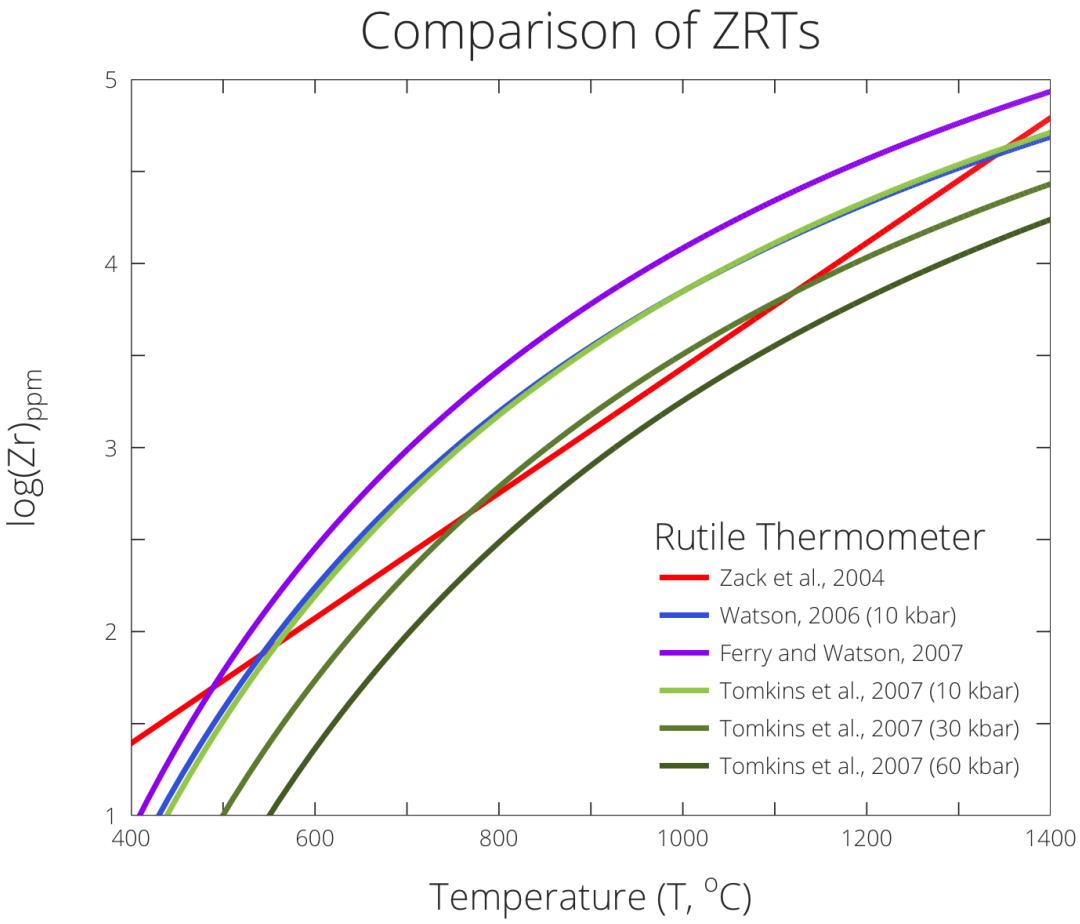

Figure 5.1: Lines representing the ZRTs of Watson et al. (2006), Ferry and Watson (2007), and Tomkins et al. (2007) are all largely parallel to one another, with the magnitude of their separation largely representing the effect of pressure. The thermometer of Tomkins et al. (2007) is currently the preferred ZRT.

and chemical and physical weathering, meaning that rutile has the capacity to preserve thermal data during burial, exhumation, and surface transport and weathering.

- Diffusion of Zr in rutile is thought to be generally slow at temperatures less than around 600 ^{o}C (Cherniak et al., 2007; Blackburn et al., 2012), meaning that in addition to being physically resistant to destruction, it's composition with respect to Zr may also resist re-equilibration at temperatures below 600 ^{o}C.

5.2 Sample Selection and Analytical Methods

The concentration of Zr in rutile is only temperature dependent when Zr is buffered by coexisting zircon (and possibly quartz). As such, the rutiles included in this study are required to have grown or equilibrated in a zircon- and quartz-present assemblage. It is not always possible to exclusively state if this is the case for separated rutile crystals, unless inclusions of either phase are observed within the separated grains. For the most part, one can assume rutiles qualify for ZRT if both zircon and quartz are identified as accessory phases in the eclogite assemblage. For most samples, quartz was identified both in thin section (e.g. Figure 5.2) and from magnetically separated mineral fractions, whereas zircon was typically only identified magnetically separated mineral fractions.

Concentrations of Zr were measured alongside other trace elements in separated rutiles using LA-ICP-MS at the University of Portsmouth. The analytical equipment and methods are described in detail in the previous chapter (page 147) and are not repeated here. Care was taken in ensuring that only rutile analyses showing stable Zr readings throughout each acquisition were included in the dataset.

5.3 Results

Over 430 Zr analyses were obtained on 237 separated crystals from 28 eclogites. A complete table of the collected data is shown in Appendix C.2.5 (page 313). Temperatures calculated using our data use the ZRT of Tomkins et al. (2007) given its proven ability to estimate temperatures that agree with other popular geothermometry

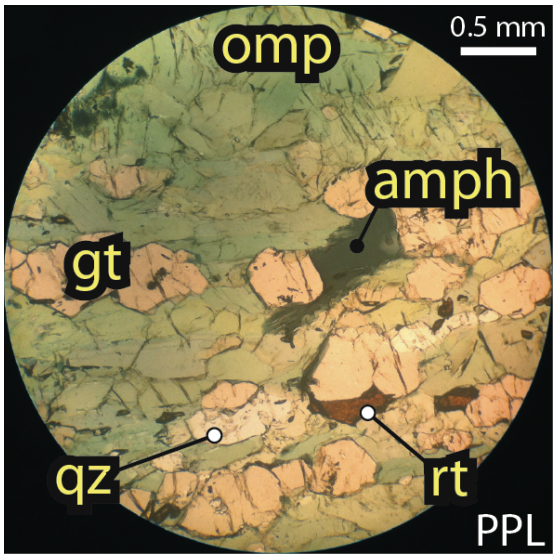

Figure 5.2: Photomicrograph of the Naustdal eclogite (WGR-65-DW) showing an example of the coexistence of rutile and quartz in the eclogite assemblage. Where quartz was observed in the same assemblage as rutile, it was assumed that rutile grew and/or equilibrated in a quartz-present assemblage.

techniques (e.g. Zhang et al., 2009; Ewing et al., 2013). A summary of the temperatures calculated for each eclogite are show in Table 5.1.

5.3.1 Error

A conservative error for LA-ICP-MS determinations of Zr concentrations is $\pm$10 %, which for most analyses in this study equates to approximately $\pm$15-25 ppm. The ZRT of Zack et al. (2004) has an inherent uncertainty of $\pm$50 ^{o}C. Watson et al. (2006) report an inherent error of $\pm$20 ^{o}C for their ZRT. Error for the Ferry and Watson (2007) ZRT is estimated to be on the order of $\pm$5-10 ^{o}C, including a reasonably minor contribution from error in α_{SiO_2}. Relative errors for the Tomkins et al. (2007) ZRT are estimated to be in the region of 4.0-5.0%, accounting for a conservative analytical error of $\pm$10 % (2.5% contribution) and 2.0-2.5% relative error for pressure estimates. A temperature of 700 ^{o}C calculated using the Tomkins et al. (2007) ZRT has a likely error of $\pm$28-35 ^{o}C at P $\approx$ 10 kbar.

The statistical transformation of mean-mean and mean-maximum temperatures require

Table 5.1: Summary of temperatures for each whole-rock eclogite calculated using the thermometer of Tomkins et al. (2007) and expressed as the mean-mean, mean-max and max temperature of the rutile population in each eclogite.

		P	**Temperature (^{o}C)**		
Sample	Locality	(kbar)	mean-mean	mean-max	maximum
08	Drøsdal	25	637 ± 10	637 ± 12	695 ± 35
14	Åsnes	20	626 ± 7	628 ± 13	686 ± 34
30	Kvalneset	28	694 ± 10	699 ± 12	712 ± 36
32	Krokaberg	23	665 ± 10	667 ± 13	692 ± 35
37	Angelshaug	27	669 ± 10	673 ± 14	737 ± 37
46	Nybø	27	719 ± 10	720 ± 11	726 ± 36
51	Flatraket	41	661 ± 11	661 ± 11	667 ± 33
53	Årsheimneset	41	717 ± 10	718 ± 11	733 ± 37
65	Naustdal	30	606 ± 9	607 ± 10	616 ± 31
67	Fossheim	17	615 ± 9	617 ± 10	628 ± 31
69	Engebøfjellet	25	623 ± 11	624 ± 12	696 ± 35
70	Åsneset	16	665 ± 11	667 ± 14	685 ± 34
71	Holmane	27	663 ± 11	663 ± 12	687 ± 34
72	Raudegga	26	642 ± 10	644 ± 11	684 ± 34
73	Almenningen	25	671 ± 6	677 ± 11	712 ± 36
74	Måløy	25	678 ± 9	682 ± 13	692 ± 35
75	Straumen	30	680 ± 11	681 ± 13	684 ± 34
76	Gangeskaret	25	675 ± 6	677 ± 10	685 ± 34
77	Seljeneset	25	661 ± 10	662 ± 12	672 ± 34
78	Vengen	25	652 ± 9	653 ± 10	669 ± 33
79	Havik	25	670 ± 9	676 ± 13	688 ± 34
80	Flister	25	687 ± 9	687 ± 10	703 ± 35
81	Runderheim	25	703 ± 10	703 ± 11	713 ± 36
82	Salt	30	711 ± 13	711 ± 13	714 ± 36
83	Årdalen	25	727 ± 11	728 ± 14	741 ± 37
85	Hareidland	30	748 ± 17	748 ± 17	769 ± 38
Lef	Lefdal	30	684 ± 11	685 ± 11	689 ± 34

Pressure estimates are averages from the literature

errors to be propagated with the following equation:

$$\delta T_{avg} = \sqrt{\frac{(\delta T_1)^2 + (\delta T_2)^2 + (\delta T_3)^2 ...}{n^2}} \tag{5.7}$$

Where δT_{avg} is the error associated with the mean, δT_1 and so on are the errors associated with each value contributing to the mean, and n is the number of values contributing to the mean.

In the case of the mean-mean temperature values, equation 5.7 is applied twice: the first time to calculate a grain mean error, and the second time to calculate the error for the mean of those values. The mean-maximum value only requires equation 5.7 to be used once on the extracted grain maximum values and associated errors, and the equation is not used at all on the maximum temperature.

5.3.2 Temperature and Zr Ranges of Rutiles

Figures 5.3 and 5.4 show box plots for the Zr concentrations and calculated temperatures for each eclogite. Both these figures show that the variation in both Zr and temperature for the majority of samples is fairly low. The concentration of Zr in rutile within each eclogite usually has a range of $<$100 ppm, with many $<$50 ppm which is equivalent to a temperature range of 50 ^{o}C or less. There are exceptions (e.g. samples 32, 69 and 85) in which both Zr concentrations and therefore temperatures are spread over much more than 100 ^{o}C. Figures 5.5 and 5.6 provide further detail by showing examples of the temperature variations in and between rutile grains in whole rocks with relatively narrow and large ranges in Zr and temperature respectively. They show that the temperatures recorded by rutiles are typically within very narrow ranges, even if the temperatures of other rutiles in the same rock are much higher.

Figure 5.7 shows another way of expressing the variation in both Zr and temperature in the dataset as a whole: density distribution curves are plotted for the standard deviation of calculated temperatures within both individual grains and whole-rock samples. The figure shows that the standard deviation of temperature variations within rutile grains is mostly below $\pm$0-15 ^{o}C with a median of $\pm$4.5 ^{o}C. Indeed, Figure 5.8 shows that the largest and most extensively sampled grain in this study (R76-13, n = 12)

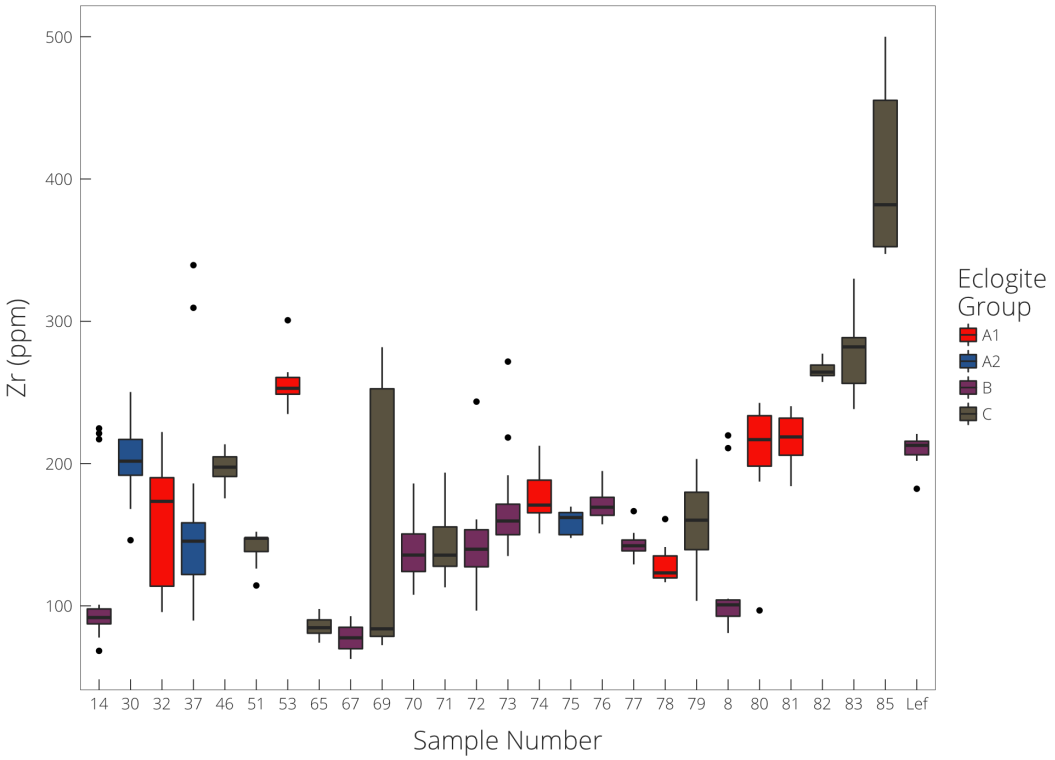

Figure 5.3: Box plots showing the distribution of measure Zr concentrations rutiles for each whole-rock sample. The plot shows that range in rutile Zr concentrations for each whole rock is generally less than 100 ppm. It is interesting to note that group C eclogites tend to have a larger range in Zr concentrations within their rutile populations compared with the other whole-rock eclogite groups.

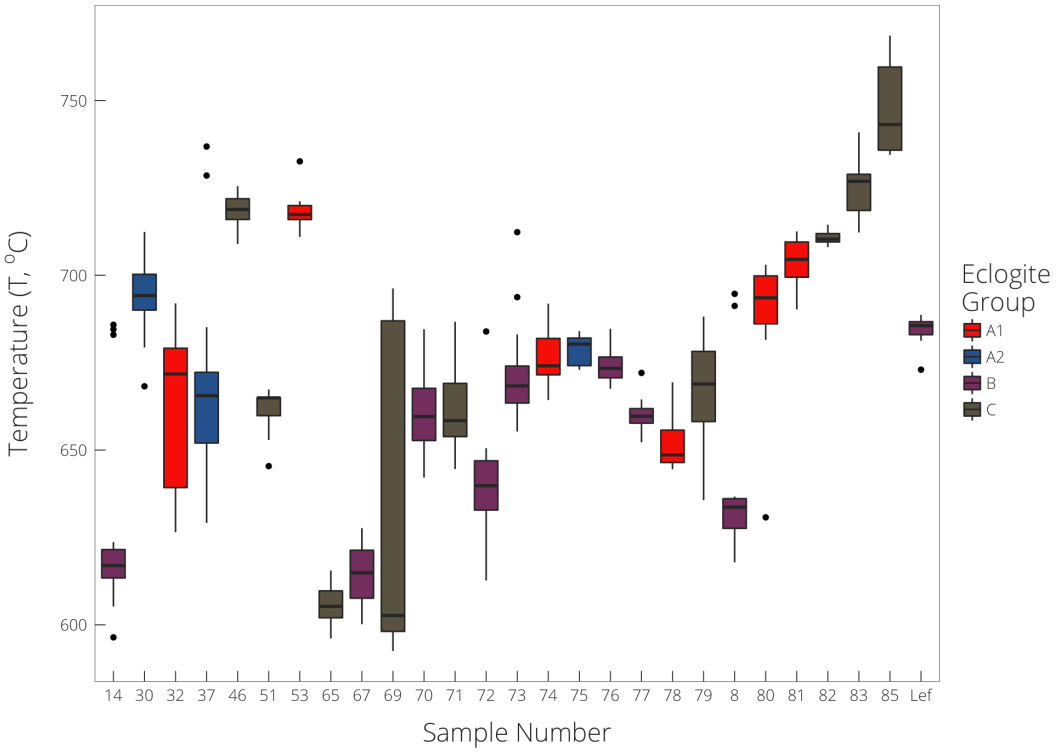

Figure 5.4: Box plots showing the distribution of temperatures in each sample, as calculated using the ZRT of Tomkins et al. (2007). The plot shows that temperatures in rutiles from Norwegian eclogites have a range that is mostly $<50\ ^{o}$C.

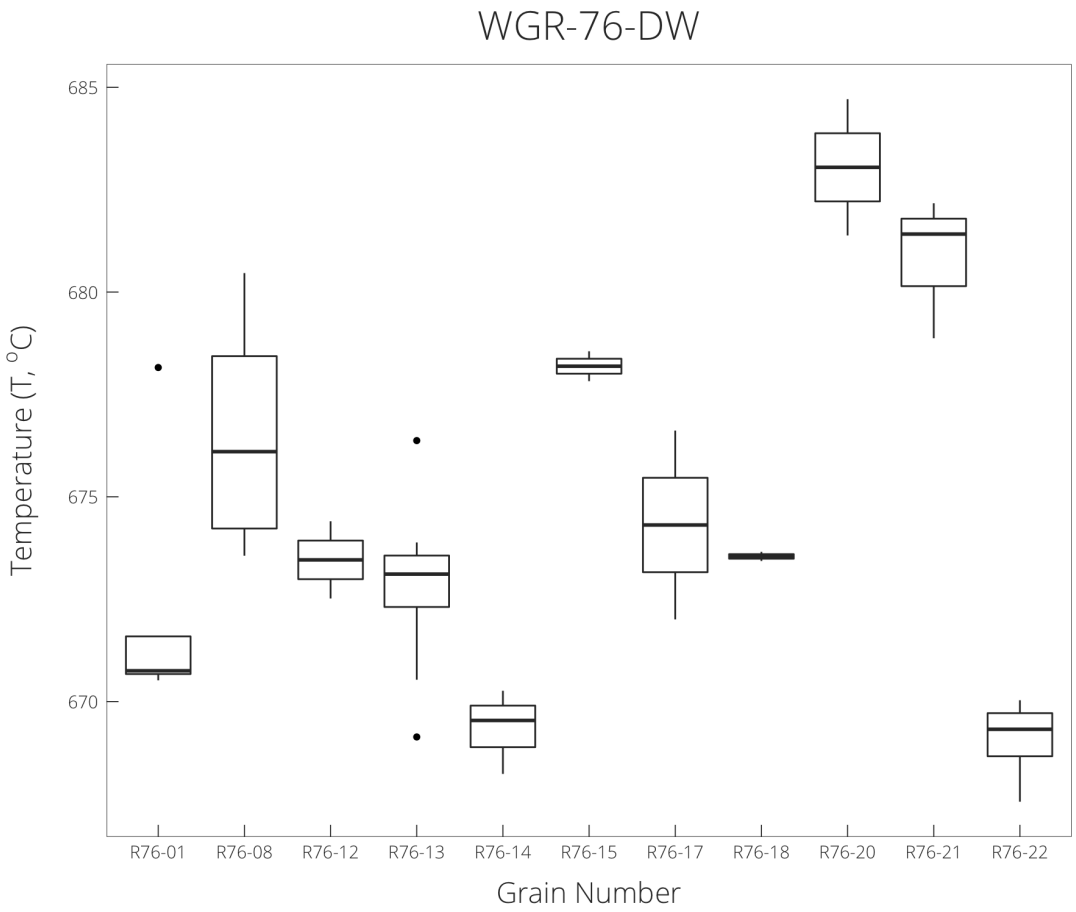

Figure 5.5: Box plot showing the distribution of temperatures in each rutile grain for WGR-76-DW, which has a relatively narrow range of Zr and temperature for the whole-rock rutile population. The plot shows that grains have very low ranges in temperatures, even within the narrow temperature range of the rutile-population as a whole.

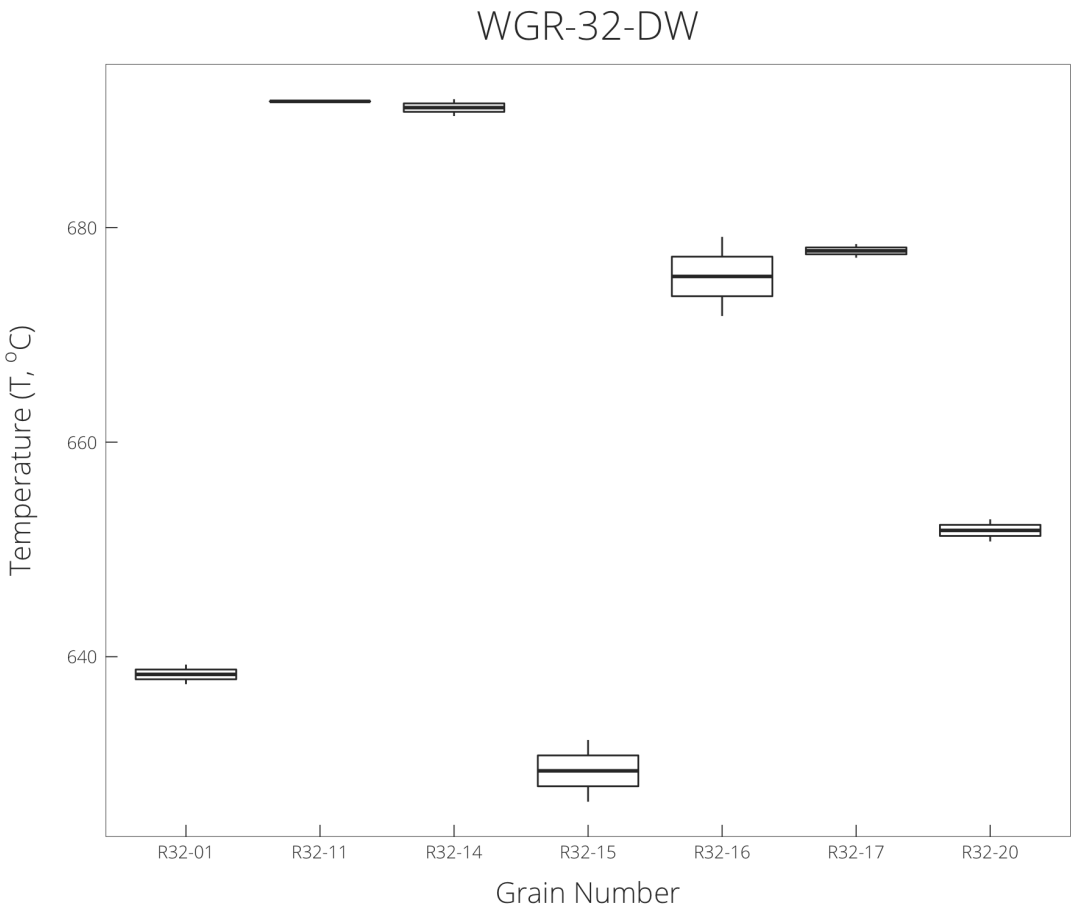

Figure 5.6: Box plot showing the distribution of temperatures in each rutile grain for WGR-32-DW, which has a relatively large range of Zr and temperature for the whole-rock rutile population. The plot that shows although the range in temperatures between rutiles is relatively large, the ranges of temperatures within rutiles remains very low.

showed a range in calculated temperatures of approximately 7 ^{o}C, with a very slight increase from core to rim. Figure 5.7 above also showed that temperature variations between average temperatures for rutiles within whole-rock samples are mostly within a range of $\pm$20-40 ^{o}C (median $\pm$17.7 ^{o}C). Outliers on the density curve for whole rock standard deviations probably belong to samples like WGR-69-DW and WGR-85-DW.

5.3.3 Mean-Mean Temperature

The mean-mean temperature is the weighted mean temperature of the rutile population in each rock, i.e. the whole-rock temperature is calculated as the average of the average temperature in each rutile. In cases where the grains were only analysed once, the value for that analysis is used as-is.

Rutile crystals in most samples indicate relatively homogeneous temperatures from each analysis, and the majority of rutile populations also have relatively narrow ranges of temperatures. A mean-mean transformation of the data is therefore a reasonably robust estimate of the equilibration temperatures of each rock's rutile population.

Figure 5.9 shows a density distribution curve for the mean-mean temperatures of all eclogites in this study. A regional gradient is known to exist in the WGR (e.g. Griffin et al., 1985) and therefore the curve is expected to be affected by the geographical distribution of samples collected from that regional gradient. Nonetheless, the curve gives an indication of the temperatures of eclogites found within the WGR. Mean-mean temperatures for eclogites are mostly in the range of 600-750 ^{o}C with a peak density at 670 ^{o}C. The nested peak in the range of 650-700 ^{o}C is most likely reflecting sampling bias in the Nordfjord-Statlandet region.

5.3.4 Mean-Max Temperature

The mean-maximum whole-rock temperature is calculated as the average of the maximum temperatures recorded in each rutile. This value is sensitive to maximum temperatures whilst remaining relatively insensitive to any anomalously high Zr readings. The mean-mean and mean-maximum temperature datasets for each whole rock are likely to be best suited to indicating the temperatures over which most

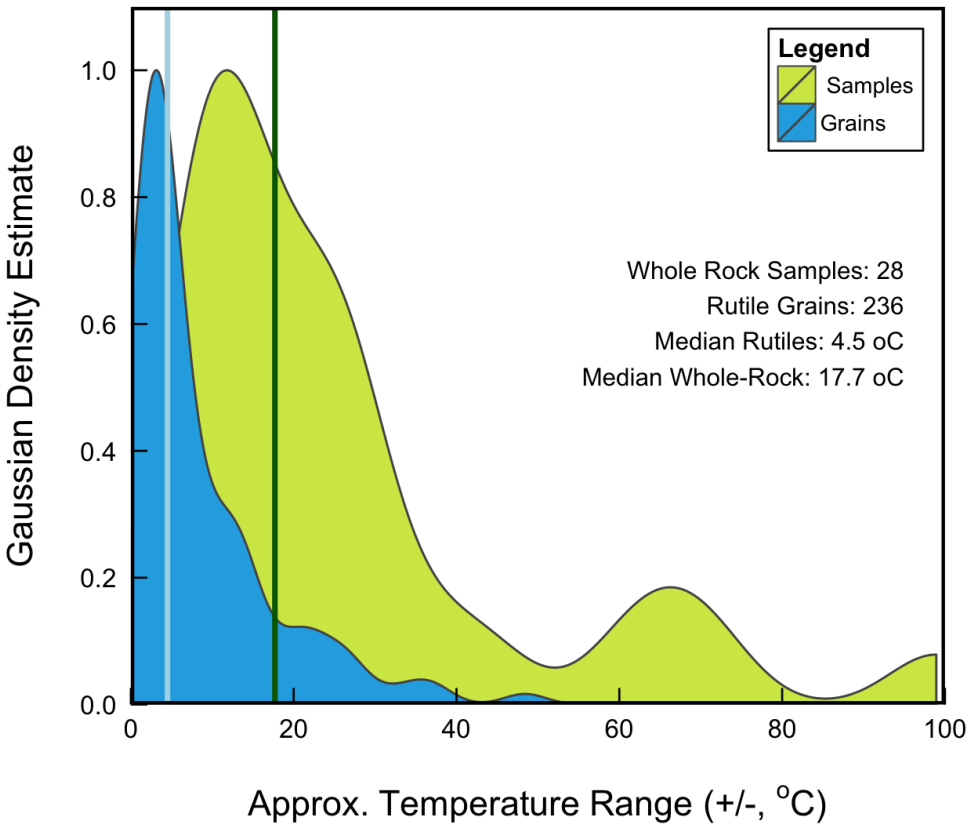

Figure 5.7: Gaussian density curve for estimated temperature ranges (using ZRT of Tomkins et al. (2007)) within grains and samples. The data show that rutile either crystallises and/or equilibrates over a relatively narrow temperature range of approximately $\pm$0-15 ^{o}C and not generally higher than $\pm$20 ^{o}C. Temperature variation within samples is much larger: typically $\pm$20-40 ^{o}C.

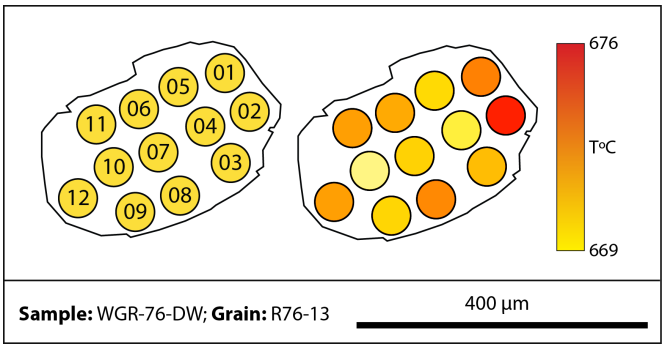

Figure 5.8: Temperature distribution in a large, highly sampled grain (R76-13) showing that typical grain temperature variations are low, even in large grains. The grain displayed shows only slight tenancy to have higher temperatures recorded closer to the grain rim. Temperatures calculated using ZRT of Tomkins et al. (2007).

analysed rutile crystals in the population grew, rather than the peak temperature experienced by the whole-rock. That is of course unless the rutile population crystallised in unicen, in which case the mean-mean, mean-max and maximum temperatures are likely to be very similar.

Figure 5.9 shows that the density distribution curve for mean-maximum temperatures for eclogites in the WGR has largely the same shape as that for mean-mean temperature. The peak of the mean-maximum curve is displaced only around 10 ^{o}C higher. It is not surprising that these two curves are highly similar, as we have already shown that the variation in temperatures in grains is very low.

5.3.5 Maximum Temperature

The maximum temperature of each sample is simply the single highest temperature calculated from a single rutile analysis for each whole-rock. Whilst this value *might* give a more accurate estimate of the whole-rock's T_{max}, the value is highly sensitive to potentially anomalous or contaminated Zr readings, and so for individual samples this maximum temperature cannot be considered to be robust. However, when considered together with the maximum temperatures of other eclogites, these values may be considered to more reliably record the regional maximum temperatures at which rutile in Norwegian eclogites equilibrated.

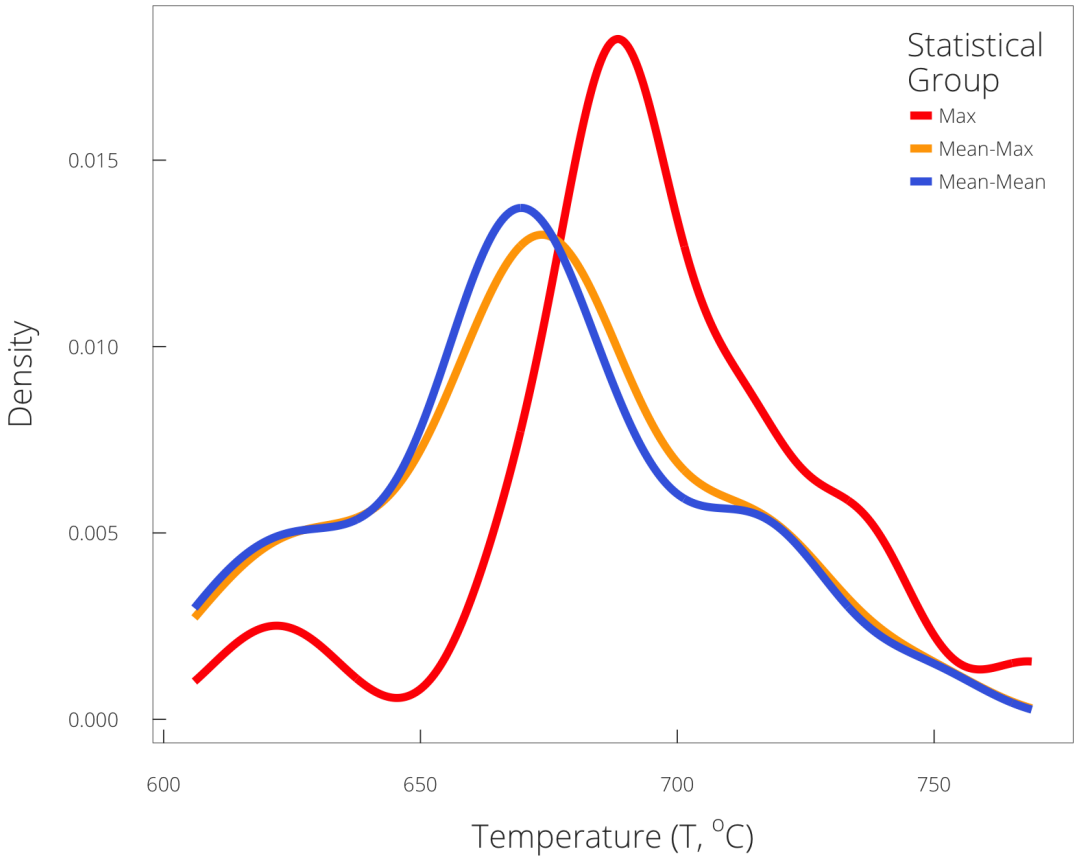

Figure 5.9: Density distribution curves (KDE) for temperatures calculated using the ZRT of Tomkins et al. (2007) in each of the statistical groups. The distribution of mean-mean and mean-max temperatures are very similar, reflecting the generally low range in temperatures preserved in each rutile and between rutiles. The shape of the curve for maximum temperatures is similar to mean-mean and mean-max, however has a narrower distribution and is displaced to temperatures around 30 ^{o}C or so higher than the other curves.

The absolute range in maximum temperatures is still 650-750 ^{o}C, however the vast majority of samples have temperatures of 650-750 ^{o}C, with a peak density at approximately 685 ^{o}C, suggesting that maximum temperatures of the whole dataset are generally 25-30 ^{o}C higher than the other two estimates.

5.4 Discussion

Until now, much of the data have been presented and treated as a whole. There are clearly limitations to treating the data in such a way, since it is expected that eclogites attained lower peak metamorphic temperatures in the south-east, and higher temperatures in the north-west (see Griffin et al., 1985; Cuthbert et al., 2000). For this reason, later in this section we address samples on a more individual basis in the form of a thermal map of the Nordfjord-Statlandet area. However, there are important observations of the data taken as a whole to be discussed first.

5.4.1 Temperature Ranges of Rutiles

Figure 5.7 showed that the temperature variation within most rutiles is less than $\pm$0-10 ^{o}C, and the variation in temperatures between rutiles is mostly around $\pm$20-40 ^{o}C. Cherniak et al. (2007) suggest that significant and ubiquitous re-equilibration of Zr is unlikely since diffusion of Zr in rutile is very slow, whereas Blackburn et al. (2012) show that isothermal residence of t>2 Ma at temperatures exceeding 600 ^{o}C allows significant internal re-equilibration of Zr in rutile to occur in grains of up to 50 μm. Two scenarios are therefore possible for our samples: either rutiles were grown rapidly over a narrow temperature range; and/or rutiles experienced significant re-equilibration at or near their peak metamorphic conditions.

In previous chapters we have shown that rutile probably initially crystallised in the lower-amphibolite facies, immobilising important HFSEs. Given that the burial trajectory of eclogites as plotted on a pressure-temperature diagram was probably very steep (discussed later), then one would expect rutiles to at least have cores that record temperatures much less than 600 ^{o}C. Given the findings of Blackburn et al. (2012) this strongly suggests that WGR eclogites spent >2 Ma at temperatures above 600 ^{o}C,

causing significant internal homogenisation of the Zr-dependent concentrations within each grain. If this is the case, temperature estimates have to be considered to be minimum estimates of T_{max} since homogenisation of rutiles with cooler cores will lower the maximum temperature estimates. Whole-rock homogenisation of Zr concentrations between rutile grains are far less likely given the slow diffusion rates of Zr, suggesting that the relatively high variation in temperatures recorded between rutiles within each whole rock (i.e. 80-100 ^{o}C) reflects the approximate range in temperatures over which rutile originally crystallised in each eclogite.

That many rutiles in eclogites record temperatures much greater than 600 ^{o}C suggests that exhumation from T_{max} to temperatures $< 600^{o}$C took less than 2 Ma. Rapid, buoyancy driven uplift of eclogites is to be expected, and is also probably the essential factor in ensuring the eclogite assemblage is preserved during uplift to the surface.

5.4.2 Pressure-Temperature Distribution

The most recent and comprehensive summary on the temperatures and pressures of WGR eclogites is provided by Cuthbert et al. (2000) who uses the garnet-clinopyroxene Fe-Mg geothermometer of Krogh-Ravna (2000) along with several geobarometers to suggest a linear relationship between temperature and pressure in the WGR (Figure 5.10), from 500 ^{o}C and 16 kbar in Sunnfjord to $>$800 ^{o}C and 32 kbar in outer Moldefjord, as preserved in some WGR eclogites and peridotites (see Figure 5.11 for geographical locations). Density distributions of temperature data from Cuthbert et al. (2000) are plotted in Figure 5.12, which shows the general increase in temperatures from southern to northern domains in the WGR. The orientation, location, and magnitude of this gradient are in general agreement with the thermal gradient mapped out by Griffin et al. (1985), shown in Figure 5.13.

Figure 5.14 shows our eclogites plotted on a pressure-temperature diagram. Our data define a gradient of around 2 ^{o}C/km on the plot that, is in general agreement with the gradient reported by Cuthbert et al. (2000) shown in Figure 5.10 and is shallower than a line of the Tomkins et al. (2007) ZRT (Zr = 125 ppm). For both our data and that of Cuthbert et al. (2000) the generally very steep linear correlation between pressure and temperature suggests suggests a 'supercool' geothermal gradient in this part of the

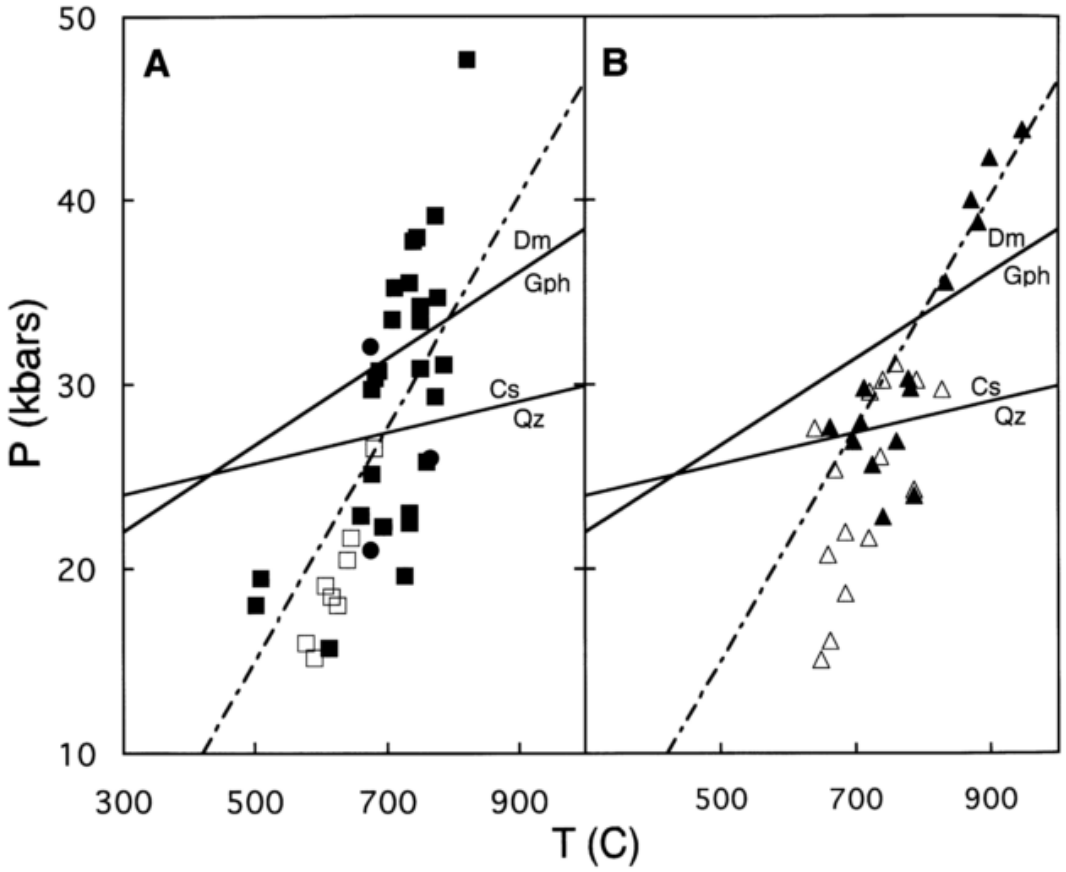

Figure 5.10: Pressure-Temperature plots of opx-eclogites and garnet peridotites in the WGR between Sunnfjord in the south and Moldefjord in the north (from Cuthbert et al., 2000). A) squares are external Opx eclogites, circles are FeTi garnet peridotites. B) Mg-Cr garnet peridotites, filled triangles are grain cores, open symbols are rims. The dashed line represents a 5 ^{o}C reference geotherm. Both plots show that there is a generally steep and linear geotherm from Sunnfjord in the south to Moldefjord in the north.

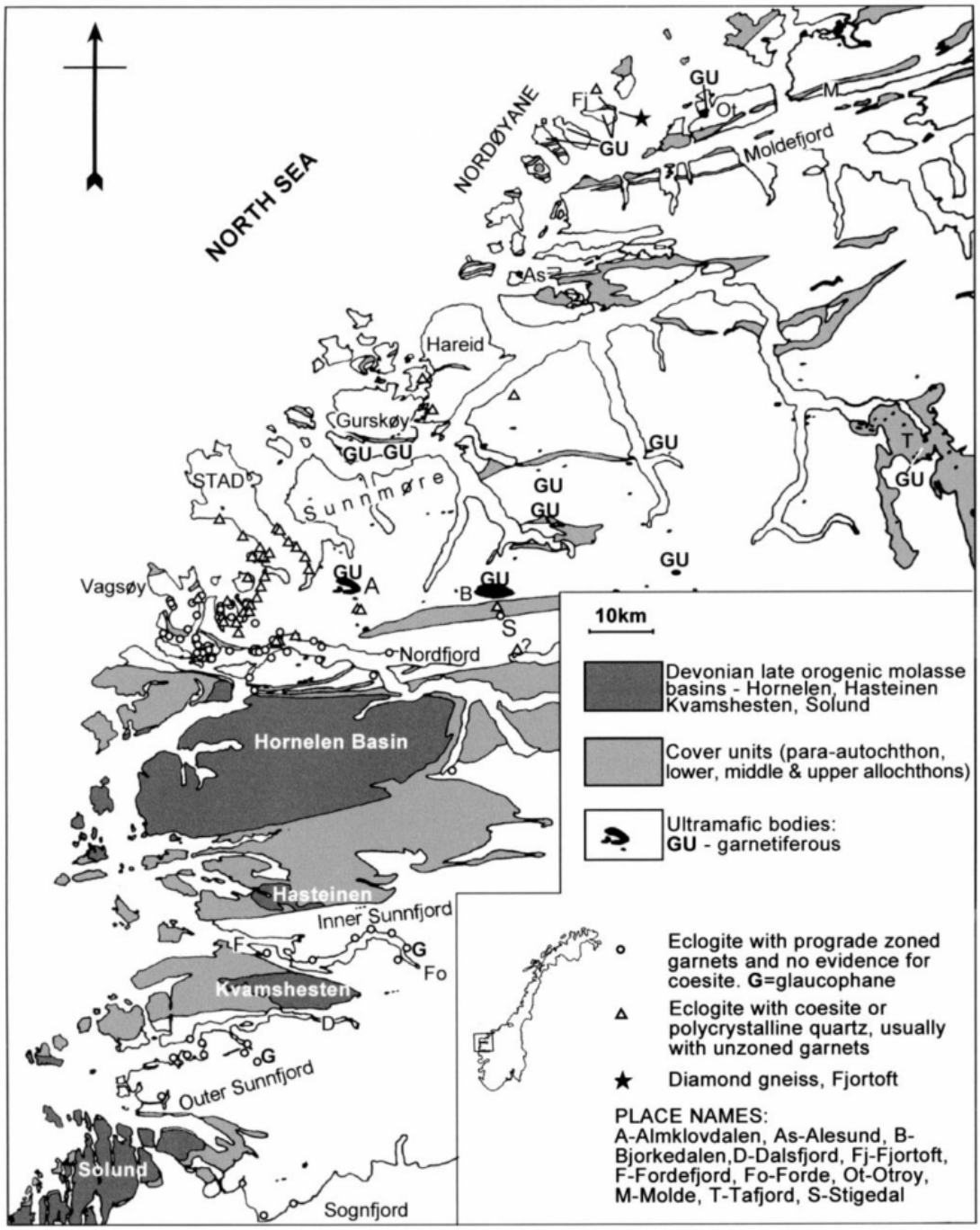

Figure 5.11: Map showing the distribution of eclogites in the WGR from Sognefjord in the south to Molde in the north. Simplified geological units are displayed, along with symbols that indicate the petrographic type of eclogite. From Cuthbert et al. (2000).

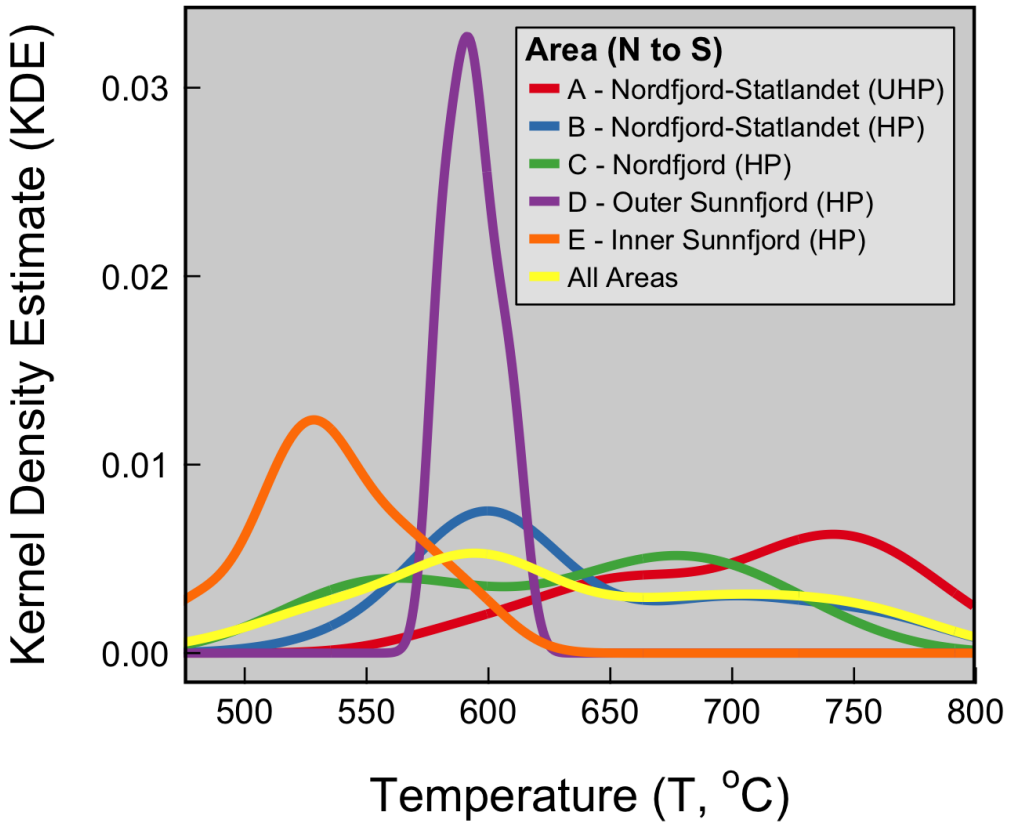

Figure 5.12: Density distribution curves for temperatures of Norwegian eclogites as summarised in Cuthbert et al. (2000). Curves are colour factored into important WGR domains, however a cumulative KDE curve is also displayed. The data show clear differences in temperatures of the different domains, which generally increase towards the North West of the WGR. The recorded temperature range is between 500 and 800 ^{o}C.

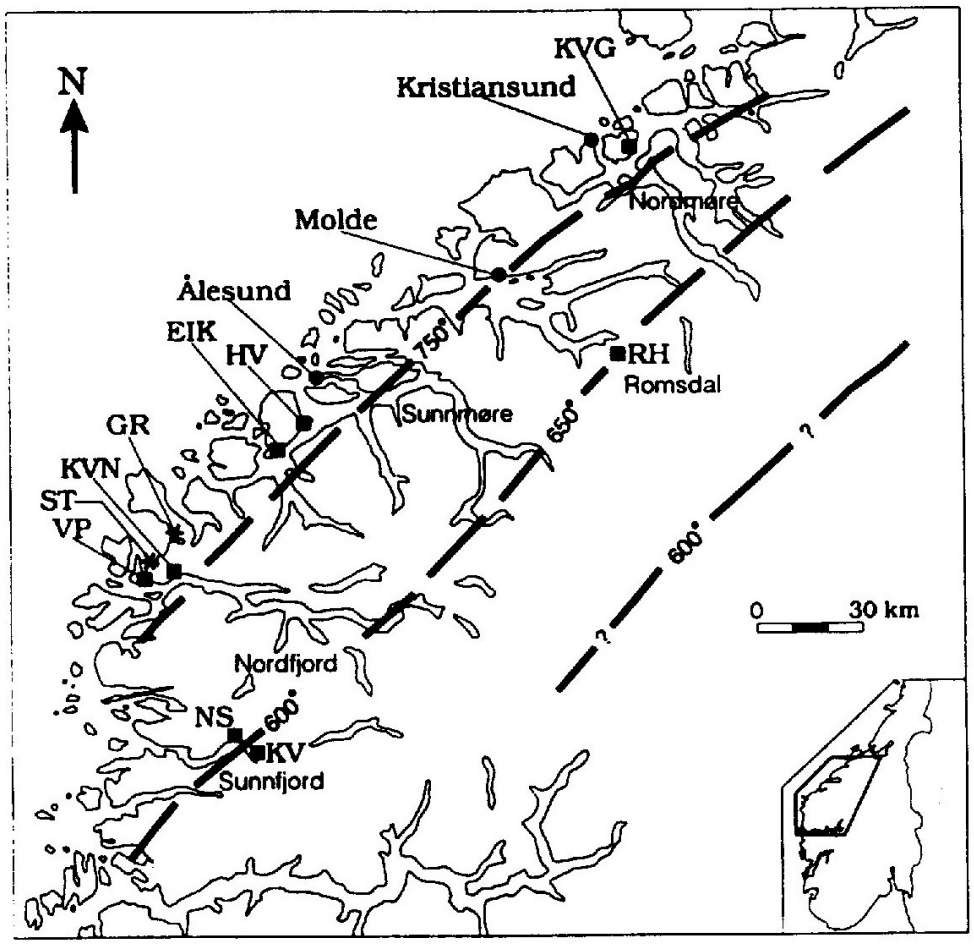

Figure 5.13: Model for peak Caledonian metamorphism preserved in the rocks of the WGR from Krogh and Carswell (1995). Geotherms from Griffin et al. (1985). Abbreviations are: EIK, Eiksunddal; GR, Grytting; HV, Hjørungavåg; KVG, KV, Kvineset; KVN, Kvalneset; ST, Straumen; VP, Verpeneset. The highly important Nordfjord-Statlandet region is below the resolution of this model.

slab.

5.4.3 Thermal Mapping

By combining ZRT data from this study with temperatures reported in Cuthbert et al. (2000), we were able to construct Figure 5.15, which is a high-resolution thermal map of the Nordfjord-Statlandet region. The isotherms in Figure 5.15 plot parallel to major amphibolite facies lineations and regional pressure domains as shown in Figure 5.16, suggesting that our thermal map is likely to be an accurate representation of the eclogite-facies thermal gradient of the Nordfjord-Statlandet region prior to late Caledonian folding. Note also that the 750 ^oC geotherm from Griffin et al. (1985) seems to fit the general position and location of the 750 ^oC geotherm in our map.

That the isotherms in Figure 5.15 appear to be folded in parallel with amphibolite facies lineaments in the area suggests that the temperature structure preserved in the basement of the region may have been subsequently folded during post-peak deformation. This deformation is probably associated with orogenic collapse and the formation of large detachment faults such as the Nordfjord-Sogn Detachment Zone (NSDZ). Furthermore, the geothermal gradient form Nordfjord in the south to Statlandet in the north is clearly not linear, instead geotherms reappear north of Nordfjord suggesting that the thermal gradient has been regionally folded not only in the horizontal plane, but the vertical plane too. Two two fold axes can explain the observations: one fold axis runs along the northern shore of Nordfjord parallel to the geotherms, describing the axial trace of an anticline; and the other running north-northwest to south-southeast describing the folding of the geotherms seen in the horizontal plane.

The most likely explanation for the folding observed in the geothermal gradient is that it was folded along with the basement during the collapse of the orogen. That the isotherms are generally aligned with amphibolite facies lineations supports this hypothesis, and shows that a more detailed integration of such high resolution temperature data needs to be considered in detail together with structural models of the area.

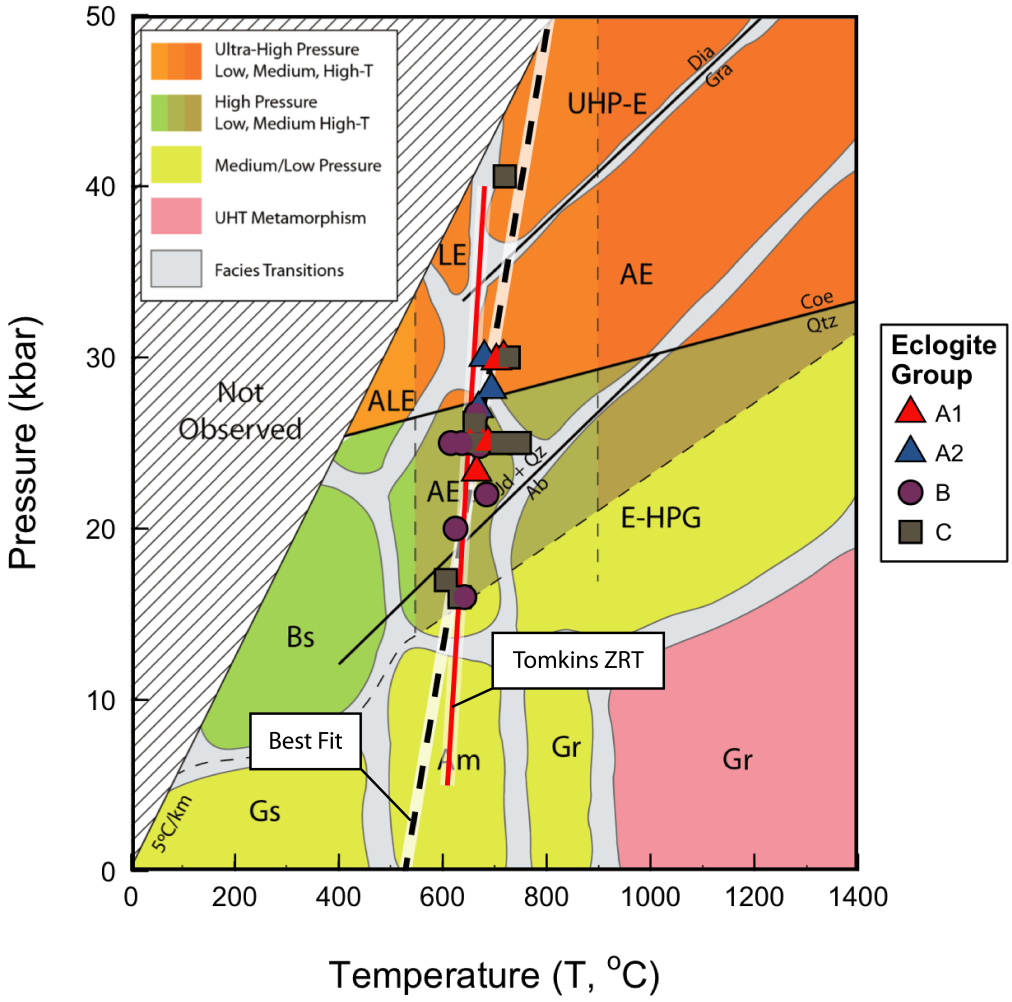

Figure 5.14: Calculated eclogite positions on a metamorphic facies diagram that concentrates on the HP-UHP facies. As can be seen, all eclogites may be classed as medium temperature. Most eclogites are High Pressure, with some UHP and MP. The majority of eclogites plot within the Amphibole-Epidote-Eclogite (AEE) or Amphibole-Eclogite facies (AE). The eclogites define a slight positive trend (dashed black line) with around 100 ^{o}C increase over the entire pressure range. The data define a line with a slope only marginally shallower than a line of the ZRT of (Tomkins et al., 2007, Zr = 125 ppm).

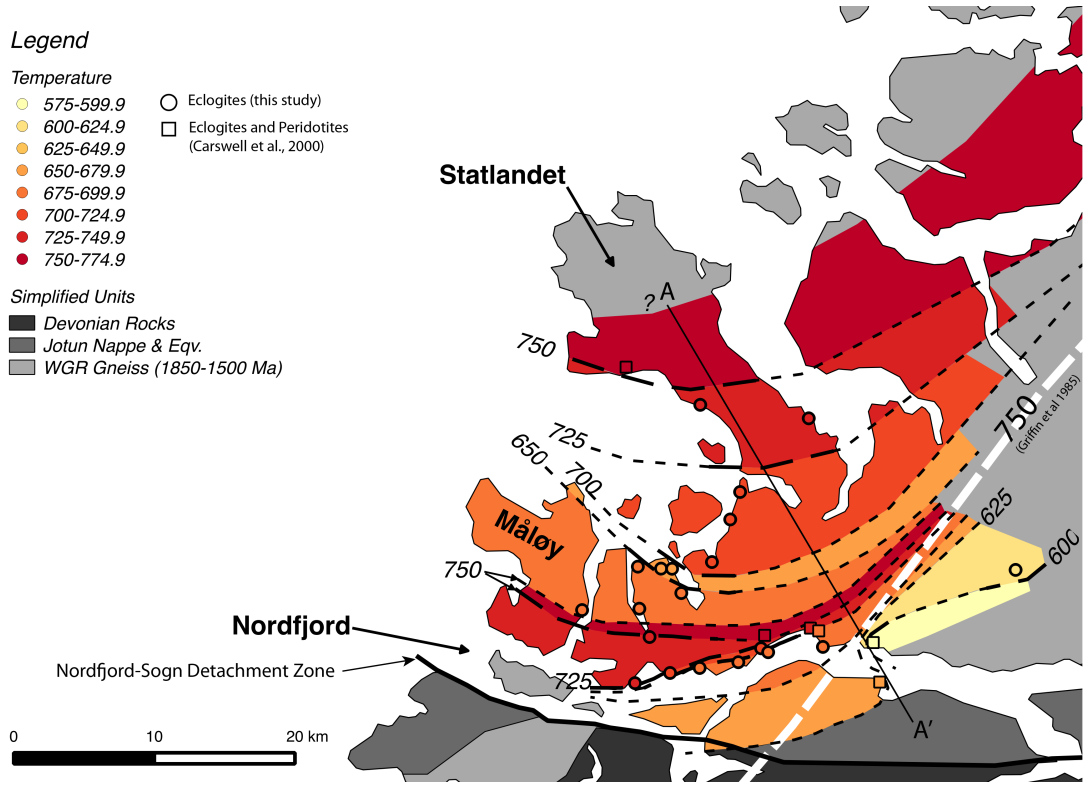

Figure 5.15: Thermal model for the Nordfjord-Statlandet Region based on ZRT conducted on eclogitic rutiles (circles), supplemented by Garnet-Clinopyroxene geothermometry Cuthbert et al. (2000) for samples not analysed in this study (squares). The white dashed line is the 750 ^oC geotherm from Griffin et al. (1985). The model shows that the thermal gradient is non-linear from north to south, suggesting the thermal gradient has been folded by subsequent deformation, presumably associated with exhumation.

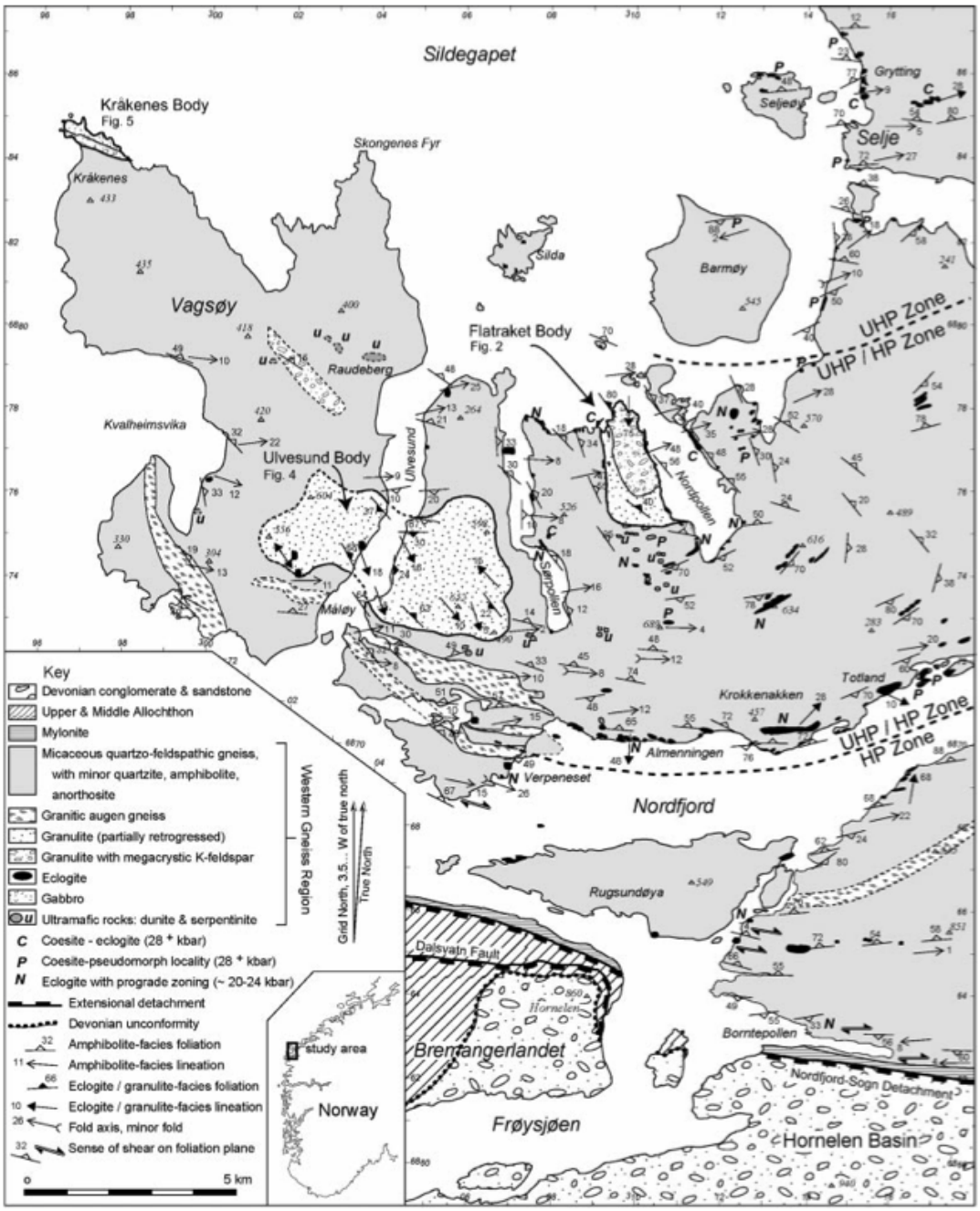

Figure 5.16: Structural geology of the Western Nordfjord-Måløy area, from Krabbendam and Wain (1997). The map shows that the general foliation in the region is largely parallel with the isotherms predicted in our thermal model for the area.

5.5 Conclusions

Using the preferred ZRT of Tomkins et al. (2007) several conclusions may be drawn from our data and applied to our understanding of the geodynamic history of the WGR and the petrogenesis of rutile along metamorphic PTt paths.

- Eclogites in this study may indeed be classed as MT eclogites, since most eclogitic rutiles record maximum temperatures in the range of 600-750 ^{o}C.

- Much of the observed range in temperatures for all eclogites in this study reflects a regional gradient of temperatures from approximately 600-650 ^{o}C in the Sognefjord and Sunnfjord area, to 625-750 ^{o}C or more in the area between southern Nordfjord and Statlandet. This agrees with other geothermometry studies in the area (e.g. Griffin et al., 1985; Cuthbert et al., 2000).

- The temperature difference between HP and UHP eclogites is only around 100-200 ^{o}C, showing that the burial trajectory of the basement was probably steep.

- We suggest that rutile crystals have experienced significant internal homogenisation together with likely significant re-equilibration at or around T_{max}. This homogenisation probably occurred during residence times likely to be $>$2 Ma at temperatures of $> 600^{o}$C.

- Lack of retrograde temperature zonation, particularly in large grains, suggests post T_{max} exhumation to temperatures below 600 ^{o}C took much less than 2 Ma.

- Such rapid exhumation was more than likely sustained to temperatures well below 600 ^{o}C, contributing to the excellent preservation of eclogites in the WGR.

- The temperature gradient preserved in the WGR basement shows convincing evidence of post-peak metamorphism amphibolite-facies deformation, probably related to the formation of large detachment zones during the collapse of the Caledonian orogen.

5.6 Proposed Future Work

Our data have raised questions which were unable to be answered given the inevitable restricted scope of this particular study. A major aspect of our investigation was to gather rutile thermometry data for a wide range of samples, whilst also gathering a breadth of data which could be used to test intra-sample variability. As a result, our rutile grains were collected by mineral separation techniques. Although this preparation technique was suited to the needs of this particular study, it limits the meta-data for each analysis. A useful complementary dataset would therefore be composed of *in-situ* analyses on the different petrographic occurrences of rutile (i.e. rutile as inclusions in garnet and pyroxene, versus rutile in the matrix).

We could also provide further context both to our eclogites and rutiles if we were to conduct U-Pb thermometry on a representative suite of rutiles from each sample. This is an area of further work on the samples we have already prepared that has much promise in leading to useful data for the WGR as a whole.

The geothermal map produced for the Nordfjord-Statlandet region has highlighted several questions about the area that can be answered by studying our data in more detail in a further study. Specifically, it is now possible to suggest a cross section of the geothermal structure of the region as preserved in the WGR eclogites, especially along line A-A' in Figure temperaturemap. It would be very interesting to see if pressure and temperature gradients correspond to sensible gradients for thickness of crust represented. One may take a thermal gradient expected for the slab top and estimate the thickness originally represented by the basement in the section, then compare that with the structural thickness now. A quick sketch analysis suggests that significant telescoping of the crust in the area may have occurred, and that a more detailed study would more than likely reach some interesting conclusions about the post-peak meatamorphic deformation of the basement in the area.

Chapter 6

Conclusions, Limitations and Further Work

In this chapter, the primary objectives of the thesis are restated along with the conclusions that came to satisfy them. Following this summary, an assessment of the main limitations is made along with suggestions for directions of future work.
The aims and objectives of this thesis can be divided into three main parts. The first part involved developing and testing a sample preparation procedure for rutile-bearing eclogites for solution ICP-MS analysis. The second part dealt with identifying likely eclogite protoliths, followed by an assessment of the overall mobilities of trace elements during eclogite formation and exhumation. Finally, attention was turned to using the geochemistry of eclogite-hosted rutiles to learn not only about the thermal histories of Norwegian eclogites, but also the role rutile played in controlling their trace element geochemistry. Aims and objectives associated with each of those three parts are detailed below:

- Part I: Development of a preparation procedure for solution-based geochemical analyses of rutile-bearing eclogites
  - Assess the extent to which typical sample digestion procedures can dissolve rutile-bearing eclogites efficiently enough to produce a solution that can be used to accurately determine trace element inventories.
  - Develop and quantitatively assess a procedure that ensures dissolution of rutile and therefore allows accurate measurements of the concentrations of important trace elements in the whole-rock to be made.
- Part II: Use whole-rock trace element geochemistry to suggest likely protolith types for Norwegian eclogites, as well as to make an assessment of the general mobility of trace elements during their eclogitisation and exhumation.

  - Identify elements that are likely to be immobile during metamorphism using both evidence from the literature and correlation analyses. Then, using elements identified as immobile perform a discriminant analysis to identify the likely igneous protoliths for Norwegian eclogites.
  - Compare the geochemistry of eclogites now with that of their likely protoliths to make quantitative and qualitative estimates of the overall mobilities of trace elements during eclogite's metamorphism and exhumation in the WGR of Norway.

- Part III: Assess the geochemistry and role of rutile in eclogites from the WGR.

  - Measure the trace element composition of a comprehensive and representative suite of rutiles separated form Norwegian eclogites.
  - Quantitatively assess the extent to which rutile, when present, controls the trace element budget of its whole rocks.
  - Investigate the apparent partitioning behaviour of trace elements identified as important in rutile. This includes identifying trace element pairs that may show analogous or coupled partitioning into rutile, as well as those which may be fractionated in by rutile.
  - Use Zr-in-rutile thermometry to suggest temperatures for the crystallisation and/or equilibration of rutiles in Norwegian eclogites.
  - Use temperatures calculated from rutiles to suggest the geographical placement of Caledonian isotherms preserved in eclogites from the Nordfjord-Statlandet region.

6.1 Conclusions

6.1.1 The Dissolution of Rutile-Bearing Lithologies

Rutile was shown to be highly resistant to very acidic solutions at room pressure and temperatures of around 100 ^{o}C. The failure of low pressure and temperature solution (LPTS) techniques to dissolve rutiles may go undetected, and will more than likely significantly reduce the accuracy of trace element determinations in rocks

where only half a percent of rutile is present. In particular, the concentrations of Ta, Nb, Hf and Mo are likely to be inaccurate. By dissolving rutile-bearing samples under pressure, i.e. high pressure and temperature solution (HPTS), one may increase the system temperatures to around 220 ^{o}C, which effectively allows all rutile to be dissolved. Whilst the accuracy of most elements is increased in such an approach, significant loss of Pb and Sn is likely to occur.

For anyone conducting whole-rock trace element analyses of rutile-bearing rocks, it is recommended that both LPTS and HPTS are undertaken to ensure accurate data are gathered.

6.1.2 The Origin of Norwegian Eclogites

Three main groups of eclogites were identified based on their bulk trace element compositions. The first group (i.e. group A) appear to be derived from basalts with MORB-like mantle sources, with geochemistries highly similar to N- and E-MORBs. The second group of eclogites (i.e. group B) are shown to have basalts that were probably sourced from enriched mantle sources, in that they have very similar geochemistries to basalts generated in subduction settings. A third group of eclogites (i.e. group C) have geochemistries that have apparently been significantly perturbed during metamorphism and/or exhumation and as such could not be reliably used to determine likely protoliths. However, it is shown that group C eclogites probably had similar protoliths to those in group A or B.

6.1.3 Element Mobility During Subduction and Exhumation

We show that, even for samples that have clearly undergone significant trace element remobilisation, the elements Nb, Ta, Zr, Hf and Y appear to remain largely immobile. Additionally, for a significant number of samples, there is good evidence that the complete suite of REEs may also remain largely immobile during metamorphism up to-, and exhumation from the eclogite facies.

An assessment of the mobility of elements generally considered to be fluid-mobile was also made. It was shown that the relative mobilities of such elements is

Ba<Rb<U<Th<Sr≈K≪Pb. Actual changes in whole-rock inventories as a result of the mobilisation of these elements either in or out of the whole-rock rarely exceed 50 %, with the exception of Pb which may be enriched by several hundred percent.

6.1.4 Rutile Geochemistry

It is shown that rutile has a highly important and often understated importance in controlling the trace element budgets of their host rocks, particularly in eclogites. For instance, rutile typically accounts for 40-70 % of TiO_2, 40-90 % of Ta, 35-85 % of Nb, up to 24 % of Sn and up to 22 % of Mo in the whole-rock. Furthermore, it was shown that rutlile has the capacity to cause significant fractionation between Nb and Ta, Nb and Mo, and Zr and Hf.

It was also shown that the concentration of Mo in rutile may be used to suggest fluid-enrichment histories of their host-rocks. Eclogites that showed evidence of fluid enrichment record elevated Mo-in-rutile concentrations. In particular, we showed that Sn and Mo concentrations are generally only correlated in rutiles that have not undergone hydrothermal enrichment. There is clear potential for these observations to be investigated further.

6.1.5 Thermal Profile of the Nordfjord-Statlandet HP-UHP Region

A study into the temperatures preserved in eclogite-hosted rutiles from the WGR confirm the presence of a regional eclogite-facies geothermal gradient in the WGR. Minimum estimates of T_{max} increase from around 600 ^{o}C the south-east of the WGR to around 750 ^{o}C or more the north-west Nordfjord-Statlandet region. It is also shown that this geothermal gradient, whilst generally linear across the WGR, has apparently been deformed along with the basement during the orogenic collapse of the Scandinavian Caledonides.

Our data showed that rutiles from Norwegian eclogites record surprisingly narrow ranges of equilibration temperatures, which is thought to be a consequence of significant time (t = $\gg$ 2 Ma) spent at T >600 ^{o}C. It is also shown that although residence time at peak conditions may have been significant in terms of the

re-equilibration of rutile, exhumation from temperatures >600 ^{o}C were probably $\ll$ 2 Ma.

6.2 Limitations

1. Several classic eclogite localities in Norway (e.g. the orthopyroxene eclogite at Selje, Statlandet) are now protected from sampling, even for scientific purposes. As a result, several localities with significant geological legacies were not included in this study.

2. Almost all analytical procedures used in this study were both highly expensive and time-intensive. For instance, the development and rigorous testing of LPTS and HPTS procedures for ICP-MS analyses of whole rock samples took more than a year of strong collaborative work at SUERC. This included the expenditure of significant manpower hours from Valerie Olive and Anne Kelly, with additional investment in new laboratory equipment from director Rob Ellam. In all analytical procedures, the relatively large number of eclogite localities included in this study multiplied the laboratory time significantly. It is for this reason that isotopic analyses of Norwegian eclogites had to be largely abandoned.

3. Geochemical and petrological heterogeneity on the centimetre- to meter scale in each of the individual eclogite exposures is likely. Such heterogeneity was below the resolution of the sampling target for this study, and as a consequence one must realise the potential for error in our geochemical data. It is clear that we would benefit from high resolution investigations of trace element geochemistry of individual eclogite bodies. This is discussed more in the following section.

4. The nature of eclogite protoliths and the relative element mobility of many trace elements is strongly dependent upon on our collective understanding of trace element mobility during subduction. The processes controlling element mobility during subduction are clearly highly complex, especially given the relatively low resolution with which we can currently study element flux in subduction zones. Therefore, we must remain relatively cautious about interpreting protoliths of such high grade rocks.

5. The spatial resolution of LA-ICP-MS (ca. 1200 μm^3) is relatively coarse compared with that of the secondary ionisation mass spectrometry (SIMS) (up to around 100 μm^3). SIMS was however, unable to provide analyses of several elements critical to the investigation of rutile geochemistry in Norwegian eclogites. Therefore, many rutile grains could accommodate only 2-3 adjacent LA-ICP-MS acquisitions. Although it appeared compositional zoning in analysed rutiles was fairly limited, the resolution of analysis could be masking important compositional zonation.

6. By analysing only separated rutiles one loses the petrological context of each grain. Since significant inter-grain compositional variation was observed in most samples, information on the petrological associations of those rutile crystals could be highly valuable, but is unfortunately missing.

6.3 Further Work

This project was undoubtedly rather explorative in nature, and thus unsurprisingly our findings have uncovered new questions which could be subjects of future research.

1. The dissolution of rutile bearing samples remains a hurdle to the geochemist. There remains much to studied about reliability of data gathered from both LPTS and HPTS techniques. In particular, the loss of volatile elements during HPTS needs to be studied more closely.

2. The breadth of localities targeted in this study has presented a double-edged sword of advantages and disadvantages. On the one hand we have been able to make regionally significant statements about eclogites in the Norwegian Caledonides, and produce a high resolution thermal map of the Nordfjord-Statlandet HP-UHP province. On the other hand, we know little about the heterogeneity on the small scale of both eclogite outcrops and individual minerals. It is clear that we could benefit from high-resolution compositional mapping of eclogite localities and important minerals (i.e. rutile) in order to better understand the geochemical evolution of not only individual samples, but the WGR as a whole.

3. Our collection of rutile crystals from Norwegian eclogites is one of the most comprehensive and highly sampled collections of natural eclogitic rutile in the world. There remains much more to learn from these samples using a variety of other analytical techniques.

   (a) Oxygen isotopes could help shed light on the finding that some rutiles may have scavenged significant amounts of Mo from high fO_2 fluids.

   (b) Rutile is also one of the most hydrous nominally anhydrous minerals on earth Bromiley et al. (2004), and therefore it would complement the oxygen isotope data to also gather data on the concentrations of hydrogen ions in rutiles, especially those with high Mo contents.

   (c) Data on uranium and lead isotopes can be combined with ZRT to study the so-called speedometry of host rock evolution (e.g. Blackburn et al., 2012). In such an investigation, temporal constraints on temperature variations in rutile can allow one to temporally constrain temperature variations both within and between rutiles from eclogites.

   (d) It was shown that geologically important relationships between the concentrations of Sn and Mo in eclogite-hosted rutiles exist. It was suggested that those samples that broke away from otherwise correlated concentrations of Sn and Mo in rutile, having Mo $>$15 ppm, were probably enriched by fluids potentially responsible for the destruction of whole-rock REE signatures. Therefore, the relationship between Sn and Mo in rutile and the fluid-history of their whole-rocks is clearly an avenue of future research with promise.

   (e) There remains much to be learned from Zr-in-rutile thermometry performed on rutiles from WGR eclogites. Performing *in-situ* analyses of Zr concentrations n rutile would certainly allow more inferences to be made about the crystallisation sequences of rutiles in the genesis of the eclogite assemblage on the prograde path. Furthermore, we identified that there remains much to be learned from studying the thermal and geographical distribution of Norwegian eclogites, particularly with respect to identifying post-collisional deformational processes. Specifically, it would be useful to use the thermal map produced of the Nordfjord-Statlandet region to

estimate any thinning of the crust that may have happened during orogenic collapse.

References

Agapova, G. F., Modnikov, I. S., and Shmariovich, Y. M. (1989). Experimental study of the behaviour of titanium in hot-sulphide-carbonate solutions. *International geology review*, 31:424–430.

Agrawal, S., Guevara, M., and Verma, S. P. (2008). Tectonic Discrimination of Basic and Ultrabasic Volcanic Rocks through Log-Transformed Ratios of Immobile Trace Elements. *International geology review*, 50(12):1057–1079.

Andersen, T. B. (1998). Extensional tectonics in the Caledonides of southern Norway, an overview. *Tectonophysics*, 285:333–351.

Andersen, T. B. and Austrheim, H. (2008). The Caledonian infrastructure in the Fjord-region of Western Norway; with special emphasis on formation and exhumation of high- and ultrahigh-pressure rocks, late- to post-orogenic tectonic processes and basin formation. *IGC excursion No 29, August 15 - 22nd*, 33.

Andersen, T. B. and Jamtveit, B. (1990). Uplift of deep crust during orogenic extensional collapse: a model based on field studies in the Sogn-Sunnfjord region of Western Norway. *Tectonics*, 9(5):1097–1111. Times Cited: 168.

Andersen, T. B., Jamtveit, B., Dewey, J. F., and Swensson, E. (1991). Subduction and eduction of continental crust: major mechanisms during continent-continent collision and orogenic extensional collapse, a model based on the south Norwegian Caledonides. *Terra Nova*, 3(3):303–310.

Andréasson, P. G. (1994). The Baltoscandian margin in Neoproterozoic-Early Palaeozoic time. Some contraints on terrane derivation and accretion in the Artic Scandinavian Caledonides. *Tectonophysics*, 231:1–32.

Arculus, R. J., Lapierre, H., and Jaillard, E. (1999). Geochemical window into subduction and accretion processes; Rapas metamorphic complex, Ecuador. *Geology*, 27:547–550.

Audetat, A. and Keppler, H. (2005). Solubility of rutile in subduction zone fluids, as determined by experiments in the hydrothermal diamond anvil cell. *Earth and Planetary Science Letters*, 232:393–402.

Aulbach, S., O'Riley, S. Y., Griffin, W. L., and Pearson, N. J. (2008). Subcontinental lithospheric mantle origin of high niobium/tantalum ratios in eclogites. *Nature Geoscience*, 1:468–472.

Austrheim, H. (1991). Eclogite formation and dynamics of crustal roots under continental collision zones. *Terra Nova*, 3(5):492–499. Times Cited: 54.

Baldwin, J. A. and Brown, M. (2008). Age and duration of ultrahigh-temperature metamorphism in the Anápolis-Itauçu complex, southern Brasília belt, central Brasil - constrains from U-PB geochronology, mineral rare earth element chemistry and trace-element thermometry. *Journal of Metamorphic Geology*, 26:213–233.

Bali, E., Keppler, H., and Audetat, A. (2012). The mobility of W and Mo in subduction zone fluids and the Mo-W-Th-U systematics in islanc arc magmas. *Earth and Planetary Science Letters*, 351-352:195–207.

Barsukova, M. L., Kuzetsov, V. A., Dorofeeva, V. A., and Khodokovsky, I. L. (1979). Experimental study of rutile-TiO_2 in flouride solutions under high-temperature. *Geokhimiya*, pages 1017–1027.

Barth, M. G., McDonough, W. F., and Rudnick, R. (2000). Tracking the budget of Nb and Ta in the continental crust. *Chemical Geology*, 165:193–213.

Bau, M. (1996). Controls on the fractionation of isovalent trace elements in magmatic and aqueous systems: Evidence from Y/Ho, Zr/Hf, and lanthanide tetrad effect. *Contributions to Mineralogy and Petrology*, 123(3):323–333. ISI Document Delivery No.: UG529 Times Cited: 235 Cited Reference Count: 67 Springer verlag New york.

Becke, F. (1903). Über Mineralbestand und Struktur der kristallinischen Schiefer. Denkschriften der k. Akademie der Wissenschaften. *Mathematisch-Naturwissenschaftliche Klasse LXXV*, pages 1–53.

Becker, H., Jochum, K. P., and Carlson, R. W. (2000). Trace element fractionation during dehydration of eclogites from high-pressure terranes and the implications for element fluxes in subduction zones. *Chemical Geology*, 163(1-4):65–99. ISI Document Delivery No.: 272MB Times Cited: 110 Cited Reference Count: 128 Elsevier science bv Amsterdam.

Binns, R. A. (1967). Barroisite-bearing eclogite from Naustdal, Sogn og Fjordane, Norway. *Journal of Petrology*, 8(3):349–371. Times Cited: 38.

Blackburn, T., Shimizu, N., Bowring, S. A., Choene, B., and Mahan, K. (2012). Zirconium in rutile speedometry: New constraints on lower crustal cooling rates and residence temperatures. *Earth and Planetary Science Letters*, 317-318:231–240.

Bonney, T. G. (1879). Notes on some Ligurian and Tuscan serpentinites. *Geological Magazine*, VI(II):362–371.

Braathen, A. e. a. (2000). Devonian, orogen-parallel, opposed extension in the Central Norwegian Caledonides. *Geology*, 28(7):615–618.

Brenan, J. M., Shaw, H. F., Phinney, D. L., and Ryerson, F. J. (1994). Rutile-Aqueous Fluid Partitioning of Nb, Ta, Hf, Zr, U and Th - implications for high-field strength element depletions in island-arc basalts. *Earth and Planetary Science Letters*, 128(3-4):327–339. Times Cited: 190.

Brewer, T. S., Daly, J. S., and Ahäll, K. I. (1998). Contrasting magmatic arcs in the Palaeoproterozoic of the south-western Baltic Shield. *Precambrian Research*, 92:297–315.

Brière, Y. (1920). Les éclogites françaises. Leur composition minéralque et chemique. Leur origine. *Bulletin de la Société française de Minéralogie XLIII*, pages 72–222.

Bromiley, G., Hilaret, N., and McCammon, C. (2004). Solubility of hydrogen and ferric iron in rutile and TiO_2 (II): Implications for phase assemblages during ultrahigh-pressure metamorphism and for the stability of silica polymorphs in the lower mantle. *Geophysical Research Letters*, 31(4). Times Cited: 16.

Brueckner, H. K. (1977). A Structural Stratigraphic and Petrologic Study of Anorthosites, Eclogites and Ultramafic Rocks and Their Country Rocks, Tafjord Area, Western Norway. *Norsk Geologisk Undersøkelse*, 332:1–53.

Brueckner, H. K. and van Roermund, H. L. M. (2004). Dunk tectonics: a multiple subduction/eduction model for the evolution of the Scandinavian Caledonides. *Tectonics*, 23:http://dx.doi.org/10.1029/2003TC001502.

Bruton, D. L. and Brockelie, J. F. (1979). The Ordovician sedimentary sequence on Smøla, west central Norway. *Norges Geologiske Undersøkelse*, 348:21–31.

Bryhni, I. (1966). Reconnaissance sudies of gneisses, ultrabasites, eclogites and anorthosites in outer Nordfjord, western Norway. *Norsk Geologisk Undersøkelse*, 241:1–68.

Bryhni, I., Bollingberg, H. J., and Graff, P. R. (1969). Eclogites in quartzofeldspathic gneisses of Nordfjord, Western Norway. *Norsk Geologisk Tidskrift*, 49:193–225.

Cabanis, B. and Lecolle, M. (1989). Le diagramme La/10-Y/15-Nb/8: un outil pour la discrimination de series volcaniques et la mise en evidence des processus de melange et/ou de contamination crustale. *Cr.R. Acad. Sci. Ser. II*, 309:2023–2029.

Carruzzo, S., Clarke, D. B., Pelrine, K., and MacDonald, M. A. (2006). Texture, composition and origin of rutile in the South Mountain Batholith, Nova Scotia. *Canadian Mineralogist*, 44:715–729.

Carswell, D. A. (1990). Eclogites and the eclogite facies: definitions and classification. In *Eclogite Facies Rocks*, pages 1–13. Blackie and Son Ltd.

Carswell, D. A., Brueckner, H. K., Cuthbert, S. J., Mehta, K., and O'Brien, P. J. (2003). The timing of stabilisation and the exhumation rate for ultra-high pressure rocks in the Western Gneiss Region of Norway. *Journal of Metamorphic Geology*, 21(6):601–612. ISI Document Delivery No.: 706RK Times Cited: 45 Cited Reference Count: 49 4th International Eclogite Conference Sep 02-04, 2001 Niihama, japan Blackwell publishing ltd Oxford.

Carswell, D. A. and Cuthbert, S. (1986). Eclogite facies metamorphism in the lower continental crust. *Geological Society, London, Special Publications*, 24(1):193–209.

Carswell, D. A. and Harvey, M. A. (1985). The intrusive history and tectonometamorphic evolution of the Basal Gneiss Complex in the Moldefjord area,

west Norway. In Gee, G. G. and Sturt, B. A., editors, *The Caledonide Orogen - Scandinavia and Related Areas*, pages 843–857. Wiley, Chichester.

Chen, Z. Y. and L., L. Q. (2008). Zr-in-rutile thermometry in eclogite at Jinheqiao in the Dabie orogen and its geochemical implications. *Chinese Science Bulletin*, 53:768–776.

Chen, Z. Y., Yu, J. J., Li, X. F., and Wang, P. A. (2007). Discussion of the application of Zr-in-rutile thermometer in the Sulu-Dabie UHP eclogites. *Acta Geologica Sinica*, 80(12):1842–1850.

Chen, Z. Y., Zeng, L. S., Li, X. F., Yu, J. J., and Xu, J. (2009). Trace elements of rutile in eclogites from CCSD main-hole: a LA-ICP-MS study and its application. *Acta Petrologica Sinica*, 25(7):1645–1657.

Chen, Z. Y., Zhang, L., Du, J. X., and Lü, Z. (2013). Zr-in-rutile thermometry in eclogite and vein from southwestern Tianshan, China. *Journal of Asian Earth Sciences*, 63:70–80.

Cherniak, D. J., Manchester, J., and Watson, E. B. (2007). Zr and Hf diffusion in rutile. *Earth and Planetary Science Letters*, 261(1-2):267–279.

Chopin, C. (1984). Coesite and pure pyrope in high-grade blueschists of the Western Alps - A first record and some consequences. *Contributions to Mineralogy and Petrology*, 86(2):107–118. Times Cited: 636.

Clark, J. R. and Willkiams-Jones, A. E. (2004). Rutile as a potential indicator mineral for metamorphosed metallic ore deposits. *Soumis a l'administration de DIVEX*.

Cocks, L. R. M. and Torsvik, T. H. (2002). Earth geography from 500 to 400 million years ago: a faunal palaeomagnetic review. *Journal of the Geological Society of London*, 159:631–644.

Coleman, R. G., Lee, D. E., Beatty, L. B., and Brannock, W. W. (1965). Eclogites and Eclogites: Their Differences and Similarities. *Geological Society of America Bulletin*, 76(5):483–508.

Corfu, F. and Andrews, J. (1986). A U-Pb age for mineralized Nipissing diabase, Gowganda, Ontario. *Canadian Journal of Earth Sciences*, 23:107–109.

Cuthbert, S. J. (1985). Petrology and tectonic settings of relatively low-temperature eclogites and related rocks in the Dalsfjord area, Sunnfjord, West Norway.

Cuthbert, S. J. and Carswell, D. A. (1990). Formation and Exhumation of medium-temperature eclogites in the Scandinavian Caledonides. In Carswell, D. A., editor, *Eclogite Facies Rocks*, pages 180–203. Blackie, Glasgow and London.

Cuthbert, S. J., Carswell, D. A., Krogh-Ravna, E. J., and Wain, A. (2000). Eclogites and eclogites in the Western Gneiss Region, Norwegian Caledonides. *Lithos*, 52:165–195.

Cuthbert, S. J., Harvey, M. A., and Carswell, D. A. (1983). A tectonic model for the metamorphic evolution of the basal-gneiss complex, Western South-Norway. *Journal of Metamorphic Geology*, 1(1):63–90. Times Cited: 82.

Czemanske, G. K., Force, E. R., and Moore, W. J. (1981). Some geologic and potential resources aspects of rutile in porphyry copper deposits. *Economic Geology*, 76:2240–2245.

Dallmeyer, R. D. (1988). *The Caledonian-Appalachian Orogen*, chapter Polyphase tectonothermal evolution of the Scandinavian Caledonides, pages 365–379. Geological Society of London, Special Publications, 38 edition.

Dallmeyer, R. D., Andréasson, P. G., and Svenningsen, O. (1991). Initial tectonothermal evolution within the Scandinavian Caledonide accretionary prism: constrains from40Ar/39Ar mineral ages within the Seve Nappe Complex, Sarek Mountains, Sweden. *Journal of Metamorphic Geology*, 9:203–218.

Dallmeyer, R. D. and Gee, D. E. (1986a). ^{40}Ar/^{39}Ar mineral ages from retrogressed eclogites within the Baltoscandinavian miogeocline: Implications for a polyphase Caledonian orogenic evolution. *Bulletin of the Geological Society of America*, 97:26–34.

Dallmeyer, R. D. and Gee, D. G. (1986b). ^{40}Ar/^{39}Ar mineral dates from retrogressed eclogites within the Basltoscandian miogeocline: implications for a polyphase Caledonian orogenic evolution. *Bulletin of the Geological Society of America*, 97:26–34.

Dawson, J. B. and Smith, J. V. (1977). The MARID (mica-amphibole-rutile-ilmenite-diopside) suite of xenoliths in kimberlite. *Geochemica et Cosmochimica Acta*, 41:309–323.

Deer, W. A., Howie, R. A., and Zussman, J. (1962). *Rock-Forming Minerals*, volume 5 Non-Silicates. Longmans.

Deer, W. A., Howie, R. A., and Zussman, J. (1992). *An Introduction to rock-forming minerals*. Longmans Scientific and Technical.

Dewey, J. F. and Strachan, R. A. (2003). Changing Silurian-Devonian relative plate motion in the Caledonides: sinistral transpression to sinistral transtension. *Journal of the Geological Society of London*, 160:219–229.

Dobrzhinetskaya, L. F., Eide, E., Larsen, R. B., Sturt, B. A., Trønnes, R. G., Smith, D. C., Taylor, W. R., and Posujhova, T. V. (1995). Microdiamond in high-grade metamorphic rocks of the Western Gneiss Region, Norway. *Geology*, 23(7):597–600.

Dolomieu, D. (1794). Mémoire sur les roches composeées en généeral, et particulièrement sur les pétro-silex, les trapps et les roches de corne, pour servir à la distribution méthodique des produits volcaniques. *Journal de Physique, de Chime, d'Historie naturalle et des Arts I*, pages 175–200, 241–263.

Dunning, G. R. (1987). U-Pb ages of Caledonian ophiolites and arc sequences: implications for tectonic settings (abstract). *Terra Abstr, EUG IV, Strasbourg*, 179.

Duretz, T., Gerya, T. V., and Kaus, B. J. P. abd Andersen, T. B. (2012). Thermomechanical modelling of slab eduction. *Journal of Geophysical Research*, 117:http://dx.doi.org/10.1029/2012JB009137.

Effenberg, G. and Ilyenko, S., editors (2007). *Non-Ferrous Metal Systems. Part 4*, chapter C-Mo-U (Carbon-Molybdenum-Uranium), pages 90–114. Non-Ferrous Metal Systems.

Eide, E. A. and Lardeaux, J. M. (2002). A relict blueschist in meta-ophiolite from the central Norwegian Caledonides-Discovery and consequences. *Lithos*, 60:1–19.

EL Korh, A., Schmidt, S., Ulianov, A., and Potel, S. (2009). Trace Element Partitioning in HP-LT Metamorphic Assemblages during Subduction-related Metamorphism, Ile de Groix, France: a Detailed LA-ICPMS Study. *Journal of Petrology*, 50(6):1107–1148.

Eskola, P. (1915). Om sambandet mellan kemisk och mineralogisk sammansättring hos Orijävitraktens metamorfabergarter. *Bulletin de la Commission géologique de Finlande*, 8(44):145.

Eskola, P. (1920). The mineral facies of rocks. *Norsk Geologisk Tidskrift*, 6:143–194.

Eskola, P. (1921). On the eclogites of Norway. *Vidensk.-Selsk. Skr. I. Mat. Naturv. Kl.*, 8:1–118.

Essex, R. M., Gronet, L. P., Andréasson, P. G., and Albrecht, L. (1997). Early Ordovician U-Pb metamorphic ages of the eclogite-bearing Seve Nappes, northern Scandinavian Caledonides. *Journal of Metamorphic Geology*, 15:665–676.

Ewing, T. A., Hermann, J., and Rubatto, D. (2013). The robustness of the Zr-in-rutile and Ti-in-zircon thermometers during high-temperature metamorphism (Ivrea-Verbano Zone, northern Italy). *Contributions to Mineralogy and Petrology*, 165:757–779.

Ferry, M. J. and Watson, E. B. (2007). New thermodynamic models and revised calibrations for the Ti-in-zircon and Zr-in-rutile thermometers. *Contributions to Mineralogy and Petrology*, 154:429–437.

Fett, A. (1995). Elementvereilung Granat, Klinopyroxen und Rutil in Eklogiten - Experiment und Natur. *Dissertation, Uniersity of Mainz, Germany*, page 227.

Fitton, J. G. (1995). Coupled molybdenum and niobium depletion in continental basalts. *Earth and Planetary Science Letters*, 136(3-4):715–721. Times Cited: 15.

Fitton, J. G. (2007). *Plates, Plumes and Planetary Processes*, volume 430, chapter The OIB Paradox, pages 387–412. Geological Society of America.

Fitton, J. G. and Godard, M. (2004). *Origin and Ecolution of the Ontong Java Plateau*, chapter Origin and evolution of magmas on the Ontong Java Plateau, pages 151–178. Number 229. Geological Society of London, Special Publications.

Fitton, J. G., Saunders, A. D., and Kempton, P. D. (2003). Does depleted mantle form an intrinsic part of the Iceland plume? *Geochemistry, Geophysics, Geosystems*, 4(doi:10.1029 / 2002GC000424).

Fitton, J. G., Saunders, A. D., Larsen, L. M., Hardarson, B. S., and Norry, M. J. (1998). Volcanic rocks from the southeast Greenland margin at 63^{o}N: composition, petrogenesis and mantle sources. *Proceedings from the Ocean Drilling Program, Scientific Results*, 152:331–350.

Fitton, J. G., Saunders, A. D., Norry, M. J., Hardarson, B. S., and Taylor, R. N. (1997). Thermal and chemical structure of the Earth. *Earth and Planetary Science Letters*, 153(197-208).

Foley, S. F., Barth, M. G., and Jenner, G. A. (2000). Rutile/melt partition coefficients for trace elements and an assessment of the influence of rutile on the trace element characteristics of subduction zone magmas. *Geochimica Et Cosmochimica Acta*, 64(5):933–938. Times Cited: 160.

Fossen, H. (2000). Extensional tectonics in the Caledonides: synorogenic or postorogenic? *Tectonics*, 19(2):213–224.

Gaál, G. and Gorbatschev, R. (1987). An Outline of the Precambrian evolution of the Baltic Shield. *Precambrian Research*, 35:15–52.

Gale, A., Dalton, C., Langmuir, C., Su, Y., and Schilling, J.-G. (2013). The mean composisition of ocean ridge basalts. *Geochem. Geophys. Geosyst.*, 14(3):489–518.

Gao, C. G., Liu, Y. S., Zong, K. Q., Hu, Z. C., and Gao, S. (2010). Microgeochemistry of rutile and zircon in eclogites from the CCSD main hole: inmplications for the fluid activity and thermo-history of the UHP metamorphism. *Lithos*, 115:51–64.

Gao, J. and Klemd, R. (2001). Primary fluids entrapped at blueschist to eclogite transition: evidence from the Tianshan meta-subduction complex in northwestern China. *Contributions to Mineralogy and Petrology*, 142(1):1–14. Times Cited: 62.

Gautneb, H. and Roberts, D. (1989). Geology and petrochemistry of the Smøla-Hitra Batholith, central Norway. *Norges Geologiske Undersøkelse*, 416:1–24.

Gebauer, D., Lappin, M., Grünenfelder, M., and Wyttenbach, A. (1985). The age and origin of some Norwegian eclogites: a U-Pb zircon and REE study. *Chemical Geology*, 52:227–247.

Gerichten, E. v. (1874). Ueber der oberfränkische Eklogit. *Annalen der Chemie und Pharmacie*, 171:183–199.

German, C. R. e. a. (1993). A geochemical study of metalliferous sediment from the tag hydrothermal mound, 26 °08'n, mid-atlantic ridge. *Journal of Geophysical Research*, 98:9683–9692.

Godard, G. (2001). Eclogites and their geodynamic interpretation: a history. *Journal of Geodynamics*, 32:165–203.

Gower, C. F., Ryan, A. B., and Rivers, T. (1990). *Mid-Proterozoic Geology of the Southern Margin of Proto-Laurentia-Baltica*, volume 38 of *Special Paper*, chapter Mid-Proterozoic Laurentia-Baltica: overview of its geological evolution and summary of the contributions made by this volume. Geological Association of Canada.

Graham, J. and Morris, R. C. (1973). Tungsten-substituted and antimony-substituted rutile. *Mineralogical Magazine*, 39(304):470–473. Times Cited: 13.

Green, D. H. (1969). Mineralogy of two Norwegian Eclogites (in Russian). *Institute fixiki tverdogotela, AN SSR*, pages 37–40.

Green, D. H. and Mysen, B. O. (1972). Genetic relationship between eclogite and hornblende + plagioclase pegmatite in western Norway. *Lithos*, 5(2):147–161.

Green, D. H. and Ringwood, A. E. (1967). An experimental investigation of the gabbro to eclogite transformation and its petrological applications. *Geochimica Et Cosmochimica Acta*, 31(5):767–833.

Green, D. H. and Ringwood, A. E. (1972). Gabbro-garnet granulite-eclogite transition. *Journal of Geology*, 80:277–288.

Green, T. H. and Pearson, N. J. (1987). An experimental study of Nb and Ta partitioning between Ti-rich minerals and silicate liquids at high pressure and temperature. *Geochemica et Cosmochimica Acta*, 51:52–62.

Griffin, W. L. (1987). On the Eclogites of Norway - 65 years later. *Mineralogical Magazine*, 51:333–343.

Griffin, W. L., Austrheim, H., Bradstad, K., Bryhni, I., Krill, A. J., and Krogh, E. J. (1985). High-pressure metamorphism in the Scandinavian Caledonides. In Gee, D. E. and Sturt, B. A., editors, *The Caledonide Orogen - Scandinavian and Related Areas*. Wiley, Chichester.

Griffin, W. L. and Brueckner, H. K. (1985). REE, RB-Sr and Sm-Nd studies of Norwegian eclogites. *Chemical Geology*, 52:249–271.

Griffin, W. L. and Mørk, M. B. (1981). Eclogites and basal gneisses in west Norway. *Uppsala Caledonide Symposium, Excursion No. B1*.

Guillong, M., Meier, D. L., Allan, M. M., Heinrich, C. A., and Yardley, B. W. D. (2008). A matlab-based program for the reduction of laser ablation ICP-MS data of homogenous materials and inclusion. *Mineralogical Society of Canada Short Courses: Laser Ablation ICP-MS in the Earth Sciences: Current Practices and Outstanding Issues*, 40:328–333.

Hacker, B. R. (2007). *Convergent Margin Terranes and Associated Regions: A tribute to W. G. Ernst.*, chapter Ascent of the ultrahigh-pressure Western Gneiss Region, Norway., pages 171–184. Geological Society of America.

Hacker, B. R. e. a. (2010). High-temperature deformation during continental-margin subduction and exhumation: the ultrahigh-pressure Western Gneiss Region of Norway. *Tectonophysics*, 480(149-171).

Hageskov, B. and Mørch, B. (2000). Adakitic high-Al tronhjemites in the Proterozoic Østfold-Marstrand Belt, W Sweden. *Bulletin of the Geological Society of Denmark*, 46:165–174.

Haggerty, S. E. (1991). Oxide mineralogy of the upper mantle. *Oxide Minerals : Petrologic and Magnetic Significance*, 25:355–416. Times Cited: 0 Lindsley, dh Short course on fe-ti oxides : their petrologic and magnetic significance May 24-27, 1991 Amer geophys union, baltimore, md.

Harley, S. L. and Motoyoshi, Y. (2000). Al zoning in orthopyroxene in a sapphirine quartzite: evidence for >1120 ^{o}C UHT metamorphism in the Napier Complex, Antarctica, and implications for entropy of sapphirine. *Contributions to Mineralogy and Petrology*, 138:293–307.

Harrison, T. (1981). Diffusion of ^{40}Ar in hornblende. *Contributions to Mineralogy and Petrology*, 78:324–331.

Hartz, E. and Torsvik, T. H. (2002). Baltica upside down: a new plate tectonic model for Rhodinia and the Iapetus Ocean. *Geology*, 30:255–258.

Harvey, M. A. (1983). A geochemical and structural study of the gneisses and eclogites on the Molde penninsula, west Norway.

Hassan, W. F. (1994). Geochemistry and mineralogy of Ta-Nb rutile from Peninsular Malaysia. *Journal of Southeast Asian Earth Sciences*, 10:11–23.

Haug, E. (1900). Les géosynclinaux et les aires continentales. *Bulletin de la Société Géologique de France*, 409-421.

Hauri, E., Wagner, T., and Grove, T. (1994). Experimental and natural partitioning of Th, U, Pb and other trace elements between garnet, clinopyroxene and basaltic melts. *Chemical Geology*, 94:149–166.

Hollocher, K., Robinson, P., Terry, M. P., and Walsh, E. O. (2007). Application of major- and trace-element geochemistry to refine U-Pb zircon, and Sm/Nd or Lu/Hf sampling targets for geochronology of HP and UHP eclogites, Western Gneiss Region, Norway. *American Mineralogist*, 29:1919–1924.

Holtedahl, O. (1920). Palaeogeography and diastrophism in the Atlantic-Arctic region during Palaeozoic time. *American Journal of Science*, 49:1–25.

Hunt, T. S. (1884). The origin of crystalline rocks. *Transactions of the royal society of Canada*, II(Section III):1–67.

Hurich, C. A. (1996). Kinematic evolution of the lower plate during intracontinental subduction: an example from the Scandinavian Caledonides. *Tectonics*, 15:1248–1263.

Ionov, D. A. and Hofmann, A. W. (1995). Nb-Ta-rich mantle amphiboles and micas - implications for subduction related metasomatic trace element fractionations. *Earth and Planetary Science Letters*, 131(3-4):341–356.

Jamtveit, B. (1987). Metamorphic evolution of the Eiksunddal eclogite complex - Western Norway, and some tectonic implications. *Contributions to Mineralogy and Petrology*, 95(1):82–99. Times Cited: 54.

Jenner, G., Foley, S., Jackson, S., Green, T., Fryer, B., and Longerich, H. (1994). Determination of partition coefficients for trace elements in high pressure-temperature experimental run products by laser ablation microprobe-inductively coupled plasma-mass spectrometry (LAM-ICP-MS). *Geochemica et Cosmochimica Acta*, 57:23–24.

Jiao, S. J., Guo, J., Mao, Q., and Zhao, R. F. (2011). Application of Zr-in-rutile thermometry: a case study from ultrahigh-temperature granulites of the Khondalite belt, north China craton. *Contributions to Mineralogy and Petrology*, 168(2):379–393.

Johansson, L., Schoberg, H., and Solyom, Z. (1993). The age and regional correlation of the Svecofennian Geitfjell Granite, Vestranden, Norway. *Norsk Geologisk Tidsskrift*, 73(2):133–143.

John, T., Klemd, R., Goa, J., and Garge-Schönberg, C. D. (2007). Trace-element mobilization in slabs due to nin steady state fluid-rock interaction: constraints from an eclogite facies transport vein in blueschist (Tianshan, China). *Lithos*, 103:1–24.

Johnson, M. R. W. and Harley, S. L. (2012). *Orogenesis: The Making of Mountains*. Cambridge University Press.

Johnston, S., Hacker, B. R., and Duecea, M. N. (2007). Exhumation of ultrahigh-pressure rocks beneath the Hornelen segment of the Nordfjord-Sogn Detachment Zone, western Norway. *Geological Society of America Bulletin*, 119:1232–1248.

Kane, J. S. (1998). A history of the development and certification of NIST Glass SRMs 610-617. *Geostandards Newsletter*, 22 (1):7–13.

Kechid, S. A. (1984). *Etude petrologique et mineralogique des eclogites de Liset (Stadlandet, Norvege)*. Ph.d.

Kildal, E. (1969). Geologisk kart over Norge, berggrunnskart Måløy, 1:25k.

Klemme, S., Blundy, J., and Wood, B. J. (2002). Experimental constraints on major and trace element partitioning during partial melting of eclogite. *Geochimica Et Cosmochimica Acta*, 66:3109–3123.

Klemme, S., Prowatke, S., Hametner, K., and Gunther, D. (2005). The partitioning of trace elements between rutile and silicate melts: Implications for subduction zones. *Geochemica et Cosmochimica Acta*, 69:2361–2371.

Koons, P. O., Rubie, D. C., and Fruch-Green, G. (1986). The effects of disequilibrium and deformation on the mineralogical evolution of quartz diorite during metamorphism in the eclogite facies. *Journal of Petrology*, 28(4):679–700.

Koto, B. (1887). A note on glaucophane. *Journal of the College of Science, imp. University, Japan (Tokyo)*, I:85–99.

Krabbendam, M. and Dewey, J. F. (1998). *Continental Transpressional and Transtensional Tectonics*, volume 135, chapter Exhumation of UHP rocks by transtension in the Western Gneiss Region, Scandinavian Caledonides, pages 159–181. London Special Publ.

Krabbendam, M. and Wain, A. (1997). Late Caledonian structures, differential retrogression and structural position of (ultra)high-pressure rocks in the Nordfjord-Statlandet area, Western Gneiss Region. *Norges Geologiske Undersøkelse*, 432:127–139.

Krogh, E. J. (1977). Crustal and in-situ origin of Norwegian eclogites. *Nature*, 269:730.

Krogh, E. J. (1980). Compatible P-T conditions for eclogite and surrounding gneisses in the Kristiansund area, western Norway. *Contributions to Mineralogy and Petrology*, 75:387–393.

Krogh, E. J. (1982). Metamorphic evolution deduced from mineral inclusions and compositional zoning in garnets from Norwegian country-rock eclogites. *Lithos*, 15:305–321.

Krogh, E. J. and Carswell, D. A. (1995). HP and UHP Eclogites and Gernet Peridotites in the Scandinavian Caledonides. In COLEMAN, R. G. and Wang, X., editors, *Ultrahigh Pressure Metamorphism*, pages 244–298. Cambridge University Press, Cambridge.

Krogh, E. J., Mysen, B. O., and Davis, G. L. (1974). A Palaeozoic age for the primary minerals of a Norwegian eclogite. *Yearb. Carnegie Inst. Washington*, 73:575–576.

Krogh-Ravna, E. J. (2000). The garnet-clinopyroxene geothermometer - an updated calibration. *Journal of Metamorphic Geology*, 18(2):211–219.

Krogh-Ravna, E. J. and Terry, M. P. (2004). Geothermobarometry of UHP and HP eclogites and schists - an evaluation of equilibria among garnet-clinopyroxene-kyanite-phengite-coesite/quartz. *Journal of Metamorphic Geology*, 22(6):579–592.

Kylander-Clark, A. R. C., Hacker, B. R., Johnson, C. M., Beard, B. L., and Mahlen, N. J. (2009). Slow subduction of a thick ultrahigh-pressure terrane. *Tectonics*, 28:http://dx.doi.org/10.1029/2007TC002251.

Kylander-Clark, A. R. C., Hacker, B. R., and Mattinson, J. M. (2008). Slow exhumation of UHP terranes; titanite and rutile ages of the Western Gneiss Region Norway. *Earth and Planetary Science Letters*, 272:531–540.

Labrousse, L. e. a. (2004). *Gneiss Domes in Orogeny*, chapter Pressure-temperature-time deofrmation history of the exhumation of ultrahigh-pressure rocks in the Western Gneiss Region, Norway, pages 155–183. Geological Society of America.

Lappin, M. A. (1966). The field relationships of basic and ultrabasic masses in the basal gneiss complex of Stdtlandet and Almklovdalen, Nordfjord, S. Norway. *Norsk Geologisk Tidsskrift*, 4:439–496.

Lappin, M. A. (1974). Eclogites from Sunndal-Grubse ultramafic mass, Almklovdalen, Norway and T-P history of Almklovdalen masses. *Journal of Petrology*, 15(3):567–601. Times Cited: 43.

Lappin, M. A. and Smith, D. C. (1978). Mantle-equilibrated Orthopyroxene Eclogite Pods from the Basal Gneisses in the Selje District, Western Norway. *Journal of Petrology*, 19(3):530–584.

Le Maitre, R. W., Bateman, P., Dudek, A., Keller, J., Lameyre Le Bas, M. J., Sabine, P. A., Schmid, R., Sorensen, H., Streckeisen, A., Wooley, A. R., and Zanettin, B. (1989). *A classification of igneous rocks and glossary of terms*. Blackwell, Oxford.

Lepsius, R. (1893). Geologie von Attika. Ein Beitrag zur Lehre von Metamorphismus der Gesteine. *Reimer, Berlin*, page 196.

Liang, J., Ding, X., Sun, X. M., Zhang, Z., Zhang, H., and Sun, W. D. (2009). Nb/Ta fractionation observed in eclogites fromthe Chinese Continental Scientific Drilling Project. *Chemical Geology*, 268:27–40.

Liou, J. G., Zhang, R., Ernst, W. G., Liu, J., and McLimans, R. (1998). Mineral paragenesis in the Pianpaludo eclogitis body, Gruppop di Voltri, western Ligurian Alps. *Schweiz. Mineral. Petrogr. Mitt.*, 78:317–325.

Lutro, O. and Tveten, E. (1996). Geologisk kart over Norge, berggrunnskart Årdal, 1:25k. *Norges Geologiske Undersøkelse*.

Luvizotto, G. L. and Zack, T. (2009). Nb and Zr behaviour in rutile during high grade metamorphism and retrogression: an example from the Ivrea-Verbano zone. *Chemical Geology*, 261(3-4):303–317.

Luvizotto, G. L., Zack, T., Meyer, T. P., Ludwig, T., Triebold, S., Kron, Munker, C., Stockli, D. F., Prowatke, S., Klemme, S., Jacob, D. E., and von Eynatten, H. (2009). Rutile crystals as a potential trace element and isotope mineral standards for microanalysis. *Chemical Geology*, 261:346–369.

MacDonald, M. A. (1968). *Studies in Volcanology: a memoir in honour of Howel Williams*, volume 116, chapter Composition and Origin of Hawaiian Lavas, pages 477–522. Geological Society of America Memoirs.

Manning, C. E. (1998). Fluid composition at the blueschist-eclogite transition in the model system Na2O-MgO-Al2O3-SiO2-H2O-HCl. *Schweiz. Mineral. Petrogr. Mitt.*, 78:225–242.

Manning, C. E. (2004). The chemistry of subduction-zone fluids. *Earth and Planetary Science Letters*, 223(1-2):1–16. Times Cited: 135.

Manning, C. E., Wilke, M., Schmidt, C., and Cauzid, J. (2008). Rutile solubility in albite-H_2O and $Na_2Si_3O_7$-H_2O at high temperatures and pressures by in-situ synchotron radiation micro-XRF. *Earth and Planetary Science Letters*, 272:730–737.

Marques, F. O., Schmid, D. W., and Andersen, T. B. (2007). Application of inclusion behaviour models to a ductile shear zone system: the Nordfjord-Sogn Detachment Zone in Western Norway. *Journal of Structural Geology*, 29:1622–1631.

Marschall, H. R., Dohmen, R., and Ludwig, L. (2013). Diffusion-induced fractionation of niobium and tantalum during continental crust formation. *Earth and Planetary Science Letters*, 375:361–371.

Marsh, S. P. (1979). Rutile mineralisation in the White Mountain andalusite deposit, California. *U.S. Geological Survey Open-File Report*, 79-1622:7.

Mauthner, J. (1872). Eklogit von Eibiswald in Steiermark. *Mineralogische Mittheilungen*, page 261.

McDonough, W. F. (1991). Partial melting of subducted oceanic curst and isolation of its residual eclogite lithology. *Philosophical Transactions of the Royal Society of London Series a-Mathematical Physical and Engineering Sciences*, 335(1638):407–418. Times Cited: 85.

McDonough, W. F. and Sun, S. (1995). Composition of the Earth. *Chemical Geology*, 120:223–253.

Mearns, E. W. (1986). Sm-Nd ages for Norwegian garnet peridotite. *Lithos*, 19:269–278.

Meinhold, G., Andersen, T. B., Kostopoulos, D., and Reischmann, T. (2008). Rutile chemistry and thermometry as provenance indicator: an example from Chios Island, Greece. *Sedimentary Geology*, 203:98–111.

Meschede, M. (1986). A method of discriminating between different types of mid-ocean ridge basalts and continental tholeiites with the Nb-Y-Zr diagram. *Chemical Geology*, 56(3-4):207–218. Times Cited: 544.

Messiga, B., Tribuzio, R., Bottazzi, P., and Ottolini, L. (1995). An ion microprobe study on trace element composition of clinopyroxenes from blueschist and eclogitized Fe-Ti gabbros, Ligurian alps, northwestern Italy. *Geochemica et Cosmochimica Acta*, 59:59–75.

Meyer, T. P., John, T., Brandt, S., and Klemd, R. (2011). Trace element composition of rutile and the application of Zr-in-rutile thermometry in an Eo-Alpine subduction zone (Eastern Alps). *Chemical Geology*, 126:388–401.

Miller, C., Zanetti, A., Thöni, M., and Konzett, J. (2007). Eclogitisation of gabbroic rocks: redistribution of trace elements and Zr in rutile thermometry in an Eo-Alpine subduction zone (Eastern Alps). *Chemical Geology*, 239:96–123.

Mørk, M. B. (1985). A gabbro to eclogite transition on Flemsøy, Sunnmøre, Western Norway. *Chemical Geology*, 50:283–310.

Mørk, M. B. (1986). Coronite and eclogite formation in olivine gabbro (Western Norway): reaction paths and garnet zoning. *Mineralogical Magazine*, 50:417–426.

Mørk, M. B. and Brunfelt, A. O. (1988). Geochemical comparisons of coronitic olivine gabbro and eclogites: metamorphic effects and the origin of eclogite protoliths (Flemsøy, Sunnmøre, Western Norway). *Norsk Geologisk Tidsskrift*, 68:51–63.

Mørk, M. B., Kullerud, K., and Stabell, A. (1988). Sm-Nd dating of seve eclogites, Norbotten, Sweden - evidence for Early Caledonian (505 Ma) subduction. *Contributions to Mineralogy and Petrology*, 99:344–351.

Mørk, M. B. and Mearns, E. W. (1986). Sm-Nd isotopic systems of a gabbro-eclogite transition. *Lithos*, 19:255–267.

Morton, A. and Chenery, S. P. (2009). Detrital rutile geochemistry and thermometry as guides to provenance of Jurassic-Palaeocene sandstones of the Norwegian Sea. *Journal of Sedimentary Research*, 79:540–553.

Mottana, A., Carswell, D. A., Chopin, C., and Oberhansli, R. (1990). *Eclogite Facies Rocks*, chapter Eclogite facies mineral parageneses, pages 14–52. Blackie, Glasgow.

Munker, C., Worner, G., Yogodzinski, G., and Churikova, T. (2004). Behaviour of high field strength elements in subduction zones: constraints from Kamachatka-Aleutian arc lavas. *Earth and Planetary Science Letters*, 224:275–293.

Murad, E., Cashion, J. D., Noble, C. J., and Pilbrow, J. R. (1995). The chemical state of Fe in rutile from an albitite in Norway. *Mineralogical Magazine*, 59:557–560.

Mutanen, T. and Huhma, H. (2003). The 3.5 Ga Siurua trondhjemite gneiss in the Archaean Pudasjärvi Granulite Belt, northern Finland. *Bulletin of the Geological Society of Finland*, 75 (1-2):51–68.

Mysen, B. O. and Heier, K. S. (1972). Petrogenesis of eclogites in high grade metamorphic gneisses, exemplified by Hareidland eclogite, Western Norway. *Contributions to Mineralogy and Petrology*, 36(1):73–94. Times Cited: 112.

Nadeau, S., Philippot, P., and Pineau, F. (1993). Fluid inclusion and mineral isotopic compositions (H-C-O) in eclogitic rocks as tracers of local fluid migration during high-pressure metamorphism. *Earth and Planetary Science Letters*, 114:431–448.

Noll, P., Newsom, H. E., Leeman, W. P., and Ryan, J. G. (1996). The role of hydrothermal fluids in the production of subduction zone magmas: Evidence from siderophile and chalcophile trace elements and boron. *Geochemica et Cosmochimica Acta*, 60:587–611.

Nordgulen, Ø., Solli, A., and Sunvoll, B. (1995). Caledonian granitoids in the Frøya-Froan area, central Norway. *Norges Geologiske Undersøkelse - Bulletin*, 427(48-51).

Norton, M. G. (1986). Late Caledonide extension in western Norway: a response to extreme crustal thickening. *Tectonics*, 5:195–204.

Nui, Y. (2004). *Advances in Earth Sciences*, chapter Geochemistry of rare earth elements in waters and sediments of alkaline lakes in the Sassykkul depression, East Pamir., pages 170–190. High Education Press, Beijing.

Nui, Y. and Batiza, R. (1997). Extreme mantle source heterogeneities beneath the northern east pacific rise – trace element evidence from near-ridge seamounts. *Proceedings of 30th ICG*, 15(109-120).

Nui, Y. and Hekinian, R. (1997). Basaltic liquids and harzburgitic residues in the Garrett Transform: A case study at fast-spreading ridges. *Earth and Planetary Science Letters*, 146:243–258.

Okamoto, H. (2012). Mo-U (Molybdenum-Uranium). *Journal of Phase Equilibria and Diffusion*, 33:497.

Pearce, J. A. (1982). *Andesites*, chapter Trace element characteristics of lavas from destructive plate boundaries, pages 525–548. Wiley.

Pearce, J. A. (1983). *Continental basalts and mantle xenoliths*, chapter Role of the sub-continental lithosphere in magma genesis at active continental margins, pages 230–249. Shiva, Nantwich.

Pearce, J. A. and Norry, M. J. (1979). Petrogenetic implications of Ti, Zr, Y and Nb variations in volcanic rocks. *Contributions to Mineralogy and Petrology*, 69:33–47.

Pearce, N. J. G., Perkins, W. T., Westgate, J. A., Gorton, M. P., Jackson, S. E., Neal, C. R., and Chenery, S. P. (1997). A compilation of new and published major and trace element data for NIST SRM 610 and NIST SRM 612 glass reference materials. *Geostandards Newsletter*, 21:115–144.

Pedersen, R. P. and Heterogen, J. (1990). Magmatic Evolution of the Karmøy Ophiolite Complex, SW Norway: relationships between MORB-IAT-Boninite-Calc-alkaline and alkaline magmatism. *Contributions to Mineralogy and Petrology*, 104:277–293.

Pertermann, M. and Hirshmann, M. (2002). Trace-element partitioning between vacancy-rich eclogitic clinopyroxene and silicate melt. *American Mineralogist*, 87:1365–1376.

Peterman, E. M., Hacker, B. R., and Baxter, E. F. (2009). Transformations of continental crust during subduction and exhumation: Western Gneiss Region, Norway. *European Journal of Mineralogy*, 21:1097–1118.

Plank, T. (2005). Constraints from Thorium/Lanthanum on Sediment Recycling at Subduction Zones and the Evolution of the Continents. *Journal of Petrology*, 46:921–944.

Ramberg, I. B., Bryhni, I., Nøttvedt, A., and Rangnes, K. (2008). *The Making of a Land: Geology of Norway*. Norsk Geologisk Forening.

Rapp, J. F., Klemme, S., Butler, I. B., and Harley, S. L. (2010). Extremely high solubility of rutile in chloride and fluoride-bearing metamorphic fluids: An experimental investigation. *Geology*, 38(4):323–326. 573XC Times Cited:5 Cited References Count:31.

Reynolds, R. C. (1963). Matrix corrections in trace element analysis by X-ray flourescence: estimation of the mass absorption coefficient by Compton scattering. *American Mineralogist*, 48:1133–1143.

Rice, C. M., Darke, K. E., Still, J. W., and Lachowski, E. E. (1998). Tungsten-bearing rutile from the Kori Kollo gold mine, Bolivia. *Mineralogical Magazine*, 62(3):421–429. Times Cited: 14.

Richards, J. P., Krogh, T. E., and Spooner, E. T. C. (1988). Fluid inclusion characteristics and U-Pb rutile age of late hydrothermal alteration and veining at the Musoshi stratiform copper deposit, Central African copper belt, Zaire. *Economic Geology*, 83:118–139.

Rickwood, P. C. (1989). Boundary lines within petrologic diagrams which use oxides of major and minor elements. *Lithos*, 22:247–263.

Ringwood, A. E. and Green, D. H. (1966). An experimental investigation of the gabbro-eclogite transformation and some geophysical implications. *Tectonophysics*, 3:383–427.

Ripp, G. S., Karmanov, N. S., Doroschkevich, A. G., Badmatsyrenov, M. V., and Izbrodin, I. A. (2006). Chrome-bearing mineral phases in the carbonatites of northern Trasnbaikalia. *Geochemistry International*, 44:395–402.

Roberts, D. (1983). Devonian tectonic deformation in the Norwegian Caeledonides and its regional perspectives. *Norges Geologiske Undersøkelse*, 380:85–96.

Roberts, D. (1990). Geochemistry of mafic dykes in the Corrovarre Nappe, Troms, north Norway. *Norges Geologiske Undersøkelse - Bulletin*, 419:45–53.

Roberts, D. (2003). The Scandinavian Caledonides: event chronology, palaeogeographic settings and likely modern analogues. *Tectonophysics*, 365:283–299.

Rocholl, A., Dulski, P., and Raczek, I. (2000). New ID-TIMMS, ICP-MS and SIMS data on the trace element composition and homogeneity of NIST certified reference material SRM 610-611. *Geostandards Newsletter*, 24:261–274.

Røhr, T. S., Corfu, F., Austrheim, H., and Andersen, T. B. (2004). Sveconorwegian U-Pb zircon and monazite ages of granulite-facies rocks,Hisaroya, Gulen, Western Gneiss Region, Norway. *Norwegian Journal of Geology*, 84:251–256.

Root, D. B., Hacker, B. R., Mattinson, J. M., and Wooden, J. L. (2004). Young age and rapid exhumation of Norwegian ultrahigh-pressure rocks: an ion microprobe and chemical abrasion study. *Earth and Planetary Science Letters*, 228:325–341.

Root, D. B. e. a. (2005). Discrete ultrahigh-pressure domains in the Western Gneiss Region, Norway: Implications for formation and exhumation. *Journal of Metamorphic Geology*, 23:45–61.

Rudnick, R. L., Barth, M., Horn, I., and McDonough, W. F. (2000). Rutile-bearing refractory eclogites: Missing link between continents and depleted mantle. *Science*, 287(5451):278–281. Times Cited: 178.

Rudnick, R. L. and Fountain, D. M. (1995). Nature and composition of the continental crust - a lower crustal perspective. *Reviews of geophysics*, 33:267–309.

Schmidt, M. W., Dardon, A., Chazgot, G., and Vannucci, R. (2004). The dependence of Nb and Ta rutile-melt partitioning on melt composition during subduction processes. *Earth and Planetary Science Letters*, 226(415-432).

Schuiling, R. D. and Vink, B. W. (1967). Stability relations of some titanium-minerals (sphene, perovskite, rutile, anatase). *Geochemica et Cosmochimica Acta*, 31:2399–2411.

Scott, K. M. (2005). Rutile geochemistry as a guide to porphyry Cu-Au mineralization, Northparkes, New South Wales, Australia. *Geochemistry: Exploration, Environment, Analysis*, 5:247–253.

Shannon, R. D. (1976). Revised effective ionic-radii and systematic studies of interatomic distances in halides and chalcogenides. *Acta Crystallographica Section A*, 32(SEP1):751–767. Times Cited: 21656.

Skår, Ø. (2000). Field relations and geochemical evolution of the Gothian rocks in the Kvamsøy area, southern Western Gneiss Complex, Norway. *Norges Geologiske Undersøkelse - Bulletin*, 437:5–23.

Skjerlie, K. P. and Patiño Douce, A. (2002). The fluid absent partial melting of a zoisite-bearing quartz eclogite from 1.0 to 3.2 GPa; implications for melting thickened continental crust and for subduction zone processes. *Journal of Petrology*, 43(2):291–314.

Smith, D. C. (1968). *The petrology and chemistry of some eclogites in the gneiss of the Selje Distric, Nordfjord, S.W. Norway*. PhD thesis.

Smith, D. C. (1976). *The geology of the Vartdal area, Sunnmøre, Norway, and the petrochemistry of the Sunnmøre eclogite suite*. Ph.d.

Smith, D. C. (1980). A tectonic melange of foreign eclogites and ultramafites in West Norway. *Nature*, 287(5780):366–367. Times Cited: 45.

Smith, D. C. (1984). Coesite in clinopyroxene in the Caledonides and its implications for geodynamics. *Nature*, 310(5979):641–644. 10.1038/310641a0.

Smith, D. C. (1988). A review of the peculiar mineralogy of the "Norwegian-Eclogite Province", with crystal-chemical, petrological, geochemical and geodynamical notes and an extensive bibliography. In *Eclogites and Eclogite Facies Rocks*, pages 1–206. Elsevier, Amsterdam.

Smith, D. C., Coleman, R. G., and Wang, X. (1995). *Microcoesites and microdiamonds in Norway: An overview Ultrahigh Pressure Metamorphism*. Cambridge University Press.

Smith, D. C. and Perseil, E. A. (1997). Sb-rich rutile in the manganese concentrations at St. Marcel-Praborna, Aosta valley, Italy: Petrology and crystal-chemistry. *Mineralogical Magazine*, 61(5):655–669. Times Cited: 17.

Solyom, Z., Gorbatschev, R., and Johansson, I. (1979). The Ottfjäll dolerites. Geochemistry of the dyke swarm. *Sverges Geologiske Undersökelse*, C756:38.

Solyom, Z., Lindqvist, J. E., and Johansson, I. (1992). The geochemistry, genesis and geotectonic setting of Proterozoic dyke swarms in southern and central Sweden. *Geol. Fören. Stockh. Förh.*, 114:47–65.

Soper, N. J., Ryan, P. D., and Dewey, J. F. (1999). Age of the Grampian Orogeny in Scotland and Ireland. *Journal of the Geological Society of London*, 156:1231–1236.

Spandler, C., Hermann, J., Arculus, R. J., and Mavrogenes, J. (2003). Redistribution of trace element during prograde metamorphism from lawsonite blueschist to eclogite facies: Implications for deep subduction-zone processes. *Contributions to Mineralogy and Petrology*, 146:205–222.

Spandler, C., Hermann, J., Arculus, R. J., and Mavrogenes, J. (2004). Geochemical heterogeneity and element mobility in deeply subducted oceanic crust; insigts from high pressure mafic rocks from New Caledonia. *Chemical Geology*, 206:21–42.

Spandler, C., Mavrogenes, J., and Hermann, J. (2007). Experimental constraints on element mobility from subducted sediments using high-P synthetic fluid/melt inclusions. *Chemical Geology*, 239(3-4):228–249.

Spencer, K. J. e. a. (2013). Campeign-style titanite U-Pb dating by laser-ablation ICP: implications for crustal flow, phase transformations and titanite closure. *Chemical Geology*, page http://dx.doi.org/10.1016/j.chemgeo.2012.11.012 .

Staudigel, H., Plank, T., White, W. M., and Schminke, H. U. (1996). *Subduction: Top to Bottom*, volume 96, chapter Geochemical fluxes during seafloor alteration od the

upper oceanic crust: DSDP Sites 417 and 418, pages 19–38. American Geophysical Union.

Stendal, H., Toteu, S. F., Frei, R., Penaye, J., Njel, U., Bassahk, J., Nni, J., Kankeu, B., Ngako, V., and Hell, J. V. (2006). Derivation of detrital rutile in the Yaoundé region from the Neoproterozoic Pan-African belt in southern Cameroon (Central Africa). *Journal of African Earth Sciences*, 44:443–458.

Stille, H. (1924). Grundfragen der vergleichenden Tektonik. *Gebrüder Borntraeger, Berlin*.

Stølen, L. K. (1994). The rift-related mafic dyke complex of the Rohkunborri Nappe, Indre Troms, northern Norwegian Caledonides. *Norsk Geologisk Tidsskrift*, 74:35–47.

Stone, P. (2012). The demise of the Iapetus Ocean as recorded in the rocks of Southern Scotland. *Open University Geological Society Journal*, 33:29–39.

Sturt, B. A. and Roberts, D. (1991). *Ophiolite Genesis and Evolution of the Ocean Lithosphere.*, chapter Tectonostratigraphic relationships and obduction histories in Scandinavian ophiolitic terranes. Sultunate of Oman.

Suess, E. (1906). The Face of the Earth. *Oxford*, 2.

Sun, S.-s. and McDonough, W. F. (1989). Chemical and isotopic systematics of oceanic basalts: implications for mantle composition and processes. *Geological Society, London, Special Publications*, 42(1):313–345.

Svenningsen, O. (1994). The Baltic-Iapetus passive margin dyke complex in the Sarektjåkkå Nappe, northern Scandinavian Caledonides. *Journal of Geology*, 29:323–354.

Svenningsen, O. (2001). Onset of seafloor spreading in the Iapetus Ocean at 608 Ma: precise age of the Sarek Dyke Swarm, north Swedish Caledonides. *Precambrian Research*, 110:241–254.

Svensen, H., Jamtveit, B., Banks, D. A., and Austrheim, H. (2001). Halogen contents of eclogite facies fluid inclusions and minerals: Caledonides, western Norway. *Journal of Metamorphic Geology*, 19(2):165–178. Times Cited: 24.

Taylor, S. R. and McLennan, S. M. (1985). *The Continental Crust: Its Composition and Evolution*. Blackwell Scientific, isbn 0 632 01148 3 edition.

Taylor, W. R. (2008). Rutile U-Pb dating in diamond exploration - application to detrital heavy mineral provenance studies and kimberlite age dating. *9th International Kimberlite Conference*, pages No. 9IKC–A–00373.

Terry, M. P. and Robinson, P. (2003). Evolution of amphibolite-facies structural features and boundary conditions for deformation during exhumation of HP and UHP rocks, Western Gneiss Region, Norway. *Tectonics*, 24(4):1036.

Terry, M. P. and Robinson, P. (2004). Geometry of eclogite-facies structural features: implications for production and exhumation of ultrahigh-pressure and high-pressyre rocks, Western Gneiss Region, Norway. *Tectonics*, 23:http://dx.doi.org/10.1029/2002TC001401.

Terry, M. P., Robinson, P., Hamilton, M. A., and Jercinovic, M. J. (2000). Monazite geochronology of UHP and HP metamorphism, deformation and exhumation, Nordøyane, Western Gneiss Region, Norway. *American Mineralogist*, 85:1651–1664.

Thompson, R. N. (1982). Magmatism of the British Tertiary Volcanic Province. *Scottish Journal of Geology*, 18:49–107. ISI Document Delivery No.: NC155 Times Cited: 299 Cited Reference Count: 163 Geological soc publ house Bath Part 1.

Tomkins, H. S., Powell, R., and Ellis, D. J. (2007). The pressure dependence of the zirconium-in-rutile thermometer. *Journal of Metamorphic Geology*, 25:703–713.

Torsvik, T. H. (2001). Palaeozoic palaeogeography: a North Atlantic viewpoint. *Geol. Fören. Stockh. Förh.*, 120:109–118.

Torsvik, T. H. and Rehnström, E. F. (2001a). Cambrian palaeomagnetic data from Baltica: Implications for true polar wander and Cambrian palaeogeography. *Journal of the Geological Society of London*, 158:321–329.

Torsvik, T. H. and Rehnström, E. F. (2001b). Cambrian palaeomagnetic data from Baltica: implications from true polar wander and Cambrian palaeogeography. *Journal of the Geological Society of London*, 158:321–329.

Torsvik, T. H., Smethurst, M., Meert, J., Van der Voo, R., McKerro, W. S., Brazier, M., Sturt, B. A., and Walderhaug, H. (1996). Continental break-up and collision in the Neo-proterozoic and Palaeozoic - a tale of Baltica and Laurentia. *Earth Science Rev.*, 40:229–258.

Tribuzio, R., Messiga, B., Vannucci, R., and Bottazzi, P. (1996). Rare earth element re-distribution during high-pressure-low-temperature metamorphism in ophiolitic Fe-gabbros (Liguria, Northwestern Italy): Implications for light REE mobility in subduction zones. *Geology*, 24:711–714.

Triebold, S., von Eynatten, H., Luvizotto, G. L., and Zack, T. (2007). Deducing source rock lithology from detrital rutile geochemistry: An example from the Erzgebirge, Germany. *Chemical Geology*, 244:421–436.

Triebold, S., von Eynatten, H., and Zack, T. (2012). A recipie for the use of rutile in sedimentary provenance analysis. *Sedimentary Geology*, 282:268–275.

Troitzsch, U. and Ellis, D. J. (2004). High-PT study of solid solutions in the system ZrO_2-TiO_2: the stability of srilankite. *European Journal of Mineralogy*, 16:577–584.

Tropper, P. and Manning, C. E. (2005). Very low solubility of rutile in H_2O at high pressure and temperature, and its implications for Ti mobility in subduction zones. *American Mineralogist*, 90(2-3):502–505. Times Cited: 36.

Tucker, R. D., Krogh, T. E., and Råheim, A. (1990). *Mid-Proterozoic Geology of the Southern Margin of Proto-Laurentia-Baltica*, volume 38 of *Special Paper*, chapter Proterozoic evolution and age province boundaries in the central part of teh Western Gneiss Region, Norway: Results of U-Pb dating of accessory minerals from Tronheimsfjord to Geiranger., pages 149–173. Geological Association of Canada.

Usui, T., Kobayashi, K., Nakamura, E., and Helmstaedt, H. (2007). Trace element fractionation in deep subduction zones inferred from a lawsonite-eclogite xenolith from the Colorado Plateau. *Chemical Geology*, 239:336–351.

Vaggelli, G., Borghi, A., Calusi, S., Cossio, R., and Giuntini, L. (2008). Micro-PIXE determination of Zr in rutile: an application of geothermometry of high-P rocks from the western Alps (Italy) and Mirko Massi. *X-Ray Spectrometry*, 37(146-150).

Vermeesch, P. (2006). Tectonic Discrimination Diagrams Revisited. *Geochemistry, Geophysics, Geosystems*, 7(6):DOI: 10.1029/2005GC001092.

Volkova, N. I., Stupakov, S. I., Babin, G. A., Rudnev, S. N., and Mongush, A. A. (2009). Mobility of Trace Elements during Subduction Metamorphism as Exemplified by the Blueschists of the Kurtushibinsky Range, Western Sayan. *Geochemistry International*, 47(4):380–392.

Von Quadt, A., Moritz, R., and Heinrich, C. A. (2005). Geochronology and geodynamics of Late Cretaceous megmatism and Cr-Au mineralisation in the Panagyurishte region of the Apuseni-Banat-Timok-Srednogorie belt, Bulgaria. *Ore Geology Reviews*, 27:95–126.

Vry, J. K. and Baker, J. A. (2006). LA-MC-ICPMS Pb-Pb dating of rutile from slowly cooled granulites: confirmation of the high closure temperature for Pb diffusion in rutile. *Geochemica et Cosmochimica Acta*, 70:1907–1820.

Wain, A. (1997). New evidence for coesite in eclogite and gneisses: defining an ultrahigh-pressure province in the Western Gneiss Region of Norway. *Geology*, 25:927–930.

Walsh, E. O. and Hacker, B. R. (2004). The fate of subducted continental margins: two-stage exhumation of the high-pressure to ultrahigh-pressure Western Gneiss Region, Norway. *Journal of Metamorphic Geology*, 22:671–687.

Walsh, E. O., Hacker, B. R., Gans, P. B., Grove, M., and Gehrels, G. (2007). Protolith ages and exhumation histories of (ultra)high-pressure rocks across the Western Gneiss Region, Norway. *Geological Society of America Bulletin*, 119:289–301.

Walsh, E. O., Hacker, B. R., Gans, P. B., Wong, M. S., and Andersen, T. B. (2013). Crustal exhumation of the Western Gneiss Region UHP terrane, Norway: 40Ar/39Ar thermochronology and fault-slip analysis. *Tectonophysics*, 608:1159–1179.

Watson, E. B., Wark, D. A., and Thomas, J. B. (2006). Crystallisation thermometers for Zircon and Rutile. *Contributions to Mineralogy and Petrology*, 151:413–433.

Weaver, B. L. and Tarney, J. (1984). Empirical approach to estimating the composition of the continental crust. *Nature*, 310(5978):575–577. 10.1038/310575a0.

Wedepohl, K. H. (1995). The composition of the continental crust. *Geochimica Et Cosmochimica Acta*, 59:1217–1232.

Werner, A. G. (1917). Abraham Gottlob Werner's lektes Mineral-System, aue desen Nachlasse aus oberbergamtliche Anordnung herausgegeben und mit Erläuterungen versehen. *Craz, Gerlach, Carl Gerold, Freyberg und Wien*, xiv:58.

Weyer, S., Munker, C., Rehkamper, M., and Mezger, K. (2002). Determination of ultra-low Nb, Ta, Zr and Hf concentrations and the chondritic Zr/Hf and Nb/Ta ratios by isotope dilution analyses with multiple collector ICP-MS. *Chemical Geology*, 187:295–313.

Williams, G. H. (1890). The Greenstone Schiest areas of the Menominee and Marquette regions of Michigan. A contribution to the subject of dynamic Metamorphism in Eruptive Rocks. *US Geological Survey Bulletin*.

Wood, D. A. (1980). The application of a Th-Hf-Ta digram to problems of tectonomagmatic classification and to establishing the nature of continental crust contamination of basaltic lavas of the British Tertiary volcanic province. *Earth and Planetary Science Letters*, 50:11–30.

Xiao, Y., Lavis, S., Niu, Y., Pearce, J. A., Li, H., Wang, H., and Davidson, J. (2012). Trace-element transport during subduction-zone ultrahigh-pressure metamorphism: Evidence from western Tianshan, China. *Geological Society of America Bulletin*, 124(7-8):1113–1129.

Xiao, Y., Niu, Y., Song, S., Davidson, J., and Liu, X. (2013). Elemental responses to subduction-zone metamorphism: Constraints from the North Qilian Mountain, NW China. *Lithos*, 160-161:55–67.

Xiong, X., Adam, J., and Green, T. H. (2005). Rutile stability and rutile/melt HFSE partitioning during partial melting of metabasalt at the amphibolite to eclogite transition, with applications to TTG gnenesis. *American Mineralogist*, 94:1175–1186.

Xiong, X., Keppler, H., Audetat, A., Ni, H., Sun, W., and Li, Y. (2011). Partitioning of Nb and Ta between rutile and felsic melt and the fractionation of Nb/Ta during partial melting of hydrous metabasalt. *Geochimica Et Cosmochimica Acta*, 75:1673–1692.

Yu, Z. S., Robinson, P., Townsend, A. T., Munker, C., and Crawford, A. J. (2000). Determination of high field strength elements, Rb, Sr, Mo, Sb, Cs, Tl and Bi at ng g-1 levels in geological rederence materials by magnetic sector ICP-MS after HF/HClO4 high-pressure digestion. *Geostandards Newsletter*, 24:39–50.

Zack, T. and John, T. (2007). An evaluation of reactive fluid flow and trace element mobility in subducting slabs. *Chemical Geology*, 239:199–216.

Zack, T., Kronz, A., Foley, S. F., and Rivers, T. (2002a). Trace element abundances in rutiles from eclogites and associated garnet mica schists. *Chemical Geology*, 184(1-2):97–122. Times Cited: 96.

Zack, T., Kronz, A., Foley, S. F., and Rivers, T. (2002b). Trace element abundances in rutiles from eclogites and associated garnet mica schists. *Chemical Geology*, 184:97–122.

Zack, T. and Luvizotto, G. L. (2006). Application of rutile thermometry to eclogites. *Mineralogy and Petrolgy*, http://dx.doi.org/10.1007/s00710-006-0145-5.

Zack, T., Rivers, T., and Foley, S. F. (2001). Cs-Rb-Ba systematics in phengite and amphibole: an assessment of fluid mobility at 2.0 GPa in eclogites from Trescolmen, Central Alps. *Contributions to Mineralogy and Petrology*, 140:651–669.

Zack, T., von Eynatten, H., and Kronz, A. (2004). Rutile geochemistry and its potential use in quantitative provenance studies. *Sedimentary Geology*, 171:37–58.

Zhang, G., David, J., Andrew, G. C., Zhang, L., and Song, S. (2010). Zr-in-rutile thermometry of HP/UHP eclogites from Western China. *Contributions to Mineralogy and Petrology*, pages http://dx.doi.org/10.1007/s00410–009–0486–2.

Zhang, G., Ellis, D. J., Christy, A. G., Zhang, L., and Song, S. (2009). Zr-in-rutile thermometry in HP/UHP eclogites from Western China. *Contributions to Mineralogy and Petrology*.

Zheng, Y. F., Gao, X. Y., Chen, R. X., and Gao, T. S. (2011). Zr-in-rutile thermometry of eclogite in the Dabie Orogen: constraints on rutile growth during continental subduction-zone metamorphism. *Journal of Asian Earth Sciences*, 40(2):427–451.

Zittel, K. v. (1899). Geschichte der Geologie und Palaontologie bis Ende des 19. Jahrhunderts. *Drud und Berlag*, (xi-868).

Appendix A

Analytical Procedures and Instrument Settings

A.1 X-ray fluorescence (XRF)

Whole rock powders were used to manufacture fused glass discs and pressed powder discs for major element and trace element analysis respectively. Procedures were as follows:
Fused glass discs:

1. Around 3 g of each powdered sample was placed in an open vile and dried overnight at 110^{o}C.

2. Around 1 g of each sample was placed into a platinum crucible and its mass (M_u) determined with high precision scales.

3. The sample was then ignited in a furnace at 1100^{o}C and its mass (M_i) redetermined. The difference between the unignited and ignited mass (i.e. M_u-M_i) was recorded as loss on ignition (LOI)

4. Lithium borate flux (Johnson Matthey Spectroflux^{TM} No. 105) was added to the unignited sample in a the M_u:M_{flux} ratio 1:5, the total mass was recorded as M_{S+F} and fused at 1100^{o}C for no less than 30 minutes.

5. The fused sample was covered and allowed to cool to room temperature, at which point its mass was re-assessed and any loss due to further ignition (of the flux) was replaced by more flux to regain a mass of M_{S+F}.

6. The sample was re-fused at 1100^{o}C until the sample was completely molten.

7. Immediately after removal from the furnace, and whilst still molten, the samples were swirled over the hot flame of a Bunsen burner for 30 seconds.

8. Once thoroughly mixed, the molten sample was then cast into a graphite disc mould held on a hotplate at 220^{o}C and flattened with a similarly hot aluminium plunger. The disc was left to anneal and then checked for cracks and heterogeneity.

Pressed Powder Discs:

1. 8 g of sample was mixed with eight drops of a 2% aqueous solution of polyvinyl alcohol.

2. The mixture was loaded into 40 mm diameter aluminium sample cups and placed in a cleaned stainless steel die with a polished tungsten carbide press face.

3. The die was loaded into a hydraulic press, and a pressure of 0.6 tons cm^{-2} applied.

Both fused glass discs and pressed powdered discs were analysed using a PANalytical PW 2404 X-ray fluorescence spectrometer fitted with a 3 kW Rh-anode end-window X-ray tube. The high precision acquisition of element abundances followed the conditions published by Fitton et al. (1998); Fitton and Godard (2004), and involved long acquisition times for background and peaks.

Matrix effects on major element acquisitions were calculated by PANalytical's software that uses theoretical alpha coefficients that take into consideration the mass of flux and loss on ignition. Alpha coefficients for long wavelength trace elements (e.g. La, Ce, Nd, Cu, Ni, Co, Cr, V, Ba, and Sc) were calculated using in-line major element measurements, whereas other trace elements were corrected using the RhK_a Compton scatter line Reynolds (1963).

A.2 Solution ICP-MS

The preparation of samples for solution ICP-MS analysis are discussed in detail in Chapter 2 (pg. 53) and are not discussed here. Dissolved samples from both LPTS and HPTS techniques were analysed using an Agilent 7500ce Octopole series ICP-MS system at theNERC and SUERC facility East Kilbride, Scotland. The new system is able to detect masses in the range 7-260 amu (i.e. Li to U). Iridium was used as an internal standard spike in each sample, which the Agillent software used to

automatically correct for mass bias (mass response), natural isotopic abundance, as well as ionisation potential. BCR-2 powder was dissolved and used as an external standard sample every 5 acquisitions to account for drift in sensitivity and used to calibrate counts per second (CPS) data into useful concentrations. Interference removal was performed using the accompanying Agilent software to account for all polyatomic interferences.

A.3 LA-ICP-MS

The separated rutile grains were analysed using LA-ICP-MS at the School of Earth and Environmental Sciences (SEES), University of Portsmouth using a New Wave (ESI) UP-213 Laser Ablation System tethered to an Agilent 7500LE Series ICP-MS. Samples of rutile grains were set into 25 mm polished epoxy resin discs, and placed in a vacuum of 4.9-5.3 $\times 10^{-6}\ pa$. A laser beam (spot: 40-50 μm; fluence: 4 $J\ cm^{-2}$; energy:43-44.5 $\%$; frequency: 10 Hz) was used to ablate the sample into a He and Ar gas (He flow rate - 0.75 $l\ min^{-1}$; Ar flow rate - 1.20 $l\ min^{-1}$) which led into the ICP mass spectrometer.

Each acquisition lasted 60 seconds. Background recording started from 0s. From 10-20 seconds the laser was fired with the aperture closed, in order for the laser energy to plateau without ablating the sample. At 20 s the aperture was opened and sample ablation began, continuing until termination of the acquisition sequence at 60 s.

Data files from each acquisition were processed using the open source program SILLS (signal integration for laboratory laser systems) developed by Guillong et al. (2008). Acquisitions were loaded into the program in batches of 20, at which point the time ranges of background and sample analysis count data to be used were manually selected on plots similar to Fig. 4.5. Samples 1, 2, 19, and 20 in every batch were analyses of standard 612 (glass), and in every other batch sample 18 was an analysis of rutile standard R10. The internal standard was assumed to be $TiO_2 = 98wt.\%$. SILLS uses all these standards as well as time stamps of each analysis to calculate the composition and accompanying statistical attributes for each analysis. After conversion to concentration format by the program SILLS, the analyses of the rutile

standard R10 were checked for consistency.

Appendix B

Petrography

B.1 Almenningen, Nordfjord - [N61 54.609, E5 15.172]

WGR-73-DW, heavily retrogressed micaceous eclogite

This eclogite sample has been significantly retrogressed. Garnets are large (>3-4 mm) and abundant (ca. 70%) contain significant number of inclusions of clinopyroxene, mica and quartz. Patches of primary omphacite and white mica can be found within the retrogressed groundmass, along with presumably primary rutile. Although peak eclogite mineralogical texture has been significantly destroyed, remnant primary minerals (clinopyroxene and mica) indicate poikiloblastic garnets and a moderately- to well developed schistosity.

B.2 Angelshaug, Nordfjord - [N61 54.222, 05 12.327]

WGR-37-DW, zoisite eclogite

The Angelshaug eclogite has a relatively diverse mineral assemblage compared with other eclogites from the region, yet it may be described as ”fresh” and largely free from the effects of obvious retrogression. As can be seen in Figure B.2, large, subhedral poikiloblastic garnets (3-9 mm) contain abundant micro-inclusions of quartz, white mica, clinozoisite, epidote, and rutile). Well defined schistosity defined mostly by omphacite, clinozoisite, and white mica. Elongate, pale-green to colourless omphacite crystals are abundant, and may contain inclusions of rutile and quartz. Clinozoisite laths are scattered throughout the rock, and are aligned with the dominant schistosity. Infrequent sections of tremolite are also present. Rutile grains are reasonably abundant and occur as either large free granules typically >1 mm in diameter, or euhedral needles <0.5 mm in diameter, mostly as inclusions in clinopyroxene and clinozoisite. Sulphides are typically pyrite with thin rims of chalcopyrite. The rock is cut by thin veins spaced at the decimetre scale. These veins cross-cut the dominant schistosity,

Sample	Locality	Gt	Omp	Amp	Qz	Coe	Rt	Phe	Ky	Zo/CZo	Ep	Su	Bt	Opx	Mag	Trem	Ser
1	Bjørnstad	6	-	5	1	-	t	3	2	-	-	t	3	-	-	-	80
8	Drøsdal	22	36	-	6	-	2	7	3	4	3	1	-	-	-	-	16
14	Åsnes	12	3	-	-	-	-	5	-	-	-	-	-	-	-	-	80
22	Lefdal	25	33	35	2	-	2	-	-	-	-	2	-	-	-	-	-
30	Kvalneset	34	43	8	1	t	2	1	t	-	t	1	-	-	-	-	11
32	Krokaberg	54	15	-	25	-	4	-	-	-	-	-	-	2	-	-	-
37	Angelshaug	25	51	3	1	-	2	3	-	11	t	1	-	-		t	3
41	Halnes	16	36	5	7	-	-	6	-	4	-	-	-	-	-	-	26
46	Nybø	46	47	-	3	-	3	-	-	-	-	-	-	1	-	-	-
47	Nybø	28	42	16	-	-	2	-	-	-	-	-	-	-	-	-	12
51	Flatraket	38	30	-	1	-	2	1	-	-	-	-	1	1	-	-	26
53	Årsheimneset	44	35	4	6	-	5	-	-	-	-	1	t	5	-	-	-
64	Sandvollen	37	-	20	2	-	2	2	-	-	-	1	-	-	-	-	36
65	Naustdal	41	48	2	1	-	8	-	-	-	-	-	-	-	-	-	-
67	Fossheim	45	23	15	-	-	3	10	-	-	-	-	-	-	-	-	4
69	Engebøfjellet	27	9	38	4	-	t	12	-	-	1	1	-	-	-	-	8
70	Åsneset	30	-	3	-	-	2	-	-	-	-	-	-	-	-	-	65
71	Holmane	22	26	-	3	-	3	-	-	-	-	-	-	-	-	-	45
72	Raudegga	39	5	16	1	-	2	2	-	-	-	-	7	-	-	-	29
73	Almenningen	67	2	7	2	-	t	2	-	-	-	-	t	-	-	-	20
74	Maløy	48	45	-	1	-	2	4	-	-	-	-	-	-	-	-	-
75	Straumen	26	-	2	6	-	2	-	-	7	-	-	-	-	-	-	57
76	Gangeskaret	17	46	20	-	-	1	15	-	-	-	-	-	-	-	-	2
77	Seljeneset	73	12	-	5	-	1	-	-	-	-	-	-	-	-	-	9
78	Vengen	71	8	-	4	-	6	-	-	-	-	-	-	-	-	-	11
79	Havik	11	19	8	-	-	4	-	-	1	-	-	-	-	-	-	57
80	Flister	47	2	42	6	-	1	-	-	-	-	1	-	-	-	-	-
81	Runderheim	47	30	3	9	-	3	-	-	-	-	-	-	-	-	-	8
82	Salt	20	1	5	6	-	6	-	-	-	-	1	11	-	-	-	50
83	Årdalen	37	4	41	2	-	1	-	-	-	-	2	11	-	t	-	2
84	Hareidland	35	23	-	4	-	1	-	-	-	-	3	9	-	t	-	26
kval	Kvalneset	-	-	-	-	-	-	-	-	-	-	-	-	-	-	-	-

Figure B.1: Estimated modal proportions for described eclogite samples. Modal proportions are given in percent, and are estimated from between 150 and 300 randomly selected point counts. The letter ”t” represents trace amounts, typically where less than one or two points coincided with the phase.

and cause very localised symplectite formation, as indicated by the presence of very fine grained green-blue amphibole.

B.3 Bjørnstad, Skifjorden - [N61 14.881, E05 06.714]

WGR-01 to 06-DW, heavily retrogressed quartz-kyanite eclogite
The Botnen eclogite sample represents a very fine grained almost totally retrogressed quartz rich eclogite located in the very south of the WGR eclogite zone. Much of the outcrop is totally retrogressed to a biotite-rich amphibolite with a well-developed schistosity otherwise absent in the relatively less retrogressed eclogite domains. Much of the exposure has clearly been sheared under a ductile regime which then turned brittle, as evidenced by deformed pre-shear quartz veins, sheared layering in the eclogite and amphibolite domains, and post-ductile cross-cutting veins filled with kyanite. A rough cleavage is present in parts of the outcrop parallel to post-ductile brittle faulting. The shear deformation observed is likely a result of the collapse of overlying nappes in the region. Differential retrogression probably pre-dates ductile shear, since the presumably more competent eclogitic parts of the exposure appear to have resisted ductile deformation more than the more amphibolitic domains.

Grain size of primary minerals is typically $<$500 μm. Only rare patches of garnet and omphacite remain, however are much coarse grained ($>$1-2 mm) than the current mineral assemblage. Current mineral assemblage is dominated by fine and microscopically heterogeneous symplectites of quartz, biotite, amphibole and kyanite. Some patches in the thin section preserve slightly larger ($>$1 mm) kyanite and quartz crystals. Rutile is present in relatively low abundance (likely $\ll$ 0.5 %) and very dark rims in places indicate likely partial to complete alteration to ilmenite for many grains.

B.4 Drøsdal, Svanetjørna - [N61 15.136, E05 10.858]

The Drøsdal eclogite body is one of the largest eclogite bodies in the WGR, with an exposure area of over 3 km^2. It contains a complex multi-phased deformational history that is summarised by Andersen and Austrheim (2008). The outcrop host many large kyanite veins up to several meters long with kyanite crystals over 10 cm in length.

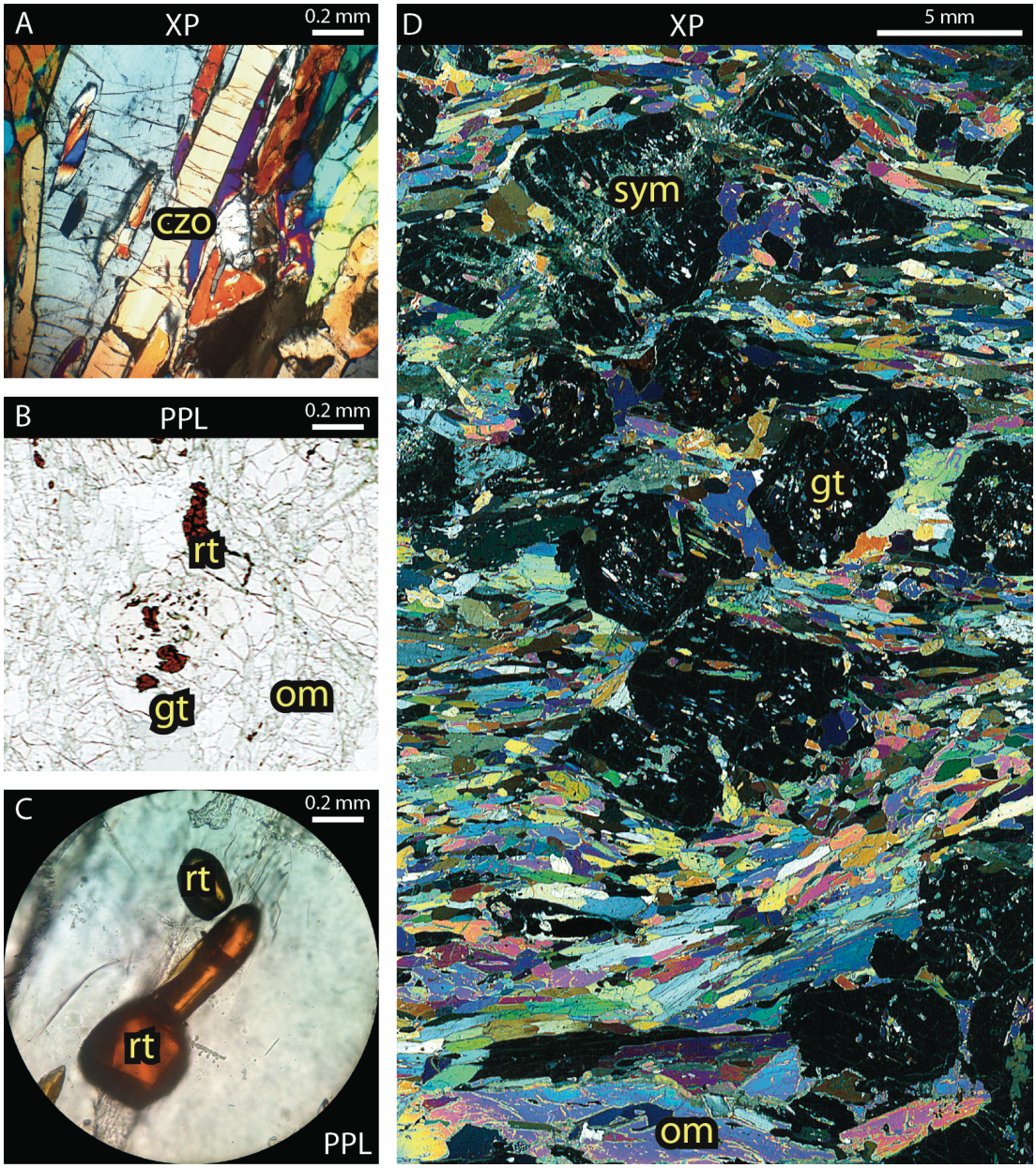

Figure B.2: Selected photomicrographs showing typical petrographic features of WGR-37-DW (Angelshaug). Sub-figures as follows: a) Clinozoisite and omphacite define the schistosity of the sample; b) rutile may occur as large granules; c) or as small often lath- or needle-shaped inclusions in either garnet or ompacite; d) XP scan of polished section showing the poikiloblastic nature of garnet and the foliation defined by clinozoisite and omphacite, along with a thin vein and associated symplectite.

WGR-08-DW, kyanite-phengite-zoisite eclogite

The eclogite mineralogy can vary on the hand sample scale and certainly across the entire body. Generally, the eclogite body is remarkably well preserved, but amphibolitisation is common at the body margins. Sample WGR-08-DW is typical of the internal portions of the eclogite. Garnets are almost always euhedral and of a uniform size (ca. 2.5-3.5 mm) with common fine (few 10s of μm) inclusions of what appear to be mostly quartz and omphacite. Garnet growth appears to define two distinct phases: inclusions are largely confined to the cores of grains (porphyroblastic), and the outer euhedral rims are mostly inclusion-free (i.e. neoblastic). The matrix is dominated by omphacite, quartz, kyanite and epidote, with minor accessories such as granular rutile and pyrite. Parts of the sample show moderate fine-grained symplectites of amphibole and quartz.

B.5 Engebøfjellet, Førdefjorden- [N61 29.526, E05 25.247]

WGR-69-DW, rutile rich eclogite

The Engebøfjellet eclogite body is one of the largest eclogite bodies in the WGR, covering an area of around 1.5 km^2, and is currently under application for rutile mining by Nordic Mining AS. It has been interpreted as a gabbroic eclogite body. The eclogite sample from the western end of the body (B.3) shows how the eclogite is rather mineralogically simple. It is fine-grained composed of abundant small garnet and cpx granules around 100-500 μm in diameter. Prograde hydrous phases are abundant (mica, amphibole, epidote) and are in relative textural equilibrium, suggesting the eclogite remained relative 'wet' under peak conditions. The rutile content of the body varies from $<$2 % to over 7-8% depending on the layer sampled, however this sample has $<$1% rutile since it was chosen from a metagabbroic layer that appeared to have a low cumulate component.

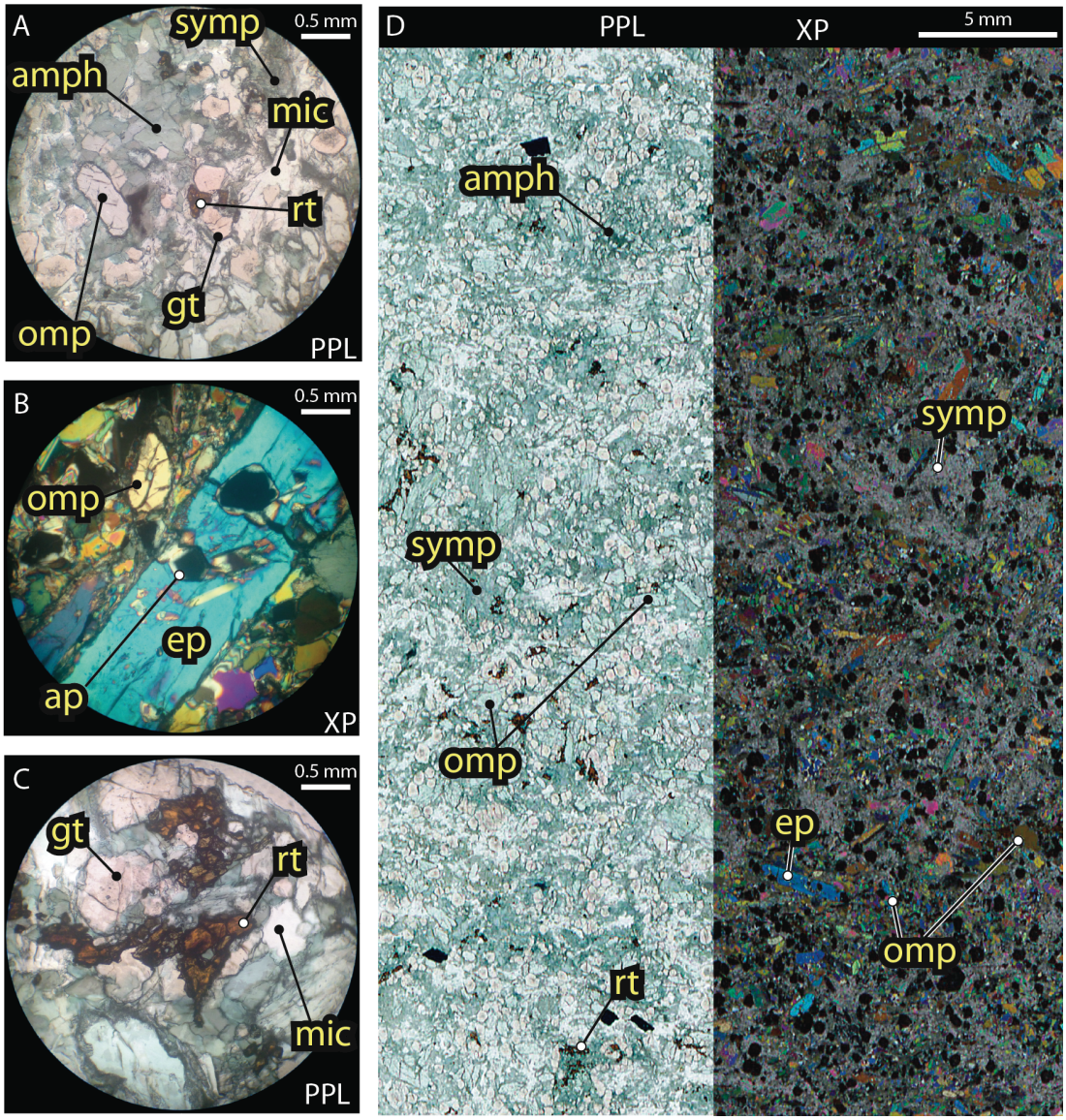

Figure B.3: Selected photomicrographs showing typical petrographic features of WGR-69-DW (Engebøfjellet). Sub-figures as follows: a) typical petrology consisting of garnet (gt), omphacite (omph), amphibole (amph) and mica (mic); b) prograde needles of epidote (ep) can be large (>1 mm); c) rutile is intercrystalline and granular in nature; d) the thin section overview shows that this particular sample is fine grained and moderately retrogressed, yet many primary minerals remain incompletely altered.

B.6 Flatraket, Nordpollen- [N61 58.582, E05 14.443]

WGR-51-DW, fine grained eclogite

This fine grained eclogite is from a dyke cutting the country gneiss near Flatraket harbour. Its mineralogy is rather simple and homogeneous. Granular, equally sized anhedral garnet and omphacite dominate the rock. Garnets typically contain significant quartz inclusions, with minor cpx and rutile needles. Granular rutile is relatively abundant in the matrix (approx. 1-2%) and is often relatively large (up to around 500μm or more). Moderate intergranular sericitisation and symplectite formation is common, however has not destroyed peak eclogite facies mineralogy.

B.7 Flister, Holmen [N61 58.832, E05 18.564]

WGR-80-DW, moderately retrogressed eclogite

A relatively coarse eclogite that has undergone significant retrograde amphibole crystallisation. Ecloigte facies garnet and clinopyroxene form large remnants (2-5 mm diameter) in a groundmass of very finely grained ($<$100 μm) amphibole and quartz. Relatively large (up to 500μm) and abundant (up to 1 %) rutile occurs as granules and needles in both intergranular spaces between eclogite facies minerals as well as in the retrogressed groundmass, suggesting that rutile petrology has been largely unaffected by retrogressive recrystallisation.

B.8 Fossheim, Førdefjord- [N61 27.254, E05 30.137]

WGR-67-DW, amphibole-mica eclogite

This well preserved medium-grained eclogite is dominated by granular- to euhedral garnet (50-100 and $>$400μm), omphacite, amphibole and white mica. Garnets have quartz and cpx as common inclusions in their cores, however more than 50 % of the garnet volume are relatively inclusion free rims. Rutile is common ($<$1-1.5 %) as inequent granules in the matrix, and is seldom observed as inclusions in any of the primary phases. Small amounts of alteration is visible along some grain boundaries, however is considered to be insignificant in volume.

B.9 Halnes, Måløy - [N61 55.462, E05 05.305]

WGR-41-DW, eclogite

The Halnes eclgotite is a fine- to medium-grained moderately retrogressed and sheared eclogite. In un-sheared zones garnets are relatively large (>3-4 mm) and euhedral with only moderate number of inclusions of predominantly quartz and clinopyroxene inclusions in the core, and relatively few if any inclusions towards the rims. Omphacite crystals outside the sheared zones are inequant laths often more than 5-10 mm in length. Small amounts of quartz and mica are present. Much of the sample is sheared, with grain size greatly reduced as a consequence. Despite this, minerals can still be identified, and mineralogy does not appear to have changed. The sample contains slight amounts of intergranular symplectite growth, typically concentrated in bands that presumably reflect fluid pathways during exhumation.

B.10 Hareidland [N62 18.603, E05 51.468]

WGR-84-DW, retrogressed biotite eclogite

This Hareidland eclogite is composed of medium- to coarse grained garnet and omphacite allied with flakes of biotite. Garnet contains relatively few inclusions, but those that are present are typically clinopyroxene, quartz, rutile or unidentifiable accessory phases. Much of the clinopyroxene and some garnet has reacted away leaving a very fine grained (sub-microscopic) retrogressive symplectite likely composed of amphibole and feldspar, and is in places kelyphitic around garnet remnants. An opaque oxide (assumed to be magnetite) is commonly associated with magnetite, whilst rutile occurs as large granules (up to 500 μm) and needles (up to 100μ) both in the rock matrix and as inclusions in garnet and clinopyroxene.

B.11 Havik, Nordpollen - [N61 57.652, E05 16.082]

WGR-79-DW, heavily retrogressed amphibole eclogite

Heavily retrogressed eclogite. Many garnet remnants remain but with kelyphitic rims and sit in a matrix of fine grained amphibole dominated symplectite. Only a few small remnants of omphacite remain to show that this was once indeed a rock with an eclogite

assemblage. Eclogitic rutiles appear to have survived reactive retrogression, and now stand out in the symplectite groundmass. Some small seemingly primary amphiboles remain partially reacted in the groundmass, suggesting this was a amphibole-bearing eclogite.

B.12 Holmane, Nordfjord- [N61 55.400, E05 23.119]

WGR-71-DW, moderately retrogressed eclogite
Eclogite facies garnet and omphacite are still visible as remnants in a matrix of amphibole and plagioclase dominated symplectite. Prograde rutile appears to have remained relatively oblivious to the surrounding recrystallisation.

B.13 Krokaberg, Nordfjord - [N61 55.019, E05 20.701]

WGR-32-DW, Eclogite
The Krokaberg eclogite is well a equilibrated, well preserved, fine grained (ca. 1 mm) eclogite. There is no perceptible compositional layering or schistosity. Garnets are euhedral, 1-1.5 mm in diameter, and contain abundant inclusions of mostly rutile and quartz from core to rim. Omphacites are nearly colourless in PPL, and show no obvious elongation or preferred orientation. Inclusions of rutile in omphacite are much less common than in rutile, and instead ompacite tends to be associated with the larger more granular crystals of rutile. Free quartz is a common free accessory phase.

B.14 Kvalneset, Nordfjord - [N61 55.549, E05 22.544]

Garnets are 1-3 mm in diameter and euhedral. They contain inclusion rich cores and inner rims (Rutile and coesite, quartz) and reasonably inclusion-free outer rims. Smaller garnets ($<$1 mm) occur in band associated with more quartz and pyrite than the rest of the slide – these garnets are relatively inclusion-free. Omphacite contains common inclusions of quartz (radial fractures indicate after coesite) and sometimes coesite with quartz rims (again associated with radial cracks). Accessories include epidote, quartz, kyanite, pyrite and rutile. Pyrite often has chalcopyrite rims.

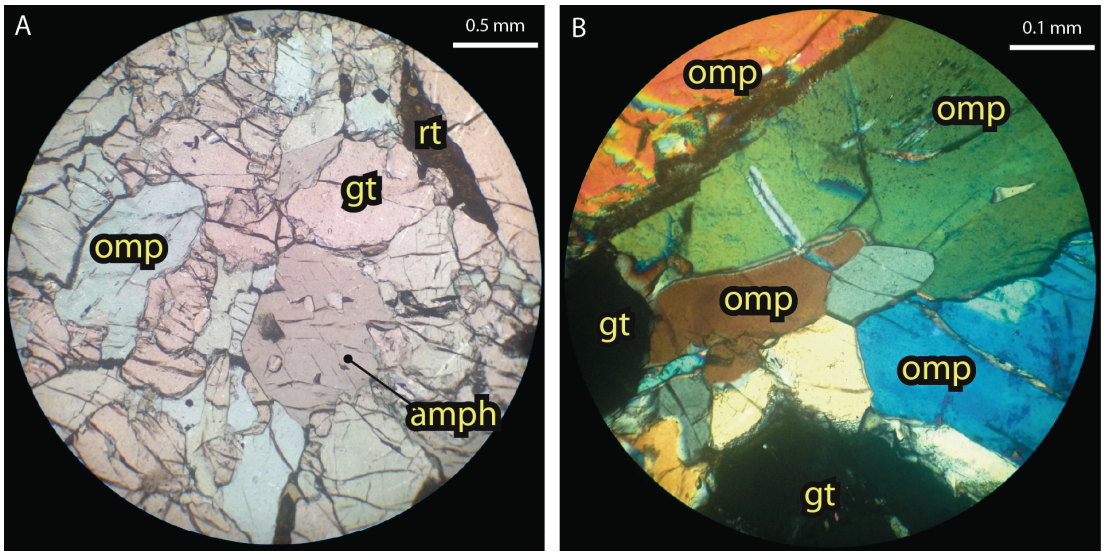

Figure B.4: Selected photomicrographs showing typical petrographic features of WGR-Lef1-DW (Lefdal). Sub-figures as follows: a) the typical petrographic appearance of an amphibole eclogite; b) omphacite grains are in most places well equilibrated, forming triple junctions between grains of all sizes.

B.15 Lefdal, Nordfjord - [N61 55.853, E05 30.565]

WGR-22-DW/Lef1/Lef2, amphibole eclogite

The Lefdal eclogite (B.4) is a good example of the amphibole eclogites found in the WGR. Garnet and omphacite texture is well equilibrated with common granular forms and triple junctions. Both garnet and clinopyroxene are typically fine- to medium grained, whereas euhedral calcic amphiboles are large (>2-4 mm). Relatively minor symplectites have formed along some grain boundaries but are considered insignificant. WGR-22-DW represents a heavily retrogressed sample from the same exposure for comparison.

B.16 Måløy, Nordfjord - [N61 57.005, E05 08.045]

WGR-74-DW, eclogite

This Måløy sample is a relatively fresh medium-grained eclogite whose mineralogy is

relatively simple. Granular garnets and pyroxenes dominate the rock, with accessories limited to relatively obvious rutile (ca. 0.5-1.0 %) and a few grains of quartz. Late stage brittle fractures cross cut the sample and have very proximal associated symplectite formation, however is insignificant in relation to the whole rock volume.

B.17 Naustdal, Nordfjord - [N61 58.533, E05 43.165]

WGR-65-DW, amphibole eclogite

The Naustdal eclogite (B.5) is another a good example of a well equilibrated granular amphibole eclogite. Euhedral pyrope garnets, typically 0.5 mm in diameter are found in crudely more garnetiferous layers, may contain inclusions of rutile, quartz and clinopyroxene. Clinopyroxene is a strongly coloured green omphacite, crystals of which are only mildly elongated parallel to garnetiferous layers, thus defining a weak schistosity. Omphacite crystals show good 1206◦ triple junctions with one another and with garnets, and may too host small euhedral rutile needles.Olive-green to deep minty green pleochroic hornblende makes up less than 5% of the section. Others – Rutile is ubiquitous in the rock. It occurs mostly in association with garnet and ranges in size from a few tens of microns in diameter to one large crystal that is around 400 microns wide and $>$10 mm long. Quartz is present as $<$5 % of the section (probably 1-2 %) and typically occurs in the garnetiferous layers.

B.18 Nybø, Sørpollen - [N61 55.979, E05 13.512]

WGR-47-DW, amphibole eclogite

Coarse grained amphibole eclogite with interesting textural relationships. Large ($>$4 mm) euhedral garnets coexist with omphacite and calcic amphibole. Many garnets are cored by, or have near-complete zones of relatively large clinopyroxenes and amphiboles. These crystals do not appear to be retrogressive, therefore it seems that the garnets have grown around these crystals whilst still achieving a euhedral shape. Rutile is a common inclusion in garnets, pyroxenes and amphiboles as well as a free phase. Quartz, phengite and kyanite are all completely absent. Some retrogressive symplectic amphibole is present along grain boundaries, but is largely confined to proximal areas, especially when away from dominant fluid pathways.

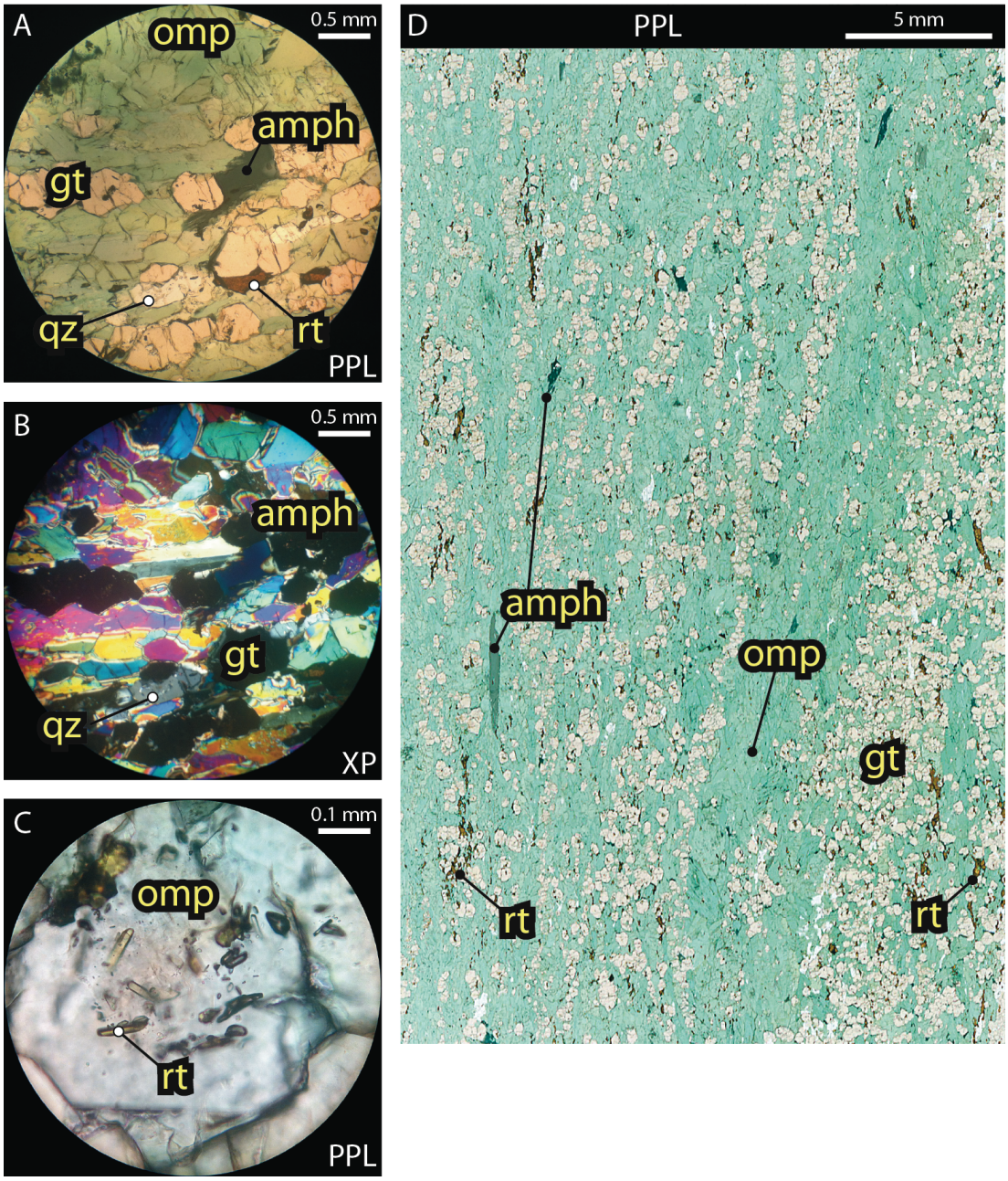

Figure B.5: Selected photomicrographs from WGR-65-DW (Naustdal). Sub-figures are: a) representative view of mineralogy and texture in PPL; b) same as (a) but in XP, c) typical needle-shaped rutile inclusions in omphacite; d) PPL scan of entire polished section showing small scale compositional layering.

B.19 Raudegga, Nordfjord - [N61 54.799, E05 17.570]

WGR-72-DW, significantly retrogressed amphibole eclogite
Almost all omphacite has reacted to amphibole dominated symplectite. Garnets remain largely euhedral and preserve inclusions. Large, apparently prograde amphiboles remain in places, but show some sieve textures especially in areas of the sample with high percentages of significant symplectite formation. Small amounts of rutile pepper the sample regardless of local alteration, indicating that it has resisted retrogressive recrystallisation.

B.20 Salt, Moldefjorden- [N62 01.494, E05 20.845]

WGR-82-DW, highly retrogressed amphibole eclogite
As with other similarly heavily retrogressed samples, cpx has almost completely been reacted to amphibole-plagioclase symplectites. Remnants of cpx are clearly omphacite, inferring an eclogitic assemblage before retrogressive alteration. In addition, garnets have largely remained unchanged during retrogression, and have preserved their inclusions that include common quartz and omphacite. The rock is also littered with granules of rutile ($<$1.0-1.5 %) that in many places exceeds 200 μm in diameter with little sign of alteration to ilmenite.

B.21 Sandvollen, Sognefjord- [N61 05.303, E05 22.999]

WGR-64-DW, highly retrogressed amphibole eclogite
The mineralogy and texture of the Sandvollen eclogite is almost identical to that of Salt above. The main difference is that garnets in the Sandvollen eclogite are larger (ca 5-10 mm) and that rutile is also typically larger and also more abundant ($>$2%).

B.22 Seljeneset, Nordpollen - [N61 58.577, E05 15.335]

WGR-77-DW, retrogressed eclogite
Very large anhedral and highly porphyroblastic garnets (5-20 mm or more) dominate the sample. Inclusions are almost impossible to identify under the microscope,

however the first order grey birefringence and high abundance of free quartz suggests that inclusions are mostly quartz. Omphacite remnants are obvious but many have been significantly recrystallised to amphibole-dominated symplectites. Free quartz stands out and accounts for around 5 % of the sample. Rutile is obviously rather abundant (>1.0-1.5 %) and is found in patches suggesting that secondary processes may be responsible for its abundance and textural placement.

B.23 Straumen, Sørpollen [N61 57.057, E05 12.684]

WGR-75-DW, retrograded coesite-amphibole eclogite

This Straumen eclogite (B.6) has undergone significant retrograde amphibolitisation, however prograde and peak eclogite mineral assemblages may still be identified. Garnets are generally large (>3-4 mm) and contain abundant inclusions of mostly rutile and quartz needles but occasionally prograde hornblende inclusions. Some prograde amphiboles remain and can be occasionally seen to include epidote needles. Garnets also have kelyphitic rims in which both calcic amphibole and plagioclase can be clearly identified. Zoisite laths 1-3 mm in length stand out clearly in the retrograded groundmass. Coesite, quartz after coesite, and diamond have all been reported by others in samples from this locality.

B.24 Vengen, Nordpollen- [N61 20.085, E05 15.697]

WGR-78-DW, eclogite

Vengen is an impressive eclogite in hand specimen, dominated by bright red garnets and deep, rich pine green omphacite. In thin section, the sample is dominated by anhedral garnets, often in layers, that contain abundant inclusions of rutile and quartz. Omphacites are a bright, saturated apple green and are generally free of inclusions except for the occasional needle of rutile. Free quartz is common (ca. 5-7 %) and typically occurs in patches of multiple anhedral crystals. Rutile is relatively coarse (typically >100-200μm) and abundant (>2-3%). Limited amphibolite dominated symplectites have formed proximal to the occasional fracture or obvious grain boundary fluid pathway, however overall retrogression is minor.

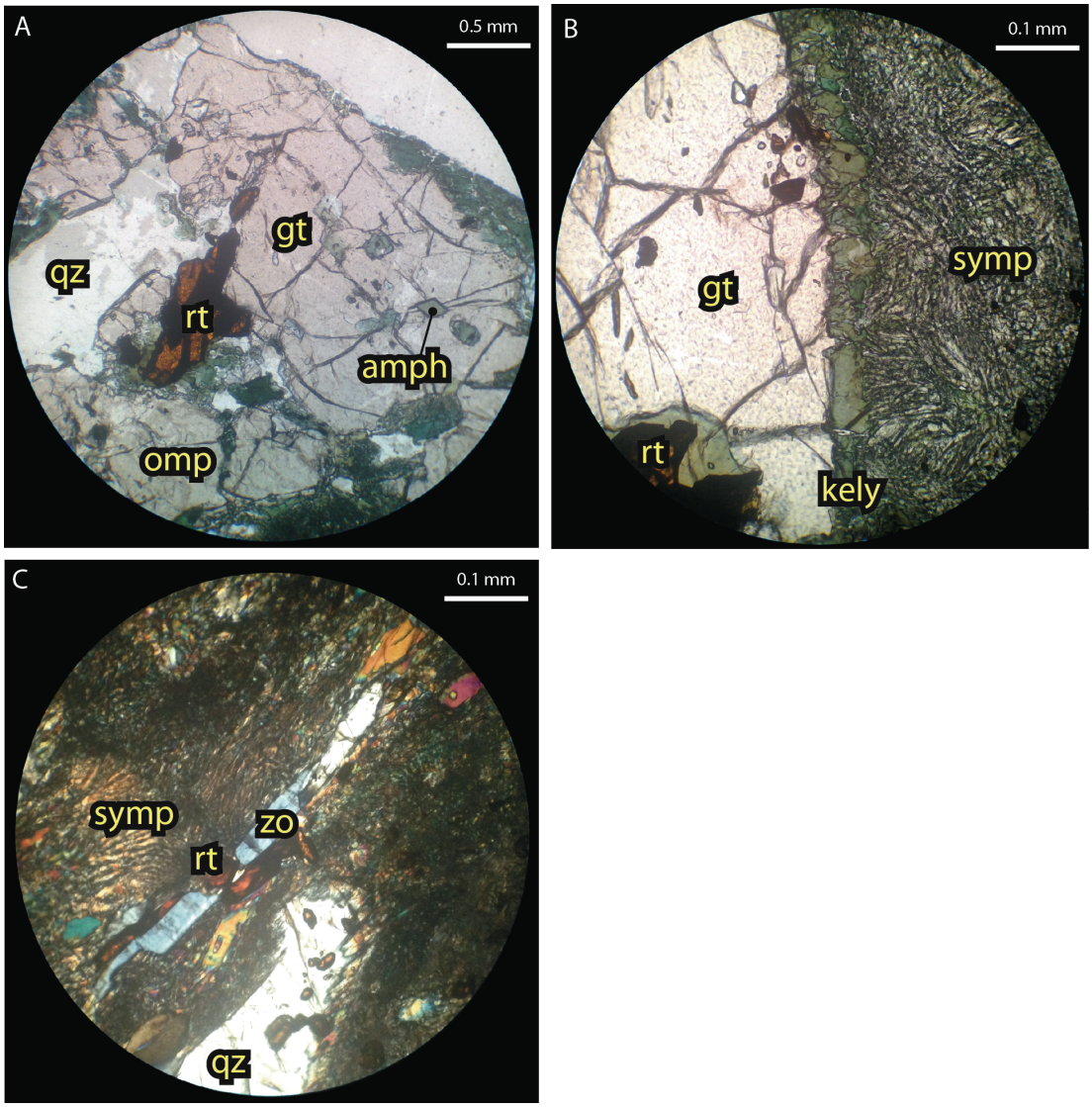

Figure B.6: Selected photomicrographs from WGR-75-DW. A: typical mineralogy consisting of garnet (gt), omphacite (omp), amphibole (amph), quartz (qz) and rutile (rt); B: amphibole-dominated kelyphitic rims around garnets are common, and can be distinguished from the finer-grained amphibole-plagioclase symplectite that fills significant portions of the groundmass; C: zoisite appears to have resisted retrograde recrystallisation in places.

B.25 Årdalen, Statlandet [N62 04.800, E05 17.619]

WGR-83-DW, retrogressed eclogite

Large garnets (>3 mm) are subhedral to euhedral and contain relatively few inclusions. When present, inclusions in garnet are mostly rutile or quartz. The majority of garnets have kelyphitic rims dominated by a Ca-rich amphibole, likely hornblende. Most clinopyroxene has reacted to form submicroscopic amphibole- dominated symplectites, again mostly hornblende. Biotite commonly surrounds opaque oxide that could be magnetite or titanite. Rutile is obvious across the whole section (<1 %) and some crystals appear to have altered to titanite around their rims. Hydrous alteration of the likely Fe-rich and potentially tianiferous oxides with a K-rich fluid could explain the presence of biotite.

B.26 Årsheimneset, Vanylvsfjorden- [N62 04.28, E05 26.407]

WGR-53 & 55-DW, orthopyroxene amphibole eclogite

As can be seen from selected photomicrographs (B.7), the Årsheimneset eclogite is dominated by heavily intergrown garnet and clinopyroxene. Garnet is often very large (>10 mm), anhedral and highly poikiloblastic. Omphacite is also often large (>5-10 mm) with well developed cleavages. The most common accessories are orthopyroxene (UHP) and quartz (HP): much of the interior of the exposure is opx-free (WGR-53-DW), whereas the lower parts of the outcrop contain uneven distribution of orthopyroxene. Sample WGR-55-DW shows that early garnet growth is associated with large well-formed colourless prograde amphibole, quartz and obvious brown biotite. Despite this seemingly HP assemblage, WGR-55-DW also contains abundant garnet-hosted palisade textures formed by the expansion of coesite inclusions as they recrystallised to quartz, showing that the Årsheimneset experienced an unequivocal UHP episode. The contrasting HP and UHP assemblages in the same rock show that lack of UHP petrographic indicators in any one sample do not necessarily mean UHP conditions were not achieved, and similarly, the presence of UHP petrographic indicators does not necessarily mean the whole rock equilibrated to UHP conditions.

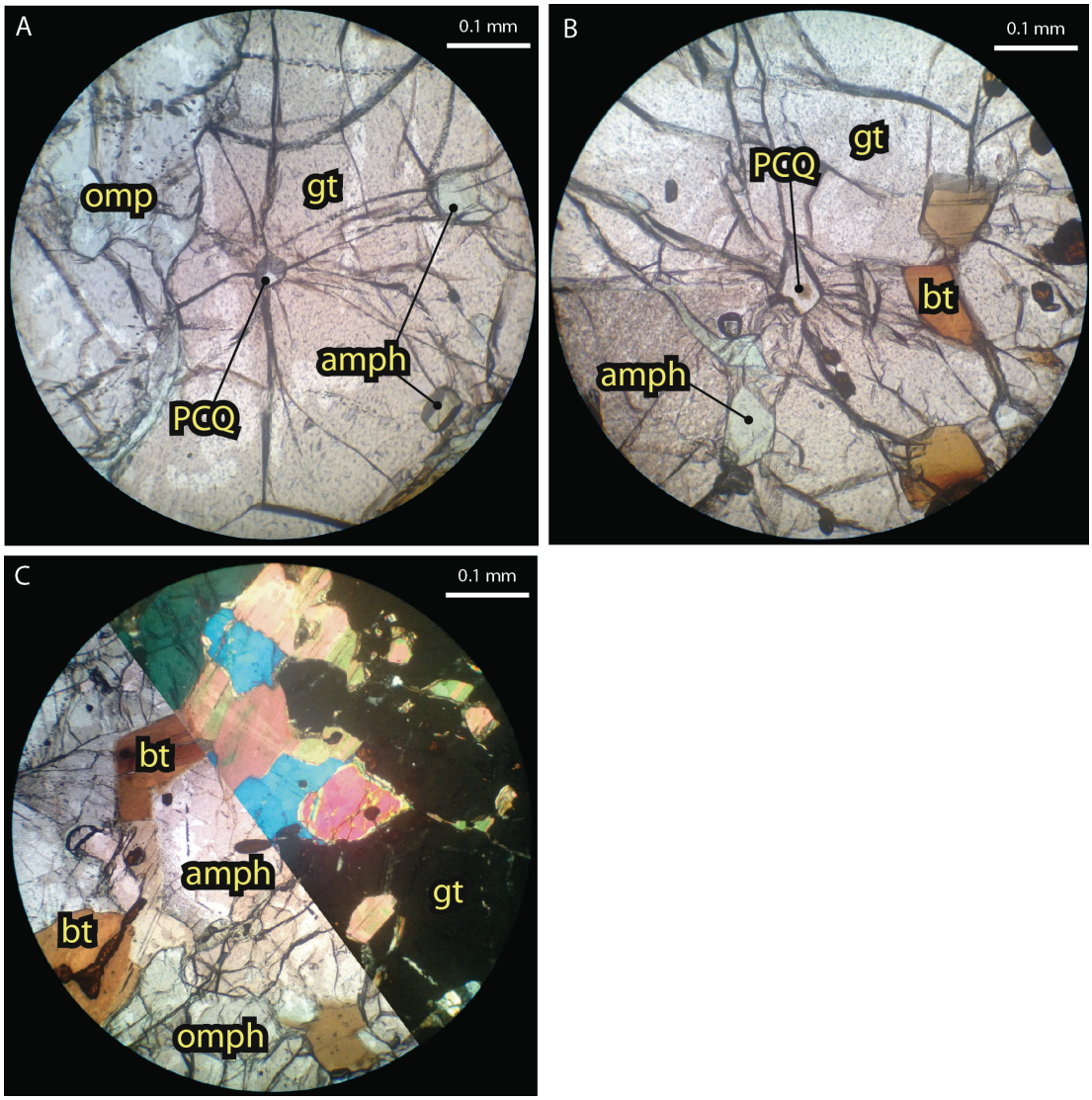

Figure B.7: Selected photomicrographs from WGR-55-DW. A & B show palisade textures caused by the formation of quartz after coesite as inclusions in garnet. The increase in volume between the two silica polymorphs results in radial fractures emanating from the inclusion, and is taken as evidence of a former UHP mineral assemblage; B and C: these images show the prograde assemblage also included amphibole and biotite.

B.27 Åsnes, Dalsfjorden - [N61 19.975, E05 12.180]

WGR-14-DW, quartz-mica eclogite

Relatively fine grained eclogite. Small (<500-750 μm) euhedral garnets are mildly poikiloblastic, and have thin kelyphitic rims. The groundmass is composed of well aligned inequant grains of omphacite, white mica and quartz, which define the rock's schistosity. Garnets do not perturb schistosity, suggesting the linear fabric in the rock formed early on the prograde path.

B.28 Åsneset, Nordfjord - [N61.9267, E5.4592333]

WGR-70-DW, eclogite

Heavily retrogressed fine grained eclogite. Only prograde garnets and very rare remnants of omphacite remain. The rocks matrix has almost completely recrystallised to a amphibole-plagioclase submicroscopic symplectite.

Appendix C

Geochemical Data

C.1 Sample Names and Locations

Table C.1: Names and locations for collected samples used in this study.

Locality	Sample	Longitude	Latitude
Årdalen	WGR-83	5.29365	62.08
Årsheimneset	WGR-53	5.4401166	62.0714833
Åsnes	WGR-14	5.203	61.3329166
Åsneset	WGR-70	5.4592333	61.9267
Almenningen	WGR-73	5.2528666	61.91015
Angelshaug	WGR-37	5.20545	61.9037
Bjørnstad	WGR-01	5.1119	61.2480166
Botnen	WGR-60	5.3515	61.0310833
Drøsdal	WGR-01	5.1809666	61.2522666
Engebøfjellet	WGR-69	5.4207833	61.4921
Flatraket	WGR-51	5.2407166	61.9763666
Flister	WGR-80	5.3094	61.9805333
Fossheim	WGR-67	5.5022833	61.4542333
Gangeskaret	WGR-76	5.20935	61.9776166
Halnes	WGR-41	5.0884166	61.9243666
Hareidland	WGR-84	5.8578	62.31005
	WGR-85	5.84105	62.3094
Havik	WGR-79	5.2680333	61.9608666
Holmane	WGR-71	5.3853166	61.9233333
Krokaberg	WGR-32	5.3450166	61.9169833
Kvalneset	WGR-Kval	5.3757333	61.9258166
	WGR-30	5.3757333	61.9258166
Lefdal	WGR-Lef1	5.5094166	61.9308833
	WGR-Lef2	5.5094166	61.9308833
	WGR-22	5.5094166	61.9308833
Måløy	WGR-74	5.1340833	61.9500833
Naustdal	WGR-65	5.7194166	61.97555
Nybø	WGR-46	5.2252	61.9329833
	WGR-47	5.2252	61.9329833
Raudegga	WGR-72	5.2928333	61.9133166
Runderheim	WGR-81	5.3341	62.0075166
Salt	WGR-82	5.3474166	62.0249
Sandvollen	WGR-64	5.3833166	61.0883833
Seljeneset	WGR-77	5.2555833	61.9762833
Straumen	WGR-75	5.2114	61.95095
Vengen	WGR-78	5.2616166	61.33475

C.2 Whole Rock Composition Data

C.2.1 XRF, Major Elements

Table C.2: Whole rock major-element data for Norwegian eclogites in this study. Data were collected via XRF at the University of Edinburgh. LOI: Loss On Ignition; LOI*: Loss On Ignition corrected for Fe oxidation; GOI: Gain on Ignition; b.d.: below detection limits.

Sample	SiO_2	Al_2O_3	Fe_2O_3	FeO	MgO	CaO	Na_2O	K_2O	TiO_2	MnO	P_2O_5	LOI	LOI*	GOI	Total
01	49.886	21.577	5.541	4.487	5.144	10.039	3.456	0.9	0.353	0.073	1.505	1.52	2.02	0.5	99.993
08	50.867	20.711	5.782	4.682	6.118	10.89	3.425	0.585	0.414	0.109	0.378	0.38	0.901	0.521	99.661
14	51.097	16.395	10.261	8.309	8.203	9.241	3.45	0.377	0.709	0.149	0.03	0.03	0.955	0.925	99.942
22	49.01	16.85	12.06	9.767	6.28	8.72	4.6	0.663	1.411	0.229	b.d.	-0.04	1.047	1.087	99.783
30	49.641	13.93	12.855	10.411	7.254	11.094	2.866	0.119	1.714	0.303	b.d.	-0.16	0.999	1.159	99.617
32	48.068	14.049	15.383	12.457	6.866	11.035	2.398	0.203	1.901	0.215	b.d.	-0.29	1.097	1.387	99.828
37	49.64	16.84	7.39	5.985	9.15	13.16	2.64	0.062	0.902	0.138	b.d.	-0.03	0.636	0.666	99.892
41	47.962	25.51	4.836	3.916	5.313	10.774	3.694	0.592	0.181	0.057	0.529	0.53	0.966	0.436	99.978
46	48.312	15.989	10.266	8.314	10.86	9.89	3.524	0.011	1.089	0.143	b.d.	-0.4	0.526	0.926	99.684
47	48.411	14.583	13.286	10.759	10.148	8.039	3.98	0.053	1.031	0.167	b.d.	-0.07	1.128	1.198	99.627
51	46.02	16.94	15.08	12.212	5.42	9.7	3.87	0.256	3.034	0.245	b.d.	-0.63	0.73	1.36	99.935
53	46.334	12.729	15.976	12.938	10.478	11.255	1.534	0.004	2.151	0.237	b.d.	-0.81	0.63	1.44	99.887
60	51.183	20.587	8.438	6.833	3.204	7.92	4.08	1.073	2.258	0.079	0.591	0.36	1.121	0.761	99.77
64	43.949	14.643	18.944	15.342	5.99	9.015	2.342	0.173	4.113	0.287	0.643	-0.372	1.336	1.708	99.727
65	40.02	13.47	22.31	18.067	5.29	9.9	2.05	0.02	4.954	0.346	1.439	-0.311	1.701	2.012	99.488
67	48.1	17.26	11.53	9.337	7.85	9.73	2.97	0.724	0.864	0.178	0.009	0.38	1.42	1.04	99.595

Continued...

Continued...

Sample	SiO_2	Al_2O_3	Fe_2O_3	FeO	MgO	CaO	Na_2O	K_2O	TiO_2	MnO	P_2O_5	LOI	LOI*	GOI	Total
69	50	18.03	10.41	8.43	6.97	8.11	3.84	0.398	0.936	0.146	0.06	0.74	1.679	0.939	99.64
70	54.054	15.354	11.016	8.921	6.219	7.659	2.862	1.226	1.187	0.175	0.037	0.19	1.183	0.993	99.978
71	49.83	16.099	12.836	10.395	6.328	9.95	3.701	0.043	1.279	0.184	0.117	-0.657	0.501	1.157	99.71
72	45.185	14.975	13.598	11.012	10.01	10.251	2.502	0.423	0.762	0.224	0.027	1.477	2.703	1.226	99.434
73	47.795	16.457	14.642	11.858	6.329	8.144	3.363	1.066	1.941	0.186	0.376	-0.387	0.933	1.32	99.912
74	46.47	16.92	13.66	11.062	9.31	9.62	2.65	0.232	1.362	0.183	0.144	-0.67	0.562	1.232	99.881
75	49.75	14.53	11.17	9.046	7.34	11.92	3.4	0.026	1.627	0.166	0.162	-0.26	0.747	1.007	99.831
76	52.17	6.55	7.5	6.074	16.33	15.09	0.95	0.15	0.268	0.157	0.022	0.64	1.316	0.676	99.827
77	47.35	15.07	19.75	15.994	5.88	7.34	1.98	0.004	2.483	0.257	1.014	-1.3	0.481	1.781	99.828
78	42.43	14.62	21.54	17.444	5.66	7.94	1.86	0.006	6.012	0.282	0.899	-1.36	0.582	1.942	99.889
79	50.5	16.87	8.6	6.965	7.6	10.23	4.12	0.593	0.493	0.133	0.039	0.18	0.955	0.775	99.358
80	52.228	15.074	13.373	10.83	6.587	7.721	2.985	0.027	1.635	0.221	0.278	-0.368	0.838	1.206	99.76
81	50.5	15	11.04	8.941	8.24	11.83	2.31	0.056	0.994	0.18	0.079	-0.51	0.485	0.995	99.719
82	49.73	13.831	15.393	12.465	5.373	10.139	2.816	0.322	2.154	0.239	0.395	-0.617	0.771	1.388	99.775
83	46.545	17.578	14.612	11.833	6.954	8.422	2.5	0.905	1.997	0.234	0.369	-0.367	0.95	1.318	99.749
84	46.16	15.8	15.78	12.779	9.6	8.23	2.41	0.566	1.51	0.202	0.243	-0.53	0.893	1.423	99.971
85	48.86	18.44	9.99	8.09	7.02	12.39	1.95	0.106	0.566	0.273	0.03	-0.18	0.721	0.901	99.445
Kval	49.53	14.096	12.797	10.364	7.373	11.758	2.757	0.075	1.891	0.216	b.d.	-0.58	0.574	1.154	99.913
Lef1	49.052	13.825	11.537	9.343	9.028	10.906	4.33	0.011	0.793	0.213	b.d.	-0.15	0.89	1.04	99.546
Lef2	48.039	13.452	12.049	9.758	11.045	11.293	3.045	0.056	0.951	0.266	b.d.	-0.38	0.706	1.086	99.816

C.2.2 XRF, Trace Elements

Table C.3: Whole rock trace-element data for Norwegian eclogites in this study. Data were collected via XRF at the University of Edinburgh (b.d.: below detection limits; - : not analysed).

Sample	Zn	Cu	Ni	Cr	V	Ba	Sc	La	Ce	Nd	Sr	U	Rb	Th	Pb	Nb	Zr	Y
01	57.2	67.2	115.1	183.2	66.6	173.9	12.8	4.6	15.9	7.4	480.4	1	32.6	2.2	12	2.1	31.5	10.4
08	38.3	33.4	93.8	391.8	144.3	206.1	30.6	7.5	13.7	4.5	250.7	0.4	18.9	1	2.6	0.8	30.7	7.3
14	95	37.5	171	150	208.7	123	30.6	8.7	24.1	14.7	54.2	0.7	10.2	2.2	2.5	3.6	70.6	26.2
22	200.6	42.8	56.2	112.9	288.7	520.4	42	29.3	61.1	28.8	86.7	2	20.9	7.8	6.6	20.8	141.6	39.9
30	107.7	62.2	77.4	231.4	379.1	29.2	46.8	0.8	13.9	11	61.7	1	3	b.d.	1.4	3.4	110.4	40.2
32	150.1	64.2	61.8	80.3	433.7	46.3	56.1	3.6	18.4	12.4	140.5	0.5	5.8	b.d.	5.8	9	105.8	41.9
37	52.9	42.9	128.8	1166.2	203.8	14.1	42.7	1.2	9.2	8.7	242.5	b.d.	1.8	b.d.	0.9	1.6	74.3	24.2
41	51.2	23.3	144.7	17.3	34.2	352.5	4.7	5.7	9.9	4.7	567.7	b.d.	12.5	b.d.	4.5	0.6	11.2	2.3
46	78.6	36.8	152.4	107	173.5	9.2	21.2	2.7	12.5	6.1	155.9	b.d.	0.5	0.9	3.6	4.7	63.6	12.9
47	125.5	62.2	438.8	144.3	142.5	3.7	20.1	0	1.7	0.6	55.1	0.5	0.2	b.d.	1.3	6.4	63.4	16.6
51	119.8	12.5	57.8	16.4	224.5	90.2	19.7	0	13.4	9.1	103	0.6	11.4	b.d.	3.6	7.9	255.5	25
53	124.3	103.3	331.3	526	406.1	20.6	36.3	15.3	40.7	24.7	102.6	b.d.	0.5	b.d.	21.4	15.6	132.5	27.3
60	65.667	33.2	73.767	19.933	162.967	796.733	8.367	17.767	39.467	19.367	1529.033	b.d.	15.533	1.533	8.267	4.6	72.033	9.333
64	188.133	110.333	116.867	66	344.8	28.3	40.5	17.133	56.133	40.1	122.433	b.d.	3.367	0.833	5.067	11.2	299.633	69.967
65	202.933	18.6	20.5	20.033	350.133	23.7	51.467	2.967	25.067	22.833	223	b.d.	0.267	b.d.	2.2	6.133	21.6	33.167
67	87.7	58.3	163	181.833	226.967	193.767	35.8	23.4	45.933	22.667	236.733	1.267	22.033	4.133	11.233	3.8	106.433	26.767
69	94.267	32.033	72.1	256.967	217.2	92.133	25.433	2.733	8.967	5.567	434.467	b.d.	14.367	0.7	7.267	1.5	31.733	10.533
70	99.133	40.8	104.233	273.967	186.667	668.7	30.4	22.533	40.1	22.167	95.2	0.833	32.933	4.2	2.4	9.233	211.5	38.933

Continued...

Continued...

Sample	Zn	Cu	Ni	Cr	V	Ba	Sc	La	Ce	Nd	Sr	U	Rb	Th	Pb	Nb	Zr	Y
71	122.733	97.767	119.367	67.4	281.333	21.267	35.1	b.d.	1.433	0.367	26.433	0.467	1.067	b.d.	0.767	3.8	80.8	30.567
72	107.867	49.5	107.6	125.533	388.9	100.9	63.267	b.d.	15.067	11.3	95.933	0.4	14.3	b.d.	7.633	1.867	33.1	17.467
73	123.167	42.667	120.333	41	231.967	473.133	23.333	13.933	34.833	22.2	184.633	0.6	25.167	0.533	10.2	4.933	120	32.933
74	100.033	73.067	217.133	72.167	173.4	73.733	22.333	4.6	12.967	8.567	83	0.9	14.833	b.d.	2.167	6.133	92.233	21.533
75	-	-	-	-	-	-	-	-	-	-	-	-	-	-	-	-	-	-
76	56.233	68.9	346.867	3601.2	191.133	17.533	55.367	1.333	3.7	3.4	79.633	b.d.	5.667	0.7	10.267	0.9	20.433	10.067
77	132.3	18.2	44.233	2.333	252.633	36.333	18.367	25.133	55.067	33.133	185.6	b.d.	0.5	1.467	2	4.467	158.967	36.667
78	103.4	12.033	40.967	b.d.	288.1	23.667	29.367	20.6	30.067	23.233	152.933	b.d.	0.933	b.d.	2.833	12.067	164.633	43.7
79	78.967	142.233	161.1	481.967	178	540.033	26.9	4.533	9.1	5.267	119.467	b.d.	4.933	0.7	1.633	0.6	29.967	9.7
80	116.433	57.967	61.9	127.367	316.633	24.967	42.1	7.1	18.533	14.733	78.967	0.8	1.767	b.d.	3.033	9.8	111.367	37.9
81	74.5	65.467	109.433	315.4	294.7	17.633	45.2	3.333	9	7.133	67.1	0.467	1.467	b.d.	6.667	5.033	55.767	23.8
82	136.6	98	44.533	71.333	410.8	165.433	45.767	19.6	42.6	27.1	188.4	b.d.	4	0.467	3.8	11.233	171.067	42.333
83	104.8	58.067	113.4	79.833	198.633	410.533	25.667	4.633	17.3	12.5	157.933	0.533	31.233	b.d.	8.9	6.833	134.033	33.867
84	120.633	47.433	218.933	197.267	157.233	180.9	21.467	11.6	25.433	17.633	267.4	b.d.	14.933	b.d.	4.767	8.133	109.5	22.233
85	74.867	15.1	83.633	165.933	365.133	17.433	47.867	38.367	66.933	30.6	347.733	1.633	2.967	7.367	11.133	1	29.733	14.633
Geg	48.5	52.2	205.2	779.6	306.2	23.8	48	4.3	12.6	7.7	36.7	0.4	3.6	b.d.	1.9	2.4	23	15.6
kval	107.2	52.7	75.3	224	401.5	30.2	48.3	1.6	16.5	14.5	182.5	0.5	2.1	b.d.	3.9	3.2	119.5	42.1
Lef1	71.1	41.1	216.7	469.1	242.1	10.2	37.2	9.2	24.3	13.1	170.4	b.d.	1.1	b.d.	1.6	3.3	58.7	19.5
Lef2	49.6	44.5	259.3	783.2	220.4	11.5	34.3	0	5.3	4.8	197.6	b.d.	0.1	b.d.	8.5	5.5	72.6	25.8

C.2.3 LPTS-ICP-MS, Incomplete Dissolutions

Table C.4: Low Pressure Temperature Solution (LPTS) ICP-MS data for Norwegian eclogites in this study. Samples were dissolved using 'standard' hotplate dissolution techniques at room pressure.

Sample	01	08	14	22	30	32	37	41	46	47	51	53	Geg	kval	Lef1	Lef2
Trace element concentration (ppm)																
La	7.92	7.47	11.51	30.00	4.00	6.90	2.77	6.54	4.02	0.43	3.20	15.06	5.49	4.58	12.86	0.72
Ce	18.08	15.69	27.99	61.55	12.62	18.95	9.62	13.50	10.30	1.04	9.26	37.41	13.72	15.47	32.29	3.59
Pr	2.15	1.90	3.64	7.62	2.09	2.79	1.64	1.64	1.37	0.18	1.48	4.90	1.87	2.72	4.20	0.82
Nd	8.21	7.43	15.57	29.92	10.92	13.91	8.74	6.47	6.27	0.98	7.48	20.95	8.12	14.75	17.09	5.25
Sm	1.70	1.50	3.86	6.22	3.62	4.42	2.93	1.12	2.04	0.67	2.93	4.83	1.99	5.26	3.00	2.39
Eu	0.59	0.63	0.98	1.56	1.23	1.48	1.04	0.94	0.85	0.34	1.31	1.51	0.67	1.82	0.88	1.05
Gd	1.67	1.47	4.13	6.10	4.81	5.44	3.48	0.94	2.59	2.00	4.72	5.24	2.32	6.47	3.05	3.71
Tb	0.27	0.22	0.71	1.02	0.99	1.01	0.64	0.11	0.43	0.49	0.87	0.90	0.41	1.14	0.50	0.71
Dy	1.68	1.33	4.55	6.62	6.81	6.81	4.20	0.53	2.60	3.15	5.15	5.40	2.70	7.14	3.23	4.53
Ho	0.34	0.28	0.92	1.38	1.42	1.45	0.87	0.09	0.51	0.57	0.90	0.97	0.55	1.48	0.67	0.92
Er	1.06	0.85	2.65	4.16	4.21	4.34	2.57	0.26	1.43	1.52	2.27	2.48	1.61	4.39	1.99	2.65
Tm	0.17	0.13	0.42	0.68	0.66	0.69	0.38	0.04	0.22	0.23	0.31	0.35	0.25	0.69	0.32	0.42
Yb	1.03	0.83	2.56	4.19	3.95	4.18	2.26	0.23	1.28	1.30	1.68	1.91	1.51	4.17	1.90	2.49
Lu	0.15	0.12	0.38	0.66	0.60	0.63	0.32	0.03	0.18	0.18	0.22	0.27	0.23	0.62	0.29	0.37
Hf	0.79	0.79	1.18	0.62	0.46	0.83	0.37	0.39	0.42	0.37	0.51	0.54	0.72	0.42	0.73	0.61
Pb	6.89	5.68	6.54	8.27	3.10	7.54	2.79	7.42	4.32	3.42	5.12	23.36	3.52	6.15	3.76	9.35
Th	1.39	1.64	1.66	6.79	0.71	0.83	0.46	0.53	0.76	0.31	0.53	0.65	1.19	0.47	0.43	0.23
U	0.37	0.38	0.48	1.31	0.20	0.31	0.08	0.18	0.10	0.03	0.73	0.74	0.15	0.14	0.06	0.03
Sn	0.30	0.15	0.20	0.65	0.21	0.49	0.18	0.15	0.27	0.20	0.45	0.59	0.17	0.17	0.17	0.20
V	2.09	1.48	1.77	2.38	1.70	2.00	1.49	1.31	1.53	2.06	2.48	1.68	1.42	1.61	1.57	1.21
Cr	64.65	135.61	188.72	268.71	343.92	403.70	186.44	34.70	163.48	136.96	217.39	365.56	277.24	358.25	220.60	201.05
Nb	171.95	344.53	149.01	117.50	220.17	85.80	889.38	27.92	100.81	142.54	33.55	503.48	657.19	198.23	383.28	621.82
Mo	1.37	0.19	1.02	9.42	1.12	7.33	0.68	0.42	3.31	1.19	4.98	10.07	0.38	0.95	0.85	1.83
Ta	0.26	0.27	0.39	0.39	0.64	0.34	0.22	0.19	1.46	0.17	1.29	1.01	0.16	0.23	0.36	0.23

C.2.4 HPTS-ICP-MS

Table C.5: High Pressure and Temperature Solution (HPTS) ICP-MS data, collected for Norwegian eclogites in this study using acid digestion vessels at the Scottish Universities Environmental Research Center (SUERC), East Kilbride, Scotland.

Sample	01	08	14	22	30	32	37	41	46	47	51	53	60	64	65	67	69	70	71	72
Trace element concentration (ppm)																				
La	7.08	8.48	11.11	26.82	4.19	6.94	2.71	4.95	4.22	0.76	3.67	13.57	18.86	19.37	7.51	23.06	3.74	18.25	0.3	5.17
Ce	17.39	16.54	26.67	59	12.4	19.27	9.65	9.98	10.32	1.2	10.13	36.44	43.65	55.54	22.95	51.68	9.33	42.44	0.84	13.19
Pr	1.92	1.91	3.25	6.62	1.89	2.71	1.53	1.25	1.24	0.19	1.44	4.42	5.37	7.47	3.4	5.94	1.25	5.31	0.12	1.8
Nd	7.57	7.57	14.37	26.87	10	13.97	8.4	5.18	5.69	1.09	7.45	19.79	22.43	35.39	18.68	23.95	5.87	23.27	0.7	8.87
Sm	1.59	1.55	3.58	5.59	3.36	4.4	2.8	0.93	1.84	0.72	2.95	4.71	4.06	9.34	5.42	4.71	1.56	5.17	0.53	2.52
Eu	0.55	0.64	0.92	1.46	1.19	1.5	0.99	0.77	0.78	0.35	1.34	1.52	1.53	2.56	2.09	0.98	0.99	1.38	0.3	0.65
Gd	1.55	1.52	3.82	5.78	4.72	5.37	3.26	0.74	2.37	2.12	4.93	5.03	3.38	10.25	6.5	4.68	1.65	5.09	2.07	2.59
Tb	0.25	0.23	0.68	1	0.98	1.02	0.61	0.09	0.4	0.5	0.9	0.91	0.42	1.83	1.02	0.74	0.29	0.91	0.61	0.45
Dy	1.54	1.36	4.36	6.56	6.65	6.81	4.01	0.41	2.38	3.17	5.18	5.4	2.08	11.7	5.99	4.5	1.79	6.33	4.79	2.95
Ho	0.32	0.28	0.89	1.37	1.4	1.44	0.84	0.07	0.46	0.58	0.92	0.96	0.36	2.33	1.16	0.94	0.38	1.38	1.06	0.63
Er	0.98	0.85	2.62	4.17	4.12	4.3	2.44	0.2	1.31	1.56	2.3	2.49	0.91	6.6	3.08	2.82	1.18	4.26	3.15	1.82
Tm	0.16	0.14	0.42	0.67	0.65	0.68	0.38	0.03	0.2	0.23	0.32	0.35	0.13	1.01	0.42	0.44	0.19	0.68	0.49	0.27
Yb	0.94	0.84	2.56	4.26	3.95	4.16	2.2	0.16	1.16	1.33	1.73	1.96	0.72	5.98	2.28	2.72	1.2	4.29	2.97	1.55
Lu	0.15	0.13	0.39	0.66	0.59	0.63	0.33	0.03	0.18	0.2	0.23	0.27	0.11	0.91	0.33	0.41	0.19	0.66	0.45	0.23

Continued...

Continued...

Sample	**01**	**08**	**14**	**22**	**30**	**32**	**37**	**41**	**46**	**47**	**51**	**53**	**60**	**64**	**65**	**67**	**69**	**70**	**71**	**72**
Trace element concentration (ppm)																				
Hf	0.99	1.08	2.11	4.13	3.19	3.35	2.12	0.47	1.87	2.05	5.93	4.53	2.32	7.94	0.78	3.06	1.04	7.48	1.89	1.34
Ta	0.12	0.05	0.15	1.22	0.15	0.44	b.d	b.d.	0.24	0.25	0.5	0.86	0.26	0.59	0.36	0.17	0.02	0.48	0.16	0.08
Pb	16.54	3.48	2.65	7.68	5.61	8.71	3	5.45	4.37	2.14	3.68	23.58	7.26	6.71	2.23	11.75	6.62	4	1.54	9.4
Th	2.8	1.3	1.54	6.32	0.5	0.47	0.04	0.06	0.6	0.05	0.29	0.27	1.6	0.84	0.11	3.19	0.2	2.68	0.04	0.79
U	0.92	0.31	0.57	1.25	0.19	0.06	b.d.	b.d.	0.12	0.06	0.88	1.04	0.34	0.46	0.09	1.29	b.d.	0.83	0.05	0.25
V	73.01	140.55	191.17	274.34	342.26	405.62	192.75	37.86	163.63	137.23	228.31	372.01	158.47	329.41	349.93	223.05	213.31	185.97	267.58	358.12
Cr	122.66	370.25	151.3	120.43	230.48	91.4	1017.37	18.39	115	145.76	35.43	505.03	37.58	79.91	33.94	151.35	212.48	227.6	85.47	129.08
Nb	2.35	0.82	3.5	22.46	2.47	8.55	1.15	0.83	4.8	6.88	7.91	16.39	5.38	11.92	6.71	4.34	1.65	10.06	4.12	1.9
Mo	0.82	0.54	0.69	0.8	0.75	0.43	0.45	0.52	1.68	0.67	1.41	1.76	0.85	1.56	0.97	0.59	0.66	0.77	0.65	0.88
Sn	1.56	0.85	1.27	2.04	1.35	1.56	1.1	1.09	1.12	1.35	1.78	1.74	1.22	2.25	0.52	1.5	0.81	1.45	1.39	1.18

Continued...

Continued...

Sample	73	74	75	76	77	78	79	80	81	82	83	84	85	Geg	kval	Lef1	Lef2
La	19.83	3.26	5.47	1.94	23.32	10.94	4.61	6.25	2.41	19.39	6.66	10.44	28.47	5.83	4.64	11.65	0.64
Ce	46.53	9.64	17.92	5.47	51.51	28.34	12.81	16.3	7.54	48.9	19.88	28.22	58.4	15.63	16.42	28.78	3.73
Pr	6.03	1.27	2.74	0.78	6.57	4.11	1.49	2.46	1.03	5.8	2.72	3.53	6.78	1.96	2.61	3.66	0.82
Nd	27.17	6.3	14.66	3.98	29.68	20.45	6.85	12.56	5.35	26.8	13.7	16.25	26.28	8.75	14.61	15.11	5.49
Sm	5.95	2.07	4.7	1.35	6.45	5.36	1.6	4.14	2.05	6.66	4.12	3.89	4.86	2.06	5.19	2.85	2.43
Eu	1.79	0.85	1.39	0.45	2.01	1.74	0.71	1.37	0.8	2.15	1.52	1.37	1.3	0.69	1.83	0.92	1.07
Gd	6.04	2.97	4.98	1.53	7.03	6.82	1.49	5.45	2.79	7.02	4.85	3.92	3.85	2.28	6.27	3.1	3.55
Tb	0.96	0.59	0.85	0.28	1.13	1.19	0.23	1.03	0.56	1.19	0.9	0.64	0.46	0.41	1.12	0.53	0.7
Dy	5.79	3.72	5.38	1.78	6.54	7.49	1.46	6.42	3.85	7.37	5.7	3.9	2.48	2.66	7.04	3.42	4.4
Ho	1.16	0.74	1.13	0.36	1.2	1.47	0.31	1.3	0.83	1.49	1.15	0.77	0.49	0.55	1.46	0.72	0.89
Er	3.36	2.14	3.41	1.06	3.1	3.85	0.93	3.83	2.49	4.32	3.3	2.23	1.46	1.6	4.37	2.14	2.59
Tm	0.51	0.33	0.54	0.16	0.42	0.53	0.15	0.6	0.4	0.66	0.5	0.34	0.23	0.25	0.68	0.33	0.4
Yb	3.11	1.94	3.37	0.96	2.4	2.93	0.89	3.66	2.44	3.99	3.06	2.05	1.46	1.51	4.17	2.08	2.44
Lu	0.47	0.3	0.51	0.15	0.35	0.42	0.14	0.55	0.37	0.6	0.46	0.32	0.23	0.23	0.63	0.32	0.37
Hf	3.53	2.65	2.88	0.84	4.39	3.6	0.87	3	1.83	4.74	3.74	2.94	0.85	0.97	3.44	2.03	2.2
Ta	0.26	0.34	0.12	b.d.	0.17	0.61	b.d.	0.56	0.25	0.64	0.32	0.46	b.d.	0.03	0.09	0.15	0.1
Pb	11.34	2.56	6.47	9.44	2.35	3.83	1.63	5.24	7.22	4.34	9.69	5.82	17.21	1.47	4.04	2.59	9.46
Th	1.61	0.34	0.34	0.15	1.66	0.33	b.d.	0.01	0.06	0.77	0.59	0.28	5.75	0.71	0.08	0.15	0.04
U	0.3	0.37	0.11	0.01	b.d.	0.15	b.d.	0.19	b.d.	0.45	0.34	0.13	1.75	b.d.	b.d.	0.03	0.03
V	222.79	166.57	352.21	194.72	250.04	287.02	174.56	288.47	287.8	395.6	180.44	145.41	335.55	289.54	371.63	232.82	204.57
Cr	50.91	64.78	242.36	3333.61	16.92	6.69	349.96	136.05	261.97	67.58	88.98	205.83	169.3	581.12	226.4	465.21	575.78
Nb	5.68	6.87	3.05	0.98	4.79	13.14	0.61	11.46	5.5	12.49	7.91	9	1.23	2.17	2.19	3.41	5.22
Mo	0.62	0.61	0.53	0.5	0.49	0.76	0.66	0.97	0.57	1.05	0.88	0.83	0.52	0.59	0.5	0.44	0.51
Sn	1.39	1.26	1.58	0.91	1.3	1.47	0.88	1.06	1.03	1.15	1.41	1.3	1.26	0.96	0.98	0.95	1.01

C.2.5 LA-ICP-MS

Table C.6: Geochemical compositions of rutiles from Norwegian eclogites as acquired by LA-ICP-MS at The University of Portsmouth in collaboration with Craig Storey. All concentrations are expressed in parts per million (ppm). Analysis code has the format R-[sample number]-[grain number]-[grain acquisition number].

Analysis	Al	Si	Sc	V	Cr	Zn	Ga	Sr	Zr	Nb	Mo	Sn	Sb	Hf	Ta	W	Pb	U
R08-03-01	267.03	373.64	2.17	779.93	1811.53	11.52	0.37	0.51	103.12	170.49	3.96	8.58	4.35	4.35	8.92	68.52	0.03	0.11
R08-03-02	153.54	353.99	1.90	770.18	1830.88	12.78	0.40	0.48	105.01	179.34	4.08	8.70	4.17	4.72	4.64	88.22		0.10
R08-08-01	37.37	330.15	2.98	603.49	1477.26	12.47	0.18	0.45	96.81	172.60	4.19	7.46	3.03	4.18	18.98	101.53		0.15
R08-08-02	36.24	382.83	3.01	600.60	1694.43	13.33	0.13	0.45	94.67	241.77	4.16	8.07	4.84	3.83	25.19	120.46		0.23
R08-09-01	296.73	361.18	1.77	1172.80	1284.52	12.54	0.58	0.47	80.92	89.89	4.31	6.82	5.63	4.71	3.81	112.90		0.02
R08-10-01	151.55	387.48	1.56	1170.73	1292.29	13.08	0.51	0.48	83.77	88.08	4.67	6.92	5.59	4.58	3.98	112.31		0.02
R08-12-01	48.12	414.02	1.15	1071.21	336.42	13.70	0.19	0.42	210.85	550.47	12.76	25.87	1.82	7.57	30.29	35.78		2.91
R08-12-02	51.32	427.04	1.26	1055.15	332.63	10.70	0.18	0.43	219.79	582.08	12.88	27.32	1.81	7.80	28.00	35.65		2.85
R08-14-01	31.20	353.74	1.10	848.65	2325.95	12.80	0.18	0.44	103.24	173.21	4.29	7.59	4.68	4.67	13.10	110.33		0.16
R08-14-02	39.38	296.09	1.06	863.76	2350.35	12.67	0.14	0.50	100.72	181.94	4.27	7.39	4.48	4.48	12.62	109.62		0.10
R08-16-01	49.93	371.71	2.06	1113.92	1099.59	12.49	0.23	0.40	90.77	73.80	4.11	5.71	5.05	4.20	2.95	108.76	0.01	0.02
R14-01-01	93.08	434.16	1.09	793.39	1852.55	20.50	0.15	0.54	89.31	268.50	4.90	10.62	5.39	4.10	14.25	2108.65	0.19	0.07
R14-01-02	102.47	428.84	1.57	794.14	1840.46	21.52	0.11	0.44	89.17	232.13	5.14	11.56	5.70	4.12	4.56	1699.30		0.06
R14-01-03	77.44	414.00	1.45	831.64	1723.52	22.16	0.10	0.48	84.87	270.61	5.56	12.60	5.29	3.76	12.75	2178.12		0.07

Table C.6: Continued...

Analysis	Al	Si	Sc	V	Cr	Zn	Ga	Sr	Zr	Nb	Mo	Sn	Sb	Hf	Ta	W	Pb	U
R14-08-01	74.65	385.48	1.83	702.37	1324.28	16.42	0.09	0.47	88.78	403.34	6.05	14.14	5.53	3.99	24.36	2848.84	0.01	0.13
R14-08-02	86.80	474.27	1.44	726.58	1329.57	16.41	0.12	0.48	95.27	420.22	5.63	12.46	5.56	3.77	25.37	2972.09		0.12
R14-08-03	61.79	456.69	1.60	745.46	1210.41	16.57	0.17	0.50	91.78	424.12	5.50	13.77	5.19	3.77	26.96	2928.52		0.13
R14-10-01	26.79	387.92	1.65	731.75	2160.39	20.41	0.05	0.45	77.87	447.73	5.75	14.44	5.24	3.47	26.93	2967.80	0.01	0.07
R14-10-02	31.40	325.44	2.29	754.29	2153.62	16.65	0.04	0.52	68.38	476.73	6.39	16.11	4.79	3.60	30.54	2662.48		0.09
R14-10-03	27.65	358.09	2.48	738.37	2152.72	17.54	0.04	0.47	77.73	438.75	6.04	14.32	4.38	3.97	26.73	2509.50		0.06
R14-12-01	39.33	422.62	1.99	733.81	1300.37	15.14	0.11	0.52	96.03	406.58	5.03	10.82	5.62	3.76	22.53	2497.24	0.02	0.19
R14-12-02	38.89	449.96	1.90	739.63	1427.21	15.76	0.09	0.42	100.81	406.37	5.29	11.00	5.37	3.89	21.33	2508.64	0.02	0.24
R14-12-03	40.91	463.33	2.07	779.29	1406.38	15.59	0.09	0.49	98.89	412.09	5.11	11.56	5.94	3.67	22.04	2511.06		0.25
R14-13-01	45.30	443.78	1.71	881.24	1130.59	16.40	0.20	0.53	93.57	458.05	5.60	11.76	5.37	4.13	31.24	2728.12	0.04	0.08
R14-13-02	75.46	479.07	2.02	867.51	1029.57	16.31	0.26	0.48	85.94	467.58	7.42	14.12	4.99	4.00	33.47	2361.11	0.01	0.09
R14-13-03	45.28	413.55	1.91	877.43	1329.38	18.03	0.18	0.51	96.78	486.71	6.56	13.29	5.29	4.00	35.81	2770.17		0.10
R14-15-01																		
R14-15-02	53.09	366.34	2.22	856.68	1412.03	15.44	0.20	0.54	90.26	457.62	5.86	13.51	5.22	3.83	32.76	2967.55		0.05
R14-16-01	80.97	432.79	5.49	1832.41	831.79	15.79	0.24	0.90	217.10	136.62	8.22	26.68	2.13	9.17	10.55	2.96	0.07	0.08
R14-16-02	85.53	424.34	4.79	1842.42	826.65	15.89	0.25	0.46	221.21	132.57	8.30	28.98	2.26	8.75	11.60	2.06		0.03
R14-16-03	61.46	470.38	5.38	1847.45	823.88	14.86	0.24	0.52	224.72	128.60	9.74	29.81	2.08	8.79	11.36	1.79		0.02
R30-04-01	74.03	643.91	1.27	1742.32	1399.27	13.69	0.33	0.70	206.32	128.98	10.35	31.72	2.21	8.34	7.96	1.49	0.15	0.08
R30-04-02	71.13	426.18	1.37	1740.86	1348.69	16.82	0.36	0.51	146.16	128.79	10.63	29.06	1.95	6.15	10.40	1.66	0.01	0.05
R30-04-03	58.19	487.20	1.54	1766.71	1326.70	16.17	0.17	0.45	189.58	117.38	11.00	29.88	2.02	7.76	9.83	1.49		0.08

Table C.6: Continued...

Analysis	Al	Si	Sc	V	Cr	Zn	Ga	Sr	Zr	Nb	Mo	Sn	Sb	Hf	Ta	W	Pb	U
R30-08-01	97.05	353.87	3.01	1573.92	1191.33	14.70	0.24	0.72	250.29	192.16	11.28	38.74	2.56	9.52	10.04	1.68		0.06
R30-08-02	160.20	430.75	2.91	1563.26	1191.26	16.05	0.35	0.53	232.43	149.04	9.99	31.11	2.09	9.01	7.21	1.58	0.01	0.06
R30-08-03	83.00	438.70	2.22	1557.53	1153.34	15.34	0.15	0.51	192.53	128.79	10.59	28.95	1.96	7.92	8.39	1.43		0.02
R30-09-01	73.81	409.60	1.41	1958.48	1061.85	16.62	0.35	0.49	205.55	129.14	9.62	28.41	1.82	7.60	7.85	1.38	0.01	0.10
R30-09-02	104.30	424.33	1.58	1969.49	1070.63	16.42	0.45	0.48	198.38	124.83	9.18	27.31	1.90	7.29	7.85	1.54		0.16
R30-13-01	65.61	463.36	1.73	2027.97	1199.90	17.48	0.80	0.52	198.39	126.09	4.51	33.44	1.81	8.21	6.96	2.03		0.06
R30-14-01	71.81	445.53	1.96	1756.25	632.24	15.87	0.32	0.52	205.00	130.11	9.13	26.74	1.93	8.02	8.57	1.34	0.03	0.10
R30-14-02	135.93	440.12	1.91	1750.66	634.22	16.67	0.72	0.43	226.50	130.99	10.14	27.72	2.28	8.90	9.22	1.57		0.29
R30-14-03	130.37	419.25	2.05	1751.96	630.23	16.25	0.84	0.48	168.09	120.03	9.35	27.37	1.95	6.25	8.67	1.52		0.06
R30-19-01	75.56	388.88	2.35	1821.08	1037.66	15.72	0.22	0.50	222.02	123.16	10.35	26.84	2.01	9.14	9.84	1.51	0.01	0.19
R30-20-01	101.60	402.63	1.84	1742.46	892.10	14.90	0.28	0.52	215.27	113.20	8.24	26.58	1.95	8.53	8.95	1.52	0.01	0.25
R30-20-02	80.55	419.53	2.00	1746.81	887.08	16.04	0.21	0.51	171.78	113.76	8.86	27.37	1.95	6.87	8.51	1.53	0.04	0.06
R30-21-01	74.47	490.40	1.93	1564.15	582.13	15.68	0.34	0.57	195.65	115.89	10.19	27.81	1.98	5.72	7.86	1.46	0.02	0.27
R32-01-01	60.20	421.04	1.86	1445.65	112.14	16.83	0.35	0.44	113.83	93.30	3.90	20.85	0.93	5.01	9.18	3.54		0.01
R32-01-02	122.64	377.22	1.65	1414.32	109.18	16.23	0.39	0.46	111.07	97.29	4.15	18.61	0.86	3.91	8.74	4.04		
R32-11-01	117.05	371.20	6.06	1770.31	1268.80	16.42	0.24	0.40	221.64	670.82	10.64	16.81	2.46	8.00	41.20	6.30		0.25
R32-14-01	129.30	425.02	2.77	1868.75	345.26	16.47	0.17	0.47	218.03	677.39	7.75	23.07	18.28	8.69	28.57	46.82		0.12
R32-14-02	138.13	389.12	2.52	1842.65	347.06	16.29	0.32	0.45	222.18	583.52	7.53	21.54	19.10	8.96	34.40	44.56		0.12
R32-15-01	40.27	410.31	3.41	790.54	1212.40	17.11	0.13	0.51	103.51	254.90	4.14	8.04	5.60	4.26	16.88	2200.33	0.06	0.35
R32-15-02	53.84	340.85	1.82	772.09	1246.74	16.32		0.40	95.65	255.69	4.24	9.24	5.75	4.37	9.29	1400.95	0.02	0.22

Table C.6: Continued...

Analysis	Al	Si	Sc	V	Cr	Zn	Ga	Sr	Zr	Nb	Mo	Sn	Sb	Hf	Ta	W	Pb	U
R32-16-01	114.46	449.53	2.23	2375.01	966.05	19.83	0.33	0.46	190.08	786.82	8.51	33.27	5.89	6.75	37.77	47.60	0.01	1.39
R32-16-02	150.24	410.99	2.19	2312.09	956.63	19.04	0.34	0.45	173.44	780.86	9.30	38.68	5.61	5.84	28.03	38.11		1.19
R32-17-01	33.91	348.39	1.42	2036.51	322.20	17.33	0.29	0.50	185.57	481.34	6.25	21.42	15.00	6.62	34.85	24.38		0.08
R32-17-02	25.08	383.37	1.82	2047.98	326.30	16.80	0.23	0.51	188.52	470.93	6.91	20.42	17.54	6.66	25.42	40.65		0.09
R32-20-01	100.74	390.20	2.32	1945.69	732.19	17.46	0.95	0.55	136.16	1583.34	10.45	48.73	5.74	6.28	123.02	33.69		1.38
R32-20-02	129.20	380.85	2.55	1958.92	738.52	16.50	1.24	0.51	132.53	1619.07	10.35	46.77	5.58	5.78	130.45	34.36	0.23	1.44
R37-04-01	62.03	418.36	1.52	1395.91	13.48	16.18	0.04	0.49	145.46	97.95	3.81	17.68	0.41	6.30	7.53	3.00		
R37-04-02	150.56	383.42	1.26	1361.84	14.69	15.93		0.55	186.04	95.42	3.44	17.35	0.60	6.97	6.77	2.68		
R37-06-01	120.06	426.14	2.52	958.51	798.50	14.49	0.04	0.44	122.05	116.88	4.46	28.22	1.36	5.12	7.46	4.34		
R37-06-02	98.36	428.93	2.48	960.19	792.02	13.81	0.09	0.53	108.53	113.41	4.35	27.01	1.30	4.93	6.90	3.67		0.01
R37-06-03	105.16	449.18	3.33	956.96	783.07	13.99		0.41	109.53	108.20	4.34	31.65	1.10	5.61	7.34	4.24	0.01	0.01
R37-07-01	132.51	402.26	4.17	1187.71	1167.24	15.59	0.47	0.53	309.47	125.71	3.98	15.51	0.91	14.09	14.41	4.44		0.14
R37-07-02	114.22	437.36	4.58	1209.12	1155.05	14.86	0.53	0.55	339.44	127.53	4.39	16.44	1.12	15.52	14.16	4.49		0.13
R37-08-01	54.58	373.25	2.67	1466.20	97.02	15.47	0.04	0.53	158.37	88.83	4.46	20.91	0.67	7.19	5.98	3.96	0.01	0.01
R37-08-02	82.32	449.43	2.65	1479.41	92.00	17.22		0.50	150.07	87.84	4.04	21.75	0.70	6.46	5.03	3.84		0.00
R37-08-03	78.76	476.51	2.84	1442.01	96.31	16.93	0.07	0.53	151.57	87.66	4.33	21.12	0.67	6.75	5.27	3.55		
R37-09-01	63.42	394.25	2.90	1599.72	4311.17	13.51	0.25	0.48	134.32	90.92	4.16	21.97	0.88	6.85	4.32	5.68	0.03	0.03
R37-09-02	43.15	403.85	2.86	1656.87	4433.74	12.45	0.15	0.40	134.68	89.28	3.81	25.35	1.45	6.54	4.17	5.83		0.02
R37-19-03	60.15	423.00	1.77	1399.55	115.05	14.70	0.20	0.42	89.67	112.35	3.77	16.23	0.88	3.68	12.12	3.28		0.03
R46-01-01	104.40	409.20	0.69	971.43	391.95	13.96	0.62	0.43	204.21	466.55	11.58	22.84	2.15	7.34	29.13	35.27		3.17

Table C.6: Continued...

Analysis	Al	Si	Sc	V	Cr	Zn	Ga	Sr	Zr	Nb	Mo	Sn	Sb	Hf	Ta	W	Pb	U
R46-06-01	113.29	389.88	1.83	1032.72	387.60	12.21	0.14	0.51	198.79	470.91	13.51	25.90	1.96	7.11	27.41	34.61	0.01	3.24
R46-06-02	95.50	355.13	1.11	1042.88	392.92	12.46	0.10	0.44	175.56	444.69	13.47	27.78	1.54	5.57	24.03	32.62		3.16
R46-08-01	177.60	383.86	0.54	1054.76	349.84	10.87	0.76	0.48	191.09	451.09	11.36	25.12	2.10	6.92	30.86	33.19		2.93
R46-08-02	101.08	428.62	0.45	1052.34	345.69	11.35	0.79	0.51	191.91	488.70	11.40	25.26	2.07	7.12	31.08	34.32	0.57	2.15
R46-09-01	33.73	341.22	1.15	1134.58	281.47	15.15	0.13	0.50	191.54	465.65	11.82	27.22	1.77	6.95	27.54	33.26		3.69
R46-09-02	27.50	403.32	1.25	1123.37	280.86	15.13	0.08	0.43	188.35	458.17	11.33	26.04	1.40	6.41	28.22	29.72		3.73
R46-11-01	160.44	364.07	0.67	1068.20	524.09	14.41	0.65	0.46	197.36	466.12	12.73	25.34	2.28	7.09	27.45	37.02		2.86
R46-11-02	86.38	428.57	0.69	1056.32	541.48	12.65	0.59	0.51	197.59	466.37	13.40	27.08	2.00	7.24	28.04	36.27	0.04	2.95
R46-16-01	35.46	407.33	1.30	1107.93	288.30	14.18	0.11	0.50	190.36	471.90	10.36	26.23	1.89	7.37	26.20	35.34		3.09
R46-16-02	42.81	356.27	1.07	1118.54	281.50	14.97	0.20	0.49	183.46	469.36	11.66	27.97	1.47	6.17	26.04	33.31		3.27
R46-17-01	244.53	396.73	0.94	1090.22	276.57	14.97	0.32	0.49	205.44	477.21	11.00	25.49	2.17	7.58	25.37	36.37		3.42
R46-18-01	57.52	398.18	1.84	1021.36	399.47	12.79	0.23	0.52	209.47	484.38	15.52	28.43	2.23	7.45	26.40	36.27		2.76
R46-18-02	224.18	421.21	1.49	1049.18	398.81	13.38	0.26	0.49	212.03	504.16	14.98	27.94	2.20	7.45	26.89	39.19	0.03	3.44
R46-19-01	78.17	369.66	1.58	1101.99	448.09	13.19	0.10	0.49	213.56	482.18	14.33	26.67	2.08	7.56	28.71	37.61		3.65
R46-22-01	37.14	367.53	1.81	1061.04	830.24	11.15	0.10	0.46	204.50	495.09	10.40	24.75	1.86	7.56	27.59	35.59		3.38
R51-04-01	87.72	337.23	1.50	1091.16	65.14	13.62	0.24	0.50	126.19	275.75	19.91	37.48	1.75	4.23	18.13	40.84		11.57
R51-05-01	81.38	456.23	1.33	926.75	61.49	14.45	0.45	0.51	147.52	229.60	20.16	37.29	2.45	5.79	17.38	53.59		9.75
R51-06-01	71.04	416.21	0.73	969.01	75.25	15.11	0.69	0.45	147.51	242.09	18.15	40.34	2.31	5.79	23.47	51.77		9.86
R51-08-01	106.46	401.12	0.43	949.47	67.39	15.16	1.04	0.51	114.31	245.88	20.96	40.65	2.02	3.93	17.06	41.20	0.05	12.76
R51-12-01	86.87	444.61	0.98	956.53	70.05	20.02	0.60	0.49	146.43	262.25	19.11	41.33	2.36	5.62	11.91	50.77	0.12	10.51

Table C.6: Continued...

Analysis	Al	Si	Sc	V	Cr	Zn	Ga	Sr	Zr	Nb	Mo	Sn	Sb	Hf	Ta	W	Pb	U
R51-13-01	84.67	380.52	1.12	824.78	72.24	15.41	0.22	0.49	152.09	228.54	20.26	37.64	2.42	5.28	17.60	50.89		10.21
R51-14-01	94.48	470.51	1.54	1108.82	57.05	16.93	0.29	0.42	147.64	302.18	19.94	40.92	2.07	4.65	19.57	41.35		11.04
R51-16-01	96.48	394.95	0.95	940.19	69.08	16.14	1.23	2.61	138.18	260.62	19.41	39.98	2.14	5.55	22.94	54.25	3.15	10.55
R51-17-01	71.26	331.59	2.56	1010.77	60.03	14.96	0.81	0.45	149.90	268.29	19.21	40.22	2.33	5.91	22.48	51.72		10.46
R53-01-01	136.37	560.40	1.03	1859.21	880.77	16.43	0.09	18.22	236.59	765.99	57.54	47.84	15.43	8.28	32.06	55.03	2.63	41.52
R53-02-01	196.58	346.35	1.02	1927.03	1104.08	16.97	0.22	0.53	258.27	764.46	56.56	48.04	15.01	9.16	48.08	64.57		43.33
R53-03-01	125.73	305.13	0.80	1901.64	1060.25	17.21	0.05	0.40	254.59	802.22	55.79	47.50	14.86	9.20	59.56	90.31		39.70
R53-07-01	165.84	387.31	1.41	2089.79	1300.97	16.36	1.16	0.39	252.90	750.34	54.26	46.49	15.12	9.62	29.72	67.87		42.06
R53-07-02	188.01	591.88	1.49	2083.66	1259.65	16.43	1.04	0.56	247.36	728.36	53.97	46.53	15.38	8.46	30.04	49.99	0.17	42.53
R53-09-01	301.44	353.71	1.20	2089.93	1121.77	17.05	0.14	0.46	264.23	769.63	53.97	47.92	15.10	9.37	50.70	126.17	0.03	43.67
R53-09-02	75.24	375.40	1.18	2028.21	1119.94	16.03		0.52	252.01	757.97	53.97	46.95	14.64	9.07	48.51	116.93		43.36
R53-12-01	255.96	395.74	1.16	1915.98	1163.08	13.50	0.28	0.43	250.99	763.53	55.25	45.17	14.91	9.60	44.08	165.69		42.79
R53-18-01	236.08	879.43	0.73	2021.98	1219.12	22.94	0.30	0.56	234.83	732.38	56.40	46.47	14.78	8.37	43.38	51.27	0.93	40.39
R53-19-01	189.32	362.24	0.83	2259.41	1209.65	15.05	0.75	0.54	300.73	735.87	53.32	44.55	15.05	11.77	41.70	127.26	0.03	41.89
R53-19-02	256.62	913.87	0.95	2272.83	1239.74	17.56	0.77	0.49	262.77	717.22	52.94	45.20	14.54	9.52	43.96	97.99	0.30	41.66
R53-19-03	130.69	398.00	0.76	2264.51	1236.49	15.33	0.81	0.53	264.16	700.10	53.79	42.52	15.18	9.58	43.43	113.98		41.19
R53-20-01	70.63	394.42	0.65	2086.25	1216.54	16.36	0.63	0.48	250.16	762.32	55.47	46.13	14.61	8.88	44.42	70.78		41.82
R53-20-02	68.11	381.88	0.61	2010.47	1205.77	16.26	0.56	0.47	244.03	746.52	52.02	47.04	13.48	9.01	37.08	167.35		40.81
R53-21-01	45.39	475.19	0.66	2021.09	1131.32	15.11	0.67	0.53	256.60	781.18	54.88	47.04	16.08	8.98	41.66	59.15	1.92	42.15
R63-01-01	49.25	351.47	1.81	1236.13	260.88	12.33	0.31	0.49	132.69	246.54	19.71	32.36	0.26	5.85	19.72	9.33		0.51

Table C.6: Continued...

Analysis	Al	Si	Sc	V	Cr	Zn	Ga	Sr	Zr	Nb	Mo	Sn	Sb	Hf	Ta	W	Pb	U
R63-01-01	81.84	403.49	2.98	1255.65	409.09	14.43	0.23	0.55	142.08	217.41	23.04	34.56	0.23	6.49	18.96	9.63		0.17
R63-01-02	54.53	416.09	1.49	1352.66	285.06	12.86	0.43	0.51	117.91	270.87	28.30	35.22	0.29	5.51	18.33	9.27		0.66
R63-02-01	15.88	374.13	1.08	1287.83	377.45	15.55	0.29	0.43	97.84	274.01	23.72	36.12	0.23	5.05	14.87	7.12		0.62
R63-05-01	62.72	379.93	1.03	1132.81	230.69	12.79	0.48	0.45	136.53	239.32	24.73	38.05	0.21	5.61	16.37	10.29	0.01	0.34
R63-05-02	71.50	406.18	1.05	1119.72	231.84	12.92	0.50	0.46	103.70	253.00	25.33	37.35	0.20	4.58	12.14	5.03		0.41
R63-06-01	45.12	419.58	1.12	1353.74	158.32	14.80	0.88	0.45	89.88	269.79	25.16	40.18	0.18	4.58	14.21	5.31		0.47
R63-06-02	50.25	408.13	0.97	1290.65	158.69	14.57	0.82	0.49	87.94	265.18	24.83	37.94	0.21	4.30	15.60	5.24		0.39
R63-09-01	129.88	569.77	1.58	1352.35	160.19	15.81	0.41	0.79	95.94	268.49	24.26	34.82	0.15	3.94	11.59	1.94	0.04	0.56
R63-09-02	91.37	391.85	1.65	1352.67	168.59	14.05	0.48	0.53	119.56	257.07	23.29	34.54	0.29	5.13	19.08	9.10		0.56
R63-10-01	169.14	374.10	1.49	1350.78	179.56	14.22	1.06	0.48	118.71	315.72	24.65	40.80	0.27	5.48	18.98	8.24		0.49
R63-10-02	105.23	391.92	1.77	1315.80	172.83	12.65	0.94	0.47	119.03	290.25	23.06	38.02	0.21	5.54	17.98	7.85		0.43
R63-12-01	131.25	419.23	1.89	1258.74	163.45	14.24	0.76	0.47	132.21	272.34	22.43	37.85	0.27	5.74	15.07	8.66		0.14
R63-15-01	94.37	422.58	1.94	1212.04	308.05	12.67	0.28	0.51	144.40	264.15	23.88	35.77	0.17	5.63	17.37	5.60	0.06	0.27
R63-16-01	94.07	414.16	1.08	1198.57	293.81	15.72	0.49	0.43	126.79	280.08	23.92	40.11	0.23	5.80	20.30	8.74		0.32
R63-16-02	171.47	425.52	0.80	1219.54	294.44	14.76	0.67	0.49	76.98	325.24	24.13	40.82	0.15	5.69	19.01	3.07		0.44
R65-01-01	283.02	377.22	1.66	1304.45	23.12	16.87	0.54	0.46	90.08	144.32	7.97	2.05	2.15	3.90	10.67	0.83		0.39
R65-02-01	296.66	393.31	2.16	1216.90	49.81	15.94	0.53	0.47	84.01	104.21	7.83	2.28	2.29	3.92	5.35	0.94		0.75
R65-02-02	305.85	424.33	1.81	1214.04	50.31	15.48	0.33	0.45	74.50	131.50	7.92	2.57	2.20	3.60	9.62	0.94		0.78
R65-05-01	122.62	386.83	1.68	1263.53	73.50	17.12	0.58	0.59	90.38	123.86	8.91	2.44	2.07	4.17	7.03	1.01		0.82
R65-08-01	143.79	470.66	1.19	1314.45	66.59	16.12	0.43	0.50	84.13	141.32	8.05	2.29	2.34	3.64	10.53	1.00		0.83

Table C.6: Continued...

Analysis	Al	Si	Sc	V	Cr	Zn	Ga	Sr	Zr	Nb	Mo	Sn	Sb	Hf	Ta	W	Pb	U
R65-08-02	155.26	485.76	1.46	1305.31	67.26	17.20	0.49	0.47	80.47	168.54	7.11	2.38	2.38	3.60	12.72	0.88		0.80
R65-09-01	126.52	446.05	1.65	1350.61	25.43	17.03	0.65	0.48	85.15	164.90	7.94	2.13	1.97	3.88	12.38	0.88	0.01	0.63
R65-11-01	100.35	401.86	1.45	1213.22	71.59	17.05	0.46	0.52	97.83	138.62	8.41	2.19	2.33	4.30	8.38	1.09		0.77
R65-13-01	105.87	452.20	1.85	1132.47	42.03	17.23	0.32	0.46	80.89	133.87	7.88	2.27	2.01	3.79	9.94	0.91		0.84
R65-14-01	156.92	386.31	1.33	1288.82	33.35	19.36	0.49	0.50	74.12	152.65	7.96	2.25	2.45	3.60	12.92	1.04		0.73
R65-16-01	130.01	367.16	2.88	1323.03	32.59	20.79	0.39	0.56	91.99	121.03	8.47	1.94	1.79	3.67	7.08	0.94		0.86
R65-17-01	101.09	394.14	1.67	1106.34	44.38	18.09	0.36	0.44	86.29	129.37	8.16	2.13	2.18	4.10	6.91	0.87		0.89
R67-01-01	100.22	453.05	3.69	872.48	884.40	20.85	0.09	0.45	77.54	572.76	8.72	32.80	10.92	4.41	45.99	29.95	0.01	0.33
R67-02-01	170.21	439.06	1.20	1038.33	494.29	19.65	0.38	0.41	75.14	565.04	7.63	32.71	10.33	4.12	40.26	30.00		0.17
R67-02-02	121.26	426.78	1.05	1022.17	561.55	19.90	0.34	0.49	92.75	556.89	8.22	27.42	11.76	4.25	39.11	29.59		0.33
R67-03-01	230.92	418.77	2.40	947.93	753.48	20.17	0.40	0.45	82.90	616.67	9.18	32.82	11.29	4.14	38.33	29.83	0.01	0.17
R67-06-01	132.79	476.85	1.92	1053.84	735.61	19.17	0.25	0.41	89.57	519.36	9.14	34.43	12.23	4.46	34.37	26.61		0.33
R67-07-01	68.19	458.87	1.49	1145.19	656.32	20.44	0.31	0.48	79.20	493.12	9.10	33.31	9.94	4.22	32.64	24.96		0.28
R67-11-01	82.39	435.55	1.74	1076.87	623.86	18.97	0.36	0.52	87.39	507.45	9.41	32.47	11.52	4.26	29.01	26.14		0.21
R67-12-02																		
R67-13-01	184.89	457.01	1.76	998.42	959.66	18.29	0.38	0.50	69.87	479.63	8.23	34.62	10.92	3.80	27.80	27.52		0.27
R67-13-02	170.69	432.25	1.94	979.07	954.64	18.27	0.29	0.41	66.96	470.07	8.24	24.74	11.21	3.66	22.45	23.85		0.27
R67-16-01	81.54	463.50	1.87	1099.68	523.03	19.62	0.14	3.03	62.68	486.45	7.26	19.97	11.96	3.90	22.33	30.17	0.38	0.26
R67-19-01	95.58	350.46	1.11	897.24	640.35	21.17	0.25	0.49	67.29	457.84	7.82	25.54	10.17	3.54	19.99	27.45		0.32
R67-19-02	75.10	349.68	1.39	897.64	662.88	18.64	0.24	0.76	76.72	443.38	7.85	23.08	12.53	4.11	11.83	28.94		0.37

Table C.6: Continued...

Analysis	Al	Si	Sc	V	Cr	Zn	Ga	Sr	Zr	Nb	Mo	Sn	Sb	Hf	Ta	W	Pb	U
R67-19-03	141.20	347.33	1.45	935.14	669.66	20.52	0.23	0.51	84.95	519.68	9.12	26.52	11.06	4.31	28.15	32.98		0.47
R69-01-01																		
R69-04-01	78.53	424.79	1.78	972.54	1791.60	13.73	0.30	0.58	83.86	117.05	2.60	7.06	14.44	3.87	5.61	3.79	0.23	0.06
R69-05-01																		
R69-05-02	141.05	360.02	5.49	1657.01	177.67	13.26	1.01	0.51	272.28	637.05	19.99	39.88	1.59	7.91	29.55	3.77		3.98
R69-11-01	79.03	362.70	4.09	1890.11	280.33	14.42	1.00	0.52	235.50	469.06	19.47	26.52	1.74	8.03	29.62	3.49		5.99
R69-12-01	52.51	463.91	0.81	879.58	2097.27	13.79	0.21	0.49	77.15	212.17	3.05	6.13	14.82	5.16	14.62	2.52	0.03	0.10
R69-16-01	42.20	375.79	0.86	838.12	5277.93	13.48	0.13	0.43	82.42	232.44	3.34	6.73	17.77	6.88	16.28	6.52	0.14	0.07
R69-19-01	62.62	408.46	1.26	882.36	3616.82	14.77	0.20	0.51	78.57	143.05	3.40	7.85	22.81	5.24	8.43	5.90		0.09
R69-20-01	148.72	369.15	1.10	840.73	1099.67	14.61	0.15	0.42	72.39	192.54	2.19	5.22	13.49	3.05	11.39	2.20		0.13
R69-23-01	53.07	371.09	6.07	1918.17	224.35	15.26	0.84	0.50	281.79	612.01	21.98	34.10	1.82	9.97	37.62	3.79		5.88
R69-23-02	89.88	297.68	5.24	1806.33	220.18	15.98	0.53	0.45	252.55	583.50	18.89	31.35	1.56	8.54	39.03	3.46		5.76
R70-04-01	104.06	383.94	3.15	853.42	574.12	10.33	0.67	0.43	144.33	995.03	9.07	36.87	10.97	4.35	45.50	24.87		4.36
R70-07-01	36.30	390.59	17.11	547.48	267.19	10.95	0.13	0.51	186.01	1164.59	12.11	37.68	8.49	7.35	48.22	31.38		4.41
R70-09-01	58.82	385.78	1.19	1284.71	168.77	11.48	0.53	0.46	152.53	312.16	24.50	43.83	0.23	6.34	16.11	10.25		0.48
R70-09-02	45.62	428.84	0.99	1320.43	170.16	11.62	0.47	0.48	148.54	297.32	23.47	44.55	0.24	6.36	16.73	10.33		0.57
R70-12-01	114.85	592.64	1.91	1214.69	194.99	11.70	0.42	0.55	135.70	271.49	21.41	35.23	0.27	5.95	16.94	10.74	0.05	0.65
R70-12-02	52.03	407.18	1.67	1238.77	204.49	11.48	0.45	0.50	119.00	304.01	23.59	38.31	0.28	5.38	18.52	9.29		0.55
R70-12-03	48.35	373.34	1.69	1224.11	201.60	11.38	0.50	0.49	107.80	305.19	24.09	37.78	0.21	5.41	16.64	8.26		0.50
R70-12-04	31.40	390.09	2.09	1240.62	204.58	11.50	0.40	0.47	121.37	304.35	22.91	38.02	0.21	5.23	14.83	9.61		0.63

Table C.6: Continued...

Analysis	Al	Si	Sc	V	Cr	Zn	Ga	Sr	Zr	Nb	Mo	Sn	Sb	Hf	Ta	W	Pb	U
R70-17-01	83.17	386.59	1.31	1234.17	156.91	12.15	0.49	0.46	127.90	331.77	22.22	38.13	0.22	5.62	16.09	9.83		0.48
R70-17-02	79.64	394.41	0.96	1237.69	161.29	11.89	0.56	0.47	126.90	260.30	23.29	36.74	0.25	5.41	17.52	9.41		0.60
R70-20-01	69.21	370.03	1.78	1285.38	314.36	13.34	0.36	0.64	154.89	295.85	22.89	37.61	0.26	6.30	12.75	10.62	0.06	0.41
R71-02-01	143.70	350.98	1.49	748.39	1267.93	14.19	0.20	0.38	125.22	863.45	19.80	26.46	3.14	4.77	34.01	12.33		1.01
R71-03-01	99.84	346.47	3.34	717.94	2047.53	13.83	0.28	0.45	113.03	749.75	16.47	23.47	3.35	4.33	26.83	13.98		1.12
R71-06-01	168.90	396.16	2.10	743.75	1097.89	13.61	0.37	0.50	178.32	699.66	17.62	24.23	4.64	6.63	32.98	14.82		1.19
R71-08-01	116.89	401.72	1.46	1863.84	225.12	14.40	0.33	0.50	135.65	458.83	4.90	50.53	9.27	6.37	24.51	21.30		0.06
R71-08-02	157.00	351.09	1.28	1836.37	218.17	14.37	0.74	0.52	129.75	458.24	5.67	50.47	10.04	5.34	22.33	19.90		0.06
R71-09-01	244.54	336.83	1.33	712.67	1281.13	14.07	0.69	0.44	127.81	700.77	16.40	24.60	2.25	4.44	26.32	11.83		0.86
R71-11-02	53.28	403.95	0.25	717.22	1423.72	15.06	0.43	0.50	193.63	827.01	17.33	23.00	4.44	6.87	38.00	15.64		1.03
R71-13-01	77.88	392.19	0.85	698.98	2109.36	14.59	0.47	0.43	155.49	799.88	18.83	22.31	5.02	5.40	23.52	15.69		1.22
R71-14-01	92.12	347.19	0.90	717.10	1338.01	13.94	0.35	0.41	137.62	941.39	17.40	24.13	3.08	4.46	33.38	14.23		0.86
R72-01-01	120.77	420.38	5.67	1780.66	278.96	14.91	0.27	0.41	151.15	169.46	16.45	39.05	26.52	8.04	8.27	117.13		3.58
R72-05-01	59.73	382.69	18.03	1346.89	262.52	25.35	0.19	0.47	243.53	314.47	32.47	38.41	20.08	11.31	11.53	71.75	0.01	4.77
R72-08-01	48.88	354.21	1.33	2070.17	365.90	12.39	0.26	0.46	142.59	272.15	19.67	34.31	22.94	7.56	12.53	49.90		2.61
R72-08-02	45.27	476.49	1.73	2036.83	357.26	13.91	0.29	0.43	137.03	268.10	22.42	35.93	24.87	7.46	10.72	60.62	0.01	2.40
R72-09-01	55.37	367.89	1.78	1888.68	275.96	15.40	0.05	0.46	122.05	187.90	18.06	37.17	25.30	8.02	11.69	80.43	0.02	2.87
R72-12-01	49.01	399.78	0.80	2121.33	359.07	25.34	0.24	0.46	160.77	274.03	18.41	38.36	23.58	8.12	12.15	61.51		2.76
R72-12-02	96.21	319.92	2.16	2219.84	331.32	12.99		0.53	129.25	232.70	21.16	46.60	19.64	7.61	10.91	47.28		3.15
R72-13-01	97.12	321.22	2.21	2173.50	329.04	13.07		0.54	132.84	233.70	20.99	45.43	19.07	7.59	11.03	45.59		2.98

Table C.6: Continued...

Analysis	Al	Si	Sc	V	Cr	Zn	Ga	Sr	Zr	Nb	Mo	Sn	Sb	Hf	Ta	W	Pb	U
R72-13-02	185.92	443.93	2.20	2209.44	341.16	12.21		0.49	114.38	230.27	19.62	49.46	18.14	7.16	10.83	41.48		2.68
R72-18-01	1.50	495.98	1.08	1281.33	13438.45	21.96	0.15	0.47	160.48	560.32	24.38	45.32	8.43	7.29	19.09	52.00	0.01	44.33
R72-18-01	131.27	358.73	1.32	1913.08	277.44	13.39	0.69	0.50	149.96	293.82	19.52	37.37	25.41	7.81	14.90	51.57		2.43
R72-20-01	122.15	360.82	3.92	2013.83	335.81	14.78	0.39	0.56	96.66	242.00	17.39	37.03	22.56	8.14	11.49	75.31		3.36
R73-01-01	92.37	412.48	5.59	1062.44	203.31	18.94	0.29	0.56	159.76	308.74	9.59	24.50	2.85	6.69	17.90	7.70		3.22
R73-01-02	93.44	492.03	6.31	1022.64	207.03	16.96	0.30	0.44	154.93	299.02	8.40	24.88	2.89	6.24	15.87	7.87		3.18
R73-01-03	101.07	456.50	5.73	1031.66	211.02	17.87	0.26	0.46	170.73	279.81	7.49	22.99	2.76	7.18	14.46	8.02		2.93
R73-02-01	104.03	416.14	2.15	1018.92	91.84	18.08	0.45	0.53	163.02	311.42	9.54	26.69	2.86	6.67	9.89	7.80		3.54
R73-02-02	86.18	450.59	1.95	1018.13	94.56	20.12	0.35	0.99	172.81	286.90	8.67	24.66	2.88	6.85	10.59	7.99	0.09	3.18
R73-02-03	90.32	457.91	2.43	1005.12	89.82	20.30	0.34	0.46	168.43	306.17	8.51	24.44	2.73	7.00	13.91	7.76		3.04
R73-02-04	86.17	488.24	2.44	1012.92	90.46	17.59	0.30	0.45	160.88	313.28	7.83	25.84	3.03	6.62	12.19	8.30		3.34
R73-03-01	25.44	408.69	4.34	976.75	121.65	40.15	0.13	0.51	191.80	323.14	9.48	28.05	2.95	6.89	13.94	8.66	0.05	2.31
R73-03-02	25.18	523.59	4.86	949.42	119.27	47.08	0.12	0.36	271.67	325.09	9.38	30.09	2.89	9.67	18.16	8.27		2.35
R73-03-03	28.43	443.68	4.15	957.52	116.59	19.60	0.13	0.47	218.29	321.34	9.95	30.59	2.85	7.45	13.85	8.05		2.57
R73-04-01	89.61	398.83	0.73	1217.12	168.86	16.80	0.26	0.44	176.77	316.99	9.27	26.69	2.50	5.78	17.06	5.62		3.64
R73-04-02	95.90	405.56	1.10	1246.26	169.23	18.20	0.16	0.52	139.66	302.39	9.22	26.07	2.40	5.09	13.21	5.88		3.59
R73-04-03	91.27	489.94	1.39	1236.18	164.96	20.04	0.17	0.63	150.34	301.10	8.52	26.47	2.28	5.42	16.32	5.93	0.04	3.58
R73-04-04	87.85	554.78	1.85	1218.74	164.31	19.90	0.19	0.47	153.85	289.72	8.86	26.72	2.73	5.42	15.02	5.86		3.38
R73-05-01	42.97	474.83	4.74	890.52	156.41	19.97	0.17	0.57	159.53	327.11	10.47	32.96	2.97	6.18	17.44	8.09	0.04	3.12
R73-05-01	38.13	450.10	4.88	893.38	160.32	18.10	0.22	0.48	171.37	315.99	9.35	30.07	2.83	6.56	12.41	7.55	0.02	3.04

Table C.6: Continued...

Analysis	Al	Si	Sc	V	Cr	Zn	Ga	Sr	Zr	Nb	Mo	Sn	Sb	Hf	Ta	W	Pb	U
R73-06-01	75.44	403.31	1.66	1163.73	42.85	19.43	0.56	0.54	183.85	278.16	9.42	25.88	2.93	6.82	18.50	9.49		3.13
R73-06-02	74.61	411.17	1.71	1169.51	41.73	19.85	0.47	0.45	181.86	259.54	9.69	26.37	3.05	7.75	15.80	9.49		2.93
R73-08-01	39.99	468.83	4.28	810.92	74.78	19.22	0.20	0.52	145.22	314.67	10.11	29.14	2.88	4.82	20.98	7.75	0.03	3.03
R73-08-02	42.99	430.45	4.19	826.28	78.73	18.25	0.13	0.44	135.03	333.01	9.34	31.37	3.25	4.95	21.73	8.23		3.56
R73-08-03	40.17	520.76	4.71	822.16	80.39	17.06	0.23	0.49	160.73	310.86	8.85	30.63	2.81	6.43	18.92	8.01		3.29
R73-09-01	24.14	391.09	0.40	1084.03	306.55	18.12	0.29	0.46	157.11	272.41	8.78	25.91	3.24	6.13	12.43	8.85		3.50
R73-09-02	28.91	443.68	0.69	1089.32	315.16	19.57	0.62	0.47	155.03	273.57	9.10	26.20	3.08	6.44	15.92	8.63		3.41
R73-09-03	27.23	443.12	0.56	1079.20	310.55	37.43	0.40	0.45	160.49	265.54	9.05	25.55	3.15	6.26	16.62	8.83		3.16
R73-10-01	83.44	357.18	0.90	1140.10	325.78	17.11	0.38	0.45	149.01	300.86	9.49	26.83	2.95	5.00	13.52	7.00	0.02	2.94
R73-10-02	101.65	454.21	1.01	1186.76	333.42	16.57	0.53	0.54	156.47	280.73	9.25	25.55	3.00	5.75	13.70	7.54	0.01	2.96
R73-10-03	118.83	470.24	0.66	1153.63	326.94	16.94	0.56	0.50	147.18	253.00	8.82	25.26	3.29	4.66	15.44	8.20		3.03
R73-16-01	41.91	440.78	1.75	913.15	376.68	15.13	0.16	0.49	171.75	259.76	7.70	24.41	2.95	6.69	15.43	8.85		3.52
R73-16-02	50.27	501.92	1.57	918.22	364.15	14.94	0.12	0.45	156.07	282.83	8.77	25.21	2.79	5.94	15.13	8.71		3.38
R73-16-03	52.74	439.68	1.71	938.43	384.66	14.74	0.24	0.45	135.47	285.03	9.83	26.32	2.88	5.20	12.20	7.99	0.06	3.57
R73-16-04	46.78	545.71	2.01	928.59	373.12	15.49	0.25	0.45	138.73	300.32	8.89	28.43	3.06	5.43	13.43	8.10		3.51
R73-16-05	48.05	424.81	1.70	926.82	391.06	16.47	0.20	0.57	142.92	295.83	9.24	27.38	3.07	5.52	12.78	8.06	0.01	3.68
R74-01-01	119.40	455.96	0.63	995.70	423.32	17.58	0.37	0.49	181.26	495.89	17.46	35.24	3.33	7.51	33.28	35.89	0.12	17.65
R74-01-03	213.89	414.07	0.79	1028.26	416.20	15.39	0.45	0.62	203.89	504.68	15.39	35.34	3.96	8.87	28.14	42.64	0.08	18.64
R74-04-01	91.93	523.75	0.80	999.40	233.91	12.44	0.38	0.55	164.70	478.84	16.66	34.98	3.35	7.35	35.33	34.39	0.02	18.79
R74-04-02	90.07	397.87	0.72	1009.61	229.55	12.72	0.25	0.48	150.95	532.04	15.95	34.18	5.92	7.06	41.79	50.52	0.01	18.53

Table C.6: Continued...

Analysis	Al	Si	Sc	V	Cr	Zn	Ga	Sr	Zr	Nb	Mo	Sn	Sb	Hf	Ta	W	Pb	U
R74-04-03	154.81	381.00	0.81	994.97	235.17	13.31	0.32	0.50	155.24	523.89	16.18	34.97	3.62	6.65	47.93	35.50		17.82
R74-11-02	95.51	512.57	0.76	1016.90	180.51	12.25	0.10	0.53	160.22	520.29	16.46	35.60	6.84	9.12	34.05	51.32	0.12	16.45
R74-11-03	67.96	489.25	0.91	1051.58	180.60	11.74	0.10	0.48	166.10	504.75	17.65	36.83	3.79	7.78	22.96	34.73	0.06	16.37
R74-12-01	85.94	335.09	0.67	1104.26	179.61	15.98	0.30	0.49	170.82	512.99	16.17	34.87	3.44	7.02	29.86	34.94		18.29
R74-12-02	151.94	377.60	0.91	1083.53	178.46	13.87	0.34	0.49	202.16	567.62	16.08	36.91	3.28	8.55	34.20	37.97		17.76
R74-13-01	156.93	461.80	0.95	927.36	366.76	16.18	0.33	0.53	212.51	468.46	15.26	34.93	3.86	9.15	27.48	36.61	1.51	18.77
R74-13-02	154.39	431.97	0.75	926.26	360.89	14.32	0.30	0.51	166.49	500.75	16.09	33.62	4.99	6.95	33.67	43.62		18.51
R74-13-03	114.10	461.74	0.86	916.48	361.55	13.91	0.23	0.45	174.69	500.68	16.35	33.85	6.80	7.59	27.90	52.16	0.27	18.60
R74-16-01	185.32	452.65	0.78	1036.22	272.49	14.64	0.31	0.58	195.46	503.81	17.13	37.37	3.64	7.46	33.22	35.27	0.02	18.58
R74-19-01	156.42	697.80	0.80	1022.03	274.42	19.78	0.24	0.62	166.62	545.20	17.59	38.18	3.67	7.10	37.08	37.11	8.31	18.33
R74-19-02	188.18	465.82	0.83	1084.59	152.75	13.45	0.49	0.48	180.68	510.45	17.10	34.91	5.36	8.04	38.02	43.34		16.56
R75-01-01	97.47	369.19	1.26	1285.13	450.37	18.10	0.08	0.43	148.22	77.13	0.90	16.99	1.40	8.16	5.49	2.21		0.13
R75-01-02	101.80	363.91	1.31	1284.84	447.05	17.57	0.09	0.46	155.29	77.49	1.29	17.33	1.39	8.65	5.30	2.55		0.10
R75-04-01	126.79	454.38	0.99	1287.60	335.88	17.34	0.03	0.54	165.96	47.70	1.16	16.01	1.18	9.59	2.55	1.25	0.01	0.07
R75-06-01	56.21	421.93	1.42	1415.04	198.88	17.43	0.07	0.54	148.26	46.19	1.30	17.00	1.96	9.98	3.43	2.08		0.04
R75-06-02	58.22	368.87	1.39	1371.02	168.30	17.70	0.11	0.43	160.03	43.27	0.84	16.75	1.43	9.99	2.79	1.57		0.03
R75-07-01	84.93	403.71	1.53	1241.24	370.04	16.77	0.22	0.45	169.74	91.39	1.17	21.14	1.36	8.35	3.91	2.48		0.11
R75-09-10	112.95	414.74	1.27	1020.27	415.24	17.16	0.08	0.47	164.10	78.09	0.95	16.48	1.48	8.72	2.54	1.76	0.01	0.09
R75-13-01	64.29	395.75	1.94	1323.63	292.31	18.11	0.34	0.57	164.41	44.27	0.95	17.50	1.34	10.04	3.93	1.53		0.04
R75-13-02	60.40	360.68	2.13	1309.26	280.19	17.60	0.21	0.45	147.71	42.85	1.23	17.04	1.22	8.88	3.18	1.23		0.01

Table C.6: Continued...

Analysis	Al	Si	Sc	V	Cr	Zn	Ga	Sr	Zr	Nb	Mo	Sn	Sb	Hf	Ta	W	Pb	U
R75-15-01	157.97	371.68	1.90	955.09	272.03	18.04	0.06	0.49	167.74	97.32	1.09	18.61	1.30	9.05	5.59	1.88		0.34
R76-01-01	1.90	439.44	1.10	1365.50	10223.98	18.69	0.07	0.51	165.54	380.73	21.75	43.16	8.90	7.13	14.40	48.52		41.35
R76-01-02	3.33	356.29	1.28	1381.42	10197.96	20.41		0.60	163.80	381.46	23.14	43.19	9.17	6.96	15.62	52.40	0.04	40.69
R76-01-03	1.64	433.56	1.13	1368.62	10073.09	19.95	0.04	0.52	179.68	372.18	23.29	42.22	9.23	7.40	15.25	51.85		43.67
R76-01-04	2.15	335.89	0.83	1363.64	9831.60	20.57		0.47	163.32	374.54	22.36	41.12	9.78	7.20	16.31	53.95	0.02	42.69
R76-01-05	8.04	548.25	1.24	1385.63	9553.91	20.85	0.03	0.45	163.64	381.04	23.19	40.78	9.74	7.32	15.65	56.06	0.02	41.61
R76-08-01	0.95	403.66	1.78	1051.07	10289.45	21.37		0.47	178.79	267.47	23.51	30.08	8.92	7.95	14.59	54.42	1.08	50.00
R76-08-02	0.99	399.42	1.87	1041.00	10351.45	20.22		0.50	171.57	267.16	24.20	29.86	8.23	7.57	14.73	49.92		41.81
R76-08-03	1.22	482.05	1.84	1035.27	10169.30	19.91		0.45	169.68	259.05	22.56	29.28	7.99	7.48	14.93	52.34		43.76
R76-08-04	3.13	520.76	2.00	1062.26	10271.15	19.78		0.58	184.88	255.41	20.86	30.53	8.56	8.10	15.33	55.55	0.09	52.67
R76-12-01	1.33	408.76	1.02	1375.70	11348.63	20.91		0.44	171.48	562.97	23.81	47.52	8.61	7.87	19.40	52.16		40.73
R76-12-02	0.95	378.49	1.00	1370.67	11447.67	19.74		0.43	167.48	555.43	22.58	46.92	9.16	7.91	19.40	50.90		39.84
R76-13-01	0.51	447.99	1.39	1237.00	11662.75	21.13		0.46	170.37	282.95	24.39	36.81	9.13	7.45	15.39	48.78		44.22
R76-13-02	1.58	500.99	1.46	1269.76	11280.82	20.92		0.50	175.74	295.95	28.48	39.94	9.63	8.18	16.62	55.35	0.05	48.67
R76-13-03	1042.43	1955.00	1.45	1326.59	9852.16	21.58	0.23	0.62	168.31	285.12	24.51	37.23	8.43	7.11	15.31	49.62	0.07	41.46
R76-13-04	1.26	393.35	1.59	1245.84	11085.83	18.61		0.41	163.35	271.86	24.99	37.48	8.80	7.00	14.25	45.34		33.08
R76-13-05	1.42	411.49	1.56	1216.35	11283.99	19.57	0.03	0.49	166.58	265.19	25.71	36.62	8.33	7.26	14.80	46.31		37.71
R76-13-06	3.77	426.50	1.49	1235.56	11511.99	20.37		0.46	169.16	269.70	25.61	37.05	8.47	7.34	14.66	47.61		35.29
R76-13-07	87.11	1824.58	1.22	1233.65	10491.94	17.76	0.03	0.97	167.30	265.21	24.93	35.54	9.40	6.69	15.21	48.32	0.12	40.98
R76-13-08	1.43	431.24	1.57	1237.52	11205.69	19.64	0.02	0.48	170.30	273.31	23.09	37.35	8.99	6.84	15.14	48.38		37.48

Table C.6: Continued...

Analysis	Al	Si	Sc	V	Cr	Zn	Ga	Sr	Zr	Nb	Mo	Sn	Sb	Hf	Ta	W	Pb	U
R76-13-09	2.38	428.26	1.48	1244.03	11175.67	19.50		0.47	167.19	282.17	25.34	38.06	9.08	7.05	15.22	47.51		38.30
R76-13-10	1.28	464.12	1.76	1249.00	11465.95	19.15		0.47	160.50	270.15	25.06	36.06	8.93	6.44	14.88	47.90		37.49
R76-13-11	1.06	477.19	1.41	1237.82	11462.02	19.72		0.50	169.31	271.62	25.52	36.55	8.87	7.12	14.93	47.59	0.01	38.80
R76-13-12	2.37	471.79	1.69	1192.87	11294.73	18.57	0.02	0.60	169.49	272.11	24.10	34.66	8.16	7.73	14.94	52.57	0.03	40.81
R76-14-01	1.62	477.56	1.18	1139.28	10752.09	20.36		0.46	161.31	593.00	26.68	47.06	8.15	7.31	18.01	49.70		34.48
R76-14-02	3.38	474.80	1.35	1119.90	11070.83	20.37		0.49	158.67	573.41	25.62	44.59	7.36	7.56	17.90	52.02		28.26
R76-14-03	2.12	470.13	1.66	1136.98	10321.95	21.19	0.04	0.41	162.80	578.46	24.05	41.92	7.22	7.67	15.98	50.79		31.67
R76-15-01	9.77	375.40	1.91	1271.41	12794.25	19.59	0.07	0.49	180.56	250.88	24.55	26.68	8.53	7.07	15.19	50.73	0.01	56.12
R76-15-02	17.20	505.62	2.47	1308.99	13048.42	21.85	0.08	0.43	178.94	256.17	25.99	28.48	11.35	6.91	15.19	49.25	0.01	48.77
R76-17-01	1.27	364.99	1.57	1445.10	12322.32	19.84		0.46	166.41	271.30	25.04	33.06	8.12	7.27	13.84	47.70		32.90
R76-17-02	1.03	408.37	1.41	1450.00	12917.00	20.53		0.55	176.28	255.19	24.20	32.89	7.72	7.83	11.36	55.65	0.01	42.22
R76-18-02	0.65	516.91	1.11	1277.25	13382.18	21.46		0.44	169.88	510.17	24.95	42.40	9.55	7.68	19.82	46.95		41.41
R76-18-03	0.93	440.28	1.07	1255.25	13282.64	20.55		0.51	169.41	522.19	23.20	43.24	9.38	7.29	19.18	50.46		40.78
R76-20-01	0.46	450.89	1.75	1264.67	10747.82	19.46	0.07	0.49	186.98	254.83	23.81	27.89	9.41	7.67	13.54	47.26		51.21
R76-20-03	0.64	390.61	1.46	1281.31	10882.61	18.29	0.04	0.45	194.78	255.92	22.30	25.92	8.32	8.02	13.59	51.15		54.93
R76-21-01	3.84	413.10	0.92	1276.60	13713.80	18.44	0.04	0.50	188.80	251.01	25.89	28.83	8.62	8.24	14.57	51.68	0.10	75.19
R76-21-02	1.67	395.28	1.32	1268.85	13604.13	20.00	0.05	0.48	181.28	246.78	26.39	28.87	9.63	7.27	13.59	47.61	0.01	63.45
R76-21-03	2.03	391.40	0.98	1262.45	13598.61	18.09	0.03	0.49	187.06	251.31	26.94	28.14	8.46	7.70	14.56	49.25		81.25
R76-22-01	0.93	402.50	1.16	1320.67	10088.42	19.37		0.53	157.32	276.83	24.82	36.37	8.64	7.13	16.34	48.36	0.01	46.55
R76-22-02	1.76	387.48	1.11	1338.95	10200.62	20.03		0.43	160.29	274.57	23.20	36.22	9.65	7.34	16.29	59.45	0.10	48.97

Table C.6: Continued...

Analysis	Al	Si	Sc	V	Cr	Zn	Ga	Sr	Zr	Nb	Mo	Sn	Sb	Hf	Ta	W	Pb	U
R76-22-03	1.40	401.28	1.06	1313.57	10010.01	18.68	0.03	0.49	161.46	271.58	23.02	36.03	8.81	7.09	15.99	47.43	0.01	47.54
R76-22-04	1.12	413.22	1.20	1320.45	10099.56	21.16		0.46	162.32	269.83	22.72	37.11	8.69	6.93	16.18	49.01		43.96
R77-01-01	58.16	359.52	1.59	1514.96	19.81	16.51	0.39	0.46	138.66	253.81	6.44	18.57	0.28	7.02	14.24	1.72	0.02	2.88
R77-01-02	76.14	355.34	1.13	1516.06	17.69	16.02	0.35	0.49	138.38	252.80	7.03	19.70	0.20	6.85	10.64	1.64	0.02	3.20
R77-03-01	61.31	384.94	0.95	1335.79	7.93	18.12	0.72	0.47	143.57	246.26	6.27	18.53	0.24	6.97	10.62	1.43		2.58
R77-04-01	87.78	365.97	1.18	1391.11	11.27	16.27	1.12	0.43	138.64	234.42	6.36	17.30	0.26	6.83	9.69	1.73		3.12
R77-04-02	111.62	401.40	1.28	1371.72	11.13	15.70	1.19	0.49	146.01	227.59	6.77	17.35	0.22	7.20	8.86	1.36	0.05	3.42
R77-05-01	25.62	391.63	1.96	1401.71	6.42	15.47	0.66	0.50	151.29	215.78	7.02	18.44	0.25	7.65	11.95	1.81	0.01	2.65
R77-09-01	129.58	390.85	1.17	1686.39	82.16	17.56	0.54	0.56	129.14	157.05	6.76	19.64	0.21	5.95	5.96	1.54		1.70
R77-11-01	180.33	341.54	0.92	1611.63	87.04	16.29	1.22	0.44	140.92	198.42	6.30	19.25	0.20	6.80	6.83	1.85		2.56
R77-11-02	81.42	357.16	1.06	1615.41	84.94	15.55	0.36	0.49	145.50	197.53	6.56	20.04	0.18	6.89	6.46	1.67		2.95
R77-16-01	93.67	367.00	1.38	1479.58	14.72	15.70	0.48	0.50	140.01	247.06	6.64	18.84	0.24	6.70	15.84	1.80		2.70
R77-16-02	65.99	392.68	1.19	1477.23	14.54	16.40	0.48	0.50	147.11	258.82	6.37	19.15	0.20	6.46	13.71	1.58	0.05	3.14
R77-17-01	17.69	390.34	1.27	1386.43	7.39	15.09	0.76	0.52	166.55	270.25	6.86	20.30	0.20	7.70	13.40	1.45		3.33
R78-01-01	65.09	379.14	0.79	1216.25	20.14	18.34	0.82	0.44	137.04	203.59	5.78	14.75	0.71	5.31	13.93	1.15		2.07
R78-03-01	100.24	259.93	0.58	1236.65	16.75	17.75	0.81	0.49	128.58	188.91	5.01	13.46	0.49	5.75	10.76	1.22		1.92
R78-03-02	100.35	386.95	0.63	1247.10	18.11	17.37	0.98	0.47	128.55	189.76	5.38	14.08	0.46	5.25	10.39	1.00		1.82
R78-03-03	127.78	357.12	0.61	1223.40	15.70	18.25	0.92	0.46	124.85	177.17	5.52	13.05	0.49	5.54	8.67	1.18		1.95
R78-05-01	92.29	430.85	0.94	1201.46	21.37	18.26	0.96	0.78	139.80	230.89	6.55	15.11	0.52	5.82	20.52	1.48	0.07	1.76
R78-05-02	78.19	382.31	0.78	1234.77	22.44	18.35	0.69	0.85	134.47	233.47	6.05	14.72	0.62	5.85	14.68	1.30	0.04	1.99

Table C.6: Continued...

Analysis	Al	Si	Sc	V	Cr	Zn	Ga	Sr	Zr	Nb	Mo	Sn	Sb	Hf	Ta	W	Pb	U
R78-06-01	129.25	416.98	1.81	1338.09	17.59	17.40	0.66	0.47	121.49	201.37	5.32	13.07	0.51	5.39	11.95	1.31		1.94
R78-09-01	94.01	415.07	1.01	1312.39	23.44	18.71	0.69	0.50	118.75	191.56	5.72	14.49	0.53	4.99	10.28	1.35		1.48
R78-10-01	196.06	368.24	1.63	1363.15	18.43	17.39	0.74	0.47	119.04	168.80	5.85	13.63	0.49	4.98	7.94	0.95		1.84
R78-10-02	121.23	392.17	1.70	1386.27	17.27	18.87	0.75	0.42	120.67	175.02	4.88	14.02	0.58	5.83	9.73	1.24		1.84
R78-10-03	150.41	416.36	1.84	1357.37	17.58	16.84	0.90	0.51	121.03	177.74	5.58	14.03	0.43	5.84	11.36	1.09		1.67
R78-11-01	141.71	313.29	0.89	1270.13	16.74	18.59	0.76	0.48	118.55	126.81	5.32	12.82	0.50	4.93	2.06	0.90		1.77
R78-16-01	84.33	332.36	0.79	1141.02	12.94	18.00	0.69	0.50	141.37	182.84	5.16	14.06	0.55	6.47	12.28	1.70		1.78
R78-18-01	51.36	431.01	1.12	1319.16	24.13	18.17	0.90	0.53	160.99	187.83	6.08	15.43	0.53	6.66	7.48	1.32		1.91
R78-19-01	285.34	391.01	1.09	1355.78	18.04	16.98	1.22	0.42	119.83	175.66	5.44	13.85	0.46	5.75	7.18	1.18	0.01	1.61
R78-19-02	107.63	400.85	1.25	1324.56	18.19	17.65	0.91	0.43	116.61	180.56	4.98	13.96	0.51	5.65	8.29	1.24		1.57
R79-01-01		382.37	2.43	1190.32	1161.17	16.13	0.12	0.44	173.28	105.55	8.69	22.98	4.96	6.74	6.69	17.84		0.05
R79-01-02	0.56	400.84	2.01	1194.17	1140.50	16.24	0.07	0.49	173.83	116.95	8.97	24.19	4.36	6.66	6.58	14.78		0.23
R79-04-01	97.53	438.78	4.78	1465.59	1042.07	13.60	0.14	0.45	136.35	104.05	8.58	28.06	4.19	5.10	6.16	16.42		0.06
R79-04-02	60.06	453.49	4.52	1458.34	1028.40	12.07	0.11	0.60	151.27	86.96	7.97	26.75	4.34	6.38	6.75	15.87		0.04
R79-05-01	53.36	383.37	2.96	1566.67	1529.24	16.05	0.18	0.53	169.15	109.72	8.37	29.15	4.58	6.30	6.30	18.12		0.07
R79-06-01	70.28	425.93	2.62	1636.80	1242.29	15.62	0.60	0.49	203.21	97.50	8.99	28.69	4.61	8.70	6.78	22.50		0.19
R79-06-01	98.93	407.94	1.93	1234.16	234.54	11.56	0.49	0.46	124.33	254.10	23.06	34.70	0.24	5.63	13.61	8.07		0.51
R79-06-02	148.06	437.49	2.68	1639.76	1255.52	13.55	0.56	0.46	194.05	107.69	8.57	27.42	4.66	7.76	8.59	21.20		0.18
R79-09-01	42.20	426.74	3.27	1684.91	934.30	13.21	0.13	0.45	140.54	109.44	8.12	28.54	4.74	5.21	7.39	25.86		0.02
R79-09-02	38.68	380.52	2.82	1663.72	915.78	13.29	0.13	0.48	192.36	107.83	9.23	27.76	4.23	8.09	7.09	15.35		0.02

Table C.6: Continued...

Analysis	Al	Si	Sc	V	Cr	Zn	Ga	Sr	Zr	Nb	Mo	Sn	Sb	Hf	Ta	W	Pb	U
R79-10-01	57.40	414.91	2.33	1533.68	949.62	14.07	0.32	0.50	149.19	116.79	8.84	28.41	3.87	5.51	7.25	15.54	0.01	0.06
R79-10-02	81.31	346.69	1.98	1551.83	939.93	13.71	0.26	0.46	127.74	120.69	8.60	28.88	4.47	5.07	9.46	15.69		0.08
R79-11-01	74.54	374.25	1.51	1505.13	951.02	15.74	0.15	0.51	148.39	114.93	8.18	28.28	4.53	5.45	7.75	17.07		0.07
R79-11-01	90.63	430.95	1.22	1192.24	266.53	12.90	0.64	0.45	103.52	336.24	25.91	40.33	0.18	4.59	18.29	6.50		0.57
R79-11-02																		
R79-15-01	75.09	378.58	2.21	1267.31	791.05	15.11	0.21	0.54	177.47	116.88	8.76	26.92	4.91	7.69	7.55	20.37		0.04
R79-15-02	34.03	387.71	2.21	1281.80	820.55	16.80	0.21	0.59	186.98	113.78	9.57	29.53	4.98	7.86	7.78	20.89		0.02
R80-01-01	57.02	351.54	2.01	1737.33	614.58	10.04	0.73	0.44	232.05	964.62	11.13	35.73	2.40	9.62	79.92	40.02	0.07	12.13
R80-01-02	53.84	396.68	1.92	1767.45	600.60	11.96	0.79	0.45	225.81	926.55	11.28	36.76	2.33	9.56	84.91	41.16	0.01	13.29
R80-02-01	168.05	504.55	6.79	1436.25	477.19	9.89	0.17	0.53	238.25	1003.34	12.75	44.97	2.52	7.87	128.90	35.86	0.05	15.27
R80-02-02	134.80	434.22	7.43	1418.66	462.31	17.41	0.32	0.48	230.83	976.68	11.71	40.87	2.52	8.14	140.30	38.36		15.27
R80-03-01	150.52	383.41	3.38	1438.76	443.20	11.78	0.38	0.47	235.23	685.67	11.97	33.62	2.39	9.03	45.56	36.04	0.01	14.27
R80-03-02	663.41	843.21	3.28	1468.15	447.32	17.50	1.03	0.53	235.61	719.80	11.69	33.46	2.42	9.01	43.14	37.83	0.04	15.06
R80-04-01	464.27	930.99	1.95	1704.75	593.98	14.14	0.81	0.58	206.55	893.75	9.98	39.96	2.49	8.21	37.73	37.69	0.18	13.05
R80-11-01	757.87	1565.84	2.44	1708.43	278.03	24.09	0.74	0.59	189.72	613.31	11.43	32.16	2.29	7.01	34.17	41.05	0.04	12.66
R80-12-01	63.32	385.60	1.73	1681.75	512.69	20.31	0.67	0.51	209.36	623.26	9.53	30.72	2.39	8.42	65.58	36.33		11.17
R80-13-01	78.53	397.95	1.67	1251.64	41.52	11.41	0.53	0.51	96.80	171.93	8.47	1.90	2.33	3.96	13.17	0.98		0.62
R80-14-01	49.41	445.63	2.00	1741.01	516.70	11.80	0.57	0.47	202.68	772.90	12.66	37.88	2.73	6.43	39.46	38.08	0.01	12.06
R80-15-01	24.71	399.30	0.40	1247.85	534.73	11.66	0.71	0.46	216.81	632.39	10.29	27.80	2.63	7.70	37.65	34.52		12.77
R80-16-01	58.12	387.33	2.23	1772.37	526.49	11.97	0.58	0.52	242.64	649.53	11.49	38.46	2.67	9.80	27.17	37.12		12.20

Table C.6: Continued...

Analysis	Al	Si	Sc	V	Cr	Zn	Ga	Sr	Zr	Nb	Mo	Sn	Sb	Hf	Ta	W	Pb	U
R80-18-01	50.16	422.31	1.90	1663.82	368.57	11.71	0.79	0.48	187.33	1003.98	12.41	43.04	1.99	7.59	93.67	45.07		12.61
R80-19-01	132.48	396.75	2.90	1732.44	496.04	12.97	0.12	0.58	193.73	657.33	10.49	34.69	3.92	5.57	56.65	29.29	0.08	13.02
R81-01-01	134.26	391.20	2.21	1419.03	650.94	15.70	0.29	0.47	201.90	570.84	7.40	23.37	1.04	6.98	32.24	5.04		0.27
R81-02-01	16.87	368.57	2.01	1312.82	894.25	13.77	0.26	0.47	218.72	623.86	7.79	22.59	1.94	8.51	32.60	13.41		0.18
R81-03-01	70.45	367.32	5.12	1375.09	907.28	13.13		0.45	231.93	387.61	6.33	18.51	2.21	9.22	30.98	12.71		0.08
R81-04-01	66.57	340.43	2.79	1249.02	767.25	15.04	0.37	0.45	217.69	569.41	7.02	20.10	1.48	7.65	34.16	7.67		0.10
R81-04-02	67.32	386.65	2.68	1284.54	781.94	14.07	0.50	0.49	226.71	650.99	7.71	20.47	1.71	8.70	34.43	10.82		0.13
R81-05-01	67.95	374.49	3.35	1232.09	1055.40	14.47	0.11	0.40	197.71	596.99	6.69	23.12	1.35	6.70	32.77	6.30	0.01	0.12
R81-06-01	41.18	377.22	1.60	1755.71	1250.65	13.64	0.35	0.52	240.32	574.92	6.51	18.96	1.75	8.57	33.62	10.96	0.02	0.13
R81-06-02	36.95	361.29	1.82	1739.47	1247.78	13.40	0.33	0.52	238.56	619.41	6.92	19.81	1.76	8.12	33.15	9.53		0.11
R81-07-01	192.26	399.72	1.39	1422.37	1099.58	14.34	1.45	0.47	219.61	539.79	6.20	22.05	1.74	8.21	31.91	10.00		0.07
R81-09-01	64.29	366.36	2.62	1691.80	947.45	13.49	0.37	0.45	184.13	552.91	6.34	24.65	1.91	7.75	33.46	13.33		0.30
R81-11-01	66.51	395.48	2.07	1507.17	1318.63	14.51	0.82	0.45	205.85	535.61	7.21	20.36	1.24	7.51	32.74	8.74		0.21
R81-12-01	86.18	399.36	1.42	1501.66	1524.96	13.85	0.58	0.43	217.67	582.43	7.29	21.66	1.65	7.63	33.11	8.32		0.12
R81-13-01	52.61	380.40	1.39	1481.80	1211.49	15.78	0.59	0.45	234.25	571.19	7.24	17.84	1.95	7.38	32.80	8.22		0.06
R82-02-01	110.28	364.11	10.07	1922.90	275.05	15.81	1.19	0.45	265.37	587.77	20.15	33.44	1.85	9.26	37.85	3.75	0.01	10.67
R82-03-01	106.42	344.43	1.55	1673.49	140.10	14.00	0.75	0.41	258.67	513.22	16.07	28.44	1.66	9.61	34.28	4.02		7.08
R82-03-02	136.82	448.32	1.52	1690.73	142.98	15.62	3.37	0.56	262.91	488.05	15.34	26.20	1.75	10.37	35.61	4.59	0.04	7.20
R82-04-01	88.79	394.33	3.46	2063.63	193.06	15.43	0.75	0.49	267.20	633.36	20.26	34.42	1.66	10.12	38.17	3.90		6.81
R82-05-01	105.37	331.02	4.19	1833.08	171.88	15.26	0.76	2.29	263.19	558.76	17.02	26.75	1.88	9.03	32.86	3.99	0.05	6.30

Table C.6: Continued...

Analysis	Al	Si	Sc	V	Cr	Zn	Ga	Sr	Zr	Nb	Mo	Sn	Sb	Hf	Ta	W	Pb	U
R82-06-01	82.00	337.14	4.67	2545.03	270.46	16.69	0.63	0.53	257.35	587.32	20.13	34.42	1.50	8.82	36.11	4.05		6.60
R82-09-01	113.93	434.15	2.19	1621.01	99.81	16.48	0.63	0.54	277.24	616.09	19.30	35.31	1.48	9.80	35.57	3.86		5.92
R82-10-01	97.04	385.12	2.62	2108.38	255.33	16.27	1.26	0.43	275.30	680.30	21.82	35.80	1.76	9.73	37.15	3.87	0.04	5.62
R83-01-01	96.03	402.03	0.43	790.73	119.33	13.88	0.82	0.45	284.52	432.79	23.01	29.02	7.79	9.25	19.18	19.85	0.03	10.56
R83-02-01	133.81	376.52	0.83	969.69	286.01	14.92	0.36	0.45	286.17	264.50	20.68	26.61	8.38	9.27	16.38	19.67	0.03	8.76
R83-04-01	28.00	358.96	6.36	622.08	140.77	17.49	0.18	0.51	319.72	363.35	38.59	50.22	8.00	10.32	17.88	17.32	0.04	10.35
R83-04-02	36.05	460.57	6.51	618.63	144.70	15.75	0.19	0.47	329.94	345.08	43.54	53.44	8.08	10.35	17.82	16.18	0.01	10.26
R83-09-01	109.65	386.43	0.42	990.18	157.98	13.64	0.77	0.42	296.18	295.52	21.82	30.94	8.39	9.67	17.84	15.70		9.46
R83-15-01	93.39	441.52	0.56	1084.49	246.11	15.13	0.45	0.51	267.60	358.01	21.84	29.32	8.10	8.10	17.15	17.70	0.01	11.20
R83-15-02	106.82	432.90	0.53	1104.68	250.94	13.97	0.76	0.45	238.31	381.62	22.12	29.40	8.34	7.09	17.55	17.25		11.91
R83-18-01	20.14	460.55	0.77	1094.97	226.50	14.24	0.10	0.48	282.00	314.89	22.65	25.94	7.52	10.22	18.57	29.32		10.49
R83-18-02	21.75	369.63	0.64	1097.05	227.54	14.78	0.11	0.47	271.03	335.01	22.90	26.16	7.92	8.56	17.93	16.82	0.01	11.05
R83-18-03	25.63	408.98	0.73	1088.72	225.81	14.51	0.10	0.93	288.50	361.17	23.52	28.09	7.50	9.72	18.78	22.13	0.17	11.42
R83-20-01	72.33	424.17	0.35	802.44	198.97	16.68	1.13	0.48	256.35	361.65	21.11	31.14	8.11	8.19	17.57	16.93		11.19
R83-20-02	73.58	404.32	0.39	793.18	200.51	16.39	0.80	0.49	253.99	343.35	21.68	29.00	8.25	8.13	16.58	17.08		10.67
R83-20-03	305.55	968.18	0.46	812.22	199.51	18.86	1.15	0.56	252.71	352.56	22.32	29.61	7.67	7.82	17.64	17.28	0.13	11.26
R85-01-01	95.76	446.49	1.19	2066.39	168.34	16.50	0.51	0.54	455.28	256.51	25.77	41.61	1.93	13.81	12.58	175.35		1.11
R85-03-01	338.36	983.61	2.68	2693.82	983.27	15.56	0.09	0.65	347.33	230.31	23.54	34.19	1.34	13.60	10.24	153.39	0.01	0.70
R85-04-01	221.96	522.22	2.23	2530.93	516.14	17.22	0.20	0.59	352.43	228.67	23.39	27.84	1.37	12.59	8.96	155.03		0.78
R85-08-01	86.00	364.01	2.67	2179.67	1466.19	14.58	0.11	0.55	381.90	241.49	25.64	25.24	1.61	13.34	10.67	159.92		0.39

Table C.6: Continued...

Analysis	Al	Si	Sc	V	Cr	Zn	Ga	Sr	Zr	Nb	Mo	Sn	Sb	Hf	Ta	W	Pb	U
R85-09-01	79.24	373.98	9.73	2331.86	528.23	14.76		0.50	499.98	228.44	23.72	27.46	1.49	17.45	8.23	139.81		0.91
RLef-01-01	61.25	421.52	0.75	806.28	2108.63	13.76	0.36	0.50	210.14	538.20	3.40	14.74	1.59	8.65	21.92	16.36	0.02	0.14
RLef-02-02	96.05	409.80	1.04	962.31	1102.01	12.09	0.37	0.57	214.40	481.06	3.44	15.59	1.28	8.52	23.77	9.54		0.14
RLef-03-01	132.66	359.93	1.84	859.45	1162.56	13.14	0.15	0.57	212.81	836.57	3.22	13.74	1.26	8.81	20.89	13.26	0.01	0.17
RLef-04-01	144.03	364.44	1.01	787.04	1117.02	12.26	0.24	0.48	182.29	500.11	3.77	15.21	1.50	5.29	16.12	20.92		0.35
RLef-05-01	178.92	400.31	1.77	980.07	1177.08	12.54	0.59	0.44	201.90	422.48	3.24	16.16	1.13	9.26	23.74	10.00		0.24
RLef-05-02	178.82	404.44	2.05	984.83	1192.45	12.71	0.36	0.46	205.25	425.26	2.98	15.81	1.03	9.67	22.08	7.16		0.25
RLef-06-01	101.63	398.59	1.02	925.22	1276.31	12.60	0.27	0.50	218.36	450.79	3.19	15.14	1.47	8.84	17.80	14.17		0.11
RLef-07-01	81.61	403.51	1.53	873.08	1144.47	14.83	0.19	0.45	217.00	542.60	2.62	16.62	1.20	7.85	20.64	27.49		0.19
RLef-08-01	206.96	433.45	1.66	946.65	959.79	12.37	0.15	0.47	213.26	409.99	3.30	15.63	1.21	9.64	21.45	9.48		0.10
RLef-08-02	174.32	404.56	1.75	933.42	968.62	12.35	0.27	0.41	207.10	429.52	2.74	16.37	1.05	9.21	19.75	7.50		0.09
RLef-11-01	119.77	372.95	1.40	976.68	948.45	11.82	0.36	0.45	220.84	554.62	3.54	14.84	1.65	8.87	21.72	17.79		0.15